NASA-CR-199802

(NASA-CR-199802)   MICROCRACKING IN   N96-16101
COMPOSITE LAMINATES UNDER THERMAL
AND MECHANICAL LOADING Thesis
(MIT)   225 p
                                             Unclas

                                        63/24   0085080

MICROCRACKING IN COMPOSITE LAMINATES UNDER THERMAL AND MECHANICAL LOADING

by
Jason R. Maddocks

Submitted to the Department of Aeronautics and Astronautics on May 12, 1995 in partial fulfillment of the requirements for the Degree of Master of Science in Aeronautics and Astronautics

ABSTRACT

Composites used in space structures are exposed to both extremes in temperature and applied mechanical loads. Cracks in the matrix form, changing the laminate thermoelastic properties. The goal of the present investigation is to develop a predictive methodology to quantify micro-cracking in general composite laminates under both thermal and mechanical loading. This objective is successfully met through a combination of analytical modeling and experimental investigation. In the analysis, the stress and displacement distributions in the vicinity of a crack are determined using a shear lag model. These are incorporated into an energy based cracking criterion to determine the favorability of crack formation. A progressive damage algorithm allows the inclusion of material softening effects and temperature-dependent material properties. The analysis is implemented by a computer code which gives predicted crack density and degraded laminate properties as functions of any thermomechanical load history. Extensive experimenation provides verification of the analysis. AS4/3501-6 graphite/epoxy laminates are manufactured with three different layups to investigate ply thickness and orientation effects. Thermal specimens are cooled to progressively lower temperatures down to -184°C. After conditioning the specimens to each temperature, cracks are counted on their edges using optical microscopy and in their interiors by sanding to incremental depths. Tensile coupons are loaded monotonically to progressively higher loads until failure. Cracks are counted on the coupon edges after each loading. A data fit to all available results provides input parameters for the analysis and shows them to be material properties, independent of geometry and loading. Correlation between experiment and analysis is generally very good under both thermal and mechanical loading, showing the methodology to be a powerful, unified tool. Delayed crack initiation observed in a few cases is attributed to a lack of pre-existing flaws assumed by the analysis. Some interactions between adjacent ply groups are attributed to local stress concentrations. These two effects are not captured by the analysis due to its global nature. The analysis is conservative in these cases and agrees well with data after the observed onset of cracking.

Thesis Supervisor: Hugh L. McManus

Title: Assistant Professor, Department of Aeronautics and Astronautics, Massachusetts Institute of Technology

PRECEDING PAGE BLANK NOT FILMED

ACKNOWLEDGMENTS

FOREWARD

This research was completed at the Technology Laboratory for Advanced Composites at the Massachusetts Institute of Technology. The work was funded by NASA Langely Research Center grant NAG-1-1463.

TABLE OF CONTENTS

LIST OF FIGURES

9

LIST OF TABLES

NOMENCLATURE

a_o	Total thickness of laminate
a_c	Thickness of cracking layer
a_q	Thickness of shear transfer region
a_r	Thickness of rest of laminate
$\mathbf{A}$	Laminate stiffness matrix
A_{11}	Component of laminate stiffness matrix
D_i	Parameter used to simplify ply stiffness expressions
E_o	Effective axial stiffness of laminate
E_c	Axial stiffness of cracking layer
E_r	Axial stiffness of rest of laminate
E_l	Longitudinal modulus of ply
E_t	Transverse modulus of ply
G	Strain energy release rate
G_{Ic}	Mode I critical strain energy release rate
G_{lt}	Shear modulus of ply
G^{eff}	Effective shear modulus of shear transfer region
h	Crack spacing
K	Stiffness constant in shear lag analysis
l	Crack length
l_c	Critical crack length
m	Number of data points for layer
n	Number of plies in laminate
N	Number of plies in layer
$\mathbf{N}$	Laminate load vector

$N_x{'}$	Laminate load in x' direction
q	Shear stress
Q	Ply stiffness matrix
Q_{11}	Component of ply stiffness matrix
Q_{12}	Component of ply stiffness matrix
Q_{22}	Component of ply stiffness matrix
Q_{66}	Component of ply stiffness matrix
S	Shear strength
t	Thickness of layer
T_o	Stress free temperature
T	Transformation matrix
u_c	Axial displacement in cracking layer
u_r	Axial displacement in rest of laminate
U	Internal strain energy of body
U_q	Strain energy contribution of shear stresses
U_σ	Strain energy contribution of normal stresses
W	Work done by external force
x	Global coordinate system axis
x'	Local coordinate system axis
X_c	Axial compressive strength
X_t	Axial tensile strength
y	Global coordinate system axis
y'	Local coordinate system axis
Y_c	Transverse compressive strength
Y_t	Transverse tensile strength
$Y_t^{\it eff}$	*In situ* transverse tensile strength
z	Global coordinate system axis

z'	Local coordinate system axis
α_c	Axial coefficient of thermal expansion of cracking layer
α_r	Axial coefficient of thermal expansion of rest of laminate
α^{eff}	Effective axial coefficient of thermal expansion of laminate
α_l	Axial coefficient of thermal expansion of ply
α_t	Transverse coefficient of thermal expansion of ply
α	Effective laminate coefficient of thermal expansion vector
ΔT	Change in temperature relative to stress free temperature
ΔU	Change in internal energy
ΔW	Change in external work
$\Delta \theta$	Minimum change in ply angle
ε_c	Axial strain in cracking layer
ε_r	Axial strain in rest of laminate
ε_α	Laminate axial strain
η	Slope of load path
Φ	Constant used to simplify strain energy release rate equation
κ	Knockdown factor
λ	Parameter used to simplify shear lag analysis
ν	Major Poisson's ratio
θ_c	Ply angle of cracking ply group
θ_i	Ply angle of ith ply
θ_i'	Ply angle of ith ply after rotation
ρ	Crack density
ρ_e	Crack density observed on specimen edge
ρ_∞	Calculated crack density
σ_c	Longitudinal stress in cracking layer
σ_r	Longitudinal stress in rest of laminate

σ_a	Applied mechanical stress
ψ	Exponential decay term
ζ	Shear lag parameter

CHAPTER 1

INTRODUCTION

Advanced composite materials have gained increasing use in aerospace structural applications in recent years. Their properties, which include high specific stiffness, low coefficient of thermal expansion (CTE), and high specific strength, have made composites extremely attractive for dimensionally critical space structures such as antennae and waveguide supports, solar reflectors, and truss tubes. A lightweight space telescope support structure, for instance, may be made very stiff and with a near-zero CTE, which would not even be possible with conventional monolithic materials.

1.1 DAMAGE CAUSED BY THE SPACE ENVIRONMENT

Composites utilized in space structures are exposed to mechanical loads and extremes in temperature. The individual truss tubes of one design for the NASA Space Station, for example, must be capable of withstanding axial loads estimated at ±5.3 kN (±1200 lb) [1]. Moreover, as the spacecraft orbits the earth, it moves in and out of the earth's shadow; as a result, a truss structure is exposed to temperature changes of up to ±139°C (±250°F) in geosynchronous earth orbit [2].

When a single composite ply undergoes a change in temperature, it expands or contracts in different directions according to its CTE. Rotating the ply changes the value of its CTE. If the ply is independent and

unconstrained, the expansion or contraction occurs freely, and no ply stresses result regardless of ply orientation. Figure 1.1(a) illustrates this phenomenon. However, when plies are rotated to different orientations and laminated together as in Figure 1.1(b), each ply will not be able to expand or contract according to its own CTE due to the constraint of adjacent plies. This creates high stresses within the plies. Since the matrix has a lower *in situ* failure strain than the fiber, cracks in the matrix form, called microcracks.

Similarly, when a mechanical load is applied to a composite laminate, some of the plies may be loaded in the direction of their fibers, where they are strongest. Laminate constraint will cause others to be loaded in their weak, matrix-dominated direction, even though those plies may not be bearing much of the total applied stress. As a result, microcracks will form in the matrices of the latter, as shown in Figure 1.1(c). For both thermal and mechanical loading, we define transverse microcracks as cracks which extend parallel to the fibers and perpendicular to the x-y plane. Typical microcracks are shown in Figure 1.2.

Microcracking in composites generally does not lead directly to failure. The fibers and adjacent plies serve as obstructions to crack propagation, preventing a dominant crack from forming as in monolithic materials. It can, however, facilitate other damage modes, such as delamination, which could in turn lead to premature failure. More importantly, microcracking may cause profound property changes, specifically in CTE, stiffness, and Poisson's ratio. The structure will subsequently respond differently to future loads. This can be detrimental in dimen-sionally critical applications. The design of the Space Station truss tubes is driven largely by a CTE requirement of $0 \pm 0.9 \times 10^{-6}/^{\circ}C$, and column buckling has been identified as the dominant mode of
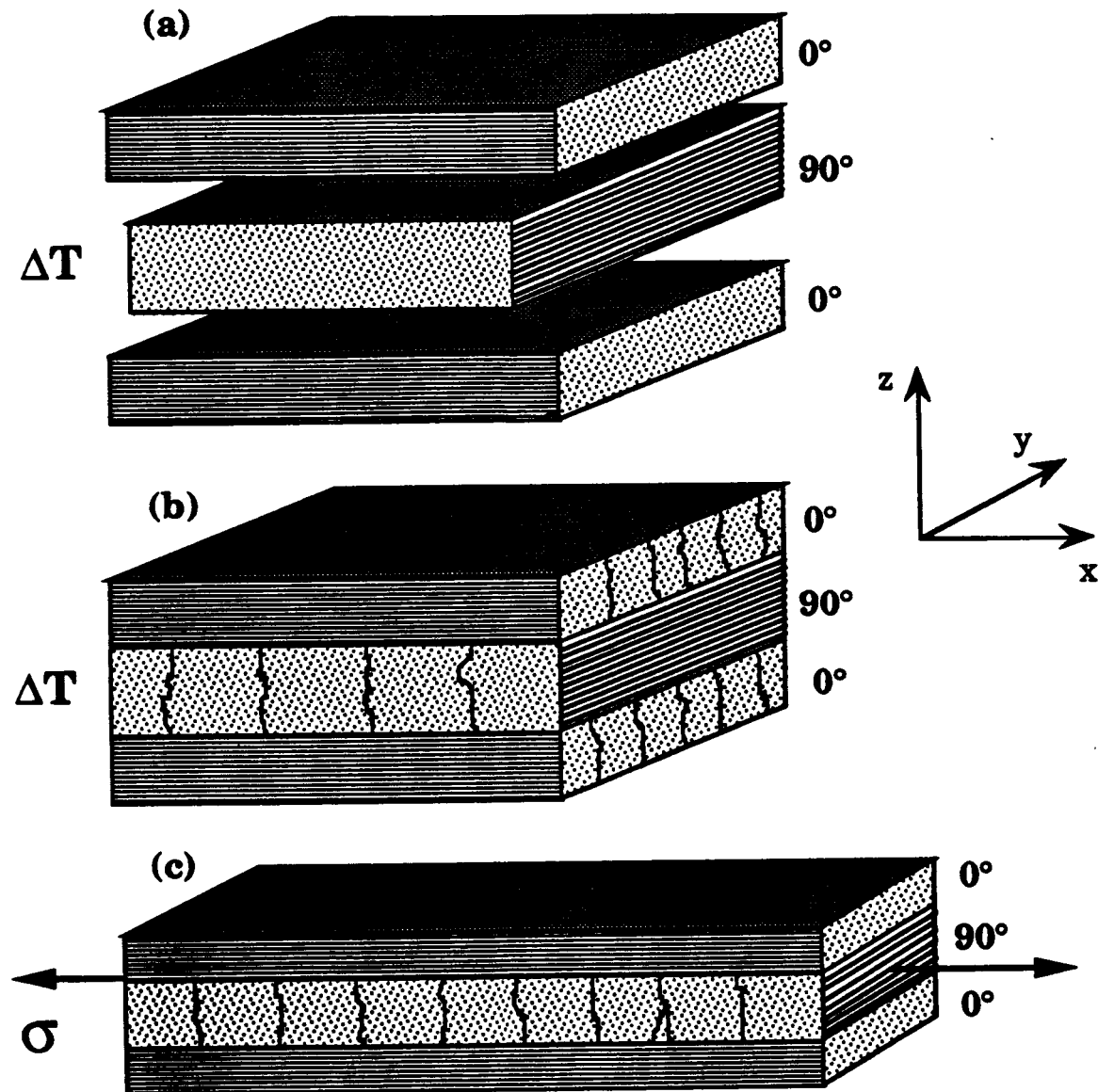
Figure 1.1 (a) Thermally loaded independent, unconstrained plies; no cracks form. (b) Thermally loaded constrained laminate; cracks form due to internal stresses. (c) Mechanically loaded laminate; cracks form in transverse ply.
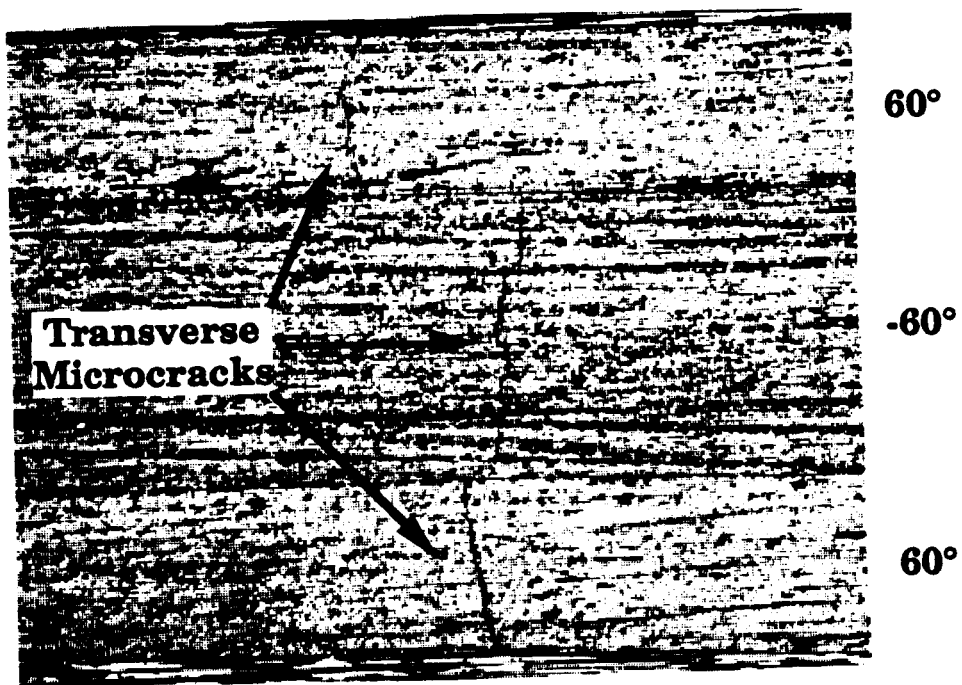
Figure 1.2　Photomicrograph of the edge of an AS4/3501-6 $[0_2/60_2/-60_2]_s$ laminate under 100x magnification. Transverse microcracks visible in all plies after mechanical loading.

failure [1]. Property changes due to microcracking, CTE and stiffness in this example, could cause the structure to stray from design criteria, with potentially disastrous consequences.

1.2 PRESENT WORK

Researchers recognized the importance of microcracking in composite structures decades ago. Since then, numerous experimental studies have confirmed the resulting property degradation and have identified some key factors in microcracking. These include material type, ply thickness, and laminate geometry. Even though an extensive data base has emerged from this work, it would be unreasonable to conduct tests on every new material that is developed and for the infinite number of laminate geometries that are possible. Instead, we need a methodology to predict the initiation and extent of microcracking analytically. We can then implement existing tools and data bases giving property changes as functions of the number of cracks. This would also help us to better understand the problem.

The goal of the present work is to develop an analytical methodology to predict the initiation and extent of microcracking in composite laminates under both thermal and mechanical loading. The analysis uses a shear lag solution of the laminate stress and displacement distributions in the vicinity of a transverse microcrack. This solution is subsequently combined with a cracking criterion based on fracture mechanics to determine whether further cracking is energetically favorable. An incremental damage model facilitates the inclusion of temperature dependent material properties and laminate softening due to cracking. The analysis is integrated into a computer code which can accommodate any user-defined thermomechanical load history. Extensive testing, using a variety of laminate geometries under thermal and

24

mechanical loading, was performed to verify the analysis. The data collection included crack counts in the specimen interiors as well as at their edges.

A data fit provided two key parameters for the analysis, both assumed to be material properties. Some interaction between cracks in adjacent plies, not included in the analytical model, was observed. In general, though, correlation between analysis and experiment was excellent under both thermal and mechanical loading and for all laminate geometries.

1.3 OVERVIEW

In Chapter 2 the previous work relevant to the problem is reviewed. This includes work which first recognized the problem, studies leading to the present work, and recent work on the problem. A problem statement summarizing the present work is presented in Chapter 3. The analytical methodology, including the shear lag model and the formulation of the energy expressions, is developed in Chapter 4. Chapter 5 describes the thermal and mechanical tests which were used to verify the analysis. The experimental results and correlation with predicted values are discussed in Chapter 6. This chapter also includes results of the data fits, parametric studies, and discussion of strengths and weaknesses of the model. Finally, conclusions and recommendations for future work are presented in Chapter 7.

CHAPTER 2

PREVIOUS WORK

Microcracking has long been recognized as an important damage mechanism in composite laminates. Early studies identified the problem and described it qualitatively, but most of these concentrated on the effects of microcracking rather than on its formation. Later studies developed predictive methodologies for both monotonic and cyclic mechanical loading. Recently work has been reported on the quantitative prediction of microcracking under thermal loading. The vast majority of studies to date have concentrated on the specific problem of cross-ply laminates under mechanical loading, a small subset of the current problem. No completed analytical methodology has demonstrated the ability to quantitatively predict microcracking under both thermal and mechanical loading in general angle laminates.

2.1 EARLY MICROCRACKING STUDIES

One of the first works to examine the implications of microcracking on dimensional stability in the space environment was that of Camahort, Rennhack, and Coons [3]. As with most of the early studies, their work was essentially phenomenological in nature. Near-zero-CTE composite specimens of five different materials were thermally cycled and then measured for CTE. Other specimens were exposed to progressive mechanical loading to evaluate residual strain as a function of applied stress. Their work confirmed that

26

near-zero-CTE laminates are indeed sensitive to thermal environments. They also showed that microcrack formation is highly dependent upon the material system.

Garrett and Bailey [4] studied transverse microcracking in cross-ply laminates under mechanical loading. They used a one-dimensional shear lag model to calculate the stress transferred from the cracked transverse plies to the uncracked longitudinal plies. Expressions for the degraded laminate properties as functions of the applied load and uncracked properties were derived. The theoretical effective moduli just before failure correlated well with experimental results. This work played a key role in characterizing the microcracking problem and emphasized the need for predictive methodologies.

2.2 PREDICTIVE METHODOLOGIES

A number of analytical approaches exist to quantitatively predict microcracking in composite laminates. All of the various methods first require knowledge of the stress distribution. This is typically determined analytically from one of the following: shear lag analysis, the self-consistent method, variational approaches, continuum mechanics, or classical laminated plate theory. The stress state can also be found numerically through finite element analyses.

Next, after the stress distribution is determined, a cracking criterion is introduced to predict whether new cracks will form. Failure criteria generally follow either the strength of materials approach or the fracture mechanics approach. Using a strength of materials criterion, the derived stress state is compared with material strengths, such as the transverse

27

failure strength of a unidirectional ply. A fracture mechanics cracking criterion, on the other hand, is based upon energy methods. From the stress distribution model, the amount of energy dissipated when a hypothetical new crack forms may be determined. If this calculated energy is greater than the critical strain energy release rate, a material property, the criterion for new crack appearance is satisfied.

Variations of the two main approaches are also used. Statistical methods may be incorporated into both. In the fracture mechanics approach, the location of a new crack may be assigned a probabilistic distribution or determined from a Monte Carlo simulation. With the strength based approach, a probabilistic distribution of the failure strength may be assumed.

Studies have also considered the problem on different scales. For example, some studies examine microcrack formation on the microstructural level, considering the fiber, matrix, and fiber-matrix properties individually. However, transverse microcracking analyses generally focus on the ply level, at which the fiber, matrix, and interface are considered homogenized.

2.2.1 Mechanical Loading Analyses

In the simplest example of a strength based analytical model, the stress state is calculated with CLPT, and the criterion for crack initiation is the transverse strength of a single lamina [5-8]. This approach relies on the assumption that *in situ* ply strength is a material property. The validity of this method was called into question by Flaggs and Kural [9], who showed that *in situ* lamina transverse strength is instead a laminate property, dependent upon laminate geometry, stacking sequence, and ply thickness.

The strength criterion has also been used by Parvizi and Bailey, along with a shear lag solution of the stress state [10]. Lee and Daniel combined this failure criterion with a "modified" shear lag model, which assumed a

28

more complex through-thickness displacement profile [11, 12]. Allen *et al.* determined the stress fields in a cracked laminate using the internal state variable concept, a continuum damage mechanics approach [5, 13]. In their method the damage, transverse microcracking in this case, was represented by a second order tensor. Calculated stresses were compared with transverse ply strength. While qualitatively useful, these approaches are still limited by the laminate dependence of the *in situ* transverse ply strength.

Peters *et al.* [14-17] used a shear lag stress solution combined with a two-parameter Weibull strength distribution as the cracking criterion. Jen and Sun [18] incorporated a similar strength distribution with a finite element stress solution. The strength and shape parameters of the Weibull distribution are determined experimentally from a single specimen. These analyses have limited application in general cases, as the Weibull parameters are related to the *in situ* transverse ply strength and are thus laminate dependent. The works are useful parametric studies, however, since the effects of laminate geometry, stacking sequence, and ply thickness on the Weibull parameters help to better characterize the transverse microcracking problem.

Many researchers have used a fracture mechanics failure criterion with a shear lag stress solution to predict transverse microcracking in cross-ply laminates [19-26]. Some, such as that of Caslini *et al.*, predict only the onset of microcracking [19]. Laws and Dvorak, in contrast, proposed a progressive damage model which determines both the onset and accumulation of cracks. It also incorporates a probabilistic distribution for the site of the next crack [24].

Hashin pioneered the variational approach to determine the thermoelastic properties of a cracked laminate [27]. In this method the

29

complementary energy is minimized to derive the stress and strain fields. Though his analysis cannot predict the onset or accumulation of microcracking, Nairn [28, 29] and Varna and Berglund [30] later combined his stress analysis technique with a fracture mechanics failure criterion to predict microcracking in cross-ply laminates.

Other energy based approaches include studies by Wang and Crossman [31] and Binienda et al. [32], who calculated stress distributions with finite element models. Nuismer and Tan developed a two-dimensional elasticity model for their analysis [33]. Laws and Dvorak [34, 35] proposed a self-consistent model in which the cracking layer is replaced by an effective homogeneous medium containing many aligned slit cracks. Wang et al. [36] used the concept of effective flaw distributions in conjunction with a Monte Carlo simulation. The size and spacing of the microflaws are determined by probability distributions. A new crack is assumed to form at the most significant microflaw. As a result, this method is often called the "weakest link" approach.

In general, the applicability of predictive methodologies for mechanical loading is confined to monotonic loading of cross-ply laminates. Only a few analyses have been derived for general angle-ply laminates. Gudmundson et al. used a variational approach to determine the stress fields and thermoelastic properties of a cracked laminate [37]. Flaggs used a shear lag stress analysis with a mixed mode fracture mechanics failure criterion to predict microcracking initiation [20]. These analyses, however, have not demonstrated the ability to predict microcrack accumulation as a function of a progressively applied load.

2.2.2 Thermal Loading Analyses

Very few predictive methodologies exist for thermal loading. A number of the mechanical loading analyses incorporate a residual thermal stress due to manufacture [5, 11, 13, 15, 16, 23, 24, 26-29, 31, 32, 34-38]. None of them have demonstrated predictive capabilities for progressive thermal loading. The residual stress is generally treated as a constant.

Thermal loading analyses have generally focused on issues other than prediction of cracking, such as microcracking effects. Bowles [39] and Adams and Herakovich [40] used finite element stress analyses to determine the effects of microcracking on longitudinal CTE. Bowles also proposed a technique to use finite element analysis in conjunction with CLPT to determine all of the thermoelastic properties, though no experimental verification was presented [39]. Tompkins *et al.* [41-44] and Camahort *et al.* [3] conducted experimental studies in which the effects of thermal cycling on laminate properties and microcrack density were measured. Manders and Maas [45] tested thin plies and Bowles and Shen [46] thin fabric to determine whether microcracking would be suppressed. Experimental testing by Knouff showed that the accumulation of microcracks under thermal cycling is dependent upon fiber type [47].

Some studies have tried to quantitatively predict microcracking under thermal loads. Bowles *et al.* [46, 48] and Adams *et al.* [49] used CLPT stress solutions with *in situ* transverse strengths to predict cracking initiation. A similar approach was taken by Peters and Andersen [38], though with Weibull distributions of the failure strengths. Chamis *et al.* developed a finite element model which calculates nodal stress resultants in complex structures under thermal loading. A combined stress failure criterion is used to simulate damage progression [50]. Herakovich and Hyer predicted

31

initiation temperature with CLPT and microcrack accumulation with finite elements in cross-ply laminates subjected to thermal loading; both stress analyses use an *in situ* ply strength failure criterion [51]. These approaches, besides having limited application to microcrack accumulation under progressive loading, suffer from the problems associated with strength based failure criteria.

A few analyses have focused on damage at the microstructural level [48, 52-55]. Their objective is to determine the effects of constituent properties, interface strengths, and other micromechanical parameters on the development of microflaws. Using finite elements, Bowles and Griffin [53, 54] modelled the thermally induced stresses associated with continuous fibers embedded in a matrix. The location and initiation temperature of fiber debonding is predicted by comparing the radial stress at the fiber-matrix interface with the radial tensile strength of the interface.

2.3 RECENT WORK

McManus *et al.* [56] developed a predictive methodology for cross-ply laminates under thermal loading. They used a shear lag stress solution with an energy based failure criterion. Crack density in one 90° ply group and knocked-down laminate properties were derived as functions of progressively decreasing temperature. An iterative degradation model included the effects of thermal cycling. A computer code was written to implement the analysis, giving crack density and reduced laminate properties as functions of progressive temperature change or number of thermal cycles.

They also collected experimental data to correlate with the analytical predictions. Cross-ply specimens were progressively cooled and thermally

cycled in an environmental chamber. Microcracks were counted on the edges of the specimens using optical microscopy.

The analysis correlated well with both the progressive cooling and thermal cycling data. One significant finding was that, in thermal cycling, the thinnest ply groups cracked much earlier and more extensively than predicted. This result is contrary to recent trends to suppress microcracking by using thinner plies. However, cracking in thin plies generally has little effect on the effective laminate properties.

This work was extended by Park [57] to predict transverse microcracking in all plies of a general angle-ply laminate. The incremental damage model was also modified to include the effects of temperature-dependent material properties. The existing computer code was changed extensively to incorporate the new approach. Crack densities were measured experimentally in a variety of laminates exposed to progressive thermal loading. Cracks were counted at the specimen edges using optical microscopy, and in the interiors using x-ray inspection and by incrementally sanding down the edges.

Edge crack counts in thin plies did not correlate well with the analytical predictions. The agreement between theoretical crack densities and interior crack counts, though, was significantly better. The poor correlation of the edge crack counts was attributed to two effects. First, observations from the interior data showed that cracks in the thin ply groups were discontinuous, but the model assumes that transverse cracks form edge-to-edge. Second, a free-edge stress analysis showed that the stresses are lower in this region. Thus fewer microcracks will form at the free edge than in the interior. As a result, edge crack counts are probably not a good indication of the damage state within the laminate.

33

An important finding of the work was that correlation between analysis and the average of the interior crack measurements was very good, even though scatter was high. Thus the analysis appears to be a useful tool for predicting mean crack densities under thermal loading, even for thin plies.

2.4 SHEAR LAG AND FRACTURE MECHANICS PARAMETERS

Two parameters are necessary when a shear lag stress solution is used in conjunction with an energy based cracking criterion to predict microcracking. The first is the critical strain energy release rate, G_{Ic}, a measure of fracture toughness. This parameter is physically meaningful but currently impossible to measure directly for microcracking. Many studies instead use the interlaminar fracture toughness, which can be measured using a double cantilever beam test. However, this property characterizes delamination formation and growth, which is an entirely separate problem from microcracking, or intralaminar fracture. Moreover, both the accuracy and precision of current measuring techniques are questionable. Figure 2.1 shows the broad range of G_{Ic} values that were measured during round-robin testing in one study [58].

The second is a non-dimensional shear lag parameter, referred to as ζ in the present study. Note that a standardized notation does not exist for this parameter. Furthermore, comparison of values from different studies must be done carefully. For example, some analyses use a shear lag parameter with dimensions of length. This semi-empirical aspect of the shear lag model is both a material property and a geometric factor. Like G_{Ic}, this parameter is impossible to measure directly. Some have assumed the shear lag parameter to be laminate dependent. Laws and Dvorak [24], for
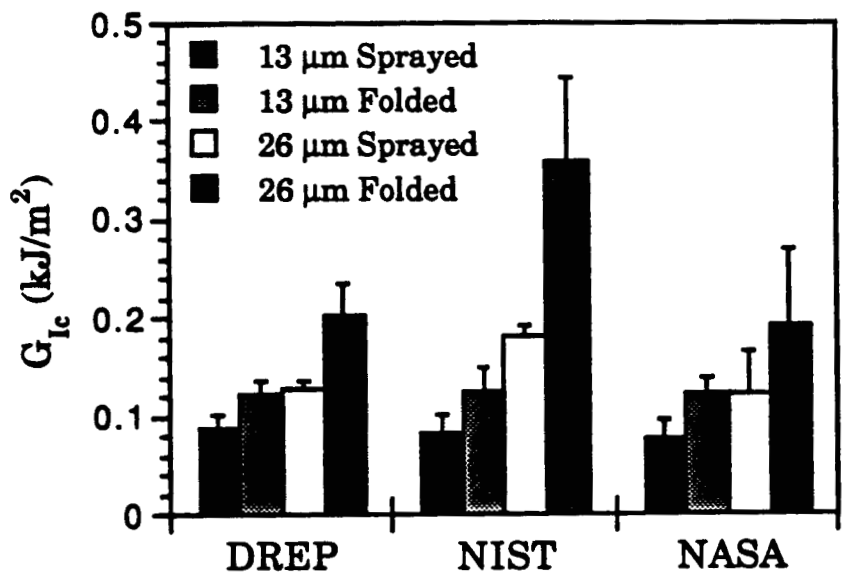
Figure 2.1   After [58].   Results of round robin G_{Ic} testing in three different
laboratories using four different test techniques.

example, back-calculated ζ from first-ply-failure and interlaminar fracture toughness data. Runkle [59] used a similar approach and attributed the laminate dependence of ζ to local delamination. Lee and Daniel [12] and Ogin *et al.* [60] derived closed-form solutions for ζ based upon kinematic assumptions. Others have determined ζ empirically, assuming its value to be fixed for a given fiber type and independent of laminate geometry [15, 16, 56, 57, 61, 62].

CHAPTER 3

APPROACH

3.1 PROBLEM STATEMENT

The objective of the present investigation is to develop an analytical methodology to predict microcracking in composite laminates under both thermal and mechanical loading. The motivation for the present work is provided by the lack of understanding in the area of microcrack formation as identified in Chapter 2. Analytical modeling in conjunction with experimental investigation is used to achieve this research objective.

The problems addressed by the analysis are threefold: (i) to provide a design capability such that given material properties, laminate geometry, and thermomechanical load history, the analysis will predict crack densities and degraded laminate properties; (ii) to aid in identifying key parameters in the microcracking problem as well as the sensitivity to these parameters; and (iii) to provide insight to the physical mechanisms involved in crack formation.

The purposes of the experimental investigation are (i) to provide input parameters for the analysis; (ii) to provide verification of the analysis; and (iii) to allow a greater qualitative understanding of the problem, including the effects of width, layer thickness, and laminate geometry.

3.2 ANALYTICAL APPROACH

The analysis is a fracture mechanics approach which uses a shear lag derivation of the stress and displacement fields. All plies in a general composite laminate are analyzed under progressive thermal and mechanical loading. Each ply is analyzed individually with the properties of the other layers smeared. The damage is modeled incrementally, allowing the inclusion of existing cracks in other layers and temperature dependent material properties.

A transverse microcrack is assumed to form parallel to the fibers in a respective layer and to extend completely through both the layer thickness and the laminate width. The analysis assumes that a crack appears instantaneously when the conditions for crack formation are met. A new crack forms when the energy released due to crack formation is greater than the energy required to form a new crack surface, the critical strain energy release rate G_{Ic}. The crack formation process is illustrated in Figure 3.1.

The analytical methodology is implemented by a computer code. A parametric study is used to determine the sensitivity of the analysis to the various input parameters. Full derivation of the analysis is presented in Chapter 4.

3.3 EXPERIMENTAL APPROACH

All laminates are fabricated at MIT Technology Laboratory for Advanced Composites (TELAC). AS4/3501-6 graphite/epoxy is chosen as the material system to build on the data base established by the laboratory. Three different layups are manufactured to identify the effects of laminate geometry and ply thickness.

45°
90°
45°

(a)

New Crack

45°
90°
45°

(b)
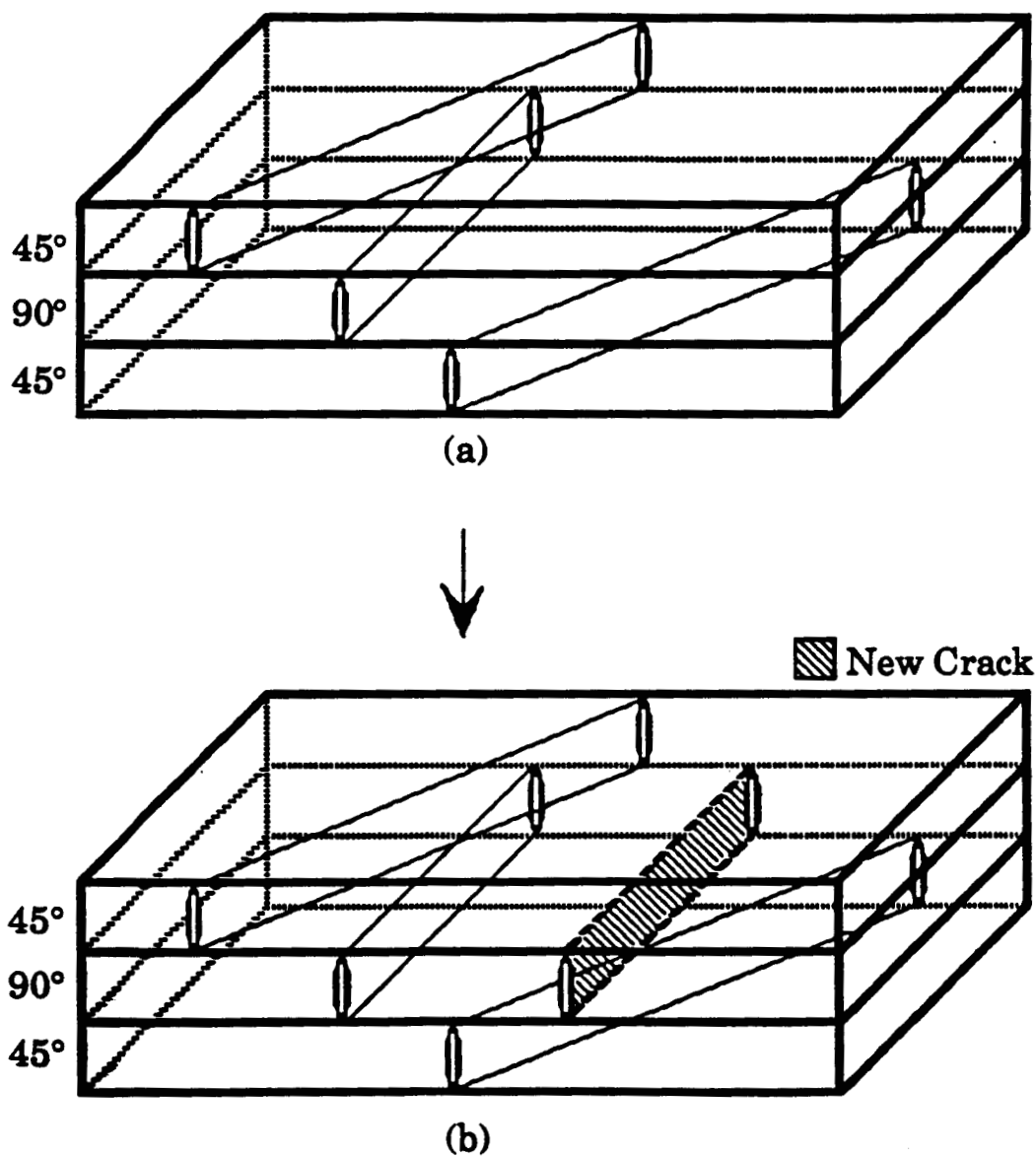
Figure 3.1   (a) Laminate containing transverse microcracks. Cracks run completely from edge to edge and through thickness. (b) Cracks assumed to appear instantaneously when conditions for new crack formation are met. (From Park, [57]).

39

Two different sizes of thermal specimens are chosen to investigate width effects. The mechanical specimens are the same width as the wider thermal specimens. Prior to testing, both long edges of every specimen are polished to minimize crack initiation sites and to facilitate microscopic inspection. Thermal specimens are progressively cooled from room temperature to -184°C in a thermal environment chamber. After cooling to each of five target temperatures, cracks are counted using optical microscopy. Some thermal specimens are used for edge crack data. Others are sacrificed to collect interior data by sanding down the edges. The mechanical specimens are loaded under monotonic tension. Edge crack data is collected at progressively higher loads until failure.

A fit of the data provides shear lag and fracture toughness parameters for the analysis. Analytical predictions are subsequently correlated with test results to validate the model and provide insight into the mechanics of the problem.

CHAPTER 4

ANALYTICAL METHODS

In this chapter the derivation of the analysis and its implementation are presented. The analysis uses a shear lag solution of the stress and displacement fields and an energy based cracking criterion. All plies in a general composite laminate are analyzed under progressive thermal and mechanical loading. Also described is a data fit procedure used to obtain key parameters for the analysis from experimental data.

4.1 DERIVATION

4.1.1 Shear Lag Stress Solution

Figure 4.1 shows a laminate aligned with a global coordinate system xyz. The laminate is made up of unidirectional plies. Stacked plies with the same ply angle are assumed to act as a single thick ply, referred to as a ply group or layer. Cracks are assumed to span the ply group thickness and propagate parallel to the fibers through the width of the composite laminate. Figure 4.1 shows cracks of this type in a laminate with three ply groups. A local coordinate system $x'y'z'$ is defined for each crack. The y' axis is aligned with the crack, parallel to the fiber direction of the ply group, the x' axis is aligned with the transverse direction of the ply group, and the origin is at the center of the crack.

To predict cracking in any one ply group, the laminate is modeled as being made up of two components: the cracking ply group and the rest of the

41
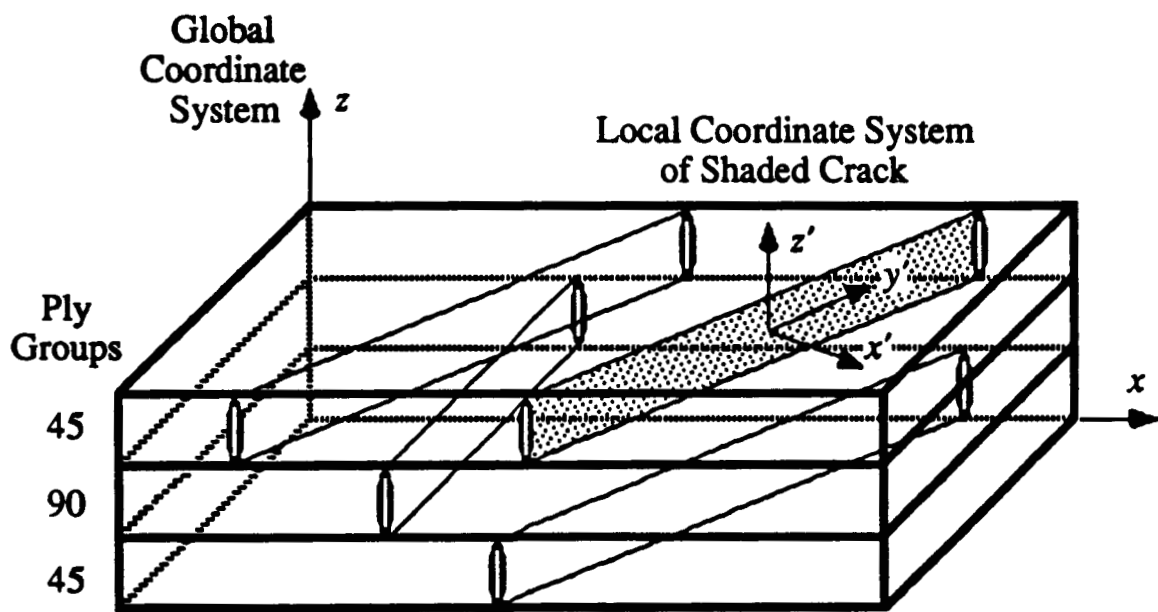
Figure 4.1 Global and local coordinate systems and assumed microcrack geometry.

laminate, which is smeared. A one-dimensional shear lag model with unit depth, shown in Figure 4.2, is used to determine the stress and displacement distributions in the vicinity of a crack in the local $x'y'z'$ coordinate system. The model assumes uniform through-thickness displacement and normal stresses in every layer. Shear stress exists only in a shear transfer region of thickness a_q between layers and is uniform through-thickness within that region.

In the shear lag solution that follows, $E, \alpha, u,$ and σ are the stiffness, CTE, displacement, and normal stress, respectively, in the x' direction. The subscripts $c, r,$ and o indicate the cracking layer, the rest of the laminate, and the entire laminate, respectively. The shear stress between uncracked and cracked layers in the $x'y'$ plane is q. The thicknesses of the cracking layer and the rest of the laminate are a_c and a_r, respectively, and a_o is the total laminate thickness.

The laminate is subjected to a thermal load, ΔT, which is the difference between the current temperature and some stress-free temperature, and an applied stress, σ_a, where

$$\sigma_a = \frac{N_{x'}}{a_o} \tag{4.1}$$

and $N_{x'}$ is the laminate load in the x' direction. $N_{x'}$ is determined by transforming $\mathbf{N}$, the laminate load vector in the global coordinate system used in CLPT [63], to the local coordinate system of the cracking layer. From equilibrium of the laminate,

$$\sigma_a a_o = \sigma_r a_r + \sigma_c a_c \tag{4.2}$$

From equilibrium of the cracked layer,
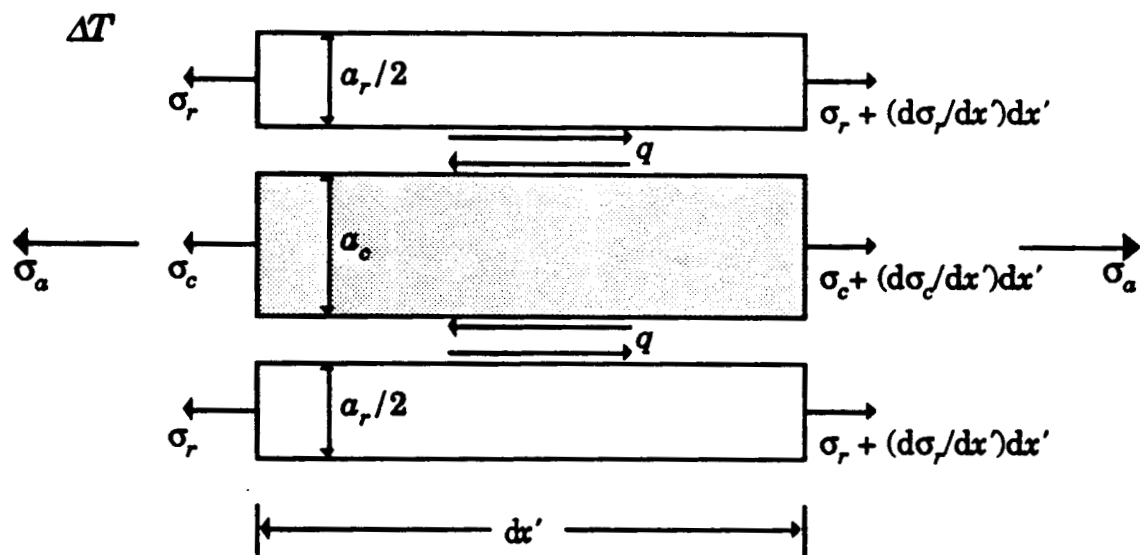
Figure 4.2   Shear lag model used to derive stress and displacement distributions.

$$q = \frac{a_c}{2}\frac{d\sigma_c}{dx'} \qquad (4.3)$$

and of the rest of the laminate,

$$q = -\frac{a_r}{2}\frac{d\sigma_r}{dx'} \qquad (4.4)$$

The stress-strain relations for the cracked layer and the rest of the laminate, respectively, are

$$\frac{\sigma_c}{E_c} = \frac{du_c}{dx'} - \alpha_c \Delta T \qquad (4.5)$$

and

$$\frac{\sigma_r}{E_r} = \frac{du_r}{dx'} - \alpha_r \Delta T \qquad (4.6)$$

Let

$$q = K(u_c - u_r) \qquad (4.7)$$

where K is a stiffness constant relating the displacements of the two layers to the shear stress between them. It can be determined from

$$K = \frac{G^{eff}}{a_q} \qquad (4.8)$$

where G^{eff} is the effective shear modulus of the shear transfer region. Placing Eq. (4.7) into Eqs. (4.3) and (4.4) and taking the derivative of both gives

$$K\left(\frac{du_c}{dx'} - \frac{du_r}{dx'}\right) = \frac{a_c}{2}\frac{d^2\sigma_c}{(dx')^2} \qquad (4.9)$$

and

$$K\left(\frac{du_c}{dx'} - \frac{du_r}{dx'}\right) = -\frac{a_r}{2}\frac{d^2\sigma_r}{(dx')^2} \qquad (4.10)$$

Subtracting Eq. (4.6) from Eq. (4.5), multiplying by K, and substituting into Eq. (4.9),

$$\frac{d^2\sigma_c}{(dx')^2} = \frac{2K}{a_c}\left[\frac{\sigma_c}{E_c} - \frac{\sigma_r}{E_r} + (\alpha_c - \alpha_r)\Delta T\right] \tag{4.11}$$

Solving Eq. (4.2) for σ_r, substituting into Eq. (4.11), and rearranging,

$$\frac{d^2\sigma_c}{(dx')^2} - 2K\left(\frac{a_rE_r + a_cE_c}{a_ra_cE_rE_c}\right)\sigma_c = \frac{2K}{a_c}\left[-\frac{\sigma_o a_o}{a_rE_r} + (\alpha_c - \alpha_r)\Delta T\right] \tag{4.12}$$

Let the shear lag parameter ζ be expressed as

$$\zeta = \sqrt{\frac{Ka_ca_oE_o}{2a_rE_rE_c}} \tag{4.13}$$

Also let

$$\lambda = \frac{2K}{a_c}\left[\frac{a_o\sigma_o}{a_rE_r} - (\alpha_c - \alpha_r)\Delta T\right] \tag{4.14}$$

It will be convenient to express this parameter as

$$\lambda = \frac{4\zeta^2}{a_c^2}\sigma_{c_\infty} \tag{4.15}$$

where σ_{c_∞}, the far-field stress in the cracking layer, is

$$\sigma_{c_\infty} = \left[\frac{E_c}{E_o}\sigma_a + E_c(\alpha_o - \alpha_c)\Delta T\right] \tag{4.16}$$

From the rule of mixtures,

$$a_oE_o = a_rE_r + a_cE_c \tag{4.17}$$

Substituting Eqs. (4.13), (4.14), and (4.17) into Eq. (4.12) gives

$$\frac{d^2\sigma_c}{(dx')^2} - \frac{4\zeta^2}{a_c^2}\sigma_c = -\lambda \tag{4.18}$$

This has a solution of the form:

$$\sigma_c = A\sinh\left(\frac{2\zeta x'}{a_c}\right) + B\cosh\left(\frac{2\zeta x'}{a_c}\right) + \frac{\lambda a_c^2}{4\zeta^2} \qquad (4.19)$$

Applying boundary conditions $\sigma_c = 0$ at $x' = \pm h$ gives

$$A = 0 \qquad B = \frac{-\lambda a_c^2}{4\zeta^2 \cosh(2\zeta h/a_c)} \qquad (4.20)$$

Placing Eqs. (4.20) into Eq. (4.19), substituting Eq. (4.15) into the result, and rearranging,

$$\sigma_c = \left[1 - \frac{\cosh(2\zeta x'/a_c)}{\cosh(2\zeta h/a_c)}\right]\sigma_{c\infty} \qquad (4.21)$$

It can be seen by examination of Eq. (4.21) that the shear lag parameter, ζ, scales the distance from the crack face over which the stress rises towards its far-field value. Solving Eq. (4.2) for σ_r, substituting into Eq. (4.21), and rearranging gives

$$\sigma_r = \frac{\sigma_o a_o}{a_r} - \frac{a_c}{a_r}\left[1 - \frac{\cosh(2\zeta x'/a_c)}{\cosh(2\zeta h/a_c)}\right]\sigma_{c\infty} \qquad (4.22)$$

Substituting Eq. (4.16) into the equation formed by placing Eq. (4.21) into Eq. (4.5), solving for du_c, and integrating from 0 to x',

$$\begin{aligned}
u_c &= \frac{a_r E_r x'}{a_o E_o}\left[\frac{a_o \sigma_o}{a_r E_r} + \alpha_r \Delta T\right]\left[1 - \frac{a_c}{2\zeta x'}\frac{\sinh(2\zeta x'/a_c)}{\cosh(2\zeta h/a_c)}\right] \\
&\quad + \alpha_c \Delta T x'\left[1 - \frac{a_r E_r}{a_o E_o}\left(1 - \frac{a_c}{2\zeta x'}\frac{\sinh(2\zeta x'/a_c)}{\cosh(2\zeta h/a_c)}\right)\right]
\end{aligned} \qquad (4.23)$$

Substituting Eq. (4.22) into Eq. (4.6), solving for du_r and integrating from 0 to x',

$$\begin{aligned}
u_r &= \frac{\sigma_o x'}{a_r E_r E_o}\left[a_o E_o - a_c E_c\left(1 - \frac{a_c}{2\zeta x'}\frac{\sinh(2\zeta x'/a_c)}{\cosh(2\zeta h/a_c)}\right)\right] \\
&\quad + \frac{\Delta T x'}{a_o E_o}\left[a_o E_o \alpha_r + a_c E_c(\alpha_c - \alpha_r)\left(1 - \frac{a_c}{2\zeta x'}\frac{\sinh(2\zeta x'/a_c)}{\cosh(2\zeta h/a_c)}\right)\right]
\end{aligned} \qquad (4.24)$$

47

The constants of integration in Eqs. (4.23) and (4.24) are set to zero to satisfy the displacement boundary conditions $u_r(0) = u_c(0) = 0$.

4.1.2 Energy Expressions

Two criteria must be met for a new crack to form. First, the crack must be energetically favorable. The strain energy release rate associated with crack growth, G, must reach a critical value G_{Ic}, viz

$$G \geq G_{Ic} \qquad (4.25)$$

where

$$G = \frac{1}{a_c} \frac{d}{dl} (W - U) \qquad (4.26)$$

W is the work done by an external load, U is the strain energy stored by the body, l is the crack length, and a_c is the thickness of the cracking body [64]. G_{Ic} is the Mode I critical strain energy release rate, a material property, also referred to as the fracture toughness. Only the Mode I fracture toughness is considered. The x'-direction stresses calculated in the one-dimensional shear lag model are Mode I opening stresses. A similar model could be used to calculate the Mode II $x'y'$ shear stresses. However, Mode II fracture is considered a secondary effect in the present investigation and is thus not included in the analysis. The Mode II fracture toughness, G_{IIc} is generally significantly greater than G_{Ic}, and the $x'y'$ shear stresses are generally lower in magnitude than the Mode I opening stresses, especially under thermal loading.

The second criterion for crack formation is that it must be mechanistically possible. The strain energy release rate in Eq. (4.26) is a function of crack length. Due to the constraint of adjacent plies, G is independent of crack length after a critical crack size l_c is reached [57], as

48

shown in Figure 4.3. Thus the strain energy release rate may be calculated from the total change in energy between uncracked and cracked states in a Griffith energy balance [64]:

$$G = \frac{\Delta W - \Delta U}{a_c} \qquad (4.27)$$

where G is the strain energy release rate and has units of energy per unit area. ΔW and ΔU are the changes in external work and internal strain energy, respectively, from the state of Figure 3.1a to that of Figure 3.1b. Equation (4.27) is derived for the case of unit depth, which is implied in the derivation of all energy expressions herein. If the cracking layer is assumed to contain initial starter cracks of length l_c [64], then Eq. (4.27) may be substituted into Eq. (4.25) to get

$$\frac{\Delta W - \Delta U}{a_c} \geq G_{Ic} \qquad (4.28)$$

which is the condition for the appearance of a new crack.

The change in internal strain energy has contributions from both the normal and shear stresses. The strain energy from normal stresses, U_σ, is

$$U_\sigma = \frac{1}{2} \oint_v \frac{\sigma^2}{E} dV \qquad (4.29)$$

The cracks are initially separated by a distance $2h$. This is shown in the volume element in Figure 4.4. The element is aligned with the local $x'y'z'$ coordinate system of the cracking layer and has unit depth. It will be used in the derivation of all energy expressions presented here. A hypothetical new crack is assumed to form midway between the existing cracks, such that the crack spacing becomes h. The change in U_σ when a new crack appears is

49
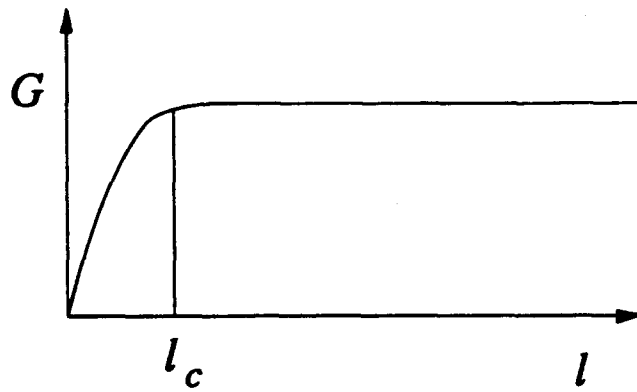
Figure 4.3   Graph of the strain energy as a function of crack length [57].
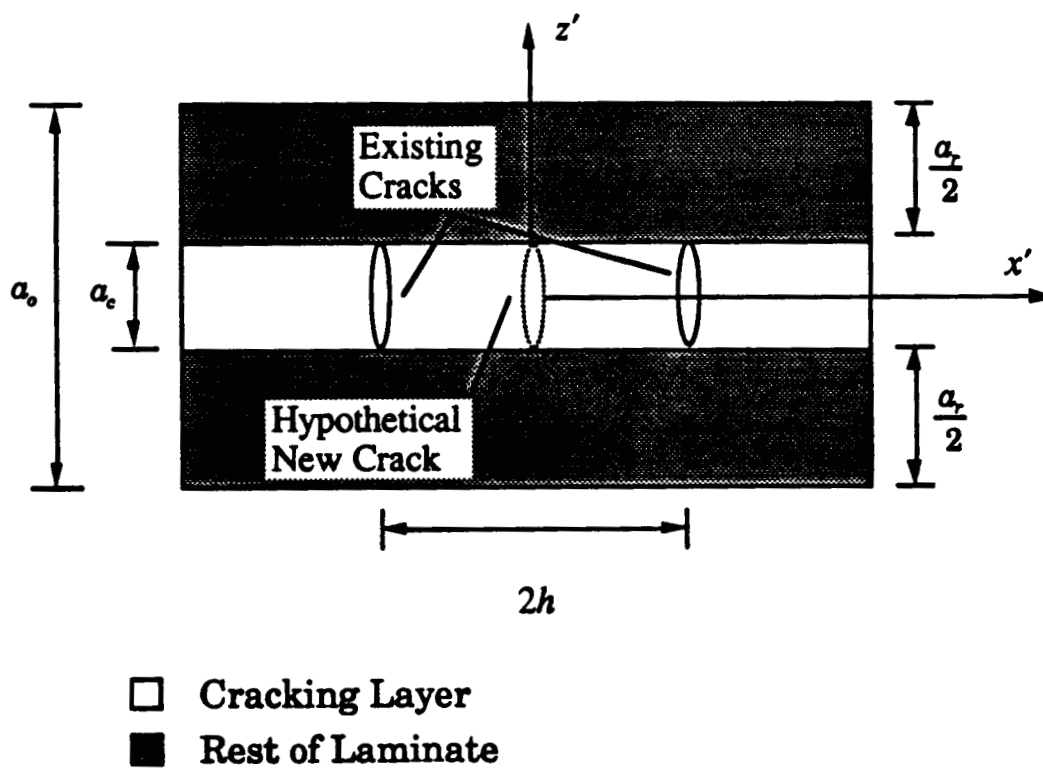
Figure 4.4 Volume element used in energy calculations, showing existing crack spacing $2h$. Hypothetical new crack forms midway between existing cracks, reducing crack spacing to h.

51

$$\Delta U_\sigma = \left[2U_\sigma \big|_h - U_\sigma \big|_{2h} \right] \tag{4.30}$$

$2U_\sigma \big|_h$ is the strain energy due to normal stresses of the volume element with cracks separated by a distance h. $U_\sigma \big|_{2h}$ is the strain energy with cracks separated by $2h$ and can be found from

$$U_\sigma \big|_{2h} = 2 \left[\underbrace{\frac{1}{2} a_r \int_0^h \frac{\sigma_r^2}{E_r} dx'}_{\text{I}} + \underbrace{\frac{1}{2} a_c \int_0^h \frac{\sigma_c^2}{E_c} dx'}_{\text{II}} \right] \tag{4.31}$$

Note that due to symmetry, we can integrate from 0 to h and multiply the result by two, rather than integrating from $-h$ to h. Substituting Eq. (4.22) into I, using the trigonometric relation $\cosh^2 x = \frac{1}{2}(\cosh 2x + 1)$, and integrating,

$$\frac{1}{2} a_r \int_0^h \frac{\sigma_r^2}{E_r} dx' = \frac{a_0^2 h}{2 a_r E_r} \sigma_a^2$$

$$+ \frac{a_c^2}{2 a_r E_r} \left[h - \frac{a_c}{\zeta} \tanh\left(\frac{2\zeta h}{a_c}\right) + \frac{\frac{a_c}{8\zeta} \sinh\left(\frac{4\zeta h}{a_c}\right) + \frac{h}{2}}{\cosh^2\left(\frac{2\zeta h}{a_c}\right)} \right] \sigma_{c\infty}^2 \tag{4.32}$$

$$- \frac{a_c a_0}{a_r E_r} \left[h - \frac{a_c}{2\zeta} \tanh\left(\frac{2\zeta h}{a_c}\right) \right] \sigma_a \sigma_{c\infty}$$

Substituting Eq. (4.21) into II, using the trigonometric relation $\cosh^2 x = \frac{1}{2}(\cosh 2x + 1)$, and integrating,

$$\frac{1}{2} a_c \int_0^h \frac{\sigma_c^2}{E_c} dx' = \frac{a_c}{2 E_c} \left[h - \frac{a_c}{\zeta} \tanh\left(\frac{2\zeta h}{a_c}\right) + \frac{\frac{a_c}{8\zeta} \sinh\left(\frac{4\zeta h}{a_c}\right) + \frac{h}{2}}{\cosh^2\left(\frac{2\zeta h}{a_c}\right)} \right] \sigma_{c\infty}^2 \tag{4.33}$$

Placing Eqs. (4.32) and (4.33) into Eq. (4.31),

$$U_\sigma\big|_{2h} = \frac{\sigma_a^2 a_0^2 h}{a_r E_r}$$

$$+ \frac{a_c a_0 E_0}{a_r E_c E_r}\left[h - \frac{a_c}{\zeta}\tanh\left(\frac{2\zeta h}{a_c}\right) + \frac{\frac{a_c}{8\zeta}\sinh\left(\frac{4\zeta h}{a_c}\right) + \frac{h}{2}}{\cosh^2\left(\frac{2\zeta h}{a_c}\right)} \right]\sigma_{c\infty}^2 \qquad (4.34)$$

$$- \frac{2a_c a_0}{a_r E_r}\left[h - \frac{a_c}{2\zeta}\tanh\left(\frac{2\zeta h}{a_c}\right)\right]\sigma_a \sigma_{c\infty}$$

The strain energy due to normal stresses in the volume element after a new crack forms and the cracks separated by a distance h is

$$U_\sigma\big|_h = 2\left[\frac{1}{2}a_r \int_0^{h/2}\frac{\sigma_r^{*2}}{E_r}dx' + \frac{1}{2}a_c \int_0^{h/2}\frac{\sigma_c^{*2}}{E_c}dx'\right] \qquad (4.35)$$

Due to symmetry, we integrate from 0 to $h/2$ and multiply the result by two. Also, in Eq. (4.35), σ_c^* and σ_r^* are the normal stresses in the cracking layer and the rest of the laminate, respectively, derived with the boundary conditions $\sigma_c^* = 0$ at $x' = \pm h/2$. Then, by analogy with $U_\sigma\big|_{2h}$,

$$U_\sigma\big|_h = \frac{\sigma_a^2 a_0^2 h}{2a_r E_r}$$

$$+ \frac{a_c a_0 E_0}{a_r E_c E_r}\left[\frac{h}{2} - \frac{a_c}{\zeta}\tanh\left(\frac{\zeta h}{a_c}\right) + \frac{\frac{a_c}{8\zeta}\sinh\left(\frac{2\zeta h}{a_c}\right) + \frac{h}{4}}{\cosh^2\left(\frac{\zeta h}{a_c}\right)} \right]\sigma_{c\infty}^2 \qquad (4.36)$$

$$- \frac{2a_c a_0}{a_r E_r}\left[\frac{h}{2} - \frac{a_c}{2\zeta}\tanh\left(\frac{\zeta h}{a_c}\right)\right]\sigma_a \sigma_{c\infty}$$

Substituting Eqs. (4.36) and (4.34) into Eq. (4.30) and using the relation $\sinh 2x = 2\sinh x \cosh x$,

53

$$\Delta U_\sigma = \frac{a_c^2 a_o E_o}{2\zeta a_r E_r E_c}$$

$$\left[\frac{3}{2}\tanh\left(\frac{2\zeta h}{a_c}\right) - 3\tanh\left(\frac{\zeta h}{a_c}\right) - \frac{\zeta h}{a_c}\left(\text{sech}^2\left(\frac{2\zeta h}{a_c}\right) - \text{sech}^2\left(\frac{\zeta h}{a_c}\right)\right)\right]\sigma_{c\infty}^2 \quad (4.37)$$

$$+\frac{a_c^2 a_o}{\zeta a_r E_r}\left[2\tanh\left(\frac{\zeta h}{a_c}\right) - \tanh\left(\frac{2\zeta h}{a_c}\right)\right]\sigma_a \sigma_{c\infty}$$

Substituting Eq. (4.16) into Eq. (4.37), expanding the loading terms, and factoring,

$$\Delta U_\sigma = \frac{a_0 a_c^2 E_c \sigma_a^2}{2\zeta a_r E_r E_0}\left[\tanh\left(\frac{\zeta h}{a_c}\right) - \frac{1}{2}\tanh\left(\frac{2\zeta h}{a_c}\right) + \frac{\zeta h}{a_c}\left(\text{sech}^2\left(\frac{\zeta h}{a_c}\right) - \text{sech}^2\left(\frac{2\zeta h}{a_c}\right)\right)\right]$$

$$+\frac{a_r a_c^2 E_r E_c (\alpha_c - \alpha_r)^2 \Delta T^2}{2\zeta E_0 a_0}\left[\frac{3}{2}\tanh\left(\frac{2\zeta h}{a_c}\right) - 3\tanh\left(\frac{\zeta h}{a_c}\right) + \frac{\zeta h}{a_c}\left(\text{sech}^2\left(\frac{\zeta h}{a_c}\right) - \text{sech}^2\left(\frac{2\zeta h}{a_c}\right)\right)\right] \quad (4.38)$$

$$+\frac{a_c^2 E_c (\alpha_c - \alpha_r)\sigma_a \Delta T}{2\zeta E_0}\left[2\tanh\left(\frac{\zeta h}{a_c}\right) - \tanh\left(\frac{2\zeta h}{a_c}\right) + \frac{2\zeta h}{a_c}\left(\text{sech}^2\left(\frac{\zeta h}{a_c}\right) - \text{sech}^2\left(\frac{2\zeta h}{a_c}\right)\right)\right]$$

The strain energy contribution from shear stresses, U_q, is given by

$$U_q = \frac{1}{2}\oint_v \frac{q^2}{G^{\text{eff}}}dV \quad (4.39)$$

Recall that shear stresses are assumed to exist only in the shear transfer region between layers. Thus Eq. (4.39) is integrated over the volume of this region alone, which has a total thickness of $2a_q$ since shear is transferred at both the top and bottom of the cracking layer. The change in U_q when a new crack forms is

$$\Delta U_q = \left[2U_q\big|_h - U_q\big|_{2h}\right] \quad (4.40)$$

$2U_q\big|_h$ is the strain energy due to shear stresses of the volume element with cracks separated by a distance h. $U_q\big|_{2h}$, the strain energy with cracks separated by $2h$, can be found by solving Eq. (4.8) for G^{eff} and substituting the result into Eq. (4.39), giving

$$U_q\big|_{2h} = \frac{2}{K}\int_0^h q^2 dx' \tag{4.41}$$

Due to symmetry, we can once again integrate from 0 to h and multiply the result by two, rather than integrating from $-h$ to h. Placing Eqs. (4.23) and (4.24) into Eq. (4.7) and squaring,

$$q^2 = \frac{K^2 a_o^2 E_o^2}{a_r^2 E_c^2 E_r^2}\left[\frac{\sinh^2\left(\dfrac{2\zeta x'}{a_c}\right)}{\cosh^2\left(\dfrac{2\zeta h}{a_c}\right)}\right]\sigma_{c_\infty}^2 \tag{4.42}$$

Substituting Eq. (4.42) into Eq. (4.41), integrating, and substituting Eq. (4.15) into the result,

$$U_q\big|_{2h} = \frac{K a_c^2 a_o^2 E_o^2}{4 a_r^2 E_c^2 E_r^2 \zeta^2}\left[\frac{\dfrac{a_c}{4\zeta}\sinh\left(\dfrac{4\zeta h}{a_c}\right) - h}{\cosh^2\left(\dfrac{2\zeta h}{a_c}\right)}\right]\sigma_{c_\infty}^2 \tag{4.43}$$

The strain energy due to shear stresses in the volume element when a new crack forms and with the cracks now separated by a distance h is

$$U_q\big|_{h} = \frac{2}{K}\int_0^{h/2}\left(q^*\right)^2 dx' \tag{4.44}$$

Due to symmetry, we integrate from 0 to $h/2$ and multiply the result by two. Also, in Eq. (4.35) q^* is the shear stress derived with the boundary conditions $\sigma_c^* = 0$ at $x' = \pm h/2$. Then, by analogy with $U_\sigma\big|_{2h}$,

$$U_q\big|_{h} = \frac{K a_c^2 a_o^2 E_o^2}{4 a_r^2 E_c^2 E_r^2 \zeta^2}\left[\frac{\dfrac{a_c}{4\zeta}\sinh\left(\dfrac{2\zeta h}{a_c}\right) - \dfrac{h}{2}}{\cosh^2\left(\dfrac{\zeta h}{a_c}\right)}\right]\sigma_{c_\infty}^2 \tag{4.45}$$

Solving Eq. (4.13) for K, placing the result into an equation found by substituting Eqs. (4.45) and (4.43) into Eq. (4.40), substituting Eq. (4.16), and using the relation $\sinh 2x = 2\sinh x \cosh x$,

$$\Delta U_q = \frac{a_c^2 a_r E_c E_r}{4 a_o E_o}\left[\frac{a_0 \sigma_a}{a_r E_r}-(\alpha_c - \alpha_r)\Delta T\right]^2$$
$$\left[2\tanh\left(\frac{2\zeta h}{a_c}\right)-\tanh\left(\frac{\zeta h}{a_c}\right)+\frac{2\zeta h}{a_c}\left(\text{sech}^2\left(\frac{2\zeta h}{a_c}\right)-\text{sech}^2\left(\frac{\zeta h}{a_c}\right)\right)\right] \quad (4.46)$$

The total change in strain energy when a crack appears, ΔU, is simply

$$\Delta U = \Delta U_\sigma + \Delta U_q \quad (4.47)$$

Substituting Eqs. (4.37) and (4.46) into Eq. (4.47) yields

$$\Delta U = \frac{a_c^2 a_o^2 E_c \sigma_a^2 - a_c^2 a_r^2 E_c E_r^2 (\alpha_c - \alpha_r)^2 \Delta T^2}{2\zeta a_r a_o E_r E_o}\left[2\tanh\left(\frac{\zeta h}{a_c}\right)-\tanh\left(\frac{2\zeta h}{a_c}\right)\right] \quad (4.48)$$

Note that the coupling between thermal and mechanical loading in Eqs. (4.37) and (4.46) drops out when the two are added. As a result, the total change in internal energy in Eq. (4.48) has no thermomechanical interactions, only pure thermal and pure mechanical loading contributions.

The change in external work when a crack forms, ΔW, is given by

$$\Delta W = \left[2W\big|_h - W\big|_{2h}\right] \quad (4.49)$$

where $W\big|_{2h}$ and $2W\big|_h$ are the work done by the applied loading before and after the new crack forms, respectively. The former is found from

$$W\big|_{2h} = 2a_o \sigma_a u_r(h) \quad (4.50)$$

Setting $x'=h$ in Eq. (4.24) and substituting into Eq. (4.50) gives

$$W\big|_{2h} = \frac{2\sigma_a^2 a_o^2 h}{a_r E_r}$$
$$-\left[\frac{a_c^2 a_o E_c \sigma_a^2 - a_c^2 a_r E_c E_r (\alpha_c - \alpha_r)\Delta T \sigma_a}{\zeta a_r E_r E_o}\right]\left[\frac{2\zeta h}{a_c}-\tanh\left(\frac{2\zeta h}{a_c}\right)\right]+2a_o \alpha_r \Delta T \sigma_a h \quad (4.51)$$

56

The work done by the applied loading after the new crack forms is given by

$$W\big|_{\hat{A}} = 2a_o\sigma_a u_r^* \left(\frac{h}{2}\right) \tag{4.52}$$

where $u_r^* \left(\frac{h}{2}\right)$ is found from Eq. (4.24), derived using the boundary conditions $\sigma_c^* = 0$ at $x' = \pm \frac{h}{2}$. By analogy with $W\big|_{2A}$,

$$
W\big|_{\hat{A}} = \frac{\sigma_a^2 a_o^2 h}{a_r E_r}
$$
$$
- \left[\frac{a_c^2 a_o E_c \sigma_a^2 - a_c^2 a_r E_c E_r (\alpha_c - \alpha_r)\Delta T \sigma_a}{\zeta a_r E_r E_o}\right]\left[\frac{\zeta h}{a_c} - \tanh\left(\frac{\zeta h}{a_c}\right)\right] + a_o \alpha_r \Delta T \sigma_a h \tag{4.53}
$$

Substituting Eqs. (4.53) and (4.51) into Eq. (4.49),

$$\Delta W = \frac{2a_c^2 a_o^2 E_c \sigma_a^2 - 2a_c^2 a_r a_o E_c E_r (\alpha_c - \alpha_r)\sigma_a \Delta T}{2\zeta a_r a_o E_r E_o}\left[2\tanh\left(\frac{\zeta h}{a_c}\right) - \tanh\left(\frac{2\zeta h}{a_c}\right)\right] \tag{4.54}$$

The change in external work in Eq. (4.54) has thermomechanical coupling and pure mechanical loading terms. The amount of work done is the displacement u_r multiplied by the magnitude of the applied force. If the laminate is simultaneously exposed to a change in temperature, u_r will have a different value than with mechanical loading alone. The work done will change as well, hence the thermomechanical interaction term. Thermal loading alone does no external work and thus has no contributions in Eq. (4.54).

Finally, the strain energy release rate is found by placing Eqs. (4.54) and (4.48) into a Griffith energy balance, Eq. (4.27), and substituting Eq. (4.16) into the result, yielding

$$G = \frac{a_c a_o E_o}{2\zeta a_r E_r E_c}\left[2\tanh\left(\frac{\zeta h}{a_c}\right) - \tanh\left(\frac{2\zeta h}{a_c}\right)\right]\sigma_{c\infty}^2 \tag{4.55}$$

The final expression for G in Eq. (4.55) has thermal loading, mechanical loading, and thermomechanical interaction contributions. The value of the

strain energy release rate is independent of load path. That is, for a given load increment, G depends only on the final load state and not on the order in which σ_a and ΔT are applied. See Appendix A for a proof of the path independence of G.

Substituting Eq. (4.55) into Eq. (4.25) and placing Eq. (4.16) into the result, the cracking criterion becomes

$$\frac{a_c E_c}{2\zeta a_r a_o E_r E_o}\left[a_o \sigma_a - a_r E_r (\alpha_c - \alpha_r)\Delta T\right]^2\left[2\tanh\left(\frac{\zeta h}{a_c}\right) - \tanh\left(\frac{2\zeta h}{a_c}\right)\right] \geq G_{Ic} \quad (4.56)$$

Eq. (4.56) must be solved numerically or graphically to find h for a given ΔT and σ_a. See Appendix B for a more detailed presentation of both the shear lag solution and the derivation of energy expressions.

4.1.3 Degradation of Laminate Properties

To include the effects of microcracks in one layer on crack formation in other layers, expressions for the reduced laminate properties as functions of crack density will be found. Cracks are assumed to reduce the properties of a ply group as a function of crack density. Using CLPT, the effective properties of the laminate are then determined from the degraded ply properties. Laws and Dvorak [24] derived the loss of longitudinal stiffness in a cracked laminate. The average strain of the segment between cracks in the uncracked portion of a mechanically loaded laminate can be shown to be

$$\varepsilon_a = \frac{\sigma_a}{E_o}\left[1 + \frac{a_c^2 E_c}{2\zeta h a_r E_r}\tanh\left(\frac{2\zeta h}{a_c}\right)\right] \quad (4.57)$$

This expression can be valid for any two cracks $2h$ apart. Substituting the expression for average crack density,

$$\rho = \frac{1}{2h} \quad (4.58)$$

58

and rearranging gives the effective stress-strain relation for the cracked laminate,

$$\sigma_a = E_o(\rho)\varepsilon_a \qquad (4.59)$$

where

$$E_o(\rho) = \cfrac{E_o}{1 + \cfrac{\rho a_c^2 E_c}{\zeta a_r E_r} \tanh\left(\cfrac{\zeta}{\rho a_c}\right)} \qquad (4.60)$$

is the new laminate stiffness as a function of crack density.

McManus *et al.* [56] went a step further to derive reduction of all laminate properties due to cracking. Considering the reduction in stiffness to be caused entirely by a reduction of the effective stiffness of the cracking ply group, they define a knockdown factor, κ, due to the microcracks

$$E_c(\rho) = \kappa E_c \qquad (4.61)$$

From Eq. (4.15),

$$E_o = \frac{a_r E_r + a_c E_c}{a_o} \qquad (4.62)$$

Substituting Eq. (4.61) into the equation formed by setting $E_o = E_o(\rho)$ and $E_c = E_c(\rho)$ in Eq. (4.62),

$$E_o(\rho) = \frac{a_r E_r + a_c \kappa E_c}{a_o} \qquad (4.63)$$

Placing Eqs. (4.62) and (4.63) into Eq. (4.60) and solving for κ,

$$\kappa = a_r E_r \left[1 - \frac{a_c \rho}{\zeta}\tanh\left(\frac{\zeta}{a_c \rho}\right)\right]\left[a_r E_r + a_c E_c \frac{a_c \rho}{\zeta}\tanh\left(\frac{\zeta}{a_c \rho}\right)\right]^{-1} \qquad (4.64)$$

This knockdown factor is used to calculate degraded laminate properties due to matrix cracks. Details of this method are given in Section 4.2.1.

4.2 IMPLEMENTATION

The implementation of the analysis follows the work of Park [57, 61], modified to include thermomechanical loading. The basic formulations for crack appearance and reduced laminate properties, Eqs. (4.56) and (4.64), respectively, are incorporated into a progressive damage model. This model is used to predict crack density and degraded ply and laminate properties at incremental loadings of an arbitrary thermo-mechanical load history. It is general enough to include any laminate geometry and includes modeling of various secondary effects.

4.2.1 Damage Progression Algorithm

Assuming an existing crack spacing $2h$, new cracks will form midway between existing cracks when the basic energy criterion in Eq. (4.56) is satisfied, resulting in a new crack spacing h. An existing crack spacing just under $2h$ will not satisfy the criteria, and no new cracks will form. In practice, the crack spacing is not uniform, and the true crack spacing will fall somewhere between these extremes. Hence, the average crack density, ρ, is:

$$\frac{1}{2h} < \rho \leq \frac{1}{h} \tag{4.65}$$

where h satisfies Eq. (4.56). For consistency, the present work will use only the minimum crack density, where all cracks are separated by $2h$. This convention has been shown to work well in previous studies [56, 57, 61]. The choice is essentially arbitrary, and it will affect the values of G_{Ic} and ζ back-calculated from the experimental data in Section 4.4.

The analysis calculates crack density for every ply of any general laminate and the resulting degraded laminate properties. The algorithm includes effects such as material softening and temperature dependent material properties. "Material softening" refers to the fact that cracking in

60
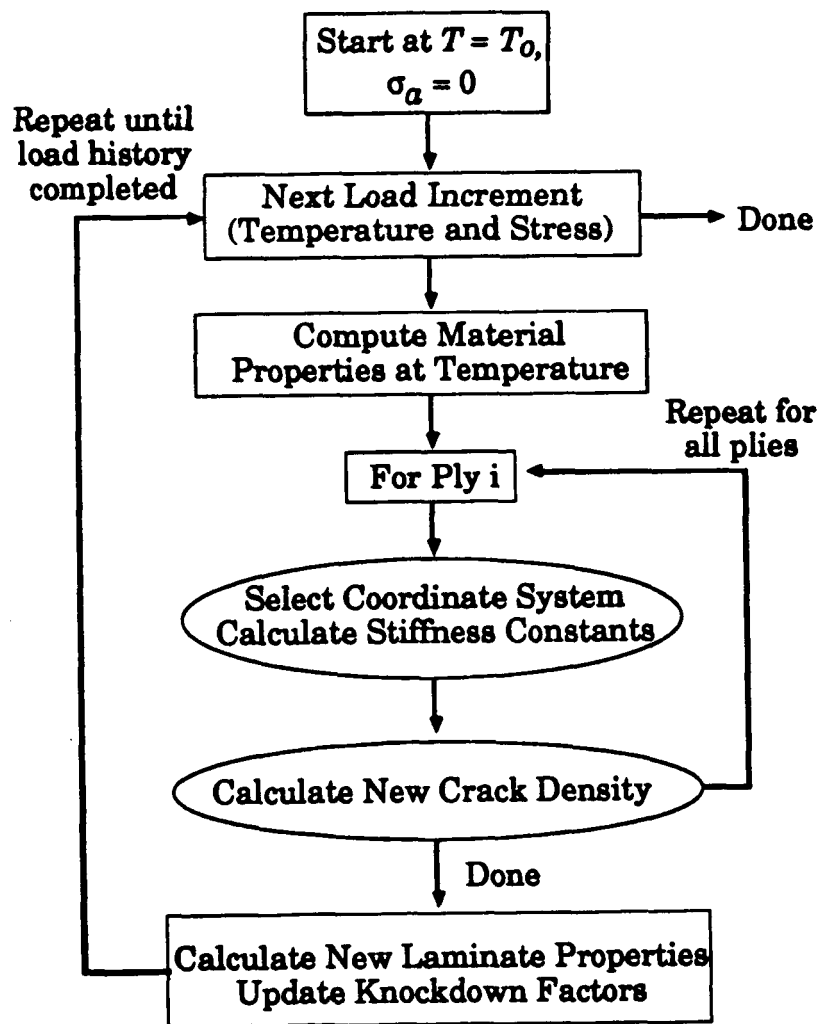
Figure 4.5   Flow chart of algorithm used to implement analysis.

61

one layer will affect the cracking behavior of the other plies in the laminate by changing the effective properties of the laminate. The reduced properties at each temperature or stress increment reflect the damage incurred in all plies at all previous loads. Material properties are also known to be dependent on temperature. The analysis includes temperature-dependent material properties, linearly interpolating between temperatures at which data is available.

Figure 4.5 shows a flow chart describing the basic algorithm. The analysis starts at the stress-free temperature and zero mechanical stress and increments to the user-specified initial conditions, accounting for any thermal residual stresses incurred during manufacture. It then increments through the temperatures and stresses in the user-defined load profile. At each new load increment, the material properties are obtained from the temperature-dependent material property data. A single ply group, referred to as ply c, is designated as the cracking layer. The crack density in ply c at this load increment is then calculated.

The analysis is carried out in the local coordinate system of the cracking layer, defined in Section 4.1.1. Properties of the rest of the laminate are smeared together, whereby existing cracks in the other layers are included. Eq. (4.56) is solved for h using a bisection iteration numerical method, and crack density ρ follows from Eq. (4.65). This procedure is repeated for every ply group in the laminate at this load increment. Finally, knockdown factors for each ply group and the effective laminate properties are updated using Eq. (4.64) and CLPT to reflect the total damage of the laminate at this load. These steps are iterated to calculate crack density and laminate properties through the entire load history.

4.2.2 Derivation of Effective Laminate and Ply Properties

Laminate theory (CLPT) [63] is used to derive the stiffness constants used in the above analysis. The equivalent stiffnesses, E_o, E_r and E_c are necessary to solve for crack spacing in Eq. (4.56). First, appropriate temperature-dependent material properties are obtained. Each ply i has material properties E_{li} (longitudinal stiffness), E_{ti} (transverse stiffness), v_i (major Poisson's ratio), G_i (shear stiffness) α_{li} (longitudinal CTE), and α_{ti} (transverse CTE). Ply i has thickness t_i. The fibers of each ply are aligned at an angle θ_i to the x axis of the global coordinate system. The cracking ply group, ply c, is treated as a single layer with orientation θ_c. The crack formation analysis is carried out in the local coordinate system $x'y'z'$ of the cracking ply group, defined in Section 4.1.1. In this coordinate system, the ply angles are defined:

$$\theta_i' = \theta_i + 90° - \theta_c \qquad (4.66)$$

The necessary laminate properties for computing crack density and property degradation can be calculated using familiar CLPT relations [61]. The laminate stiffness in the $x'y'z'$ system is

$$A = \sum_{i=1}^{n} \overline{Q}_i t_i \qquad (4.67)$$

The rotated reduced ply stiffnesses in the $x'y'z'$ system are

$$\overline{Q}_i = T_i^{-1} Q_i T_i^{-T} \qquad (4.68)$$

where

$$Q_i = \begin{bmatrix} Q_{11(i)} & Q_{12(i)} & 0 \\ Q_{12(i)} & Q_{22(i)} & 0 \\ 0 & 0 & Q_{66(i)} \end{bmatrix} \qquad (4.69)$$

and

63

$$\mathbf{T}_i = \begin{bmatrix} \cos^2 \theta_i' & \sin^2 \theta_i' & 2\sin \theta_i' \cos \theta_i' \\ \sin^2 \theta_i' & \cos^2 \theta_i' & -2\sin \theta_i' \cos \theta_i' \\ -\sin \theta_i' \cos \theta_i' & \sin \theta_i' \cos \theta_i' & \cos^2 \theta_i' - \sin^2 \theta_i' \end{bmatrix} \qquad (4.70)$$

and the reduced ply stiffnesses are

$$Q_{11(i)} = \frac{E_{ll}}{D_i} \qquad Q_{12(i)} = \kappa_i \frac{v_i E_{tt}}{D_i}$$

$$Q_{22(i)} = \kappa_i \frac{E_{tt}}{D_i} \qquad Q_{66(i)} = \kappa_i \frac{G_{lt}}{D_i} \qquad (4.71\text{a-e})$$

$$D_i = 1 - v_i^2 \frac{E_{tt}}{E_{ll}}$$

Here, κ_i is the knockdown factor for ply i defined by Eq. (4.64) which accounts for the effects of pre-existing cracks. It has the value 1 until ply i begins to crack. Note that all matrix-dominated properties are assumed to be reduced by the same knockdown factor. The CTEs of each ply are

$$\alpha_i = \begin{Bmatrix} \alpha_{ll} \\ \alpha_{tt} \\ 0 \end{Bmatrix} \qquad (4.72)$$

In the $x'y'z'$ system, the ply CTEs are

$$\bar{\alpha}_i = \mathbf{T}_i^T \alpha_i \qquad (4.73)$$

The laminate constants required in Eqs. (4.56) and (4.64) are now calculated. The total laminate thickness, a_o, is

$$a_o = \sum_{i=1}^{n} t_i \qquad (4.74)$$

The necessary constants for the cracking layer are

$$E_c = \frac{E_{ll}}{D_c} \qquad \alpha_c = \alpha_{lc} \qquad a_c = t_c \qquad (4.75)$$

and the smeared properties of the rest of the laminate are

$$E_r = \frac{A_{11} - E_c a_c}{a_r} \qquad \alpha_r = \alpha_1^r \qquad a_r = a_o - a_c \qquad (4.76)$$

64

where α_1' is the first element of the vector of CTEs which are calculated from

$$\alpha' = \left[\mathbf{A} - \overline{\mathbf{Q}}_c t_c\right]^{-1}\left(\sum_{i=1}^{n} \overline{\mathbf{Q}}_i \overline{\alpha}_i t_i - \overline{\mathbf{Q}}_c \overline{\alpha}_c t_c\right) \tag{4.77}$$

Eq. (4.56) is now used to predict the crack density in the cracking ply group. The knockdown factor for this group is also recalculated using Eq. (4.64).

After all the ply groups have been analyzed in this manner, the degraded effective laminate properties in the global x direction are calculated from

$$E^{eff} = \frac{1}{A_{11}^{inv} a_o} \qquad \mathbf{A}^{inv} = \mathbf{A}^{-1} \qquad \alpha^{eff} = \alpha_1^e \tag{4.78}$$

where α_1^e is the first element of

$$\alpha^e = \mathbf{A}^{-1} \sum_{i=1}^{n} \overline{\mathbf{Q}}_i \overline{\alpha}_i t_i \tag{4.79}$$

and $\mathbf{A}$, $\overline{\mathbf{Q}}$, and $\overline{\alpha}$ are calculated from Eqs. (4.67) to (4.73) with $\theta_i' = \theta_i$. Note that bending is not incorporated into this method, so it is strictly valid for symmetric laminates only. All of the above steps are repeated for each load increment until completion of the entire load history. Each increment incorporates the knocked down properties of all the plies from the previous increment and temperature-dependent properties for the conditions of the current increment.

4.2.3 Computer Code

The computer code CRACKOMATIC II was modified to implement the present methodology. Given material properties, laminate geometry, and user-defined thermomechanical load history, it predicts crack density and corresponding degraded laminate properties. Also included are user options to incorporate or omit material softening effects and temperature-dependent material properties. The output of the code is a table with columns listing

65

temperature, applied stress, corresponding crack density in any selected plies, and effective laminate properties. These can be used to generate plots of cracking and changing laminate properties as the laminate is exposed to a given load profile.

The program output reports crack densities as they could be observed on the edge of a specimen. The crack density calculated from Eqs. (4.56) and (4.65) is expressed in the local $x'y'z'$ coordinate system. The calculated results are transformed to the global xyz-coordinate system, accounting for the geometric effect illustrated in Figure 4.6. The reported crack density, ρ_c, is the calculated density, ρ_∞, multiplied by a geometric factor:

$$\rho_c = \rho_\infty \sin(\theta_i) \tag{4.80}$$

The manual for CRACKOMATIC II is in Appendix C. The document describes the program in detail and shows sample sessions. The source code is available by request from the author or the TELAC laboratory.

4.3 LAMINATE SELECTION

Preliminary analysis was necessary to select the three laminate geometries to be used in the experimental investigation. Several criteria were used to determine the layups. First, in order to capture both the onset and accumulation of cracking, microcracking in the laminates had to initiate within the available temperature range of the environmental chamber. If cracking initiated at one of the lowest temperature increments or not at all, then the test would yield little useful data. Furthermore, the laminates had to be initially uncracked at room temperature following cure in order to capture the onset of cracking. Using the existing progressive thermal analysis of Park [57], it was found that all plies of a $[0_2/45_2/90_2/-45_2]_s$ laminate

Crack density measured on this side

$$\rho_{90°} > \rho_{45°}$$
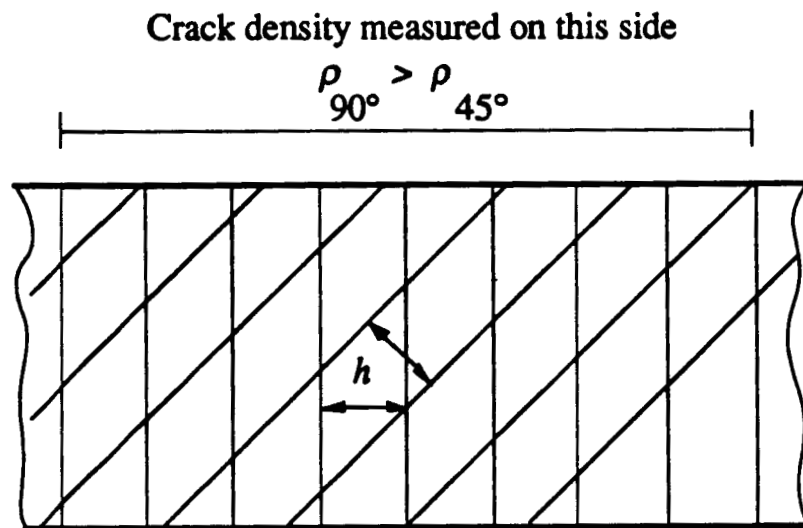
Figure 4.6 Higher crack density observed in 90° layer than in 45° layer during edge inspection, though crack spacing same in both [57].

would indeed begin cracking by -184°C, the lowest temperature possible in the chamber, and would be uncracked at room temperature. Table 4.1 lists the material properties used in these preliminary calculations. The values of G_{Ic} and ζ were estimated from those of T300/934 graphite/epoxy, found in a previous study [56].

Based on these preliminary thermal calculations, shown in Table 4.2, two additional layups were chosen. A $[0_2/45_2/90_2/-45_2]_s$ laminate would be used to investigate the effects of layer thickness by comparing its cracking behavior with that of the $[0_4/45_4/90_4/-45_4]_s$ laminate. Second, a $[0_2/60_2/-60_2]_s$ layup was chosen to examine ply orientation effects by comparison with the $[0_2/45_2/90_2/-45_2]_s$ laminate. The progressive thermal analysis indicated that the onset of cracking in both of these laminates should occur near the lower temperature limit of the environmental chamber, limiting the number of temperature increments at which useful crack density data could be collected. However, Park's work showed that thin ply groups tend to initiate cracking at a higher temperature than predicted by that analysis [57], and it was suspected that these two laminates might demonstrate this "thin ply" behavior.

Further preliminary calculations were necessary to check whether the three laminates chosen would yield useful data under mechanical loading. These are summarized in Table 4.3. In order to maximize the range of loading under which microcrack data can be collected, crack initiation could not occur just before or simultaneously with laminate failure. CLPT was used in conjunction with a maximum stress failure criterion to predict first ply failure. A thermal residual stress, assuming a stress-free temperature equal to the cure temperature (177°C), was included.

68

Table 4.1 AS4/3501-6 Material Properties Used in Preliminary Calculations

E_l (GPa)	142.0	G_{lc} (J/m^2)	250
E_t (GPa)	9.81	ξ	0.9
ν	0.30	X_t (MPa)	1661
G_{lt} (GPa)	6.0	X_c (MPa)	1698
t_{ply} (mm)	0.134	Y_t (MPa)	53.9
T_o (°C)	177	Y_c (MPa)	221
α_l (με/°C)	-0.36	S (MPa)	105
α_t (με/°C)	28.8		

Table 4.2   Summary of Preliminary Calculations Using Progressive Thermal Analysis from [57]

Laminate	Crack Initiation Temperature (°C)
$[0_4/45_4/90_4/-45_4]_s$	-58
$[0_2/45_2/90_2/-45_2]_s$	-156
$[0_2/60_2/-60_2]_s$	-124

Table 4.3 **Summary of Preliminary Calculations for Crack Initiation and Final Failure under Mechanical Loading**

Laminate	Crack Initiation (kN)		Final Failure (kN)	
	CLPT/ Max Stress	CLPT/ Max Stress, *in situ* Y_t	CLPT/ Max Stress	CLPT/ Max Stress, *in situ* Y_t
$[0_2/45_2/90_2/-45_2]_s$	14.8	26.8	61.4	62.7
$[0_2/45_2/90_2/-45_2]_s$	7.40	17.2	30.7	34.7
$[0_2/60_2/-60_2]_s$	9.52	17.8	21.4	22.7

71

Final failure of the laminate was calculated using the ply discount method [63]. In this method, CLPT was used with a maximum stress failure criterion to predict first ply failure. If the axial failure stress (X_c or X_t) was exceeded, E_l, E_t, ν, and G_{lt} for the failed ply were set to zero, corresponding to fiber failure. If, on the other hand, the transverse (Y_c or Y_t) or shear (S) failure stress was exceeded, E_t, ν, and G_{lt} for that ply were set to zero, corresponding to matrix failure. The stress was subsequently increased until the next ply failed, and the properties of that ply were knocked down as after first ply failure. This procedure was repeated until fiber failure in the 0° plies is predicted, which was presumed to indicate final failure. The predicted behavior of all three laminates, including both first ply failure and final failure, was deemed acceptable.

Next, the preceding analysis was repeated using an *in situ* transverse tensile strength $Y_t^{\it eff}$ [65],

$$Y_t^{\it eff} = Y_t \left(1 + A \frac{\sin(\Delta\theta)}{N^B} \right) \qquad (4.81)$$

where $\Delta\theta$ is the minimum ply angle change between the ply under consideration and its neighboring plies, N is the number of consecutive plies in that layer, Y^t is the transverse tensile strength of a unidirectional ply, and A and B are constants of the strength distribution, respectively, for T300/934. This empirical formula was originally derived for T300/934, for which A and B are usually taken to be 1.3 and 0.7, respectively. It is applicable to AS4/3501-6 as well, since the cracking behaviors of the two material systems are similar. The predicted first ply failure and final failure loads using this *in situ* transverse tensile strength were deemed acceptable for all three laminates.

4.4 DATA FIT

As discussed in Section 2.4, the critical strain energy release rate is impossible to measure directly. Many researchers use the interlaminar fracture toughness as a value for G_{Ic}. However, as this property is measured in double cantilever beam tests, it essentially characterizes delamination rather than microcracking. Moreover, measured values of the interlaminar fracture toughness vary considerably, as shown in Figure 2.1. The shear lag parameter is a semi-empirical aspect of the shear lag model which likewise cannot be measured directly. This parameter has not been standardized, rendering values used in different studies difficult to compare.

Consequently, the critical strain energy release rate and shear lag parameter will be determined from experimental data using the following data fit. First, crack density is predicted as a function of applied load or progressive cooling using a particular G_{Ic} and ζ. The predicted and observed crack densities are normalized by the highest density recorded for that laminate, and the applied load or change in temperature is normalized by the largest load or ΔT to which the laminate was exposed experimentally. Next, a single error value is calculated for each experimental data point using

$$Error_j = \min\left(\sqrt{\left[\overline{\Delta T_{a_k}} - \overline{\Delta T_{e_j}}\right]^2 + \left[\overline{\rho}_{a_k} - \overline{\rho}_{e_j}\right]^2} \right) \tag{4.82}$$

for thermal loading. $\overline{\Delta T_{a_k}}$ and $\overline{\rho}_{a_k}$ are the normalized change in temperature and predicted crack density, respectively, at the kth load increment of the analysis. $\overline{\Delta T_{e_j}}$ and $\overline{\rho}_{e_j}$ are the normalized change in temperature and observed crack density, respectively, at the jth data point. The value used for $Error_j$ is the minimum value calculated using any k. Similarly, under mechanical loading,

$$Error_j = \min\left(\sqrt{\left[\overline{P}_{a_k} - \overline{P}_{e_j}\right]^2 + \left[\overline{\rho}_{a_k} - \overline{\rho}_{e_j}\right]^2}\right) \qquad (4.83)$$

where $\overline{P}_{a_k}$ and $\overline{P}_{e_j}$ are the normalized applied load at the kth load increment of the analysis and j^{th} data point, respectively. Conceptually, this method is equivalent to plotting the normalized experimental data and analytical predictions on the same graph and finding the error for each data point from the absolute distance between that data point and the nearest point on the analysis curve.

The mean square error (MSE) is then determined for every layer in each laminate using [66]

$$MSE = \frac{1}{m}\sum_{j=1}^{m} Error_j^2 \qquad (4.84)$$

where m is the total number of data points for the layer. This is repeated for both thermal and mechanical loading, for each layer in every laminate. A simple computer code was written to carry out the calculations. Finally, all the MSEs are summed, giving a single total MSE value for that G_{Ic} and ζ. The procedure is repeated for different values of the shear lag parameter and critical strain energy release rate until the single set of values which minimizes the total MSE is found. Those values can then be used in Eq. (4.56) to analyze any laminate, provided that the material system does not change.

This data fit has several important advantages over the other methods used to determine G_{Ic} and ζ described in Section 2.4. A large amount of experimental data may be reduced to a single set of G_{Ic} and ζ values. The data fit can be used to check for laminate dependence of these parameters by finding the variation in values fit for the individual laminates. Finally, if

74

found to be laminate independent, G_{Ic} and ζ only need to be measured once for a given material system.

CHAPTER 5

EXPERIMENTAL PROCEDURES

An experimental investigation was carried out to provide greater qualitative understanding of the microcracking problem, determine input parameters for the analysis, and provide verification of the analytical model. In this chapter the specimen matrix used in the investigation, and the rationale behind its design, are presented. Manufacturing, pre-test preparation, and instrumentation of the specimens are then described. Finally, specimen conditioning and data collection procedures are presented.

5.1 TEST MATRICES

Small, rectangular graphite/epoxy specimens, referred to as thermal specimens, and larger tensile coupons were manufactured using three different layups. Thermal specimens were cooled to progressively lower temperatures. After reaching each target temperature, specimens were returned to room temperature. Microcrack density data was then collected on the specimen edges and in their interiors by optical microscopy. Tensile coupons were loaded monotonically to progressively higher loads. Edges were inspected for cracks after unloading the coupons from each load level. Stress-strain data was also collected.

AS4/3501-6 graphite/epoxy was chosen as the material system for this investigation. It is a well understood material, and an extensive database of its properties has been established at TELAC. Three different laminates

76

were used: $[0_4/45_4/90_4/-45_4]_s$, $[0_2/45_2/90_2/-45_2]_s$, and $[0_2/60_2/-60_2]_s$. The layups were selected based upon the procedure described in Section 4.3. Two different sizes of thermal specimens were chosen. The first, 7.62 cm x 1.27 cm, was identical to that used by Park [57], so that data collected might be compared with the results of that study. To investigate width effects, a second size was chosen, 7.62 cm x 2.54 cm. The width of the tensile coupons was selected to be the same as these wider thermal specimens to allow thermal and mechanical crack density data to be compared. Their length was subsequently chosen to be 25.4 cm, based on ASTM D3039.

A matrix of all of the specimens manufactured is shown in Table 5.1. Table 5.2 is a test matrix, which shows the conditioning and examination performed on the specimens from a single layup. Specimens made from all three layups were tested in the same way.

5.2 TEST SPECIMEN MANUFACTURE AND PREPARATION

All laminates were manufactured at TELAC using standard procedures of the laboratory [67]. 35.6 cm x 30.5 cm panels were fabricated using standard hand layup techniques. A total of six panels, two of each layup, were made. The material for the layup was furnished as 30.5 cm wide, continuous AS4/3501-6 unidirectional prepreg tape. Nominal ply thickness was 0.134 mm. The panels were autoclave cured according to the manufacturer's cure cycle. Following cure, the panels were postcured at 177°C for eight hours.

Fewer than twelve hours after postcure, the panels were cut into individual thermal and mechanical specimens as per the cutting plan in Figure 5.1. The same cutting plan was used for all panels. The cutting plan was randomized so that the effects of manufacturing variations, such as

77

Table 5.1   Specimen Matrix

Layup	Test type/ Data Collected	Specimen Size (cm)	Number of Specimens
$[0_4/45_4/90_4/-45_4]_s$	Thermal/Edge	7.62 x 2.54	5
		7.62 x 1.27	5
	Thermal/Interior	7.62 x 2.54	5
		7.62 x 1.27	5
	Mechanical/Edge	25.4 x 2.54	15
$[0_2/45_2/90_2/-45_2]_s$	Thermal/Edge	7.62 x 2.54	5
		7.62 x 1.27	5
	Thermal/Interior	7.62 x 2.54	5
		7.62 x 1.27	5
	Mechanical/Edge	25.4 x 2.54	15
$[0_2/60_2/-60_2]_s$	Thermal/Edge	7.62 x 2.54	5
		7.62 x 1.27	5
	Thermal/Interior	7.62 x 2.54	5
		7.62 x 1.27	5
	Mechanical/Edge	25.4 x 2.54	15

Table 5.2   Test Matrix Repeated for All Laminates

Conditioning	Data Collected	Wide Thermal Specimens	Narrow Thermal Specimens	Tensile Coupons
Cool to -18°C, -73°C, -129°C, and -184°C; return to RT after each	Measure cracks on edge at RT before conditioning, and at RT after each target temperature	5	5	0
RT	Measure cracks in interior	3	3	0
Cool to -18°C, return to RT	Measure cracks in interior	3	3	0
Cool to -18°C, return to RT, cool to -73°C, return to RT	Measure cracks in interior	3	3	0
Cool to -18°C, return to RT, cool to -73°C, return to RT, cool to -129°C return to RT	Measure cracks in interior	3	3	0
Cool to -18°C, return to RT, cool to -73°C, return to RT, cool to -129°C return to RT, cool to -184°C return to RT	Measure cracks in interior	3	3	0
Tensile loading to 2.22 kN, 4.44 kN, 6.66 kN, etc. until failure; return to no load after each	Measure cracks on edge before conditioning and after each loading	0	0	5

† Room Temperature (21°C)

79

spatial variability in laminate thickness and fiber volume fraction, would not create a systematic bias in the results. A water cooled diamond blade was used for cutting.

Both long edges of every specimen were wet sanded with 600 grit sandpaper and polished with 0.7 micron grit powder on a polishing wheel. The reasons for polishing were to standardize crack initiation sites and to facilitate optical microscopy of the specimen edges. Immediately after polishing, all specimens were dried at 93°C for 14 hours. They were stored in airtight containers with desiccant for the remainder of the experimental investigation to minimize moisture absorption effects.

Some additional preparation was necessary for the tensile coupons. A total of 3 width and 6 thickness measurements were taken from each coupon. This was done to ensure specimen uniformity and to compare measured values with nominal ones. A template of the positions at which thickness and width measurements were to be made was aligned to the center of the test section of each specimen, and the positions were marked out for measurements. Figure 5.2 shows a schematic of a tensile coupon with the measuring points. The average width of the coupons was 2.53 cm, compared to the nominal width of 2.54 cm. Average ply thickness was found to be 0.135 mm, compared to the nominal value of 0.134 mm. Standard deviations were small, 0.00292 cm for the width measurements and 0.00422 mm for the thickness measurements. All subsequent calculations in the present work use nominal values for both width and thickness.

Next, fiberglass end tabs were bonded to the ends of the mechanical coupons to reinforce the gripping section where the tensile loading was applied. The end tabs had a nominal thickness of 5.3 mm. To ensure smooth transfer of loads from the end tabs to the specimens and to minimize stress
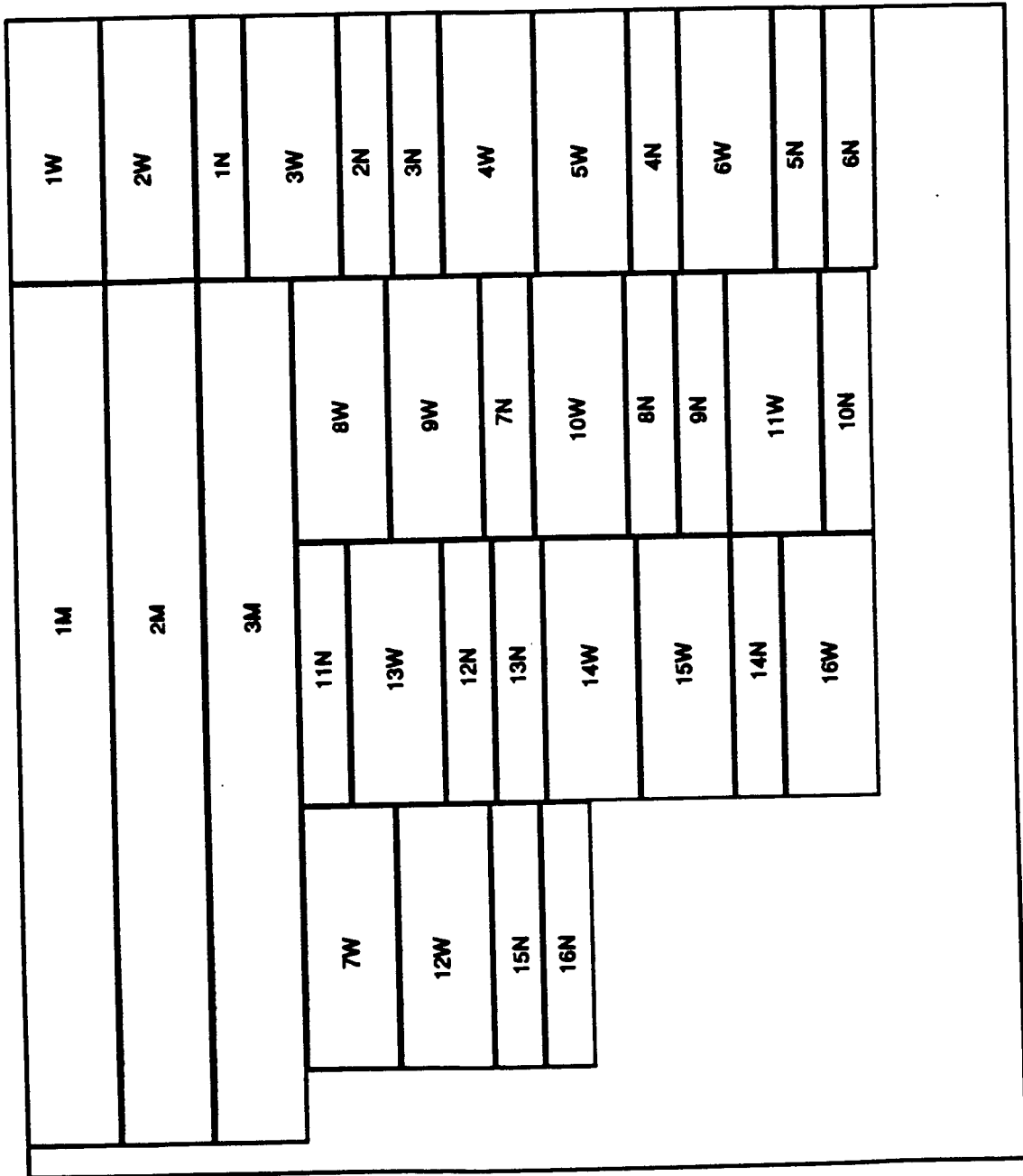
Figure 5.1 Cutting plan used for all panels.

81
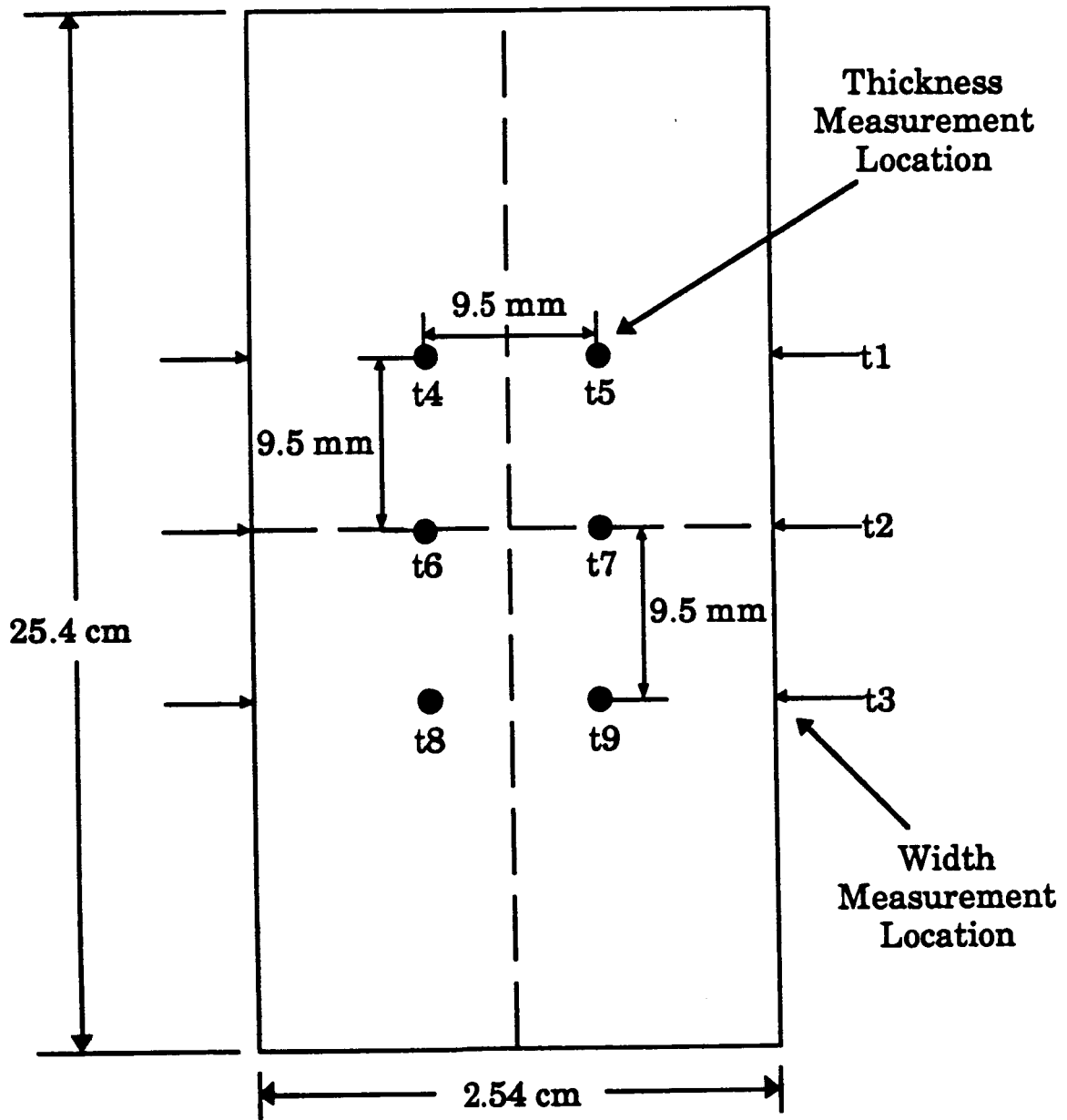
Figure 5.2　　Schematic of tensile coupon measurement locations.

concentrations, the ends of the tabs nearest to the test section were beveled 30°. The dimensions of the end tabs were 2.54 cm x 5.08 cm, leaving a 15.2 cm test section.

The end tabs were cut from 21-ply, pre-cured sheets of fiberglass with a bandsaw. A belt sander was used to bevel one of the edges of each tab. Prior to bonding, both the tabs and the coupons were cleaned with cheesecloth. Following a standard TELAC procedure [67], the tabs were placed on the coupons at room temperature with a layer of adhesive film between the tab and specimen. A total of four tabs were placed on each specimen. The adhesive used for bonding was Cyanamid 123-2 Adhesive Film. The end tabs were bonded to the coupons using a secondary bond cure in an autoclave, carried out at 1.45 mPa gage vacuum and 107°C for two hours [67].

Tensile coupons were instrumented with EA-06-125AD-120 strain gages manufactured by Micro Measurements. The gages were 5 mm x 10 mm with a gage factor of 2.080 and an accuracy of ±0.5%. One gage was mounted longitudinally on each coupon at the center of the test section, as shown in Figure 5.3. After cleaning the specimens thoroughly with cheesecloth, the gages were bonded to them using a catalyst and M-Bond 200 adhesive supplied by Micro Measurements. Electrical leads, 91 cm in length, were soldered to the gages.

5.3 TESTING PROCEDURES

5.3.1 Thermal Conditioning

Thermal loading specimens were progressively cooled in a thermal environment chamber. The chamber used electrical resistance rods for heating and liquid nitrogen injection for cooling, allowing a temperature

Top View

Side View

25.4 cm

5.08 cm

0°

90°

Graphite/Epoxy

30°

Strain Gage

7.62 cm

Film Adhesive

5.08 cm

Glass/Epoxy
End Tab

2.54 cm
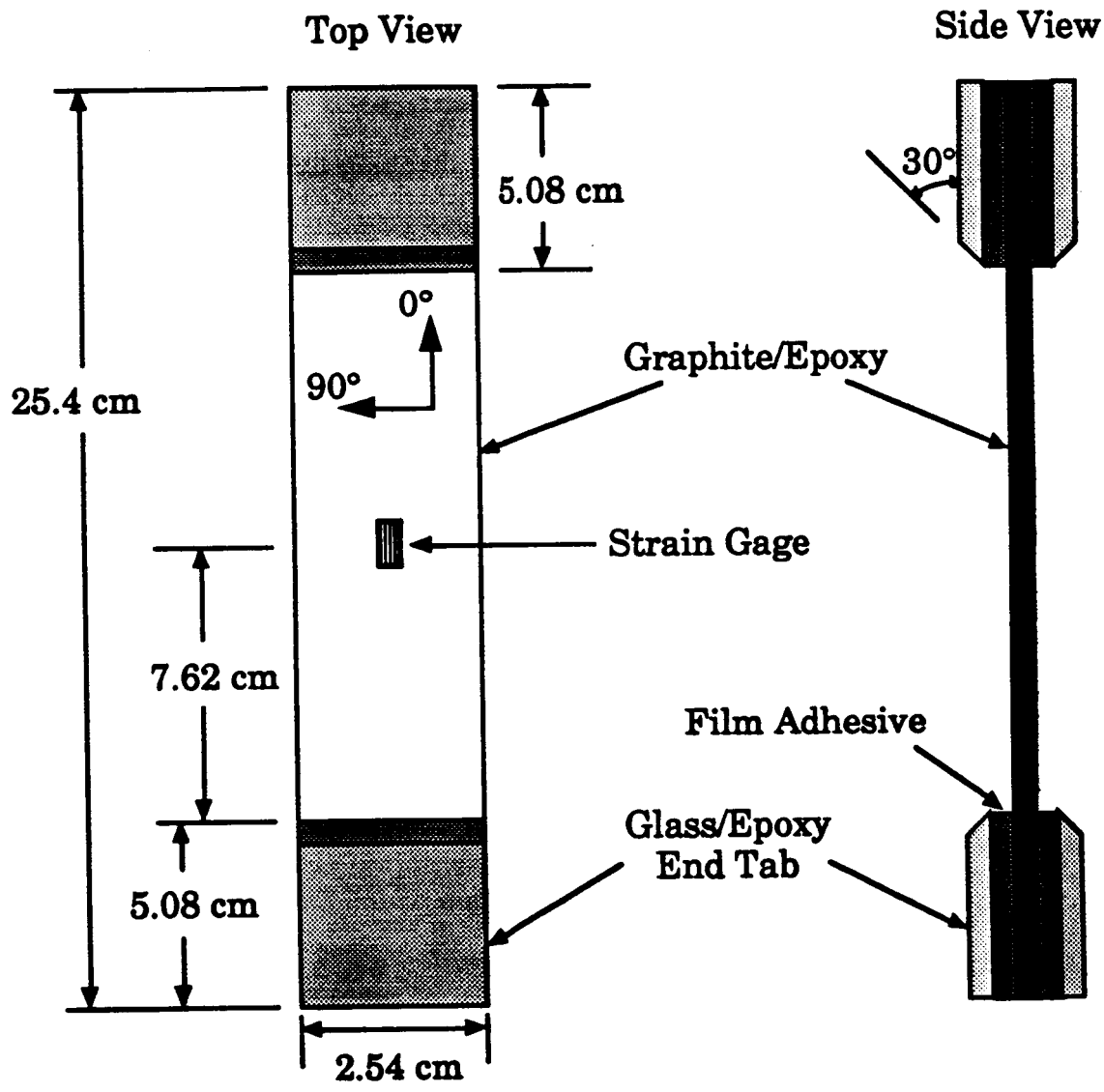
Note: Not to Scale

Figure 5.3   Tensile coupon configuration.

range of -184°C to 427°C. Specimens were placed on stainless steel racks in the 30.5 cm x 10.2 cm x 10.2 cm test volume within the chamber. The specimens were shielded from direct heat radiation and contact with liquid nitrogen and were directly heated and cooled by fan-circulated air only. The temperature of the chamber was precisely controlled with an Omega temperature controller. The microprocessor-based controller could be programmed to a desired thermal profile comprising a series of linear segments. A single J-type thermocouple provided feedback to the controller. Prior to testing, over 100 tuning runs were done to determine the optimum controller tuning settings and feedback thermocouple location.

Five additional K-type thermocouples were mounted within the chamber. One of these was epoxied to a graphite/epoxy specimen to simulate the thermal response of an actual test specimen. Thermocouple outputs were fed into a MacADIOS breakout box, which was in turn interfaced with an Apple Macintosh IIx through a MacADIOS analog/digital converter card supplied by GW Instruments. Thermocouple readings were recorded and displayed in a virtual strip chart by the LabVIEW®2 data acquisition program. The thermocouples were used in the tuning runs to determine the controller settings and specimen rack locations which provided stable control and minimized the effects of temperature gradients. During thermal testing the thermocouples were used to record the actual temperature profile.

Thermal specimens were first inspected for both edge and interior microcracks at room temperature using the procedure described in Section 5.4. They were then cooled to progressively lower temperatures down to -184°C. The target temperatures for all thermal specimens were -18°C, -73°C, -129°C, and -184°C. Since multiple runs were necessary to cool all the specimens, the individual specimens included in each run as well as their

distribution on the specimen racks were always randomized to prevent these factors from causing a consistent bias in the results. The randomization procedure involved gently shaking the bottle in which the specimens were stored and simply pulling them out randomly. Cooling and heating were carried out at 13.9°C per minute, slow enough to minimize both rate effects and thermal gradients. Figure 5.4 shows the temperature profile of the thermal environment chamber during a test run to -73°C, as measured by the thermocouple epoxied to a specimen.

The specimens designated for edge crack data, referred to as "edge" specimens, were cooled to the target temperature, soaked at that temperature for 5 minutes, returned to room temperature, and soaked at room temperature for 5 minutes. Crack density data was subsequently collected on their edges. They were then returned to the environment chamber and cooled to the next target temperature. This procedure was repeated until all edge specimens were conditioned to every target temperature.

The specimens used for internal crack counting, referred to as "interior" specimens, were separated into five different groups for each of the five target temperatures. Each interior specimen was conditioned to every target temperature down to and including its designated target temperature, after which it was destroyed by the inspection procedure. The specimens were cooled to a target temperature, soaked at that temperature for 5 minutes, returned to room temperature, and soaked at room temperature for 5 minutes. The specimens designated for that target temperature were inspected for internal crack density, rendering them useless for further testing. The remainder of the specimens were then conditioned to the next target temperature, and the specimens designated for that temperature were

86
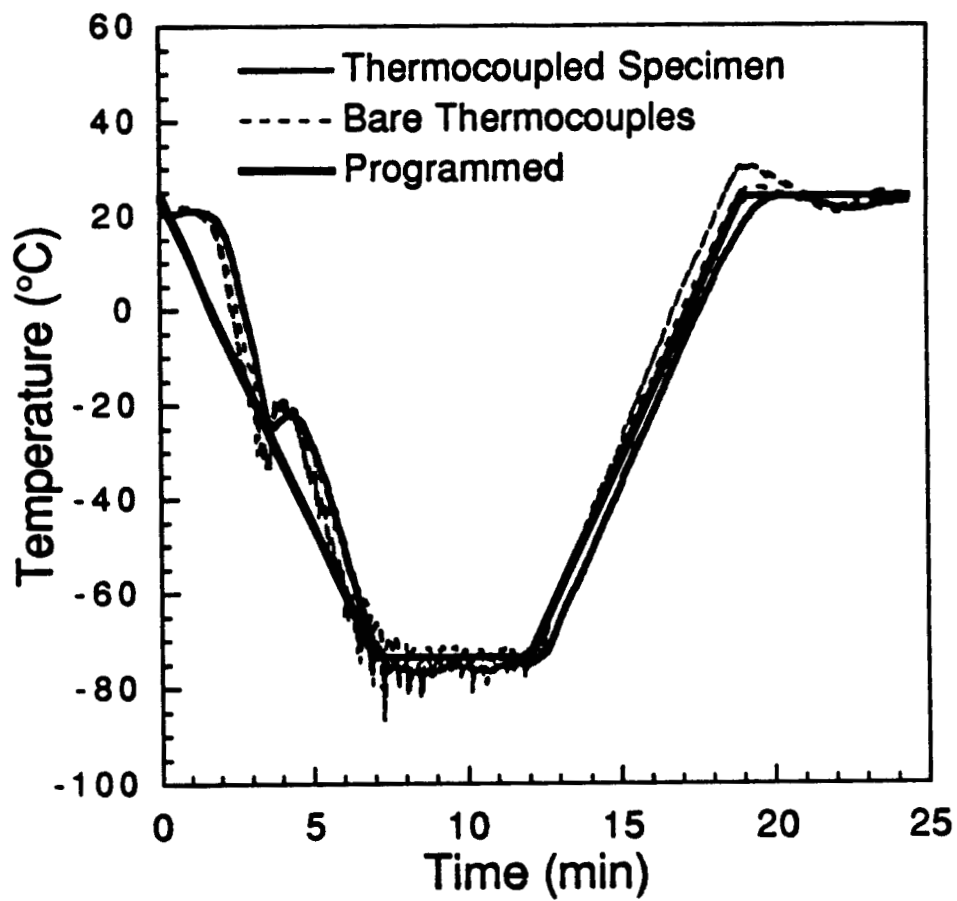
Figure 5.4 Temperature profile of thermal environment chamber during test run to -73°C.

inspected. This procedure was repeated until all target temperatures were reached.

No more than one day was allowed to pass between conditioning the specimens to a target temperature and inspecting them for microcracks.

5.3.2 Mechanical Conditioning

The mechanical specimens were first inspected for edge microcracks at room temperature using the procedure described in Section 5.4. Tensile coupons were then loaded monotonically under load control to progressively higher target loads. The coupons were loaded to a target load, unloaded, removed from the test machine, and inspected for cracks on their edges. They were then placed back in the testing maching, and loaded to the next target load, which was 2.22 kN higher the previous maximum load, unloaded, and inspected again. This procedure was repeated until other damage modes, particularly delamination, were observed. The coupon was then loaded to failure, and no further microcrack data was collected.

All tensile tests were performed on an MTS 810 test machine equipped with hydraulic grips. To mount a tensile coupon in the machine, one end was first placed in the upper hydraulic grips. Once alignment of the coupon was achieved by means of a machinist's square, gripping pressure was applied. Next the upper crosshead was lowered until the bottom of the specimen was between the lower hydraulic grips. Before gripping the lower jaws, the strain gage was balanced and calibrated. Loading and unloading rates were held constant at 89 N/s. The strain gage output was fed through Vishay Instruments strain gage amplifiers/balances, into the MacADIOS breakout box and analog/digital converter card, and recorded by LabVIEW®2. Load and stroke information from the test machine was also recorded.

88

5.4 MICROCRACK INSPECTION

5.4.1 Edge Examination

Microcracking damage was quantified by optical examination of the polished free edge of a specimen. Cracks were counted in a 2.54 cm section in the center of one edge of each specimen. The boundaries of the section were precisely marked with a white paint marker. A tally counter was used in crack counting to minimize error. Each ply group was inspected individually, and only microcracks which spanned at least half the thickness of the ply group were counted as cracks. Shorter cracks or fiber/matrix debonding were often visible but never counted. The crack density recorded was that observed on the edge, and does not account for the geometric effect shown in Figure 4.6.

Specimens were randomly assigned for inspection to two different people. Each used an identical optical microscope at a magnification of 100x. Cross checks were done by having both persons inspect the same specimen. Generally, both observed and recorded the same results.

5.4.2 Interior Crack Counts

Interior specimens were used to determine the crack density within the volume of the laminate. These specimens were cooled in the thermal environment chamber with the edge specimens. Then their edges were inspected using the procedure described in Section 5.4.1. Next, (1) material was sanded away from the inspection edge until reaching a desired depth, (2) the edge was polished and the 2.54 cm center section marked, and (3) the edge was inspected once again. Steps 1-3 were repeated at a total of four incremental depths until approximately half of the laminate volume was inspected, as shown in Figure 5.5. The 1.27 cm-wide specimens were

89

25.4 mm

■ Section in which
Cracks Counted

21.4 mm

17.4 mm

13.4 mm
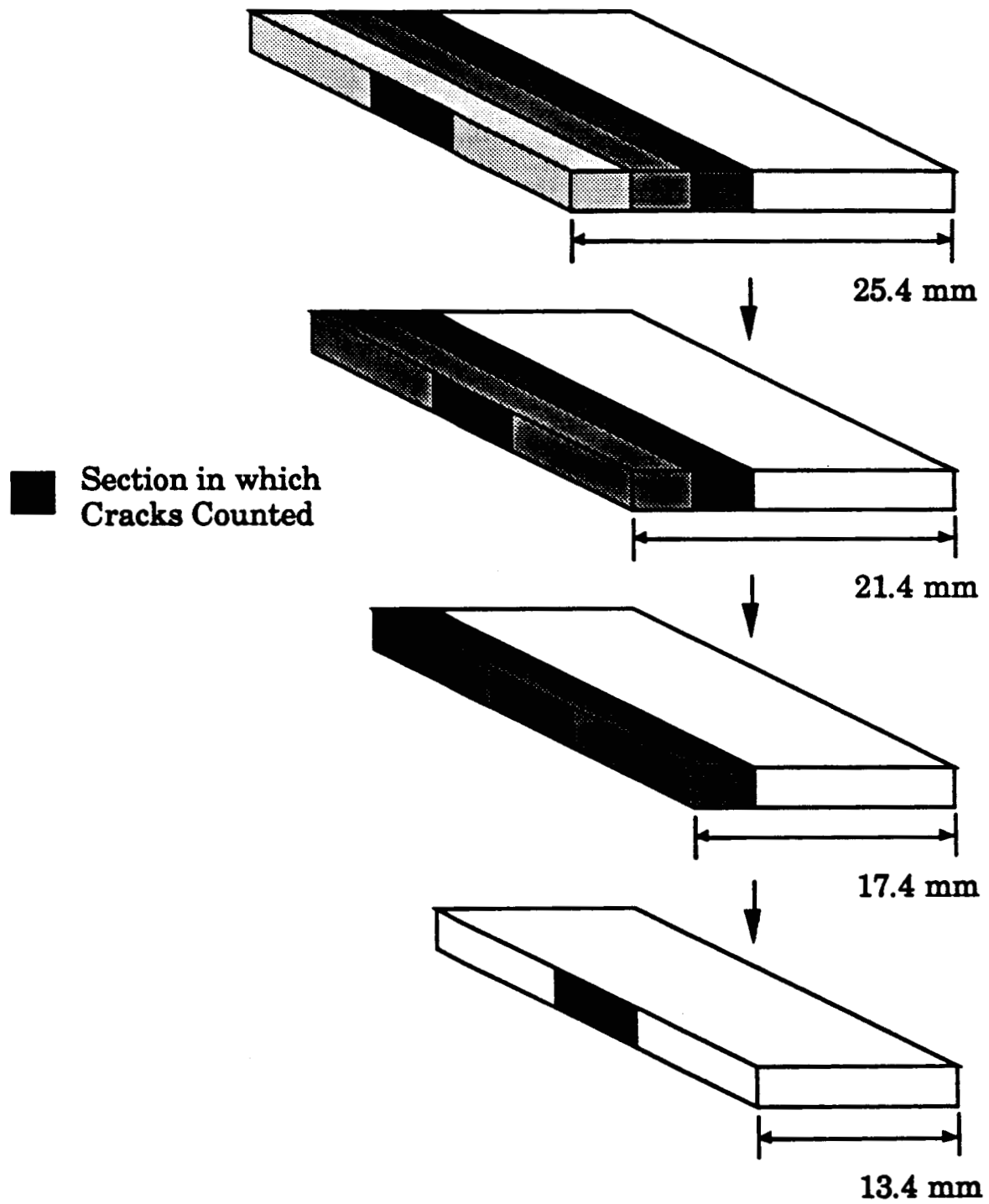
Figure 5.5 Schematic of procedure for interior crack counts.
7.62 cm x 2.54 cm thermal specimen shown.

examined at depths of 0 mm, 2 mm, 4 mm, and 6 mm. The 2.54 cm-wide specimens were examined at depths of 0 mm, 4 mm, 8 mm, and 12 mm.

In Step 1, the edge was sanded to within approximately 10% of the next depth increment using dry 180 grit sandpaper. Care was taken not to allow the specimens to become hot to the touch during sanding. The remainder of the material was removed with dry 600 grit sandpaper. The width of the specimen was frequently measured with a vernier caliper to ensure even, accurate sanding. Following sanding, the edge was polished with 0.7 micron grit powder on a polishing wheel. This sanding procedure was shown by Park [57] to cause minimal additional damage to the specimens. Finally, a 2.54 cm section was marked in the center of the edge, and cracks were inspected as in Section 5.4.1.

CHAPTER 6

RESULTS AND DISCUSSION

Analytical and experimental results are presented in this chapter. First, the results of the data fit used to determine G_{Ic} and ζ are reviewed. Mechanical loading results and correlations with analytical predictions are then presented. Thermal loading results and correlations follow. A parametric study is presented to examine the sensitivity of the analysis to different variables. Finally, the results and correlations are discussed. The effects of laminate geometry, specimen width, and layer thickness are examined. The validity of the analytical model and its assumptions is also addressed.

6.1 DATA FIT

The results of the data fit are presented in Table 6.1. The values of the critical strain energy release rate and shear lag parameter which minimize the overall mean square error for all layers are G_{Ic} = 141 J/m² and ζ = 1.0. Both thermal and mechanical loading results were used in this data fit. It is important to note that all subsequent analyses in the present study will use these values.

Also shown are the G_{Ic} and ζ values which minimize the mean square error for each of the three layups individually. These were determined by fitting the analysis to the mechanical cracking data for each laminate. Values fit to the thermal data of the $[0_4/45_4/90_4/-45_4]_s$ laminates are also

Table 6.1   Data Fit Results

Laminate	G_{Ic} (J/m²)	ζ
All Data[†]	141	1.0
$[0_4/45_4/90_4/-45_4]_s$	141	1.1
$[0_2/45_2/90_2/-45_2]_s$	141	1.2
$[0_2/60_2/-60_2]_s$	120	1.2
Thermal[††]	156	0.6

[†] Fit to all data available; subsequently used in all analyses.

[††] Fit to data from $[0_4/45_4/90_4/-45_4]_s$ thermal specimens

shown. Thermal results of the $[0_2/45_2/90_2/-45_2]_s$ and $[0_2/60_2/-60_2]_s$ laminates were not included in the data fit, as very little cracking was observed in those specimens under progressive cooling. The material properties used in the data fit and every analysis thereafter are shown in Table 6.2. These values were assumed to be independent of temperature.

The G_{Ic} and ζ values fit to individual layups and loading conditions are, in general, very close to those fit to all measurements. G_{Ic} fit to data from mechanically loaded $[0_2/60_2/-60_2]_s$ specimens is approximately 15% lower, and G_{Ic} fit to data from thermally loaded $[0_2/45_2/90_2/-45_2]_s$ specimens is 10% higher, than that fit to all data. The only severe disagreement is the ζ fit to data from thermally loaded $[0_2/45_2/90_2/-45_2]_s$ specimens.

6.2 MECHANICAL LOADING RESULTS

6.2.1 Crack Density Data and Analytical Predictions

In this subsection, selected analytical and experimental crack density correlations for the tensile coupons are presented. Average measured crack densities are plotted with error bars representing one standard deviation. All such results not presented here may be found in Appendix D.

Microcracks observed on the coupon edges generally appeared continuous through the thickness of the ply group and were nearly perpendicular to the coupon sides. Some cracks were observed which formed less than halfway through the thickness of the ply group. These not were not included in the reported crack density because they did not meet the counting criterion defined in Section 5.4.1. At higher load increments, cracks were often observed to branch off of existing cracks. These were only counted if the "branch" formed across at least half of the layer thickness. Some of these formed at very shallow angles to the xy plane. Figure (6.1) shows one such

94

Table 6.2   AS4/3501-6 Material Properties Used in All Analyses

E_l (GPa)	142.0	α_l ($\mu\varepsilon/°C$)	-0.36
E_t (GPa)	9.81	α_t ($\mu\varepsilon/°C$)	28.8
ν	0.30	T_g (°C) [68]	177
G_{lt} (GPa)	6.0	t_{ply} (mm)	0.134

45₄

90₄

-45₈

Figure 6.1   Photomicrograph of edge of $[0_4/45_4/90_4/-45_4]_s$ tensile coupon at 100x magnification. Local delamination propagates from shallow-angle cracks visible in 90_4 layer.

crack. Local delamination propagated from these kinds of cracks at the highest load levels.

Analytical and experimental results for the 45_4 ply group in the mechanically loaded $[0_4/45_4/90_4/-45_4]_s$ specimens are shown in Figure 6.2. Correlation between experiment and analysis is very good. The layer has a small number of cracks before any conditioning. The analysis predicts the onset of extensive cracking nearly perfectly and generally falls within the error bars during crack accumulation. Scatter is relatively low, except in the region where cracking initiates.

The results for the 90_4 ply group in the same laminate are shown in Figure 6.3. The crack density rises to a significantly higher value than in the 45_4 ply group, though both show the same trends. Cracks initiate at a slightly lower load than predicted. The analysis also underpredicts crack density through the entire range of cracking. A slight increase in the slope of the crack data is visible at approximately 30 kN. This load coincides with the first observation of microcracks at very shallow angles during microscopic inspection. Local delamination was observed to propagate from these cracks at higher load increments, as shown in Figure 6.3. The increase in slope also coincides approximately with the onset of cracking in the adjacent 45_4 ply group.

Correlation between experiment and analysis is not as good for the -45_8 layer, shown in Figure 6.4. As predicted, fewer cracks form in this layer than in the 90_4 and 45_4 layers. However, crack initiation occurs at a much higher load than predicted. After the onset of cracking, the analysis captures the cracking trend satisfactorily. A comparison of Figure 6.4 with Figure 6.2 shows that cracking initiates in the middle -45_8 layer at exactly the same load as in the adjacent 90_4 layer. Additionally, an increase in the slope of the

97

C-2

$[0_4/45_4/90_4/-45_4]_s$

45_4 Ply Group

Figure 6.2   Experimental results and analytical predictions of crack density vs. progressive applied load. 45_4 ply group of $[0_4/45_4/90_4/-45_4]_s$ laminate.

$[0_4/45_4/90_4/-45_4]_s$
90_4 Ply Group
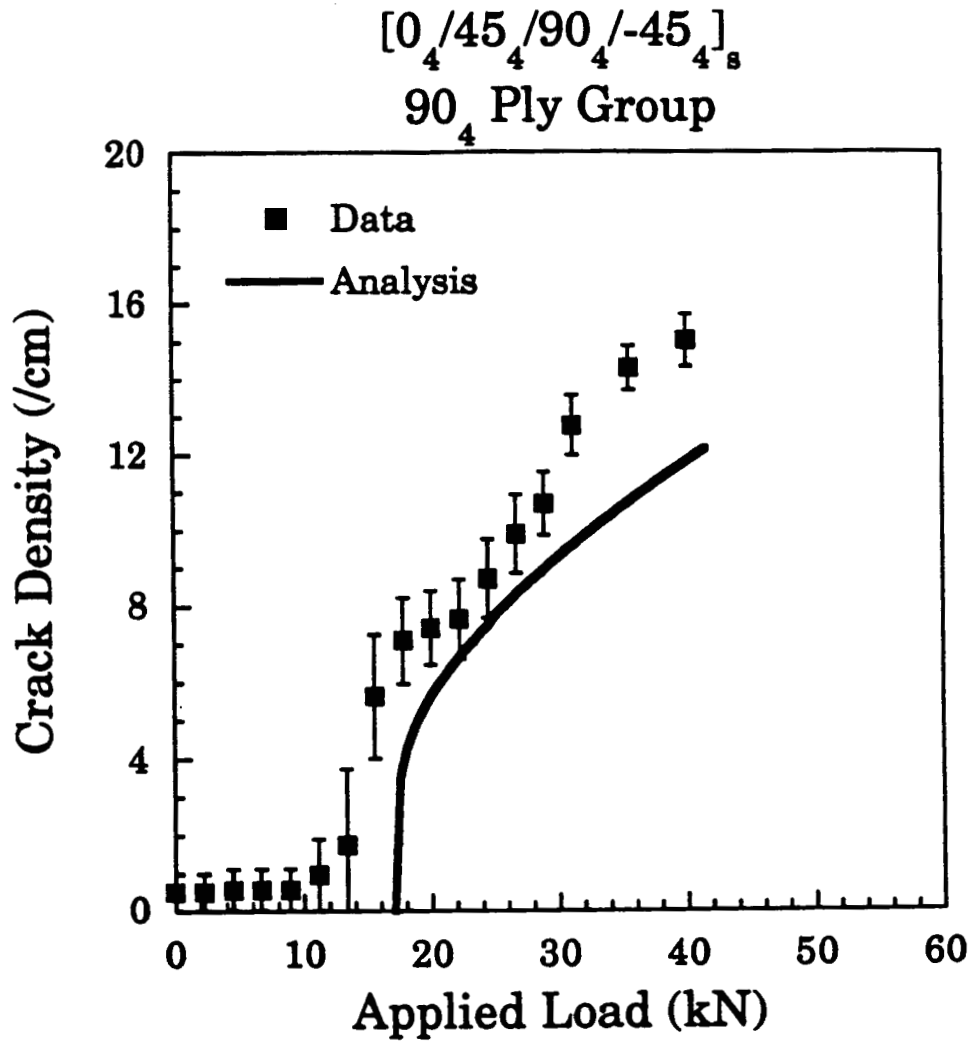
Figure 6.3   Experimental results and analytical predictions of crack density vs. progressive applied load. 90_4 ply group of $[0_4/45_4/90_4/-45_4]_s$ laminate.

99
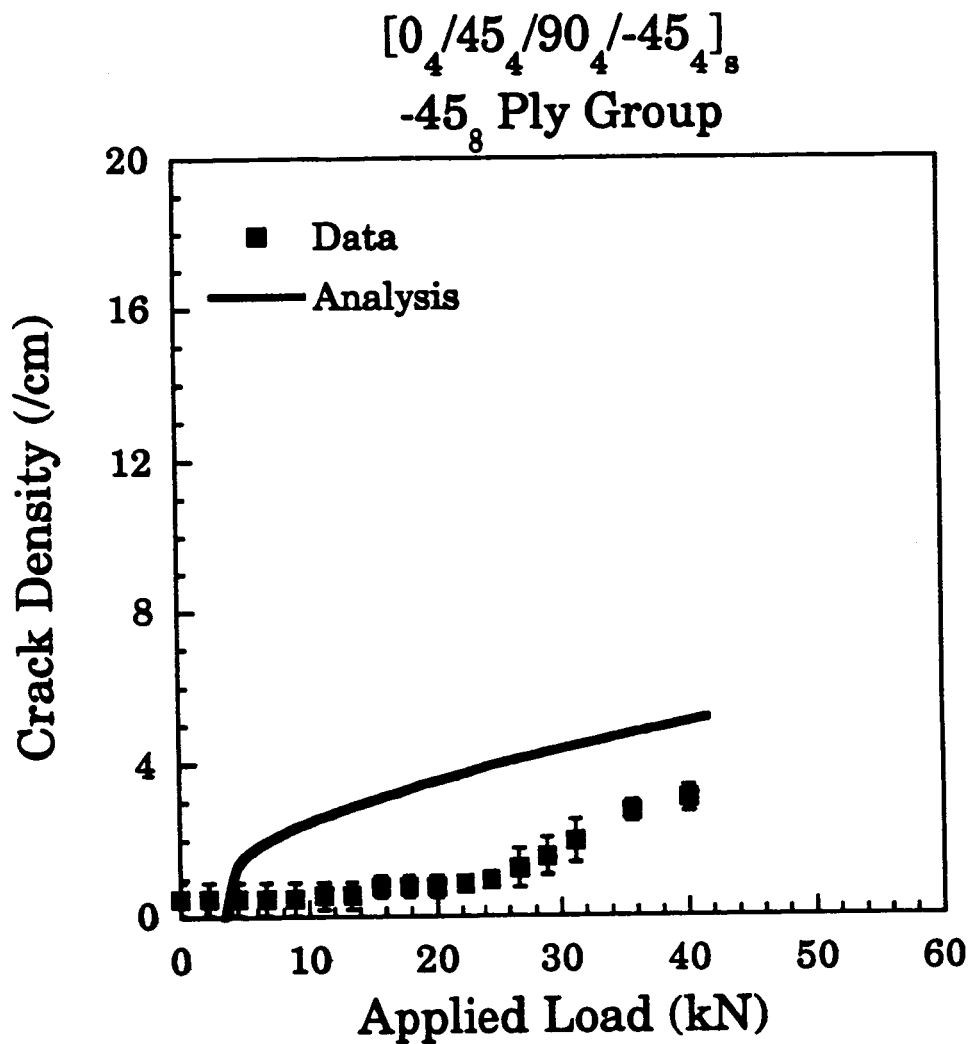
Figure 6.4 Experimental results and analytical predictions of crack density vs. progressive applied load. -45$_8$ ply group of [0$_4$/45$_4$/90$_4$/-45$_4$]$_s$ laminate.

crack density data in the -45$_8$ ply group can be seen at about 27 kN, the load at which cracking initiates in the 45$_4$ ply group.

The applied stress at which cracking occurs in the 16-ply [0$_2$/45$_2$/90$_2$/-45$_2$]$_s$ specimens is double that in the 32-ply specimens. Scatter is relatively high in the region of crack initiation. Once cracking initiates, the predicted and measured crack densities reach much higher values than in the 32-ply [0$_4$/45$_4$/90$_4$/-45$_4$]$_s$ specimens. Anomalous behavior in the [0$_2$/45$_2$/90$_2$/-45$_2$]$_s$ tensile coupons shows nearly identical trends with the [0$_4$/45$_4$/90$_4$/-45$_4$]$_s$ laminate data. This resemblance is readily seen in the 45$_4$ and 90$_4$ layer data in Figure 6.5. The -45$_4$ ply group shows the same middle-layer behavior discussed earlier, shown in Figure 6.6. Crack initiation in this ply group coincides with initiation in the adjacent 90$_4$ layer. A slight increase in the observed crack density slope occurs simultaneously with the onset of cracking in the 45$_4$ layer.

Analytical and experimental correlation for the 60$_2$ layer in the [0$_2$/60$_2$/-60$_2$]$_s$ tensile coupons is shown in Figure 6.7. The analysis captures the onset of cracking but slightly underpredicts the accumulation of cracks. The applied stress at which cracking occurs is comparable to that in the 16-ply [0$_2$/45$_2$/90$_2$/-45$_2$]$_s$ laminates. The middle-layer crack suppression discussed earlier is readily apparent in the -60$_4$ layer data, shown in Figure 6.8. Cracking in this ply group, though predicted at a much lower load, initiates simultaneously with the adjacent layer. After the onset of cracking, the analysis captures the accumulation of cracking nearly perfectly.

6.2.2 Stress-Strain Data

In the present investigation, the first observation of extensive microcracking during edge inspection will be referred to as first ply failure. When the laminates were conditioned at levels above the first-ply-failure
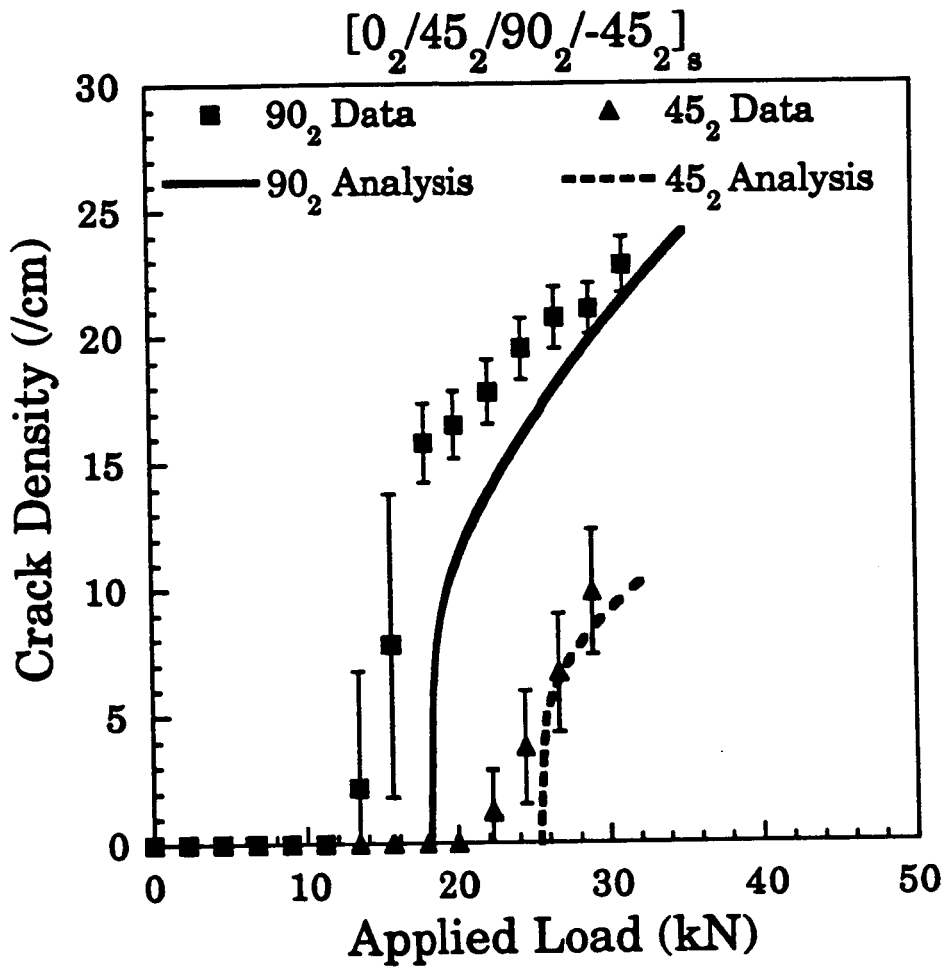
$[0_2/45_2/90_2/-45_2]_s$

Figure 6.5   Experimental results and analytical predictions of crack density vs. progressive applied load. 45_2 and 90_2 ply groups of $[0_2/45_2/90_2/-45_2]_s$ laminate.

$[0_2/45_2/90_2/-45_2]_s$
-45$_4$ Ply Group
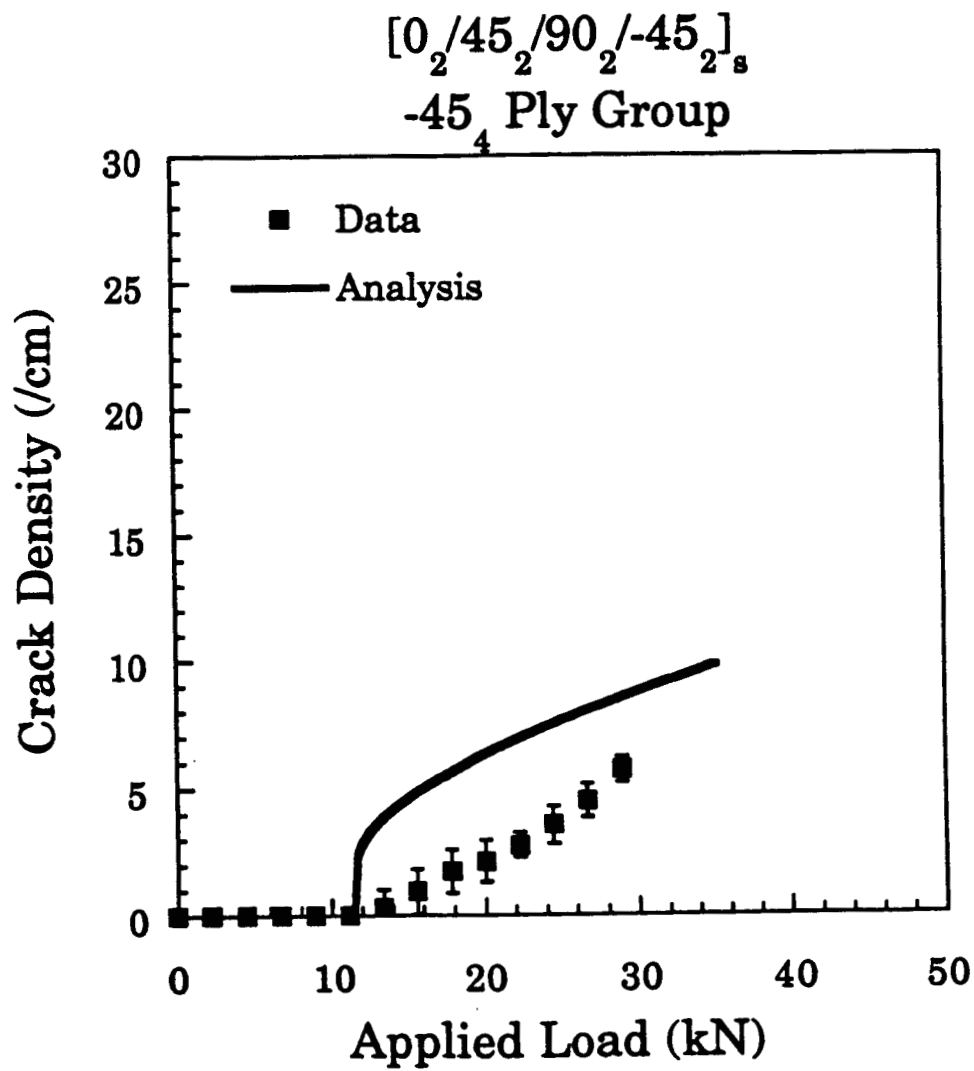
Figure 6.6   Experimental results and analytical predictions of crack density vs. progressive applied load.   -45$_4$ ply group of $[0_2/45_2/90_2/-45_2]_s$ laminate.

$[0_2/60_2/-60_2]_s$
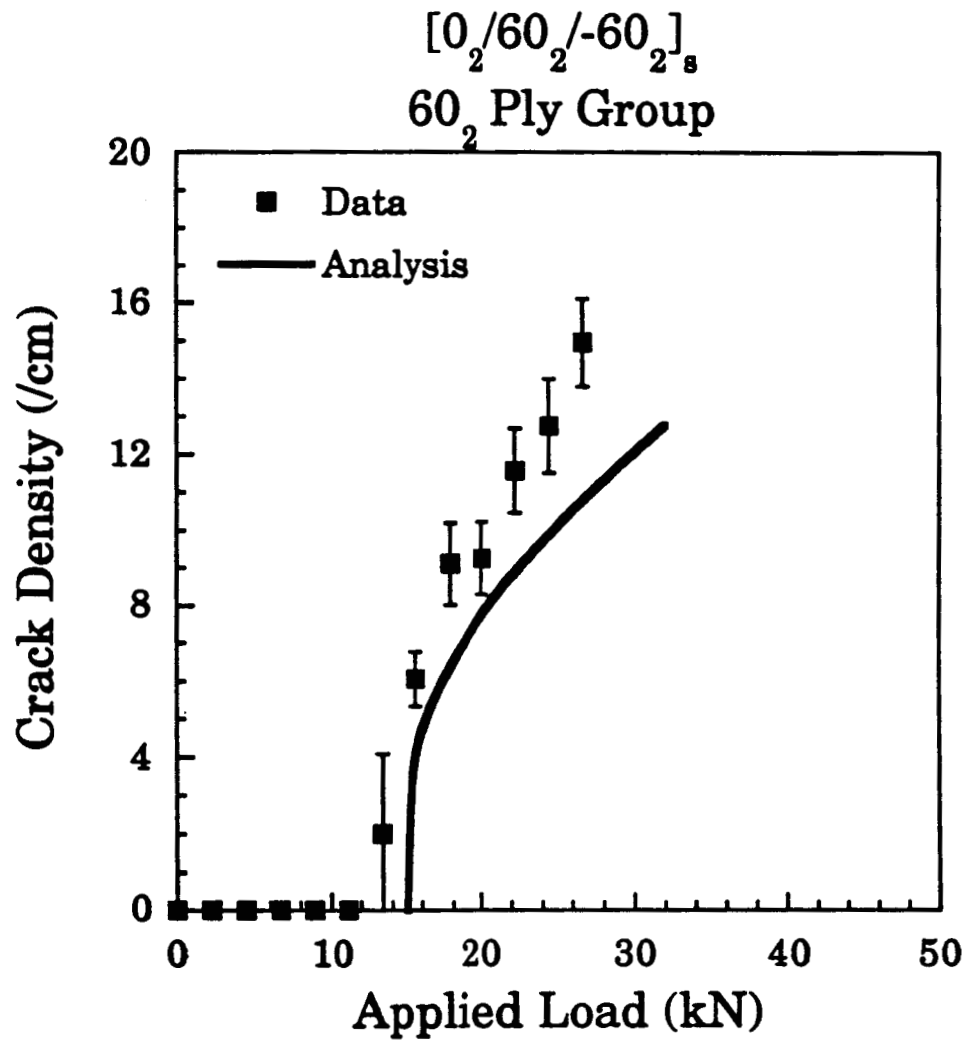
60_2 Ply Group

Figure 6.7 Experimental results and analytical predictions of crack density vs. progressive applied load. 60_2 ply group of $[0_2/60_2/-60_2]_s$ laminate.

$[0_2/60_2/-60_2]_s$

-60_4 Ply Group

Crack Density (/cm) vs. **Applied Load (kN)**

- ■ Data
- — Analysis

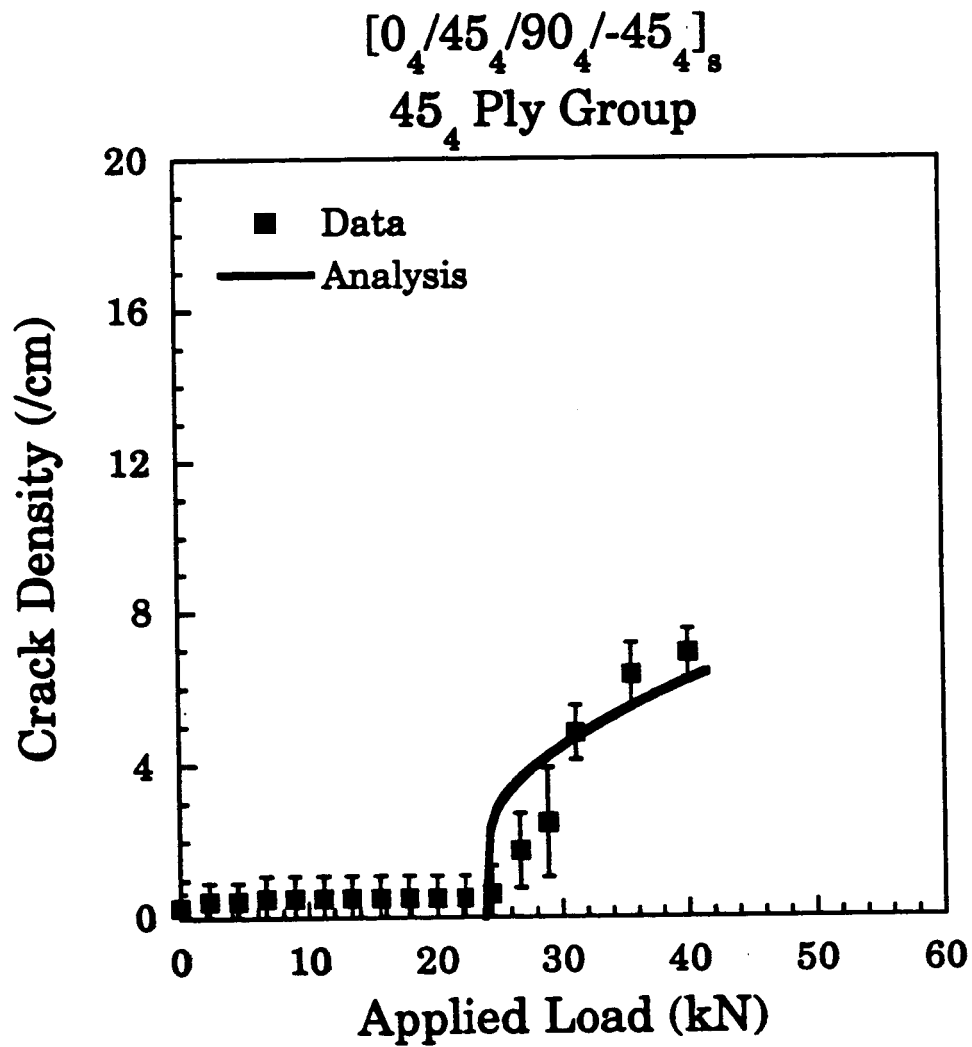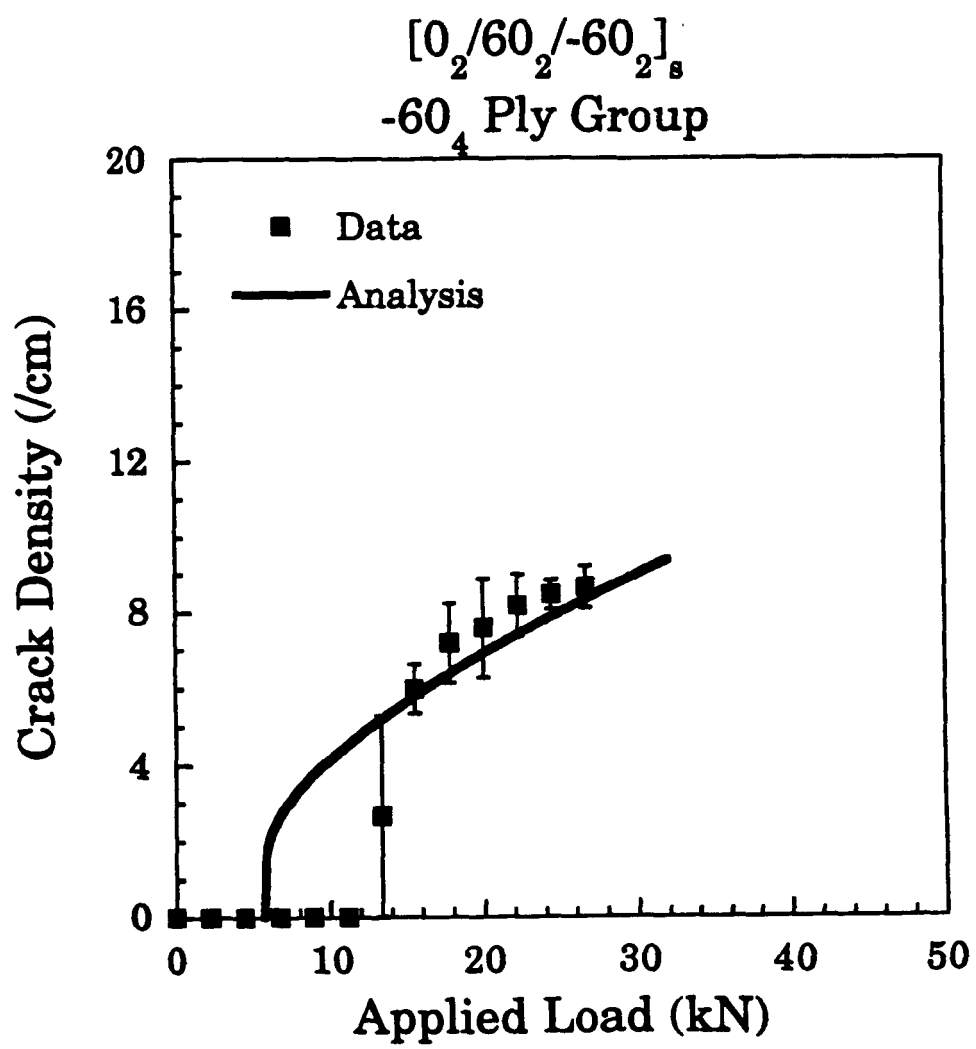Figure 6.8 Experimental results and analytical predictions of crack density vs. progressive applied load. -60_4 ply group of $[0_2/60_2/-60_2]_s$ laminate.

load, cracking and popping noises were clearly audible. These acoustic emissions presumably coincided with the formation of new microcracks. They were only heard when the load exceeded the target load of the previous loading. Reloading to the previous maximum load caused no further cracking or popping noise. This behavior indicates that unloading and reloading to previous target loads had little effect on the internal damage.

The stress-strain curve of the $[0_2/45_2/90_2/-45_2]_s$ tensile coupons loaded to 15.6 kN, below its first-ply-failure load, is shown in Figure 6.9. The loading and unloading paths appear straight and nearly identical. No cracks were observed during edge inspection after unloading. After conditioning this coupon to the next target load, 17.8 kN, extensive cracking was observed during edge inspection, indicating first ply failure. The stress-strain curve for this target load is shown in Figure 6.10.

An abrupt decrease in slope of this stress-strain curve can be seen at 300 MPa, which is the peak stress of the previous load increment, shown in Figure 6.9. The change in slope corresponds to first ply failure and indicates a loss of stiffness due to microcracking. It also coincides with the acoustic emissions described earlier. Superimposing Figures 6.9 and 6.10 shows that the loading region of the stress-strain plot for the 17.8 kN target load has the same slope as both the loading and unloading regions of that for the 15.6 kN target load. The unloading region of the 17.8 kN stress-strain plot has a slightly lower slope than the loading region, indicating a loss of stiffness due to microcracking. All stress-strain curves for target loads where first ply failure was observed may be found in Appendix E. First-ply-failure loads are summarized in Table 6.3.

After first ply failure, subsequent loadings produced cracking and popping noises when the load exceeded the target load of the previous

106

Specimen FA-2M
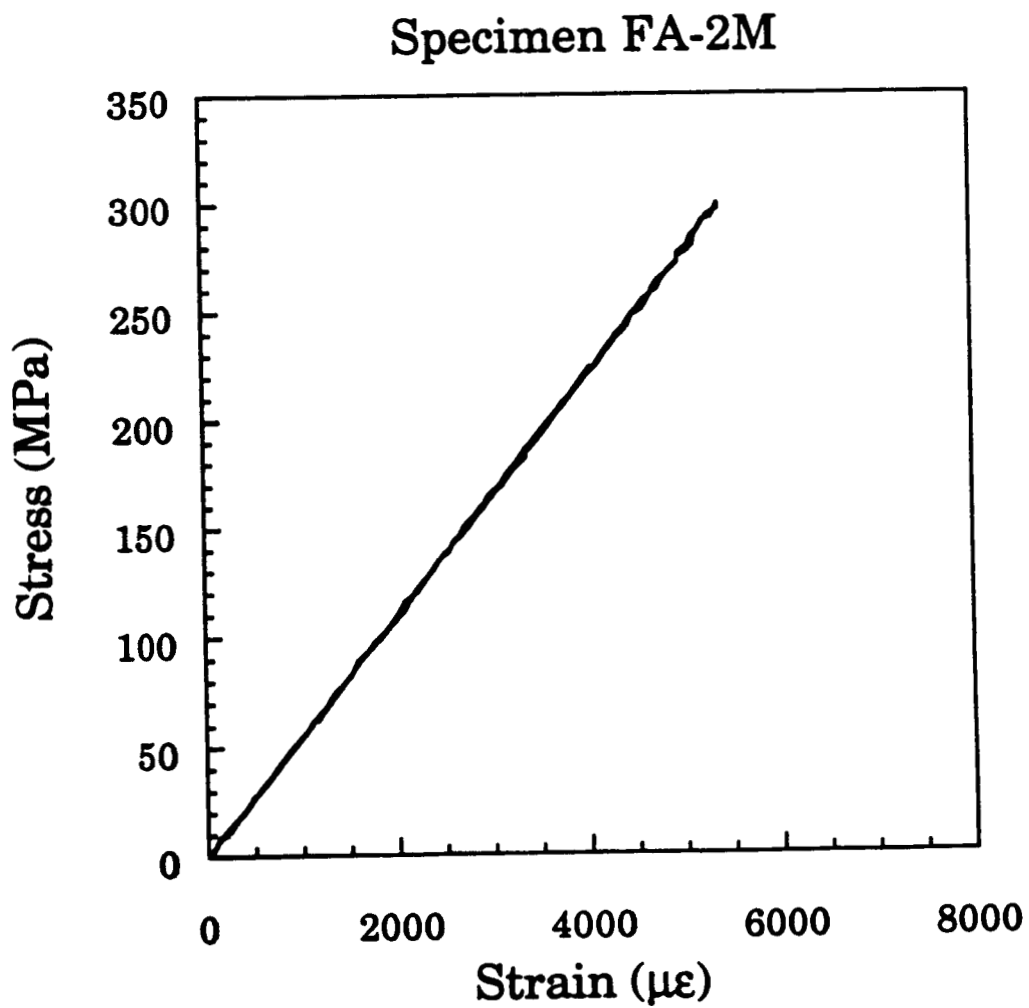
Figure 6.9 Stress-strain plot for FA-2M [0$_2$/45$_2$/90$_2$/-45$_2$]$_s$ tensile coupon progressively loaded to 15.6 kN.

Specimen FA-2M
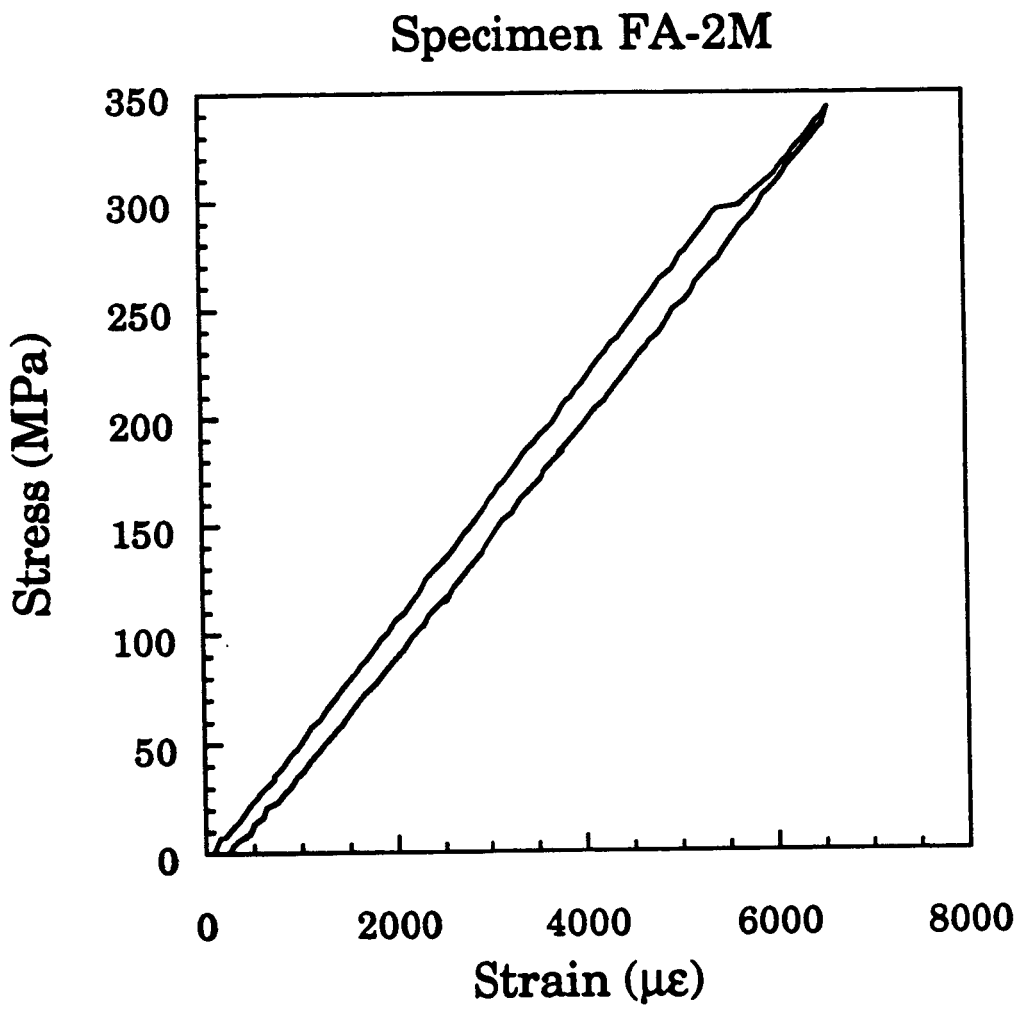
Figure 6.10 Stress-strain plot for FA-2M [0₂/45₂/90₂/-45₂]ₛ tensile coupon progressively loaded to 17.8 kN.

loading. However, no further anomalies were observed in the stress-strain curves during these loadings. All of the stress-strain curves for loadings beyond first ply failure were linear to within the resolution of the data.

6.2.3 Ultimate Failure Stress

Ultimate failure stress data for the three laminate geometries is presented in Table 6.3. The $[0_2/45_2/90_2/-45_2]_s$ specimens failed at an average of 592 MPa with a standard deviation of just 2.77 MPa. The $[0_2/60_2/-60_2]_s$ specimens also had very low variability in failure stress. The failure stresses of the $[0_4/45_4/90_4/-45_4]_s$ coupons varied considerably, however. These failed at an average of 453 MPa with a standard deviation of 40.1 MPa.

It is also significant to note that the failure stress of the $[0_4/45_4/90_4/-45_4]_s$ coupons was 32% lower than that of the $[0_2/45_2/90_2/-45_2]_s$ coupons. The only distinction between the two laminates was layer thickness, which caused their microcracking behavior to be different. Therefore microcracking probably played a significant role in the failure mechanisms, dominating the failure of the $[0_4/45_4/90_4/-45_4]_s$ coupons.

6.3 THERMAL LOADING DATA

6.3.1 Interior vs. Edge Data

As discussed in Section 5.4, some thermal specimens were used to collect interior crack data at various depths. This data was subsequently averaged over the measurement depths. Other thermal specimens were used for edge crack data only. Very little disparity between the interior and edge data is observed. This is in contrast to previous studies [57, 61], where interior and edge data were significantly different, and crack density varied erratically with measurement depth. The interior data in the present work shows very little variation of crack density with depth.

109

Table 6.3   First Ply Failure and Ultimate Failure Data

Laminate	First-Ply-Failure Stress (MPA)		Ultimate Failure Stress (MPa)	
	Average	Standard Deviation	Average	Standard Deviation
$[0_4/45_4/90_4/-45_4]_s$	138	19.3	453	40.1
$[0_2/45_2/90_2/-45_2]_s$	319	38.5	592	2.77
$[0_2/60_2/-60_2]_s$	368	31.5	666	14.2

Cracks observed on the specimen edges and in their interiors had the same appearance as those on the edges of the tensile coupons, described in Section 6.2.1. New cracks were observed to branch from existing cracks following conditioning to the lowest target temperatures. Delamination was never observed during the inspection of thermal specimens.

6.3.2 Crack Density Data and Analytical Correlations

In this subsection, selected correlations between analytical and experimental crack densities are presented. Average measured crack densities are plotted with error bars representing standard deviation. All thermal loading results may be found in Appendix D.

Crack data and predictions for the 45_4 ply group in the thermally loaded $[0_4/45_4/90_4/-45_4]$, interior specimens are shown in Figure 6.11. The interior of this layer is initially uncracked at room temperature. The analysis appears to successfully capture crack initiation. Agreement at lower temperatures as cracks accumulate is also very good. The predicted crack density falls within the error bars at all but the lowest temperature increment, where the analysis slightly overpredicts the amount of cracking. Note that the crack density under thermal loading in this layer is almost the same in magnitude as under mechanical loading, shown in Figure 6.1. The variability is slightly higher in the thermal specimens, however.

The results for the 90_4 ply group in the same laminate are shown in Figure 6.12. The crack density rises to a slightly higher value than in the 45_4 ply group, though both show the same trends. The analysis captures crack densities at the lowest temperature increments. The laminate is initially cracked at room temperature, obscuring the temperature at which cracking initiates. It appears that new cracking initiates at the -73.3°C temperature increment, which the analysis appears to capture fairly well. Thermal

111

$[0_4/45_4/90_4/-45_4]_s$
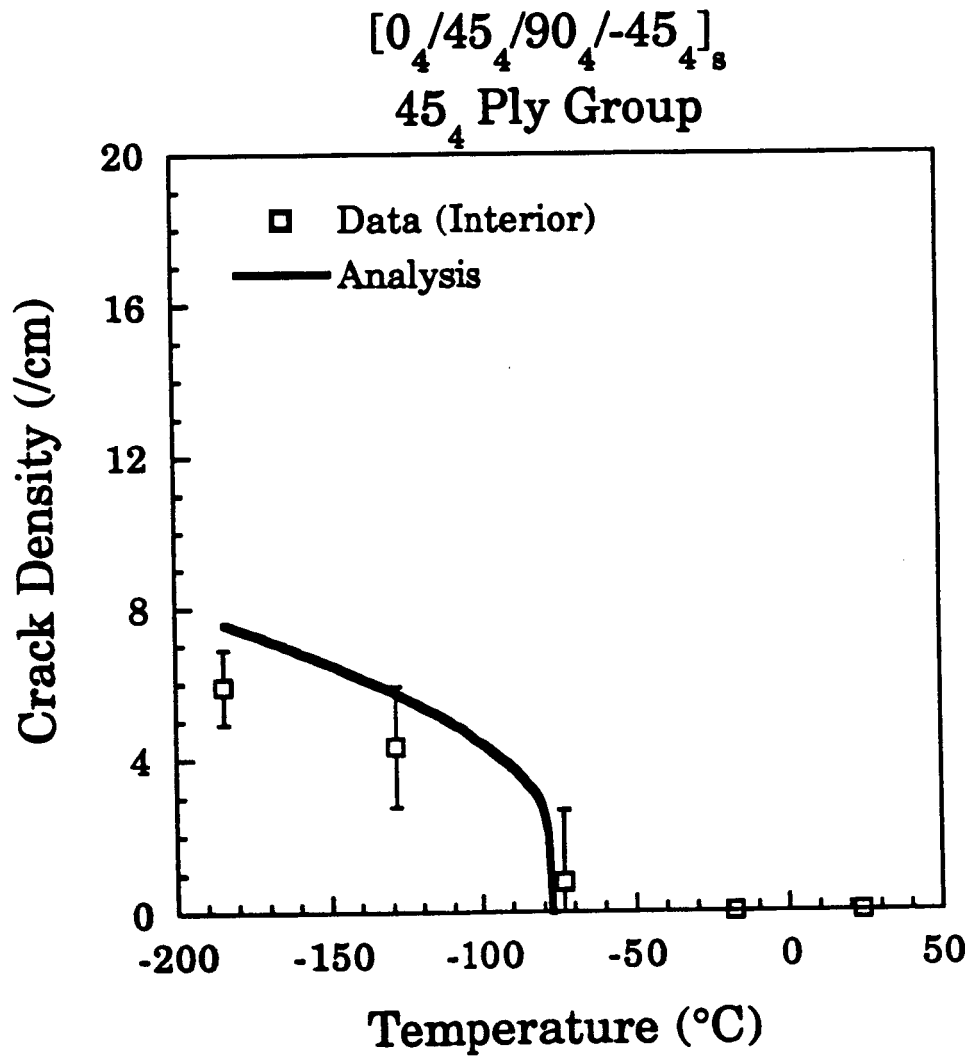
45_4 Ply Group

Figure 6.11 Experimental results and analytical predictions of crack density vs. progressively decreasing temperature. 45_4 ply group of $[0_4/45_4/90_4/-45_4]_s$ interior specimens.

$[0_4/45_4/90_4/-45_4]_s$
90$_4$ Ply Group
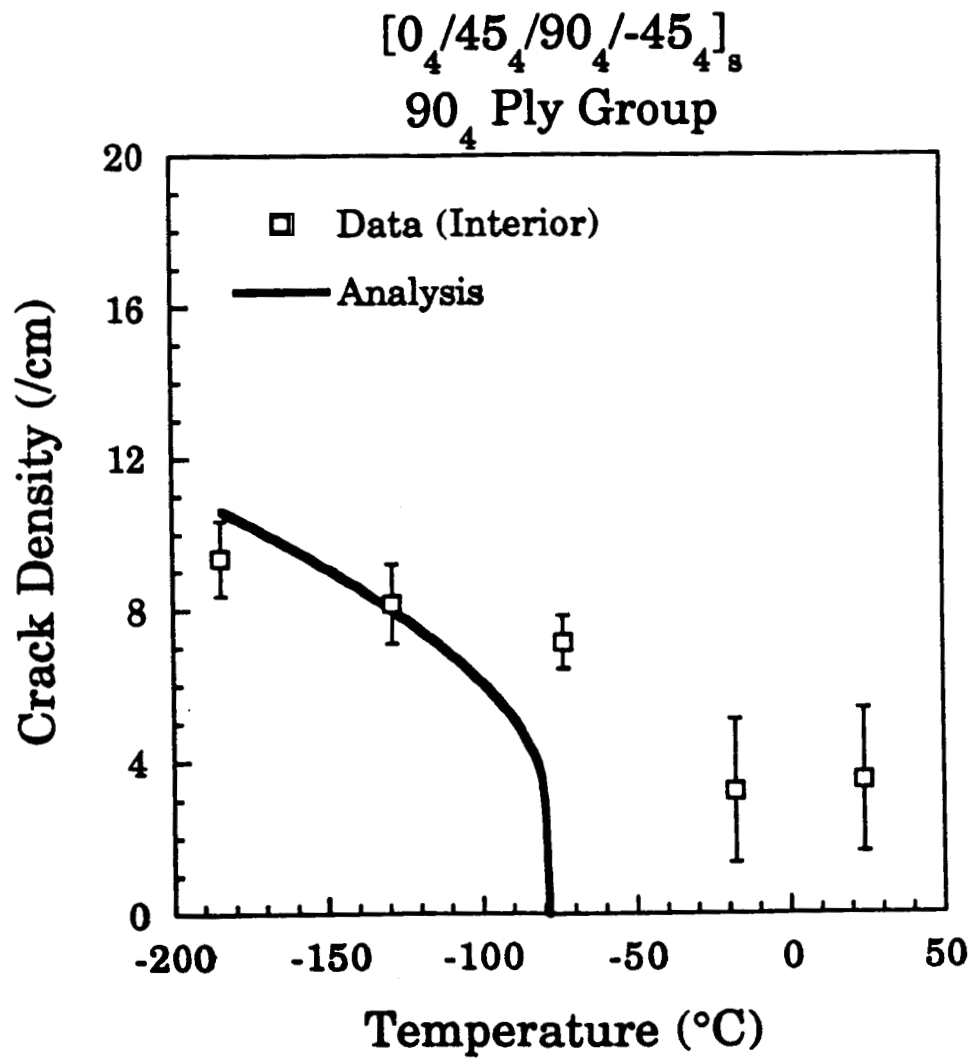
Figure 6.12 Experimental results and analytical predictions of crack density vs. progressively decreasing temperature. 90$_4$ ply group of $[0_4/45_4/90_4/-45_4]_s$ interior specimens.

initiation is more clearly seen in the edge data, shown in Figure 6.13, which is very similar to the interior data but shows fewer initial cracks. The analysis clearly predicts thermal initiation but slightly overpredicts crack density at the lowest temperature increment.

Correlation between analysis and experiment for the -45_8 layer, shown in Figure 6.14, shows the same trends as the mechanical loading results. As predicted, fewer cracks form in this layer than in the 90_4 and 45_4 layers, a result of the thickness effects discussed earlier. The analysis seems to capture crack accumulation well. Further cracking (from the initially cracked state) appears to initiate at $-73.3°C$, the temperature at which extensive cracking was first observed in the adjacent 90_4 layer. However, the temperature at which cracking initiated in the -45_8 layer is difficult to assess, due to the limited number of data points available and the presence of cracks prior to conditioning.

Few cracks are observed in the other two laminates under thermal conditioning. Analytical and experimental correlations for the 90_2 and 45_2 layers in the $[0_2/45_2/90_2/-45_2]_s$ specimens are shown in Figure 6.15. The analysis predicts the onset of cracking in both layers nearly perfectly. Edge data and interior data are similar for both layers. Cracking in the -45_4 ply group of this laminate, shown in Figure 6.16, begins at a lower temperature than predicted. Crack initiation occurs at the same temperature increment as in the adjacent 90_2 layer. Edge and interior data for the -45_4 layer are almost indistinguishable. All crack densities in the $[0_2/45_2/90_2/-45_2]_s$ specimens under thermal loading are significantly lower in magnitude than under mechanical loading.

Experimental results and analytical predictions for the 60_2 and -60_4 layers are presented in Figure 6.17. The analysis predicts cracking in both

114

$$[0_4/45_4/90_4/-45_4]_s$$
$$90_4 \text{ Ply Group}$$
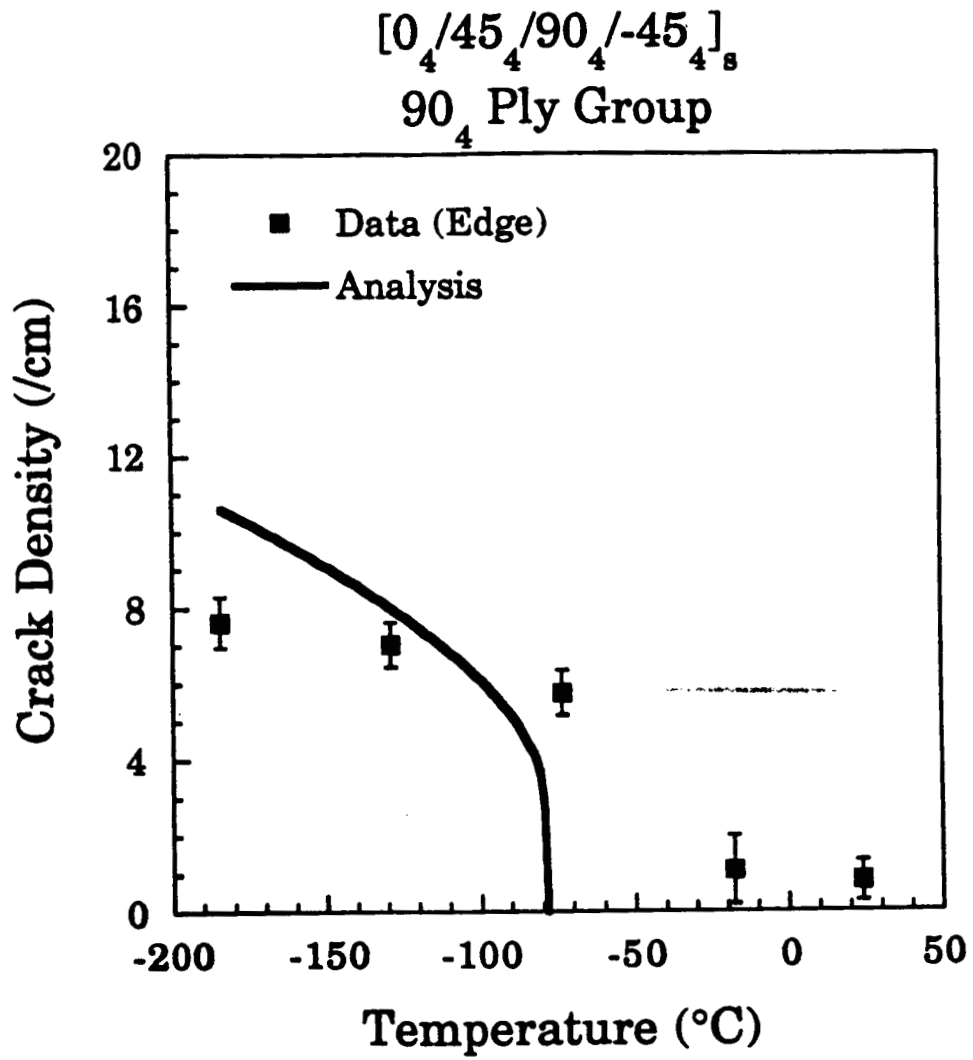
Figure 6.13 Experimental results and analytical predictions of crack density vs. progressively decreasing temperature. 90_4 ply group of $[0_4/45_4/90_4/-45_4]_s$ edge specimens.

$[0_4/45_4/90_4/-45_4]_s$
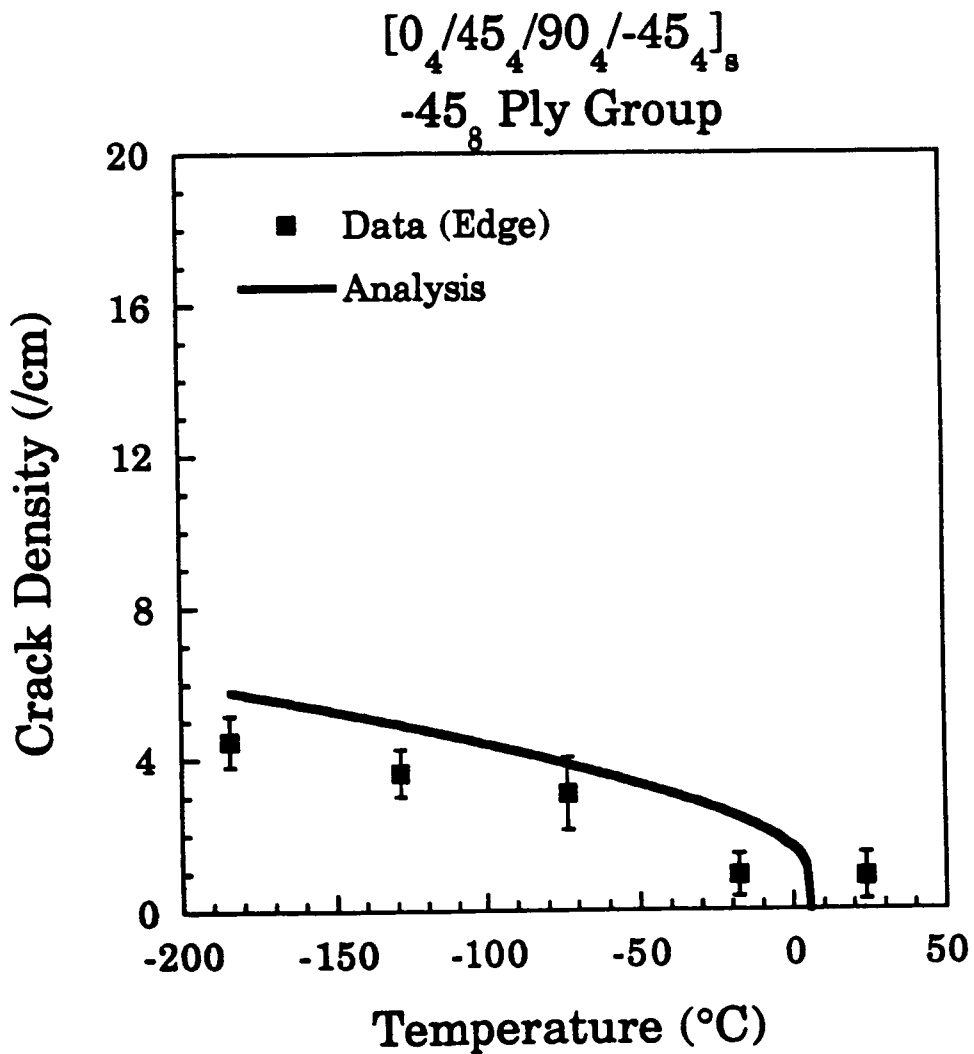
-45_8 Ply Group

Figure 6.14 Experimental results and analytical predictions of crack density vs. progressively decreasing temperature. -45_8 ply group of $[0_4/45_4/90_4/-45_4]_s$ edge specimens.

116
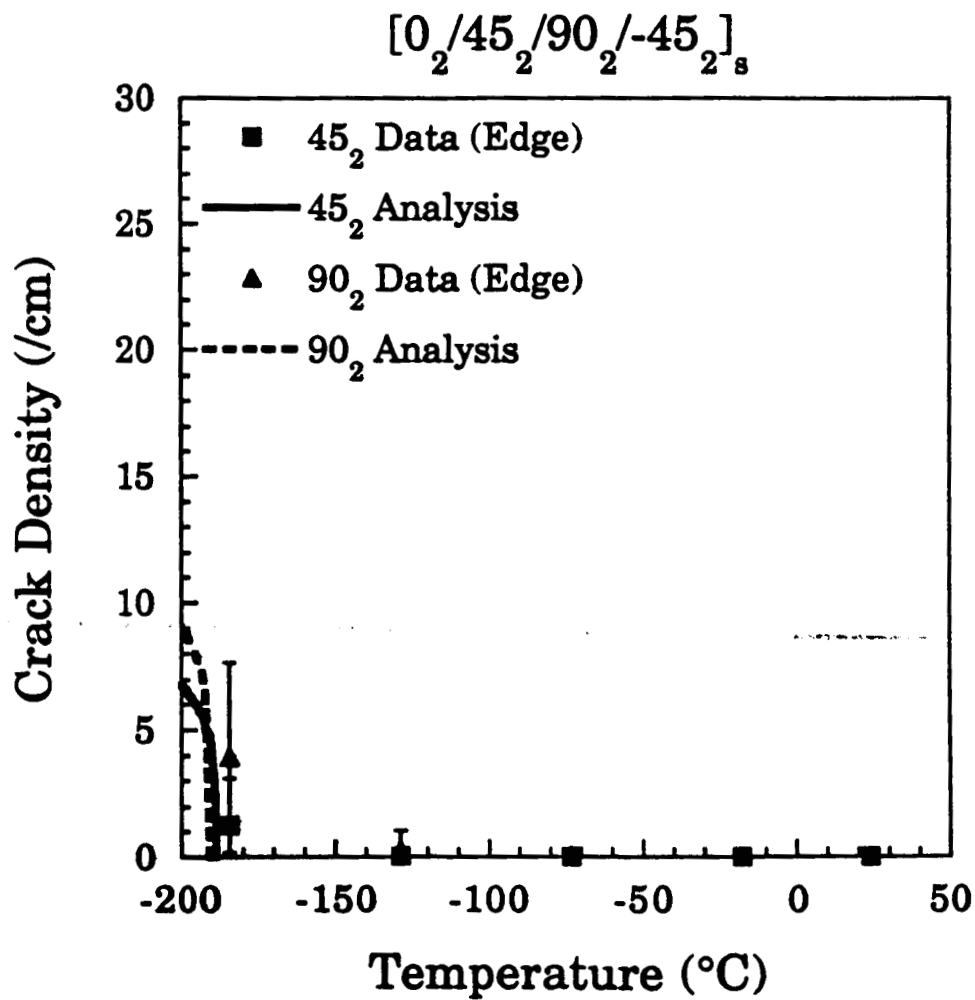
$[0_2/45_2/90_2/-45_2]_s$

Figure 6.15 Experimental results and analytical predictions of crack density vs. progressively decreasing temperature. 90_2 and 45_2 ply groups of $[0_2/45_2/90_2/-45_2]_s$ interior specimens.

$$[0_2/45_2/90_2/-45_2]_s$$
$$-45_4 \text{ Ply Group}$$
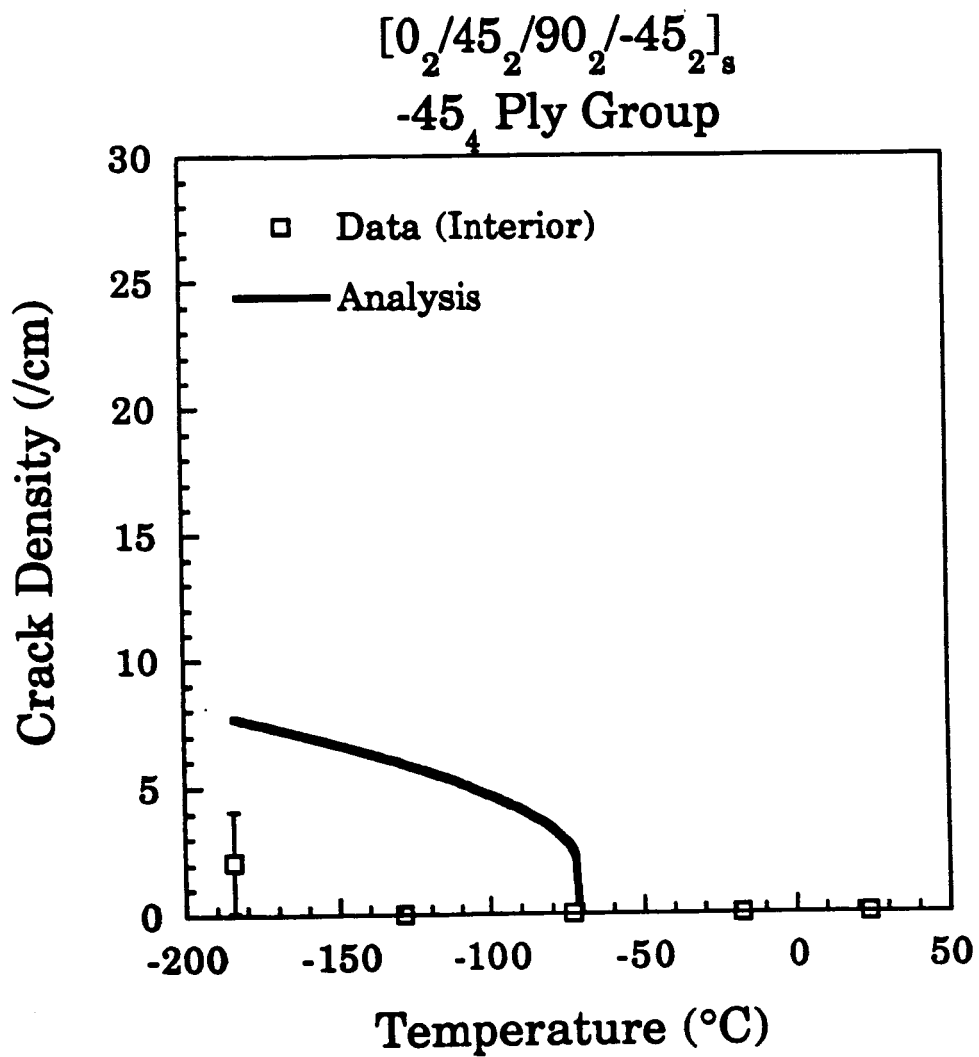
Figure 6.16 Experimental results and analytical predictions of crack density vs. progressively decreasing temperature. -45_4 ply group of $[0_2/45_2/90_2/-45_2]_s$ interior specimens.
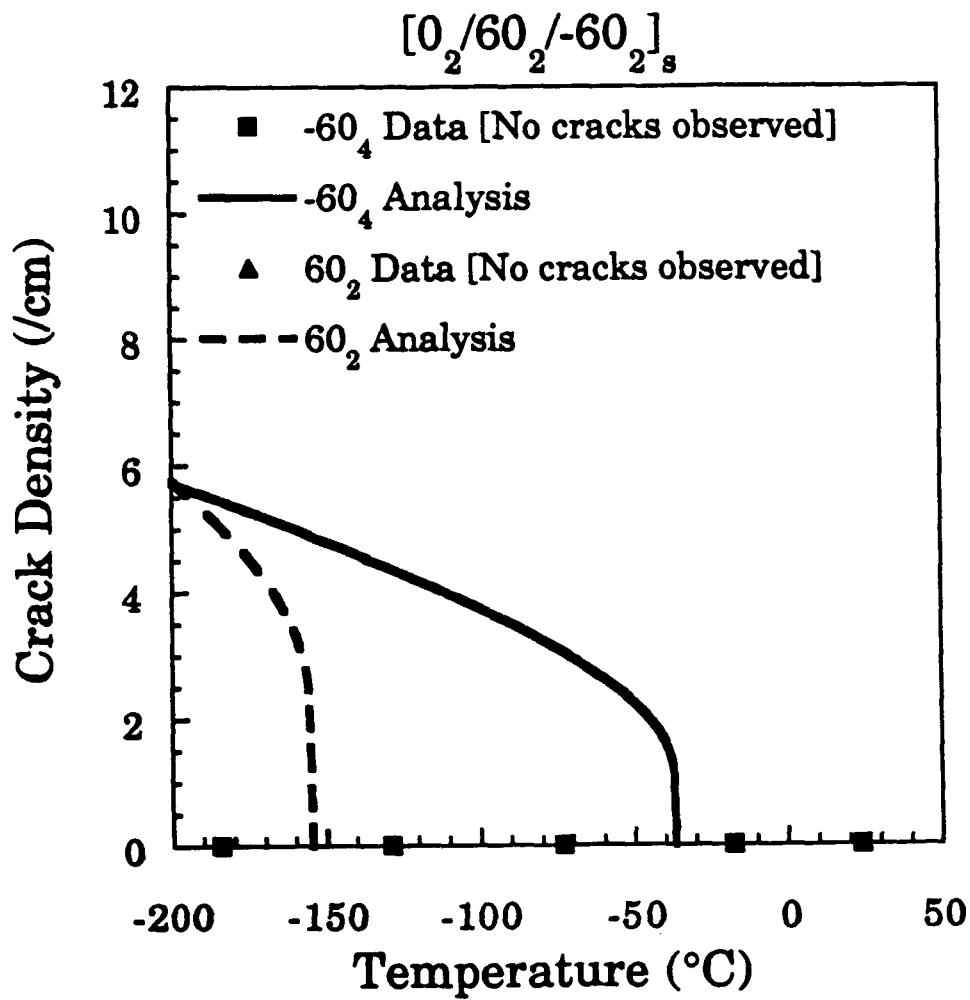
$$[0_2/60_2/-60_2]_s$$

Figure 6.17 Experimental results and analytical predictions of crack density vs. progressively decreasing temperature. -60_4 and 60_2 ply groups of $[0_2/60_2/-60_2]_s$ edge specimens.

layers within the temperature range of the environmental chamber. However, no microcracks are observed in any of the $[0_2/60_2/-60_2]_s$ thermal specimens during progressive cooling. In specimens conditioned to the lowest temperature increment, -184°C, very small microcracks are visible at the interface between the 60_2 and -60_4 layers under 200x magnification. These cracks span much less than half the layer thickness. Since they would have had to span at least half the layer thickness to be counted as microcracks, as per the counting criterion given in Section 5.4.1, these cracks are not included in the crack density data.

6.3.3 Width Effects

Thermal specimens were cut to two different widths, 1.27 mm and 2.54 mm, to investigate width effects. Specimen width does not appear to correlate with any of the observed cracking behaviors. The crack densities measured for both the narrow and wide specimens for each target temperature appear to have very similar distributions. Moreover, internal inspections show that crack density is virtually constant with measurement depth in all interior specimens, regardless of width. Thus no width effects are observed in the present investigation.

6.4 PARAMETRIC STUDY

The sensitivity of the analysis to the input parameters is presented in this section. The parameter under examination is varied while all others are fixed at the values used in the analytical correlations, given in Tables 6.1 and 6.2. The effects of the properties are plotted for the 45_4 layer of a $[0_4/45_4/90_4/-45_4]_s$ laminate.

The effect of longitudinal ply stiffness E_l on predicted crack density curves under mechanical loading is shown in Figure 6.18. Increasing stiffness has the effect of raising the laminate's resistance to microcracking. Crack initiation occurs later, and microcracks accumulate at a lower rate. Under mechanical loading, transverse microcracking in a layer is suppressed by the constraint of adjacent layers. If the adjacent layers are stiffer, they will provide more constraint, explaining the trends in Figure 6.18. Stiffer longitudinal plies also carry more of the applied stress. This lowers the stress in the transverse plies, and fewer microcracks form. Completely different behavior is seen under thermal loading. Here the adjacent layers provide constraint, but in this case the constraint causes mechanical stresses to arise within the laminate when it is exposed to a change in temperature. It is these mechanical stresses which give rise to microcracks. Thus the analysis predicts more cracking as E_l is increased under thermal loading, as shown in Figure 6.19. The analysis is more sensitive to E_l under mechanical loading than thermal loading.

If the transverse ply stiffness E_t is increased, more of the applied mechanical load will be carried by the transverse plies. Under thermal loading, increasing the transverse ply stiffness will raise the stresses due to constrained thermal deformations. As a result, cracking initiates more easily, under both thermal and mechanical loading, when E_t is increased. This effect is predicted by the analyses shown in Figures 6.20 and 6.21. The analysis curve is shifted horizontally with only a very slight change in shape. The sensitivity of the analysis to E_t under both types of loading appears to be about the same.

Similar trends are seen with critical strain energy release rate G_{Ic}. This parameter is a measure of fracture toughness by definition, so one

$[0_4/45_4/90_4/-45_4]_s$
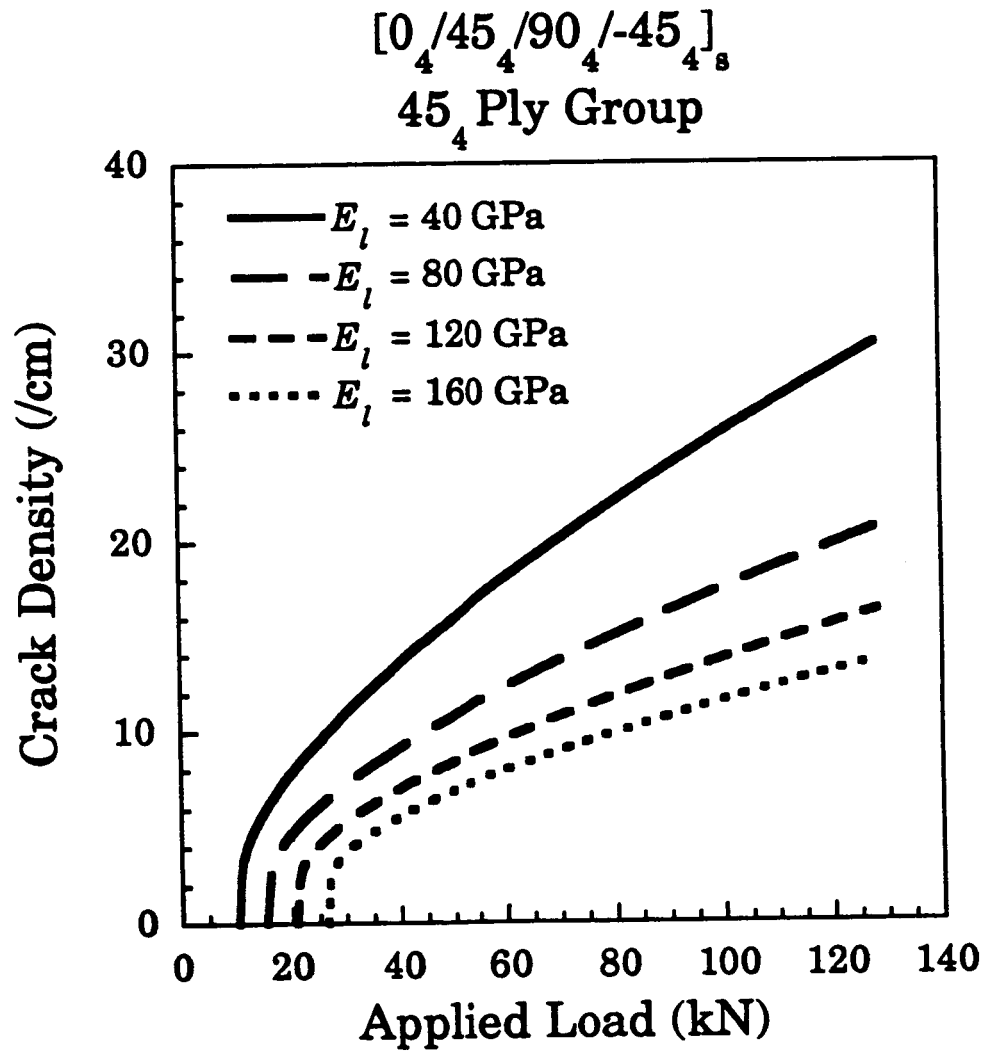
45_4 Ply Group

Figure 6.18   Effects of longitudinal ply stiffness E_l on predicted cracking behavior under mechanical loading. 45_4 ply group of $[0_4/45_4/90_4/-45_4]_s$ laminate.

$[0_4/45_4/90_4/-45_4]_s$
45$_4$ Ply Group

Figure 6.19 Effects of longitudinal ply stiffness E_l on predicted cracking behavior under thermal loading. 45$_4$ ply group of $[0_4/45_4/90_4/-45_4]_s$ laminate.

$[0_4/45_4/90_4/-45_4]_s$
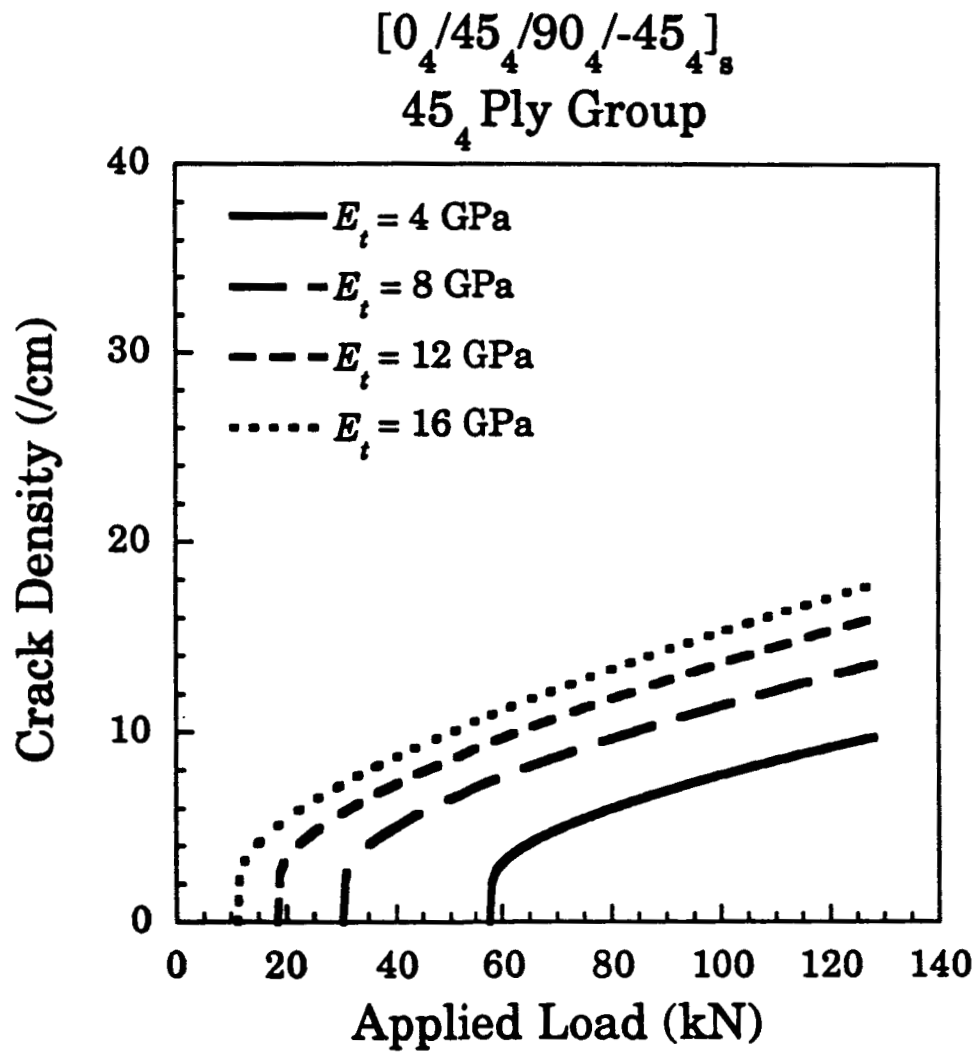
45_4 Ply Group

Figure 6.20 Effects of transverse ply stiffness E_t on predicted cracking behavior under mechanical loading. 45_4 ply group of $[0_4/45_4/90_4/-45_4]_s$ laminate.

$[0_4/45_4/90_4/-45_4]_s$
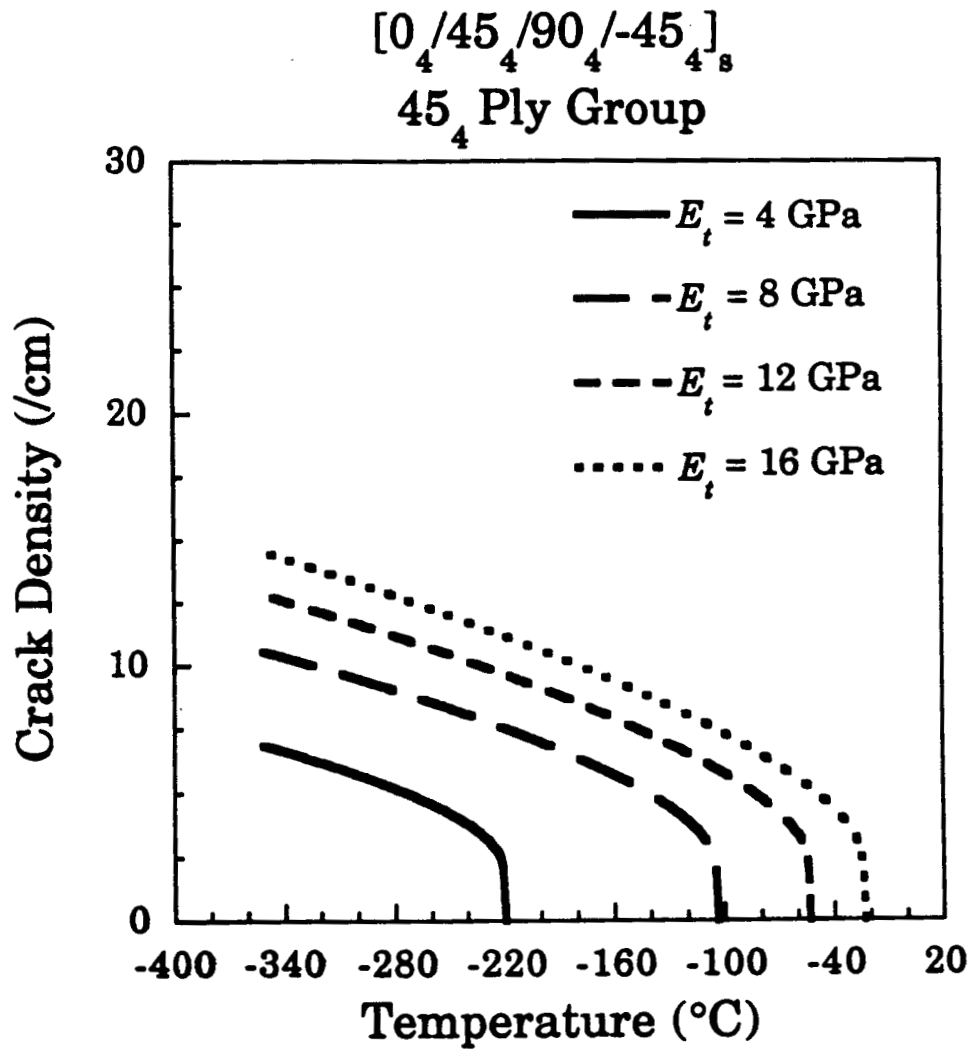
45_4 Ply Group

Figure 6.21   Effects of transverse ply stiffness E_t on predicted cracking behavior under thermal loading. 45_4 ply group of $[0_4/45_4/90_4/-45_4]_s$ laminate.

expects that the laminate's resistance to fracture will rise when G_{Ic} is increased. The analysis curve shifts horizontally, and its shape changes only slightly. Thus cracking initiates at a higher load or lower temperature, but the accumulation of cracks occurs at about the same rate. The effect is the same for mechanical and thermal loading, shown in Figures 6.22 and 6.23, respectively. Note that the analysis in some cases predicts initial cracking at room temperature, due to the $\Delta T = 170°C$ from the stress free temperature.

Layer thickness has an interesting effect on predicted cracking behavior. Predicted crack densities are plotted in Figure 6.24 for the 45_n layer in a $[0_n/45_n/90_n/-45_n]$ laminate as n varies from 1 to 4. There is little difference in the $n=3$ and $n=4$ curves. However, decreasing n to 1 increases the initiation load significantly. The rate at which cracks accumulate increases significantly as n is decreased. The crack density curve shifts horizontally, and its shape changes as well. The same trends are seen under progressive cooling, shown in Figure 6.25.

Figures 6.26 and 6.27 show the effect of varying the shear lag parameter ζ. Increasing ζ delays the onset of cracking. The slope of the crack density curve is increased, so cracks accumulate at a higher rate. This effect is similar to the effect of decreasing the layer thickness, and it is observed under both thermal and mechanical loading.

6.5 DISCUSSION

In this section, the results and correlations presented in Sections 6.1 through 6.3 will be discussed. The assumptions used to derive the analysis will be critically examined.

$$[0_4/45_4/90_4/-45_4]_s$$
$$45_4 \text{ Ply Group}$$
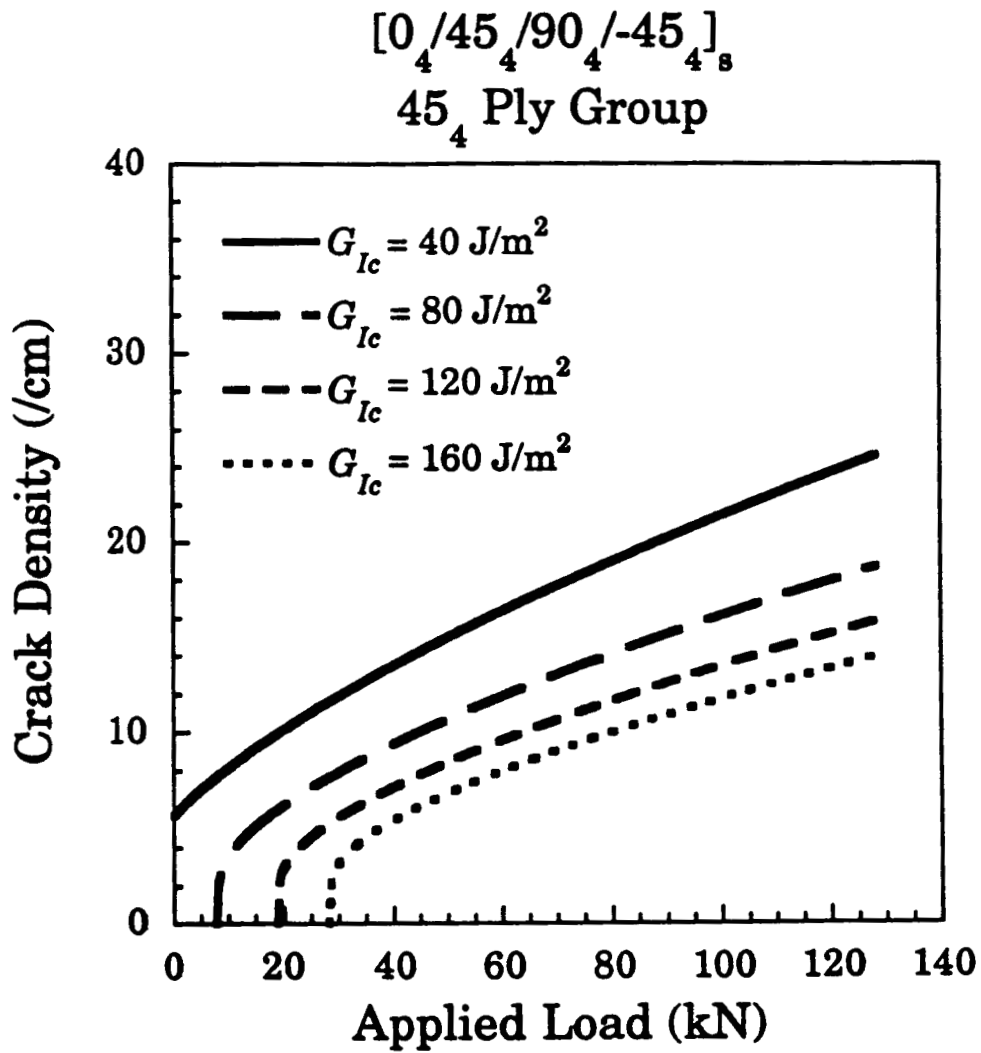
Figure 6.22   Effects of critical strain energy release rate G_{Ic} on predicted cracking behavior under mechanical loading. 45_4 ply group of $[0_4/45_4/90_4/-45_4]_s$ laminate.

$[0_4/45_4/90_4/-45_4]_s$
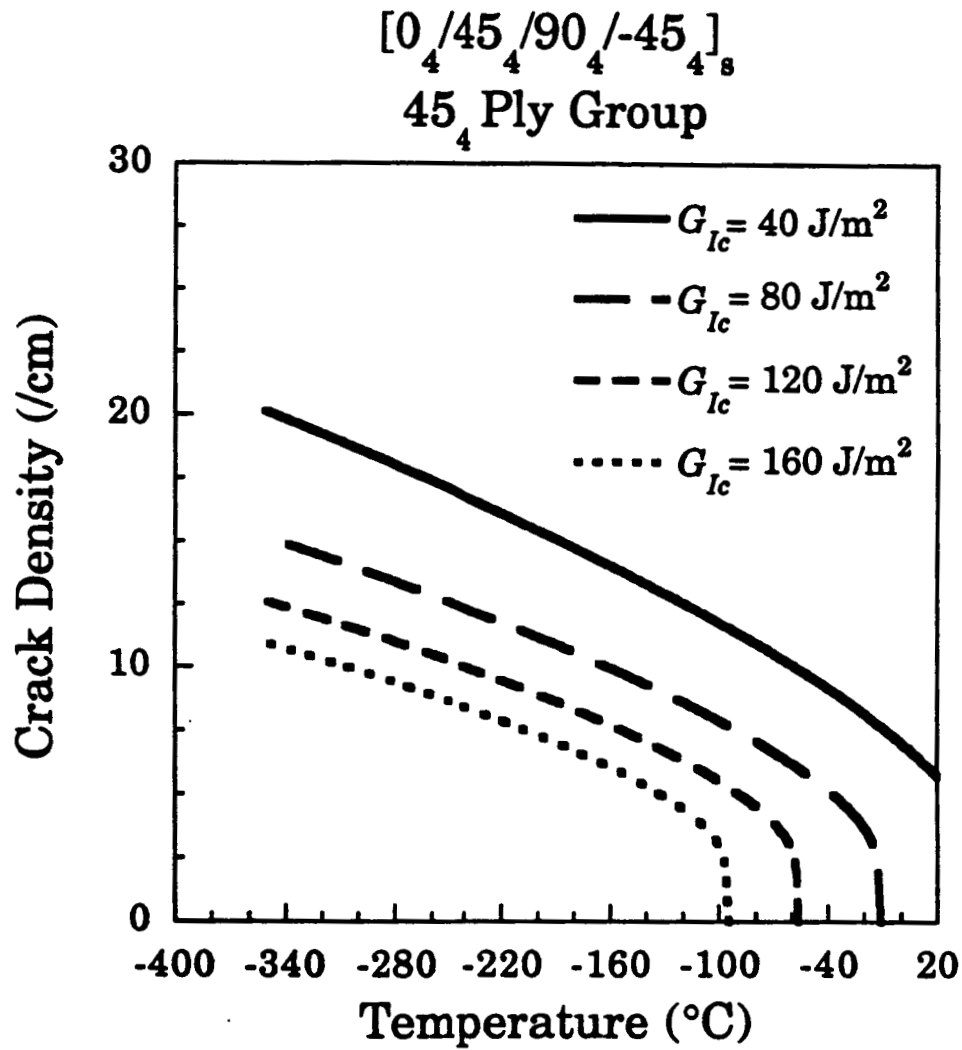
45_4 Ply Group

Figure 6.23 Effects of critical strain energy release rate G_{Ic} on predicted cracking behavior under thermal loading. 45_4 ply group of $[0_4/45_4/90_4/-45_4]_s$ laminate.

128

$$[0_n/45_n/90_n/-45_n]_s$$
$$45_n \text{ Ply Group}$$
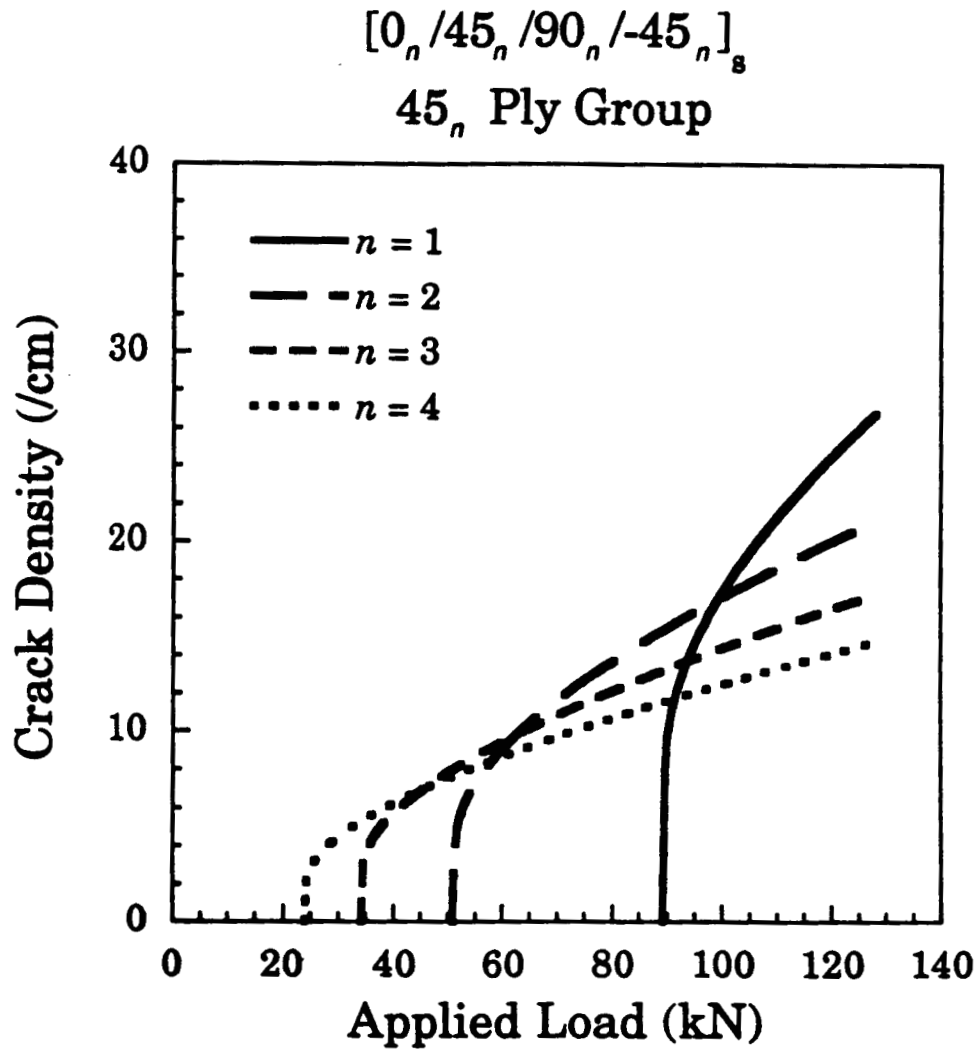
Figure 6.24 Effects of layer thickness on predicted cracking behavior under mechanical loading. 45_n ply group of $[0_n/45_n/90_n/-45_n]_s$ laminate.

$$[0_n/45_n/90_n/-45_n]_s$$
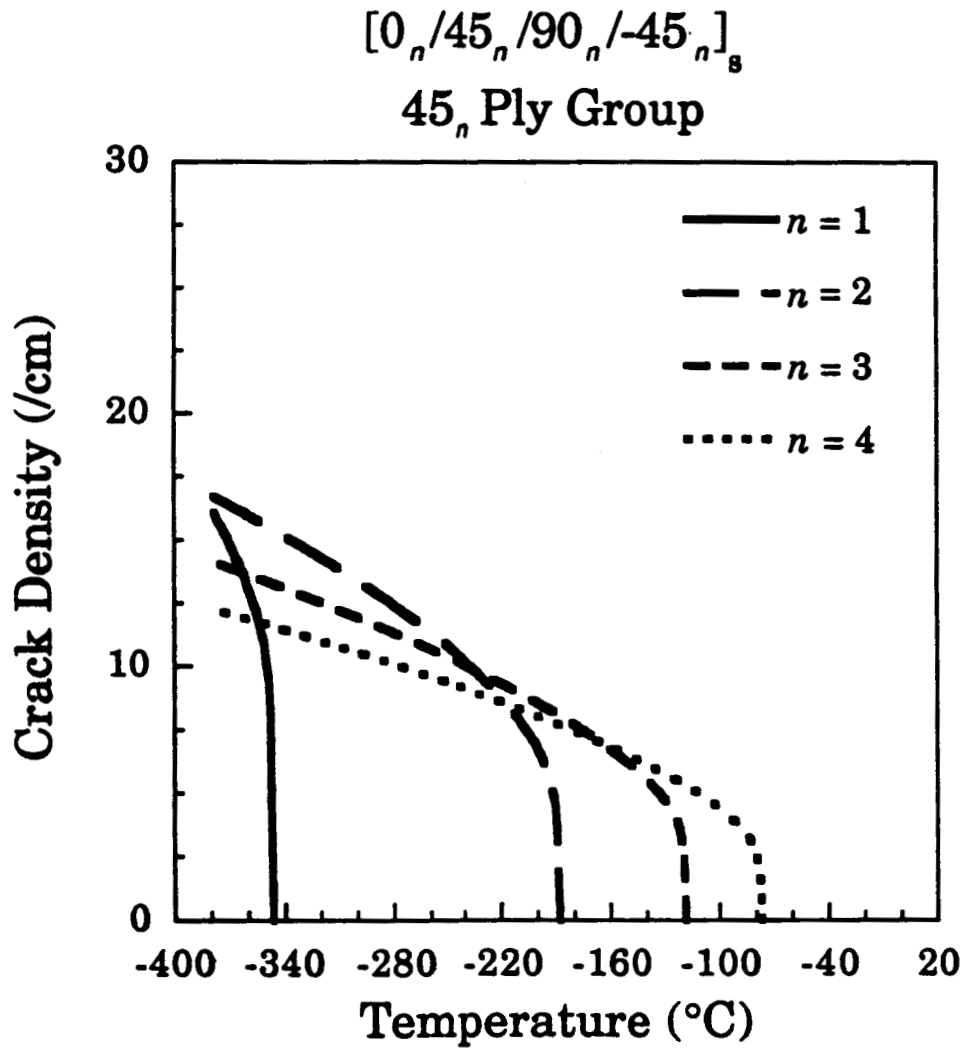
$$45_n \text{ Ply Group}$$

Figure 6.25   Effects of layer thickness on predicted cracking behavior under thermal loading. 45_n ply group of $[0_n/45_n/90_n/-45_n]_s$ laminate.

$$[0_4/45_4/90_4/-45_4]_s$$
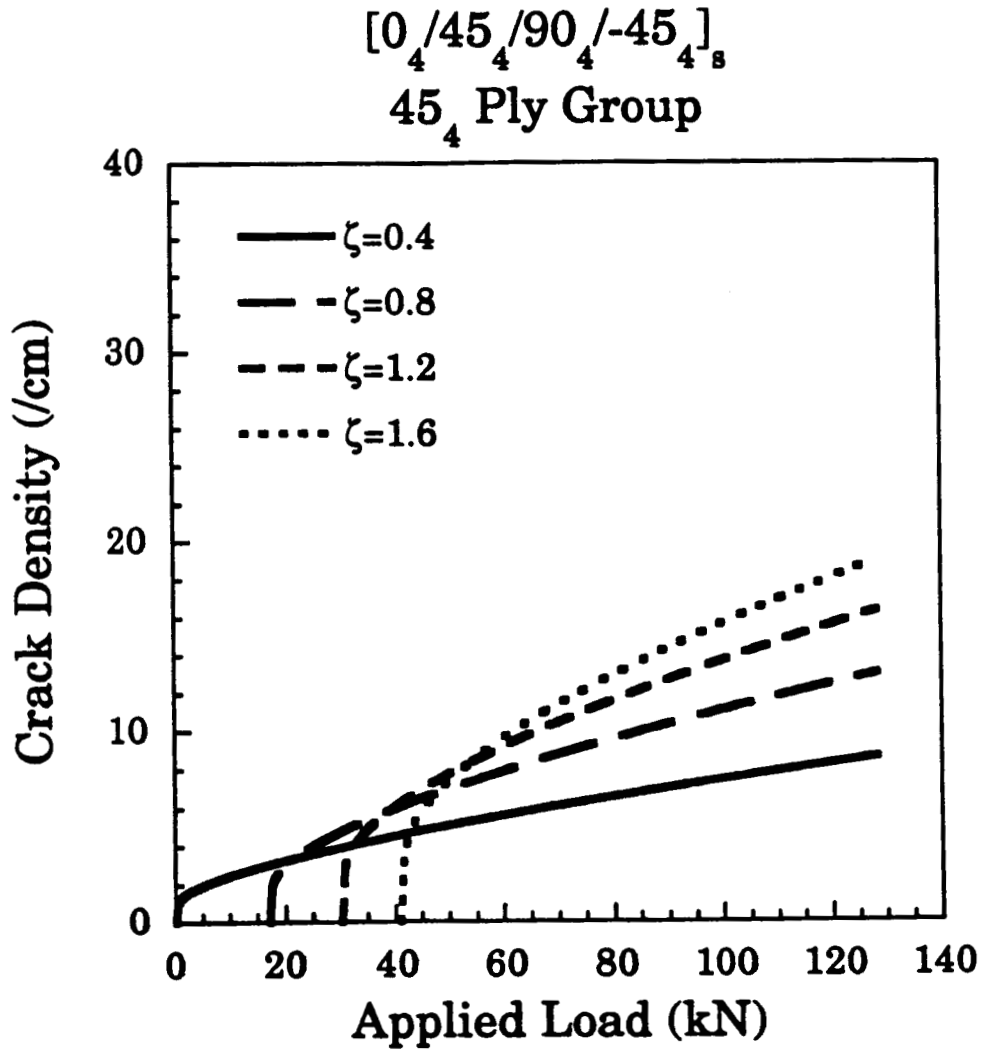
$$45_4 \text{ Ply Group}$$

Figure 6.26   Effects of shear lag parameter ζ on predicted cracking behavior under mechanical loading. 45_4 ply group of $[0_4/45_4/90_4/-45_4]_s$ laminate.

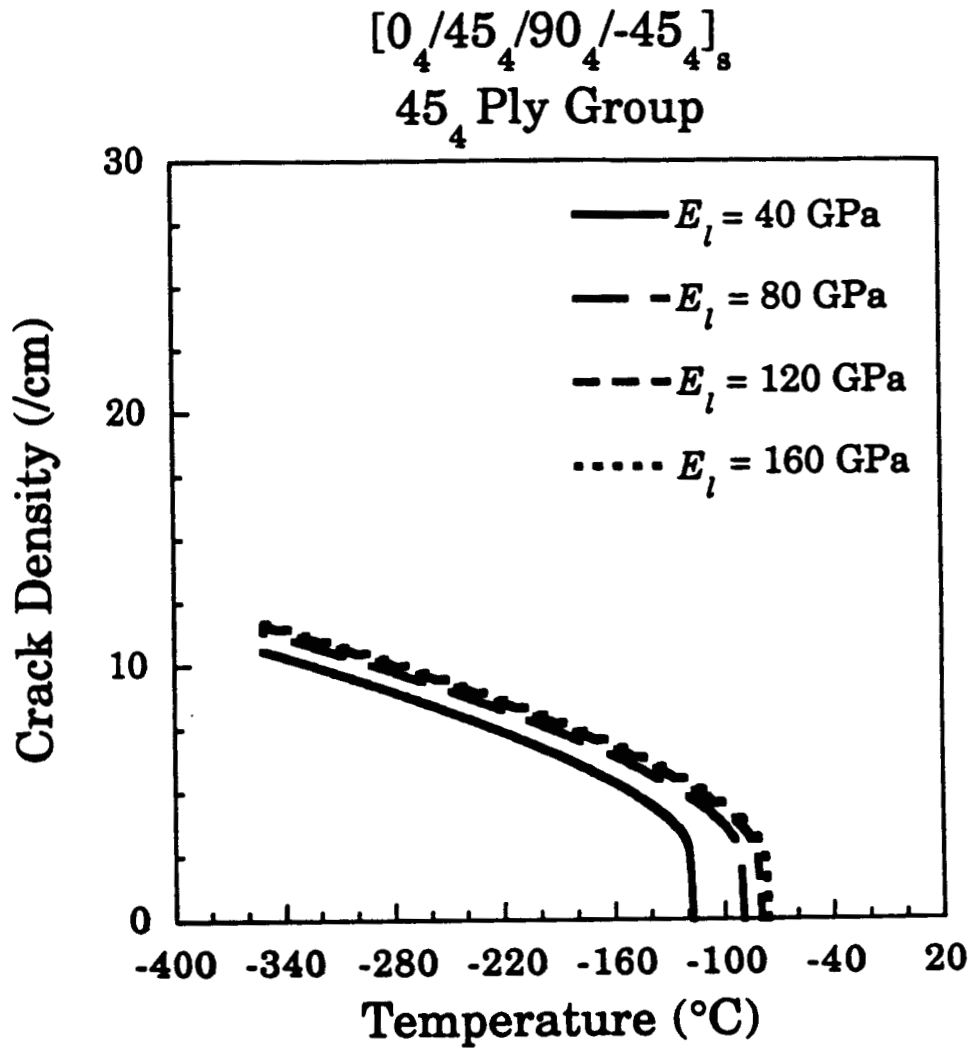$$[0_4/45_4/90_4/-45_4]_s$$
$$45_4 \text{ Ply Group}$$
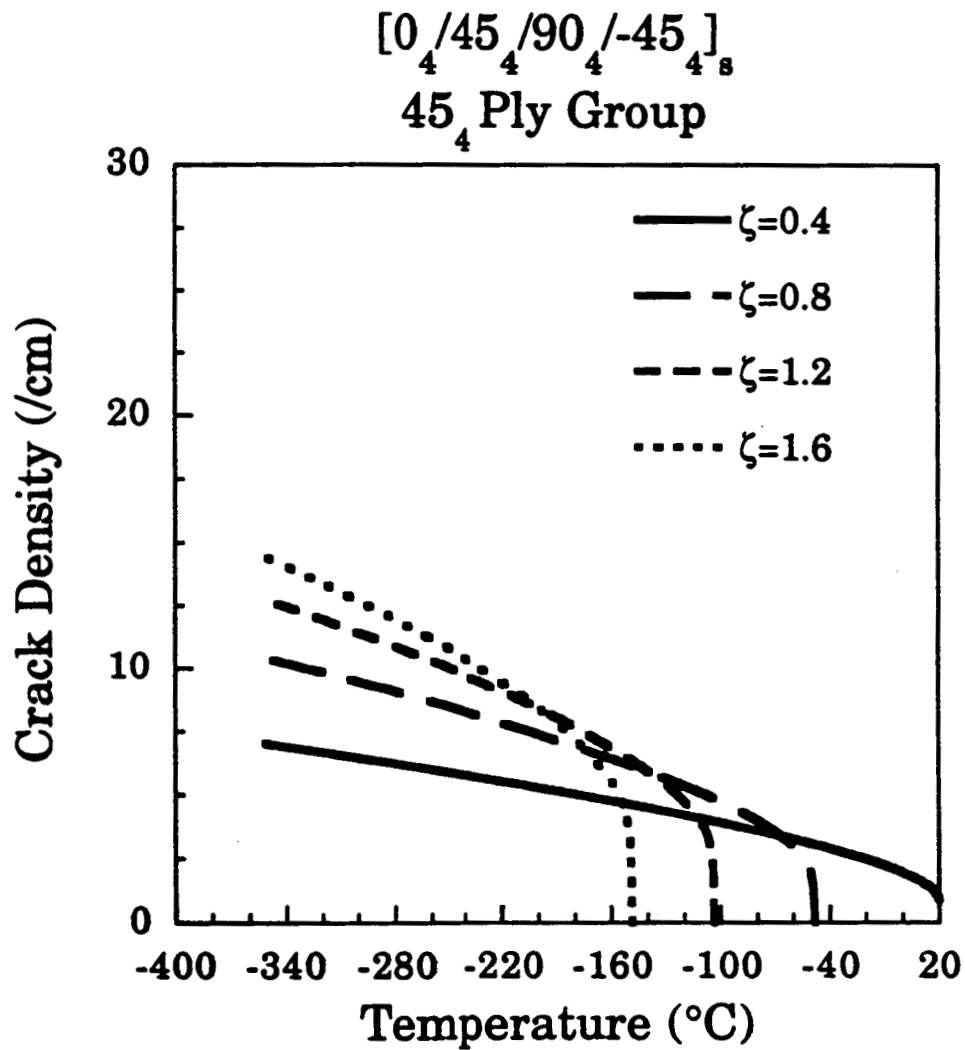
Figure 6.27   Effects of shear lag parameter ζ on predicted cracking behavior under thermal loading. 45_4 ply group of $[0_4/45_4/90_4/-45_4]_s$ laminate.

6.5.1 Data Fit

The fact that the fitted G_{Ic} and ζ values for the $[0_4/45_4/90_4/-45_4]_s$ and $[0_2/45_2/90_2/-45_2]_s$ laminates are nearly identical is a strong indication that G_{Ic} and ζ are independent of layer thickness. The shear lag parameter found for the $[0_2/60_2/-60_2]_s$ specimens is the same as that for the $[0_2/45_2/90_2/-45_2]_s$ specimens. Thus ζ appears to be insensitive to laminate geometry. The fitted G_{Ic} value for the $[0_2/60_2/-60_2]_s$ data shows only a slight disagreement with that for the $[0_4/45_4/90_4/-45_4]_s$ and $[0_2/45_2/90_2/-45_2]_s$ data.

The value of G_{Ic} fit to the thermal data from the $[0_4/45_4/90_4/-45_4]_s$ specimens agrees well with the value fit to all data. The shear lag parameter fit to the thermal data was significantly lower than that fit to all data. This is due to the fact that cracks were observed to accumulate at a slightly lower rate with thermal conditioning. This may indicate temperature dependence of the shear lag parameter, which is a function of the layer moduli. However, as the crack density data used for this fit was limited to a single laminate with relatively few data points, the results of the thermal data fit are inconclusive.

The G_{Ic} and ζ values found by fitting to data from the individual layups in the present study show very little variation. The data shown here supports the view that the critical strain energy release rate and shear lag parameter are material properties, although they may be temperature dependent. This justifies the subsequent use of the same G_{Ic} and ζ values for all analyses.

6.5.2 Crack Density Results and Correlations

Nearly all of the $[0_4/45_4/90_4/-45_4]_s$ tensile coupons and thermal specimens have cracks in some layers at room temperature prior to any thermal or mechanical conditioning. The analysis predicts this laminate to

be uncracked at room temperature following cure. A possible explanation for this is that the laminates were cooled too quickly at the end of the cure cycle. They may also have incurred damage when cut into individual specimens. These explanations are supported by the fact that the crack density of these specimens remains unchanged for several load or temperature excursions. If crack initiation due to thermomechanical loading had been reached at room temperature, one would expect further cracking in these specimens after the first loading. Furthermore, the load or temperature at which further cracking from this initially damaged state is observed usually coincides with predicted initiation.

Decreasing the thickness of the cracking layer has an effect seen in the crack density data of the present study and in many other investigations. The layer appears to become more resistant to cracking, since initiation is delayed to a lower temperature or higher applied load. Decreasing the layer thickness *increases* the rate at which cracks accumulate after initiation, as shown by the parametric study in Section 6.4.

Very little difference was observed between the crack density data collected from the interiors and edges of the thermal specimens. Crack density was virtually constant across all measurement depths in the interior specimens. Moreover, width effects did not appear to be significant. These observations are consistent with one of the most important assumptions of the analytical model, that cracks are continuous through the specimen width.

In every laminate in the present investigation, the onset of cracking in the middle ply group coincides with crack initiation in adjacent layers. This phenomenon is clearly visible under mechanical loading; thermal results were less conclusive. One of the key assumptions of the analytical model is that critical starter cracks exist in the cracking layer from which new cracks

134

may nucleate. These defects should be on the order of one ply group thickness in extent. In the thicker middle layers, this starter-crack condition may not satisfied until the adjacent layer cracks. Then cracks in the adjacent layer cause local stress concentrations which act as effective starter cracks.

There appears to be a correlation between the first observation of shallow-angle microcracks in the 90_4 ply group of the $[0_4/45_4/90_4/-45_4]_s$ tensile coupons and the abrupt increase in slope of the cracking data. As shown in Figure 6.3, local delamination later propagated from these cracks. Thus the appearance of the shallow-angle cracks may have coincided with the onset of other damage modes, particularly delamination. The change in slope may also be explained by the fact that it coincides with crack initiation in the adjacent 45_4 ply group. The microcracks in the 45_4 layer cause local stress concentrations at the interface between the ply groups. These may behave as initiation sites for both further cracking in the 90_4 layer and delaminations between the ply groups. Similar behavior is observed in the $[0_2/45_2/90_2/-45_2]_s$ tensile coupons. The rate of cracking in the -45_4 ply group increases slightly at the load increment where cracking initiates in the 45_2 ply group.

The two behaviors described above are not represented by the analytical model. The model assumes that critical starter cracks exist which act as crack nucleation sites. If these starter cracks are not present, initiation will be suppressed. The model also assumes that cracks in different ply groups interact through material softening only, described in Section 4.1.3, and does not consider local stress concentrations. Thus it does not capture some of the observed interactions. However, the analysis is conservative in the sense that it always assumes that defects exist. If these defects are not present, then crack initiation is suppressed, and the analysis gives a conservative prediction of crack density. After the onset of cracking,

135

the starter-crack assumption is satisfied, and the observed cracking behavior again agrees with that predicted by the model. This effect can be seen rather dramatically in Figure 6.8.

CHAPTER 7

CONCLUSIONS AND RECOMMENDATIONS

The present work was conducted to investigate microcracking in composites. The primary research goal was to develop an analytical methodology to predict microcracking in composite laminates under thermal and mechanical loading. This goal was met through a combination of analytical modeling and experimental investigation. In this chapter, conclusions are drawn from the findings of the present work, and directions for future research are recommended.

7.1 CONCLUSIONS

The discussion presented in Chapter 6 leads to the following conclusions:

1. The primary objective of the present investigation was met. Correlation between analysis and experiment was generally very good, verifying the analytical methodology.

2. The same analytical model successfully predicts cracking behavior under both progressive cooling and mechanical loading. This indicates that the cracking mechanisms are similar for each and may be captured by a unified analytical model. Though no combined thermomechanical loading was used, whereby progressive cooling and mechanical loading occur simultaneously, the mechanical loading included thermal residual stresses due to manufacture.

3. The shear lag parameter and critical strain energy release rate did not show laminate dependence, verifying the assumption that they are material properties. This has important implications for the future use of the methodology, as these parameters need to be measured only once for a given material system. This may be done relatively simply by loading a cross-ply laminate under monotonic tension, collecting crack data at progressive loads, and using the analysis to back out the parameters.

4. The laminates in the present work did not demonstrate the "thin ply" behavior observed in previous studies [57]. Crack densities were similar at specimen edges and throughout specimen interiors, and no dependence on specimen width was seen. These results are consistent with one of the most important assumptions of the analytical model, that cracks are continuous through the specimen width.

5. Ply groups appeared to interact with one another through local stress concentrations caused by cracking in adjacent layers. This behavior is not predicted by the analytical model, which is global in nature.

6. The onset of microcracking was suppressed in middle layers, presumably due to a lack of crack nucleation sites. The analysis assumes that critical starter cracks always exist, which may not have been true in these cases. Cracking initiated instead after adjacent layers began to crack, whereby local stress concentrations probably acted as nucleation sites.

7. The analysis is inherently conservative in the sense that it assumes that damage is always present. In the case where cracking was suppressed in the middle layers, the analysis instead predicted that cracking would occur. After the observed initation of cracking, the

138

presence of damage is consistent with the analytical model, and the observed behavior nearly matches the predicted behavior.

7.2 RECOMMENDATIONS

The present work raises a number of issues which warrant further investigation:

1. Further data collection is necessary, including

   a) more thermal data, over a broader temperature range and with more closely spaced target temperatures, to provide better verification of the methodology under thermal loading and assess the temperature dependence of the material properties;

   b) true thermomechanical loading to verify the thermal and mechanical coupling predicted by the analysis and to confirm the path independence of the strain energy release rate; and

   c) data for a larger number of laminates to verify the laminate independence of G_{Ic} and ζ.

2. Some interesting cracking mechanisms should be explored, such as

   a) whether the analysis has the ability to capture cracking behavior in "thin" ply groups (as defined by Park [57]) and

   b) whether the observed suppression of crack initiation in the middle ply groups is a general phenomenon.

3. More complicated global-local models may allow the present methodology to predict nearly all of the observed behavior. This includes modeling of

   a) local stress concentrations to capture the anomalous interactions between adjacent layers,

   b) crack nucleation sites to predict the suppression of crack initiation, and

139

c) interaction between microcracking and delamination to allow the prediction of failure dominated by these mechanisms.

4. The method could be applied to laminates made with materials other than AS4/3501-6 by collection of G_{Ic} and ζ values for these materials. G_{Ic} and ζ appear to be material properties. They could be collected by fitting to data from simple tests, such as mechanically loaded cross-ply laminates, using the analysis presented here.

REFERENCES

1. Bowles, D. and Tenney, D., "Composite Tubes for the Space Station Truss Structure", *SAMPE Journal*, May/June, 1987, pp. 49-56.

2. Crossman, F. and Johnson, R., "Spacecraft Material Applications—Long-term Stability Questions", *NASA Conference on Large Space Antenna Systems Technology*, Nov. 30-Dec. 3, 1982.

3. Camahort, J., Rennhack, E., and Coons, W., "Effects of Thermal Cycling Environment on Graphite/Epoxy Composites", *Environmental Effects on Advanced Composite Materials, ASTM STP 602*, ASTM, 1976, pp. 37-49.

4. Garrett, K. and Bailey, J., "Multiple Transverse Fracture in 90° Cross-Ply Laminate of a Glass Fibre-Reinforced Polyester", *Journal of Material Science*, Vol. 12, 1977, pp. 157-168.

5. Allen, D. and Lee, J., "Matrix Cracking in Laminated Composites under Monotonic and Cyclic Loadings", *Microcracking-Induced Damage in Composites*, Dallas, TX, 1990, pp. 65-75.

6. Carlsson, L., Eidefeldt, C., and Mohlin, T., "Influence of Sublaminate Cracks on the Tension Fatigue Behavior of a Graphite/Epoxy Laminate", *Composite Materials: Fatigue and Fracture, ASTM STP 907*, ASTM, 1986, pp. 361-382.

7. Hahn, H. and Tsai, S., "On the Behavior of Composite Laminates after Initial Failures", *Journal of Composite Materials*, Vol. 8, 1974, pp. 288-305.

8. Kistner, M., Whitney, J., and Browning, C., "First-Ply Failure of Graphite/Epoxy Laminates", *Recent Advances in Composites in the U.S. and Japan, ASTM STP*, Vol. 864, 1985, pp. 44-61.

9. Flaggs, D. and Kural, M., "Experimental Determination of the In Situ Transverse Lamina Strength in Graphite/Epoxy Laminates", *Journal of Composite Materials*, Vol. 16, March, 1982, pp. 103-116.

10. Parvizi, A. and Bailey, J., "On Multiple Transverse Cracking in Glass Fibre Epoxy Cross-ply Laminates", *Journal of Materials Science*, Vol. 13, 1978, pp. 2131-2136.

11. Tsai, C., Daniel, I., and Lee, J., "Progressive Matrix Cracking of Crossply Composite Laminates under Biaxial Loading", *Microcracking-Induced Damage in Composites*, Dallas, TX, 1990, pp. 9-18.

12. Lee, J. and Daniel, I., "Progressive Transverse Cracking of Crossply Composite Laminates", *Journal of Composite Materials*, Vol. 24, November, 1990, pp. 1225-1243.

13. Allen, D., Harris, C., and Groves, S., "A Thermomechanical Constitutive Theory for Elastic Composites with Distributed Damage–

I. Theoretical Development", *International Journal of Solids and Structures*, Vol. 23, No. 9, 1987, pp. 1301-1318.

14. Peters, P., "The Strength Distribution of 90° Plies in 0/90/0 Graphite-Epoxy Laminates", *Journal of Composite Materials*, Vol. 18, November, 1984, pp. 545-555.

15. Peters, P., "Constrained 90-Deg Ply Cracking in 0/90/0 and ±45/90/45 CFRP Laminates", *Composite Materials: Fatigue and Fracture, ASTM STP 907*, 1986, pp. 84-99.

16. Peters, P. and Chou, T.-W., "On cross-ply cracking in glass and carbon fibre-reinforced epoxy laminates", *Composites*, Vol. 18, No. 1, January, 1987, pp. 40-46.

17. Peters, P., "An Experimental Element Technique for Transverse Fracture in CFRP and GFRP", *International Union of Theoretical and Applied Mechanics (IUTAM)*, Blacksburg, VA, 1991.

18. Jen, K. and Sun, C., "Matrix Cracking and Delamination Prediction in Graphite/Epoxy Laminates", *Journal of Reinforced Plastics and Composites*, Vol. 11, October, 1992, pp. 1163-1175.

19. Caslini, M., Zanotti, C., and O'Brien, T., "Study of Matrix Cracking and Delamination in Glass/Epoxy Laminates", *Journal of Composites Technology & Research*, Vol. 9, No. 4, Winter, 1987, pp. 121-130.

20. Flaggs, D., "Prediction of Tensile Matrix Failure in Composite Laminates", *Journal of Composite Materials*, Vol. 19, January, 1985, pp. 29-50.

21. Han, Y. and Hahn, H., "Ply Cracking and Property Degradations of Symmetric Balanced Laminates Under General In-Plane Loading", *Composite Science and Technology*, Vol. 35, 1989, pp. 377-397.

22. Lim, S. and Hong, S., "Prediction of Transverse Cracking and Stiffness Reduction in Cross-Ply Laminated Composites", *Journal of Composite Materials*, Vol. 23, 1989, pp. 695-713.

23. McCartney, L., "Analytical Models of Stress Transfer in Unidirectional Composite and Cross-Ply Laminates, and Their Application to the Prediction of Matrix/Transverse Cracking", *International Union of Theoretical and Applied Mechanics (IUTAM)*, Blacksburg, VA, 1991.

24. Laws, N. and Dvorak, G., "Progressive Transverse Cracking in Composite Laminates", *Journal of Composite Materials*, Vol. 22, October, 1988, pp. 900-916.

25. Thomas, D. and Wetherhold, R., "Progressive Matrix Crack Modeling in Off-Axis Plies", *Proceedings of the American Society of Composites*, Cleveland, Ohio, 1993, pp. 683-692.

26. Bailey, J., Curtis, P., and Parvizi, A., "On the Transverse Cracking and Longitudinal Splitting of Glass and Carbon Fibre Reinforced Epoxy

Cross Ply Laminates and the Effect of Poisson and Thermally Generated Strain", *Proceedings of the Royal Society of London*, Vol. A366, 1979, pp. 599-623.

27. Hashin, Z., "The Effect of Microcracking on Thermal Expansion and Cyclic Stress-Strain Relations of Composites", *Microcracking-Induced Damage in Composites*, Dallas, TX, 1990, pp. 35-39.

28. Liu, S. and Nairn, J., "The Formation and Propagation of Matrix Microcracks in Cross-Ply Laminates during Static Loading", *Journal of Reinforced Plastics and Composites*, Vol. 11, February, 1992, pp. 158-178.

29. Nairn, J., "The Strain Energy Release Rate of Composite Microcracking: A Variational Approach", *Journal of Composite Materials*, Vol. 23, November, 1989, pp. 1106-1129.

30. Varna, J. and Berglund, L., "Multiple Transverse Cracking and Stiffness Reduction in Cross-Ply Laminates", *Journal of Composites Technology and Research*, Vol. 13, No. 2, 1991, pp. 99-106.

31. Crossman, F. and Wang, A., "The Dependence of Transverse Cracking and Delamination on Ply Thickness in Graphite/Epoxy Laminates", *Damage in Composite Materials*, *ASTM STP 775*, ASTM, 1982, pp. 118-139.

32. Gyekenyesi, A., Hemann, J., and Binienda, W., "Crack Development in Carbon/Polyimide Cross-Ply Laminates under Uniaxial Tension", *SAMPE Journal*, Vol. 30, No. 3, May/June, 1994, pp. 17-28.

33. Tan, S. and Nuismer, R., "A Theory for Progressive Matrix Cracking in Composite Laminates", *Journal of Composite Materials*, Vol. 23, 1989, pp. 1029-1047.

34. Dvorak, G., Laws, N., and Hejazi, M., "Analysis of Progressive Matrix Cracking in Composite Laminates I. Thermoelastic Properties of a Ply with Cracks", *Journal of Composite Materials*, Vol. 19, May, 1985, pp. 216-234.

35. Dvorak, G. and Laws, N., "Analysis of Progressive Matrix Cracking in Composite Laminates II. First Ply Failure", *Journal of Composite Materials*, Vol. 21, April, 1987, pp. 309-329.

36. Wang, A., Chou, P., and Lei, S., "A Stochastic Model for the Growth of Matrix Cracks in Composite Laminates", *Journal of Composite Materials*, Vol. 18, May, 1984, pp. 239-254.

37. Gudmunson, P., Ostlund, S., and Zang, W., "Local Stresses and Thermoelastic Properties of Composite Laminates Containing Microcracks", *International Union of Theoretical and Applied Mechanics (IUTAM)*, Blacksburg, VA, 1991.

38. Peters, P., "The Influence of Fiber, Matrix, and Interface on Transverse Cracking in Carbon Fiber-Reinforced Plastic Cross-Ply Laminates`", *Composite Materials: Fatigue and Fracture, Second Volume, ASTM STP 1012*, ASTM, 1989, pp. 103-117.

39. Bowles, D., "Effect of Microcracks on the Thermal Expansion of Composite Laminates", *Journal of Composite Materials*, Vol. 18, 1984, pp. 173-187.

40. Adams, D. and Herakovich, C., "Influence of Damage on the Thermal Response of Graphite-Epoxy Laminates", *Journal of Thermal Stresses*, Vol. 7, 1984, pp. 91-103.

41. Tompkins, S. and Williams, S., "Effects of Thermal Cycling on Mechanical Properties of Graphite Polyimide", *Journal of Spacecraft and Rockets*, Vol. 21, No. 3, May, 1984, pp. 274-279.

42. Tompkins, S., Bowles, D., Slemp, W., and Teichman, A., "Response of Composite Materials to the Space Station Orbit Environment", *AIAA/NASA Space Station Symposium*, Williamsburg, VA, 1988.

43. Tompkins, S., "Effects of Thermal Cycling on Composite Materials for Space Structures", *NASA/SDIO Space Environmental Effects on Materials Workshop*, 1989, pp. 447-470.

44. Tompkins, S., Funk, J., Bowles, D., Towell, T., and Connell, J., "Composite Materials for Precision Space Reflector Panels", *SPIE*

International Symposium and Exhibition on Optical Engineering and Photonics, Orlando, FL, 1992.

45. Manders, P. and Maas, D., "Thin Carbon Fiber Prepregs for Dimensionally Critical Structures", *SPIE Advances in Optical Structure Systems*, Orlando, Florida, 1990, pp. 536-545.

46. Bowles, D. and Shen, J., "Thermal Cycling Effects on the Dimensional Stability of P75 and P75-T300 (Fabric) Hybrid Graphite/Epoxy Laminates", *33rd International SAMPE Symposium and Exhibition*, Anaheim, CA, March, 1988.

47. Knouff, B., Tompkins, S., and Jayaraman, N., "The Effect of Graphite Fiber Properties on Microcracking Due to Thermal Cycling of Epoxy-Cynate Matrix Laminates", *ASTM Fifth Symposium on Composite Materials: Fatigue and Fracture*, Atlanta, Georgia, 1993, pp. 2-27.

48. Bowles, D., Tompkins, S., and Funk, J., "Residual Thermal Stresses in Composites for Dimensionally Stable Spacecraft Applications", *SEM Seventh International Congress on Experimental Mechanics*, Las Vegas, NV, April, 1992.

49. Adams, D., Bowles, D., and Herakovich, C., "Thermally Induced Transverse Cracking in Graphite/Epoxy Cross-Ply Laminates", *Journal of Reinforced Plastics and Composites*, Vol. 5, No. 3, 1986, pp. 152-169.

50. Chamis, C., Murthy, P., and Minnetyan, L., "Progressive Fracture of Polymer Matrix Composite Structures: A New Approach", *14th Annual Energy-Sources Technology Conference and Exhibition*, Houston, TX, 26-29 January 1992.

51. Herakovich, C. and Hyer, M., "Damage-Induced Property Changes in Composites Subjected to Cyclic Thermal Loading", *Engineering Fracture Mechanics*, Vol. 25, No. 5/6, 1986, pp. 779-791.

52. Bowles, D., "Thermal Stress Analysis of Composites in the Space Environment", *Fifth International Symposium on Materials in a Space Environment*, Cannes Mandelieu, France, 1991.

53. Bowles, D. and Griffin, O., "Micromechanics Analysis of Space Simulated Thermal Stresses in Composites. Part II: Multidirectional Laminates and Failure Predictions", *Journal of Reinforced Plastics and Composites*, Vol. 10, 1991, pp. 522-539.

54. Bowles, D. and Griffin, O., "Micromechanics Analysis of Space Simulated Thermal Stresses in Composites. Part I: Theory and Unidirectional Laminates", *Journal of Reinforced Plastics and Composites*, Vol. 10, 1991, pp. 505-521.

55. Hiemstra, D. and Sottos, N., "Thermally Induced Interfacial Microcracking in Polymer Matrix Composites", *Journal of Composite Materials*, Vol. 27, No. 10, 1993, pp. 1030-1051.

56. McManus, H., Bowles, D., and Tompkins, S., "Prediction of Thermally Induced Matrix Cracking", *Proceedings of the American Society of Composites*, Cleveland, Ohio, 1993.

57. Park, C., "Analysis of Thermally Induced Damage in Composite Space Structures", Massachusetts Institute of Technology, Masters Thesis, 1994.

58. O'Brien, T. and Martin, R., "Round Robin Testing for Mode I Interlaminar Fracture Toughness of Composite Materials", *Journal of Composites Technology and Research*, Vol. 15, No. 4, Winter, 1993, pp. 269-281.

59. Runkle, J., "Progressive Transverse Cracking and Local Delamination in Composite Laminates", *Proceedings of the American Society for Composites*, University Park, PA, 1992, pp. 276-285.

60. Ogin, S., Smith, P., and Beaumont, P., "Matrix Cracking and Stiffness Reduction during the Fatigue of a $(0/90)_S$ GFRP Laminate", *Composites Science and Technology*, Vol. 22, 1985, pp. 23-31.

61. Park, C. and McManus, H., "Thermally Induced Damage in Composite Space Structure: Predictive Methodology and Experimental Correlation", *Composites Science and Technology*, 1995.

62.   Highsmith, A. and Reifsnider, K., "Stiffness-Reduction Mechanisms in Composite Laminates", *Damage in Composite Materials, ASTM STP 775*, 1982, pp. 102-117.

63.   Jones, R., *Mechanics of Composite Materials*, McGraw-Hill, 1975.

64.   Anderson, T., *Fracture Mechanics, Fundamentals and Applications*, CRC Press, Inc., Boca Raton, FL, 1991.

65.   Lessard, L., "Compression Failure in Laminated Composites Containing an Open Hole", Stanford University, PhD. Thesis, 1989.

66.   Hogg, R. and Ledolter, J., *Applied Statistics for Engineers and Physical Scientists*, MacMillan Publishing Co., New York, 1992.

67.   Lagace, P. A., Brewer, J. C., and Varnerin, C., "TELAC Manufacturing Course Notes", TELAC Report 88-4B, Massachusetts Institute of Technology, 1990.

68.   Crasto, A. and Kim, R., "On the Determination of Residual Stresses in Fiber-Reinforced Thermoset Composites", *Journal of Reinforced Plastics and Composites*, Vol. 12, No. 5, Oct., 1993, pp. 545-558.

APPENDIX A

PATH INDEPENDENCE OF STRAIN ENERGY RELEASE RATE

A brief proof of the path independence of the strain energy release rate, G, is presented in this section. From Eq. (4.54),

$$G = \psi\left[a_o\sigma_a - a_r E_r(\alpha_c - \alpha_r)\Delta T\right]^2 \Phi \qquad (A.1)$$

where

$$\psi = \frac{a_c E_c}{2\zeta a_o a_r E_r E_a} \qquad (A.2)$$

and

$$\Phi = \left[2\tanh\left(\frac{\zeta h}{a_c}\right) - \tanh\left(\frac{2\zeta h}{a_c}\right)\right] \qquad (A.3)$$

Taking the partial derivative of Eq. (A.1) in I, the load increment path,

$$
\begin{aligned}
\frac{\delta G}{\delta I} = \ \psi\Bigg[& 2a_o^2\sigma_a\frac{\delta\sigma_a}{\delta I} - 2a_o a_r E_r(\alpha_c - \alpha_r)\left(\sigma_a\frac{\delta\Delta T}{\delta I} + \Delta T\frac{\delta\sigma_a}{\delta I}\right) \\
& + 2a_r^2 E_r^2(\alpha_c - \alpha_r)^2 \Delta T\frac{\delta\Delta T}{\delta I}\Bigg]\Phi
\end{aligned}
\qquad (A.4)
$$

Three different load paths (A, B, and C) are shown in Figure A.1. The initial and final load states for all three are points 1 and 3, respectively. The stress and change in temperature at the final load state are σ_f and ΔT_f, respectively. The strain energy release rate at point 3 is found by integrating Eq. (A.4) along line I.

Path A is a single continuous line from points 1 to 3 given by

$$\sigma_a = \eta \Delta T \tag{A.5}$$

Substituting Eq. (A.5) into Eq. (A.4) and integrating along I,

$$G_A = \psi \left[\int_0^{\sigma_f} 2a_o^2 \sigma_a \delta\sigma_a - 2a_o a_r E_r (\alpha_c - \alpha_r) \left(\int_0^{\sigma_f} 2\frac{\sigma_a}{\eta} \delta\sigma_a \right) \right. \\ \left. + \int_0^{\sigma_f} 2a_r^2 E_r^2 (\alpha_c - \alpha_r)^2 \frac{\sigma_a}{\eta^2} \delta\sigma_a \right] \Phi \tag{A.6}$$

From Eq. (A.6),

$$G_A = \psi \left[\sigma_f \left(a_o - \frac{a_r E_r (\alpha_c - \alpha_r)}{\eta} \right) \right]^2 \Phi \tag{A.7}$$

Path B is piecewise continuous, represented by a line from points 1 to 2 and one from points 2 to 3. These are given by

$$\sigma_a = 0 \tag{A.8}$$

and

$$\Delta T = \Delta T_f \tag{A.9}$$

respectively, where

$$\Delta T_f = \frac{\sigma_f}{\eta} \tag{A.10}$$

Substituting Eqs. (A.8) to (A.10) into Eq. (A.4) and integrating along I,

$$G_B = \psi \left[\int_0^{\frac{\sigma_f}{\eta}} 2a_r^2 E_r^2 (\alpha_c - \alpha_r)^2 \Delta T \delta\Delta T \right] \Phi \\ + \psi \left[\int_0^{\sigma_f} 2a_o^2 \sigma_a \delta\sigma_a - \int_0^{\sigma_f} 2a_o a_r E_r (\alpha_c - \alpha_r) \frac{\sigma_f}{\eta} \delta\sigma_a \right] \Phi \tag{A.11}$$

which gives

$$G_B = \psi \left[\sigma_f \left(a_o - \frac{a_r E_r (\alpha_c - \alpha_r)}{\eta} \right) \right]^2 \Phi \tag{A.12}$$

153

Path C is piecewise continuous, represented by a line from points 1 to 2' and one from points 2' to 3. These are given by

$$\Delta T = 0 \tag{A.13}$$

and

$$\sigma_a = \sigma_f \tag{A.14}$$

Substituting Eqs. (A.13) and (A.14) into Eq. (A.4) and integrating along I,

$$G_C = \psi \left[\int_0^{\sigma_f} 2a_o^2 \sigma_a \delta\sigma_a \right] \Phi \tag{A.15}$$
$$- \psi \left[\int_0^{\frac{\sigma_f}{\eta}} 2a_o a_r E_r (\alpha_c - \alpha_r) \sigma_f \delta\Delta T + \int_0^{\frac{\sigma_f}{\eta}} 2a_r^2 E_r^2 (\alpha_c - \alpha_r)^2 \Delta T \delta\Delta T \right] \Phi$$

which gives

$$G_C = \psi \left[\sigma_f \left(a_o - \frac{a_r E_r (\alpha_c - \alpha_r)}{\eta} \right) \right]^2 \Phi \tag{A.16}$$

From Eqs. (A.7), (A.12), and (A.16),

$$G_A = G_B = G_C \tag{A.17}$$

Thus the strain energy release rate is path independent.
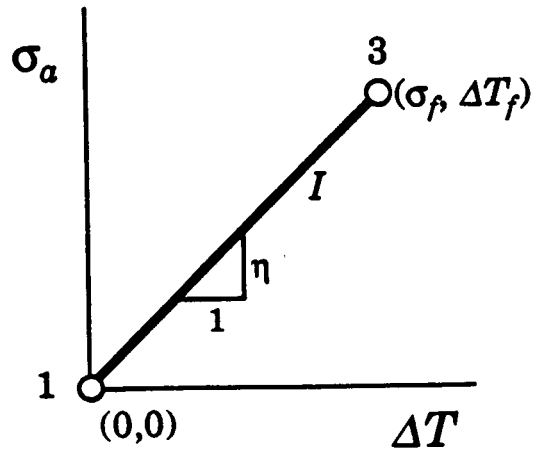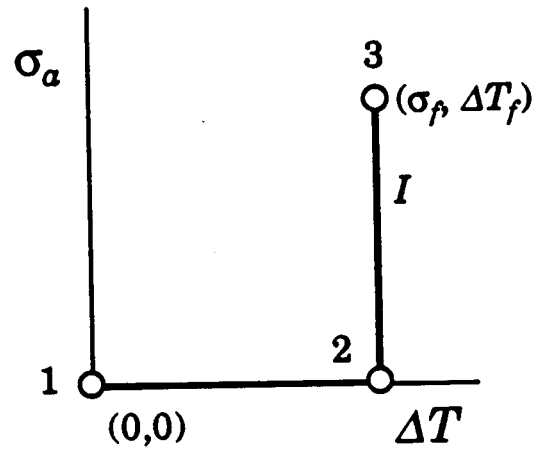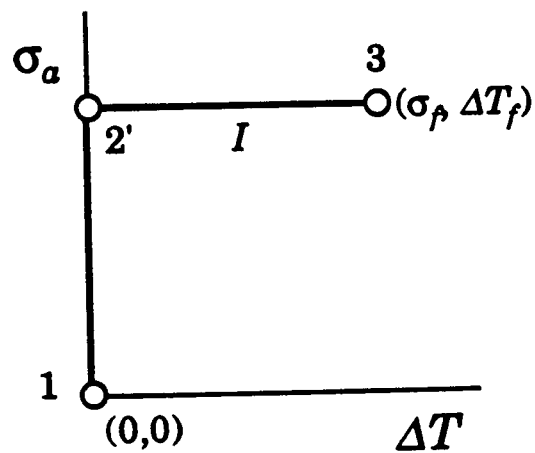
Figure A.1   Three load paths used in proof.

APPENDIX B

DERIVATION OF SHEAR LAG SOLUTION AND ENERGY EXPRESSIONS

B.1 SHEAR LAG SOLUTION

From equilibrium of the laminate,

$$\sigma_a a_o = \sigma_r a_r + \sigma_c a_c \tag{B.1}$$

From equilibrium of the cracked layer,

$$-\sigma_c a_c + \left(\sigma_c + \frac{d\sigma_c}{dx'} dx'\right) a_c - 2q\,dx' = 0 \tag{B.2}$$

and solving for q,

$$q = \frac{a_c}{2}\frac{d\sigma_c}{dx'} \tag{B.3}$$

From equilibrium of the rest of the laminate,

$$-\sigma_r \frac{a_r}{2} + \left(\sigma_r + \frac{d\sigma_r}{dx'} dx'\right)\frac{a_r}{2} + q\,dx' = 0 \tag{B.4}$$

and solving for q,

$$q = -\frac{a_r}{2}\frac{d\sigma_r}{dx'} \tag{B.5}$$

The stress strain relation for the cracking layer is

$$\sigma_c = E_c(\varepsilon_c - \alpha_c \Delta T) \quad \text{where} \quad \varepsilon_c = \frac{du_c}{dx'} \tag{B.6}$$

so

156

$$\frac{\sigma_c}{E_c} = \frac{du_c}{dx'} - \alpha_c \Delta T \qquad (B.7)$$

The stress strain relation for the rest of the laminate is

$$\sigma_r = E_r(\varepsilon_r - \alpha_r \Delta T) \quad \text{where} \quad \varepsilon_r = \frac{du_r}{dx'} \qquad (B.8)$$

so

$$\frac{\sigma_r}{E_r} = \frac{du_r}{dx'} - \alpha_r \Delta T \qquad (B.9)$$

Let

$$q = K(u_c - u_r) \qquad (B.10)$$

K is a stiffness constant relating the displacements of the two layers to the shear stress between them. It can be determined from

$$K = \frac{G^{\text{eff}}}{a_q} \qquad (B.11)$$

where G^{eff} is the effective shear modulus of the shear transfer region. Placing Eq. (B.11) into Eqs. (B.3) and (B.5),

$$K(u_c - u_r) = \frac{a_c}{2}\frac{d\sigma_c}{dx'} \qquad (B.12)$$

$$K(u_c - u_r) = -\frac{a_r}{2}\frac{d\sigma_r}{dx'} \qquad (B.13)$$

Taking the derivatives of Eqs. (B.12) and (B.13) in x',

$$K\left(\frac{du_c}{dx'} - \frac{du_r}{dx'}\right) = \frac{a_c}{2}\frac{d^2\sigma_c}{(dx')^2} \qquad (B.14)$$

and

$$K\left(\frac{du_c}{dx'} - \frac{du_r}{dx'}\right) = -\frac{a_r}{2}\frac{d^2\sigma_r}{(dx')^2} \qquad (B.15)$$

Subtracting Eq. (B.9) from Eq. (B.7),

$$\frac{\sigma_c}{E_c} - \frac{\sigma_r}{E_r} = \left(\frac{du_c}{dx'} - \frac{du_r}{dx'}\right) + (\alpha_r - \alpha_c)\Delta T \tag{B.16}$$

Multiplying Eq. (B.16) by K and substituting Eq. (B.14),

$$K\left(\frac{\sigma_c}{E_c} - \frac{\sigma_r}{E_r}\right) = \frac{a_c}{2}\frac{d^2\sigma_c}{(dx')^2} + K(\alpha_r - \alpha_c)\Delta T \tag{B.17}$$

Rearranging,

$$\frac{d^2\sigma_c}{(dx')^2} = \frac{2K}{a_c}\left[\frac{\sigma_c}{E_c} - \frac{\sigma_r}{E_r} + (\alpha_c - \alpha_r)\Delta T\right] \tag{B.18}$$

Solving Eq. (B.1) for σ_r,

$$\sigma_r = \frac{\sigma_o a_o - \sigma_c a_c}{a_r} \tag{B.19}$$

Substituting Eq. (B.19) into Eq. (B.18),

$$\frac{d^2\sigma_c}{(dx')^2} = \frac{2K}{a_c}\left[\frac{\sigma_c}{E_c} - \frac{\sigma_o a_o}{a_r E_r} + \frac{\sigma_c a_c}{a_r E_r} + (\alpha_c - \alpha_r)\Delta T\right] \tag{B.20}$$

Factoring and rearranging,

$$\frac{d^2\sigma_c}{(dx')^2} - 2K\left(\frac{a_r E_r + a_c E_c}{a_r a_c E_r E_c}\right)\sigma_c = \frac{2K}{a_c}\left[-\frac{\sigma_o a_o}{a_r E_r} + (\alpha_c - \alpha_r)\Delta T\right] \tag{B.21}$$

Let the shear lag parameter ζ, which controls the thickness of the shear transfer region, be expressed as

$$\zeta = \sqrt{\frac{K a_c(a_r E_r + a_c E_c)}{2a_r E_r E_c}} \tag{B.22}$$

Also let

$$\lambda = \frac{2K}{a_c}\left[\frac{a_o \sigma_o}{a_r E_r} - (\alpha_c - \alpha_r)\Delta T\right] \tag{B.23}$$

From the rule of mixtures,

$$a_o E_o = a_r E_r + a_c E_c \tag{B.24}$$

and

$$a_o E_o \alpha_o = a_r E_r \alpha_r + a_c E_c \alpha_c \qquad \text{(B.25)}$$

Substituting Eqs. (B.24) and (B.25) into Eq. (B.23), λ can be conveniently expressed as

$$\lambda = \frac{4\zeta^2}{a_c^2} \sigma_{c\infty} \qquad \text{(B.26)}$$

where $\sigma_{c\infty}$, the far-field stress in the cracking layer, is

$$\sigma_{c\infty} = \left[\frac{E_c}{E_o} \sigma_a + E_c (\alpha_o - \alpha_c) \Delta T \right] \qquad \text{(B.27)}$$

Substituting Eqs. (B.22) and (B.24) into Eq. (B.21) gives

$$\frac{d^2\sigma_c}{(dx')^2} - \frac{4\zeta^2 \sigma_c}{a_c^2} = \frac{2K}{a_c} \left[-\frac{\sigma_a a_0}{a_r E_r} + (\alpha_c - \alpha_r)\Delta T \right] \qquad \text{(B.28)}$$

Placing Eq. (B.23) into Eq. (B.28),

$$\frac{d^2\sigma_c}{(dx')^2} - \frac{4\zeta^2}{a_c^2} \sigma_c = -\lambda \qquad \text{(B.29)}$$

This has a solution of the form,

$$\sigma_c = A\sinh\left(\frac{2\zeta x'}{a_c}\right) + B\cosh\left(\frac{2\zeta x'}{a_c}\right) + \frac{\lambda a_c^2}{4\zeta^2} \qquad \text{(B.30)}$$

Applying boundary conditions $\sigma_c = 0$ at $x' = \pm h$,

$$0 = A\sinh\left(\frac{2\zeta h}{a_c}\right) + B\cosh\left(\frac{2\zeta h}{a_c}\right) + \frac{\lambda a_c^2}{4\zeta^2} \qquad \text{(B.31)}$$

$$0 = -A\sinh\left(\frac{2\zeta h}{a_c}\right) + B\cosh\left(\frac{2\zeta h}{a_c}\right) + \frac{\lambda a_c^2}{4\zeta^2} \qquad \text{(B.32)}$$

Adding Eqs. (B.31) and (B.32) to find B,

$$B = \frac{-\lambda a_c^2}{4\zeta^2 \cosh(2\zeta h/a_c)} \tag{B.33}$$

Subtracting Eq. (B.32) from (B.31) and solving for A,

$$A = 0 \tag{B.34}$$

Substituting Eqs. (B.33) and (B.34) into Eq. (B.30),

$$\sigma_c = -\frac{\lambda a_c^2}{4\zeta^2 \cosh\left(\dfrac{2\zeta h}{a_c}\right)} \cosh\left(\frac{2\zeta x'}{a_c}\right) + \frac{\lambda a_c^2}{4\zeta^2} \tag{B.35}$$

Factoring,

$$\sigma_c = \frac{\lambda a_c^2}{4\zeta^2}\left[1 - \frac{\cosh(2\zeta x'/a_c)}{\cosh(2\zeta h/a_c)}\right] \tag{B.36}$$

Substituting Eq. (B.26) into Eq. (B.36),

$$\sigma_c = \left[1 - \frac{\cosh(2\zeta x'/a_c)}{\cosh(2\zeta h/a_c)}\right]\sigma_{c\infty} \tag{B.37}$$

Substituting Eq. (B.37) into Eq. (B.19),

$$\sigma_r = \frac{\sigma_o a_o}{a_r} - \frac{a_c}{a_r}\left[1 - \frac{\cosh(2\zeta x'/a_c)}{\cosh(2\zeta h/a_c)}\right]\sigma_{c\infty} \tag{B.38}$$

Substituting Eq. (B.37) into Eq. (B.7) and solving for $\dfrac{du_c}{dx'}$:

$$\frac{du_c}{dx'} = \frac{1}{E_c}\left[1 - \frac{\cosh(2\zeta x'/a_c)}{\cosh(2\zeta h/a_c)}\right]\sigma_{c\infty} + \alpha_c \Delta T \tag{B.39}$$

Placing Eq. (B.27) into Eq. (B.39), substituting Eqs. (B.24) and (B.25), factoring the loading terms, and integrating,

$$u_c = \frac{a_r E_r}{a_o E_o}\left[\frac{a_o \sigma_o}{a_r E_r} + \alpha_r \Delta T\right]\int_0^{x'}\left[1 - \frac{\cosh(2\zeta x'/a_c)}{\cosh(2\zeta h/a_c)}\right]dx'$$
$$+ \alpha_c \Delta T \int_0^{x'}\left[1 - \frac{a_r E_r}{a_o E_o}\left(1 - \frac{a_c}{2\zeta}\frac{\cosh(2\zeta x'/a_c)}{\cosh(2\zeta h/a_c)}\right)\right]dx' \tag{B.40}$$

which gives

$$u_c = \frac{a_r E_r x'}{a_o E_o} \left[\frac{a_o \sigma_a}{a_r E_r} + \alpha_r \Delta T \right] \left[1 - \frac{a_c}{2\zeta x'} \frac{\sinh(2\zeta x'/a_c)}{\cosh(2\zeta h/a_c)} \right]$$
$$+ \alpha_c \Delta T x' \left[1 - \frac{a_r E_r}{a_o E_o} \left(1 - \frac{a_c}{2\zeta x'} \frac{\sinh(2\zeta x'/a_c)}{\cosh(2\zeta h/a_c)} \right) \right] \quad \text{(B.41)}$$

Substituting Eq. (B.38) into Eq. (B.9) and solving for $\dfrac{du_r}{dx'}$:

$$\frac{du_r}{dx'} = \frac{\sigma_a a_o}{a_r E_r} - \frac{a_c}{a_r E_r} \left[1 - \frac{\cosh(2\zeta x'/a_c)}{\cosh(2\zeta h/a_c)} \right] \sigma_{c_\infty} + \alpha_r \Delta T \quad \text{(B.42)}$$

Placing Eq. (B.27) into Eq. (B.42), substituting Eqs. (B.24) and (B.25), factoring the loading terms, and integrating,

$$u_r = \int_0^{x'} \left\{ \frac{a_o \sigma_a}{a_r E_r} - \frac{a_c E_c}{a_o E_o} \left[\frac{a_o \sigma_a}{a_r E_r} - (\alpha_c - \alpha_r) \Delta T \right] \left[1 - \frac{\cosh(2\zeta x'/a_c)}{\cosh(2\zeta h/a_c)} \right] + \alpha_r \Delta T \right\} dx' \quad \text{(B.43)}$$

which gives

$$u_r = \frac{a_o \sigma_a x'}{a_r E_r} - \frac{a_c E_c}{a_o E_o} \left[\frac{a_o \sigma_a}{a_r E_r} - (\alpha_c - \alpha_r) \Delta T \right] \left[x' - \frac{a_c}{2\zeta} \frac{\sinh(2\zeta x'/a_c)}{\cosh(2\zeta h/a_c)} \right] + \alpha_r \Delta T x' \quad \text{(B.44)}$$

Factoring Eq. (B.44),

$$u_r = \frac{\sigma_a x'}{a_r E_r E_o} \left[a_o E_o - a_c E_c \left(1 - \frac{a_c}{2\zeta x'} \frac{\sinh(2\zeta x'/a_c)}{\cosh(2\zeta h/a_c)} \right) \right]$$
$$+ \frac{\Delta T x'}{a_o E_o} \left[a_o E_o \alpha_r + a_c E_c (\alpha_c - \alpha_r) \left(1 - \frac{a_c}{2\zeta x'} \frac{\sinh(2\zeta x'/a_c)}{\cosh(2\zeta h/a_c)} \right) \right] \quad \text{(B.45)}$$

The constants of integration in Eqs. (B.41) and (B.45) are set to zero to satisfy the displacement boundary conditions $u_r(0) = u_c(0) = 0$.

B.2 ENERGY EXPRESSIONS

The energy criterion can be expressed as functions of the strain energy and external work alone in a Griffith energy balance:

$$G = \frac{\Delta W - \Delta U}{a_c} \tag{B.46}$$

The condition for instantaneous appearance of a new crack is

$$G \geq G_{Ic} \tag{B.47}$$

The change in internal strain energy, ΔU, has contributions from both the normal and shear stresses. The strain energy from normal stresses, U_σ, is

$$U_\sigma = \oint \int_v \sigma d\varepsilon^m dV \tag{B.48}$$

where

$$d\varepsilon^m = \frac{d\sigma}{E} \tag{B.49}$$

Substituting Eq. (B.49) into Eq. (B.48) and integrating over $d\sigma$,

$$U_\sigma = \frac{1}{2} \oint_v \frac{\sigma^2}{E} dV \tag{B.50}$$

The change in U_σ when a new crack appears is

$$\Delta U_\sigma = \left[2U_\sigma\big|_h - U_\sigma\big|_{2h} \right] \tag{B.51}$$

$2U_\sigma\big|_h$ is the strain energy due to normal stresses of the volume element with cracks separated by a distance h. $U_\sigma\big|_{2h}$ is the strain energy with cracks separated by $2h$ and can be found from

$$U_\sigma\big|_{2h} = 2 \left[\underbrace{\frac{1}{2} a_r \int_0^h \frac{\sigma_r^2}{E_r} dx'}_{\text{I}} + \underbrace{\frac{1}{2} a_c \int_0^h \frac{\sigma_c^2}{E_c} dx'}_{\text{II}} \right] \tag{B.52}$$

Note that due to symmetry, we can integrate from 0 to h and multiply the result by two, rather than integrating from $-h$ to h. Substituting Eq. (B.38) into I,

$$\frac{1}{2}a_r\int_0^h\frac{\sigma_r^2}{E_r}dx' =$$

$$\int_0^h\left\{\frac{a_o^2\sigma_o^2}{2a_rE_r}+\frac{a_c^2}{2a_rE_r}\left[1-\frac{2\cosh\left(\dfrac{2\zeta x'}{a_c}\right)}{\cosh\left(\dfrac{2\zeta h}{a_c}\right)}+\frac{\cosh^2\left(\dfrac{2\zeta x'}{a_c}\right)}{\cosh^2\left(\dfrac{2\zeta h}{a_c}\right)}\right]\sigma_{c_\infty}^2\right.$$

$$\left.-\frac{a_ca_o}{a_rE_r}\left[1-\frac{\cosh\left(\dfrac{2\zeta x'}{a_c}\right)}{\cosh\left(\dfrac{2\zeta h}{a_c}\right)}\right]\sigma_o\sigma_{c_\infty}\right\}dx' \qquad (B.53)$$

Substituting the trigonometric relation $\cosh^2x=\frac{1}{2}(\cosh 2x+1)$ into Eq. (B.53) and integrating,

$$\frac{1}{2}a_r\int_0^h\frac{\sigma_r^2}{E_r}dx' =$$

$$\frac{\sigma_o^2a_o^2h}{2a_rE_r}+\frac{a_c^2}{2a_rE_r}\left[h-\frac{a_c}{\zeta}\tanh\left(\frac{2\zeta h}{a_c}\right)+\frac{\dfrac{a_c}{8\zeta}\sinh\left(\dfrac{4\zeta h}{a_c}\right)+\dfrac{h}{2}}{\cosh^2\left(\dfrac{2\zeta h}{a_c}\right)}\right]\sigma_{c_\infty}^2 \qquad (B.54)$$

$$-\frac{a_ca_o}{a_rE_r}\left[h-\frac{a_c}{2\zeta}\tanh\left(\frac{2\zeta h}{a_c}\right)\right]\sigma_o\sigma_{c_\infty}$$

Substituting Eq. (B.37) into II,

$$\frac{1}{2}a_c\int_0^h\frac{\sigma_c^2}{E_c}dx' =\int_0^h\left\{\frac{a_c}{2E_c}\left[1-\frac{2\cosh\left(\dfrac{2\zeta x'}{a_c}\right)}{\cosh\left(\dfrac{2\zeta h}{a_c}\right)}+\frac{\cosh^2\left(\dfrac{2\zeta x'}{a_c}\right)}{\cosh^2\left(\dfrac{2\zeta h}{a_c}\right)}\right]\sigma_{c_\infty}^2\right\}dx' \qquad (B.55)$$

Substituting the trigonometric relation $\cosh^2x=\frac{1}{2}(\cosh 2x+1)$ into Eq. (B.55) and integrating,

$$\frac{1}{2}a_c\int_0^h\frac{\sigma_c^2}{E_c}dx' =$$

$$\frac{a_c}{2E_c}\left[h-\frac{a_c}{\zeta}\tanh\left(\frac{2\zeta h}{a_c}\right)+\frac{\frac{a_c}{8\zeta}\sinh\left(\frac{4\zeta h}{a_c}\right)+\frac{h}{2}}{\cosh^2\left(\frac{2\zeta h}{a_c}\right)}\right]\sigma_{c_\infty}^2 \qquad (B.56)$$

Placing Eqs. (B.54) and (B.56) into Eq. (B.52),

$$U_\sigma\big|_{2h} = \frac{\sigma_a^2 a_0^2 h}{a_r E_r}$$

$$+\frac{a_c a_o E_o \sigma_{c_\infty}^2}{a_r E_c E_r}\left[h-\frac{a_c}{\zeta}\tanh\left(\frac{2\zeta h}{a_c}\right)+\frac{\frac{a_c}{8\zeta}\sinh\left(\frac{4\zeta h}{a_c}\right)+\frac{h}{2}}{\cosh^2\left(\frac{2\zeta h}{a_c}\right)}\right] \qquad (B.57)$$

$$-\frac{2a_c a_o \sigma_a \sigma_{c_\infty}}{a_r E_r}\left[h-\frac{a_c}{2\zeta}\tanh\left(\frac{2\zeta h}{a_c}\right)\right]$$

The strain energy due to normal stresses in the volume element after a new crack forms and the cracks separated by a distance h is

$$U_\sigma\big|_h = 2\left[\frac{1}{2}a_r\int_0^{h/2}\frac{\sigma_r^{*2}}{E_r}dx'+\frac{1}{2}a_c\int_0^{h/2}\frac{\sigma_c^{*2}}{E_c}dx'\right] \qquad (B.58)$$

Due to symmetry, we integrate from 0 to $h/2$ and multiply the result by two. Also, in Eq. (B.58), σ_c^* and σ_r^* are the normal stresses in the cracking layer and the rest of the laminate, respectively, derived with the boundary conditions $\sigma_c^* = 0$ at $x' = \pm h/2$. Then, by analogy with $U_\sigma\big|_{2h}$,

164

$$U_\sigma\big|_h = \frac{\sigma_o^2 a_o^2 h}{2 a_r E_r}$$

$$+ \frac{a_c a_o E_o}{a_r E_c E_r} \left[\frac{h}{2} - \frac{a_c}{\zeta} \tanh\left(\frac{\zeta h}{a_c}\right) + \frac{\frac{a_c}{8\zeta} \sinh\left(\frac{2\zeta h}{a_c}\right) + \frac{h}{4}}{\cosh^2\left(\frac{\zeta h}{a_c}\right)} \right] \sigma_{c\infty}^2 \qquad \text{(B.59)}$$

$$- \frac{2 a_c a_o}{a_r E_r} \left[\frac{h}{2} - \frac{a_c}{2\zeta} \tanh\left(\frac{\zeta h}{a_c}\right) \right] \sigma_a \sigma_{c\infty}$$

Substituting Eqs. (B.57) and (B.59) into Eq. (B.51),

$$\Delta U_\sigma = \frac{a_c^2 a_o E_o}{a_r E_c E_r \zeta}$$

$$\left[\tanh\left(\frac{2\zeta h}{a_c}\right) - 2\tanh\left(\frac{\zeta h}{a_c}\right) - \frac{\frac{1}{8} \sinh\left(\frac{4\zeta h}{a_c}\right) + \frac{\zeta h}{2 a_c}}{\cosh^2\left(\frac{2\zeta h}{a_c}\right)} + \frac{\frac{1}{4} \sinh\left(\frac{2\zeta h}{a_c}\right) + \frac{\zeta h}{2 a_c}}{\cosh^2\left(\frac{\zeta h}{a_c}\right)} \right] \sigma_{c\infty}^2$$

$$+ \frac{a_c^2 a_o}{a_r E_r \zeta} \left[2\tanh\left(\frac{\zeta h}{a_c}\right) - \tanh\left(\frac{2\zeta h}{a_c}\right) \right] \sigma_a \sigma_{c\infty}$$

$$\text{(B.60)}$$

Using the trigonometric identity $\sinh 2x = 2 \sinh x \cosh x$,

$$\Delta U_\sigma = \frac{a_c^2 a_o E_o}{a_r E_c E_r \zeta}$$

$$\left[\tanh\left(\frac{2\zeta h}{a_c}\right) - 2\tanh\left(\frac{\zeta h}{a_c}\right) - \frac{\frac{1}{4} \sinh\left(\frac{2\zeta h}{a_c}\right) \cosh\left(\frac{2\zeta h}{a_c}\right) + \frac{\zeta h}{2 a_c}}{\cosh^2\left(\frac{2\zeta h}{a_c}\right)} + \frac{\frac{1}{2} \sinh\left(\frac{\zeta h}{a_c}\right) \cosh\left(\frac{\zeta h}{a_c}\right) + \frac{\zeta h}{2 a_c}}{\cosh^2\left(\frac{\zeta h}{a_c}\right)} \right] \sigma_{c\infty}^2$$

$$+ \frac{a_c^2 a_o}{a_r E_r \zeta} \left[2\tanh\left(\frac{\zeta h}{a_c}\right) - \tanh\left(\frac{2\zeta h}{a_c}\right) \right] \sigma_a \sigma_{c\infty}$$

$$\text{(B.61)}$$

Simplifying,

$$\Delta U_\sigma = \frac{a_c^2 a_o E_o}{2 a_r E_r \zeta}$$

$$\left[\frac{3}{2} \tanh\left(\frac{2\zeta h}{a_c}\right) - 3\tanh\left(\frac{\zeta h}{a_c}\right) - \frac{\zeta h}{a_c}\left(\text{sech}^2\left(\frac{2\zeta h}{a_c}\right) - \text{sech}^2\left(\frac{\zeta h}{a_c}\right) \right) \right] \sigma_{c\infty}^2 \quad \text{(B.62)}$$

$$+ \frac{a_c^2 a_o}{a_r E_r \zeta}\left[2\tanh\left(\frac{\zeta h}{a_c}\right) - \tanh\left(\frac{2\zeta h}{a_c}\right) \right] \sigma_a \sigma_{c\infty}$$

Placing Eq. (B.27) into Eq. (B.62), substituting Eqs. (B.24) and (B.25), and expanding the loading terms,

$$\Delta U_\sigma = \frac{a_o^2 \sigma_a^2}{a_r^2 E_r^2}\left\{ \frac{a_r a_c^2 E_r E_c}{2\zeta a_o E_o}\left[\frac{3}{2}\tanh\left(\frac{2\zeta h}{a_c}\right) - 3\tanh\left(\frac{\zeta h}{a_c}\right) - \frac{\zeta h}{a_c}\left(\text{sech}^2\left(\frac{2\zeta h}{a_c}\right) - \text{sech}^2\left(\frac{\zeta h}{a_c}\right) \right) \right] \right.$$

$$+ \frac{a_c^2 a_r E_r E_c}{2\zeta a_o E_o}\left[4\tanh\left(\frac{\zeta h}{a_c}\right) - 2\tanh\left(\frac{2\zeta h}{a_c}\right) \right] \Big\}$$

$$+ (\alpha_c - \alpha_r)^2 \Delta T^2 \left\{ \frac{a_r a_c^2 E_r E_c}{2\zeta a_o E_o}\left[\frac{3}{2}\tanh\left(\frac{2\zeta h}{a_c}\right) - 3\tanh\left(\frac{\zeta h}{a_c}\right) - \frac{\zeta h}{a_c}\left(\text{sech}^2\left(\frac{2\zeta h}{a_c}\right) - \text{sech}^2\left(\frac{\zeta h}{a_c}\right) \right) \right] \right.$$

$$+ \frac{\sigma_a a_c^2 E_c}{2\zeta E_o(\alpha_c - \alpha_r)\Delta T}\left[4\tanh\left(\frac{\zeta h}{a_c}\right) - 2\tanh\left(\frac{2\zeta h}{a_c}\right) \right] \Big\} \quad \text{(B.63)}$$

$$- \frac{\sigma_a(\alpha_c - \alpha_r)\Delta T a_c^2 E_c}{\zeta E_o}\left[\frac{3}{2}\tanh\left(\frac{2\zeta h}{a_c}\right) - 3\tanh\left(\frac{\zeta h}{a_c}\right) - \frac{\zeta h}{a_c}\left(\text{sech}^2\left(\frac{2\zeta h}{a_c}\right) - \text{sech}^2\left(\frac{\zeta h}{a_c}\right) \right) \right]$$

Factoring,

$$\Delta U_\sigma = \frac{a_o a_c^2 E_c \sigma_a^2}{2\zeta a_r E_r E_o}\left[\tanh\left(\frac{\zeta h}{a_c}\right) - \frac{1}{2}\tanh\left(\frac{2\zeta h}{a_c}\right) + \frac{\zeta h}{a_c}\left(\text{sech}^2\left(\frac{\zeta h}{a_c}\right) - \text{sech}^2\left(\frac{2\zeta h}{a_c}\right) \right) \right]$$

$$+ \frac{a_r a_c^2 E_r E_c(\alpha_c - \alpha_r)^2 \Delta T^2}{2\zeta a_o E_o}\left[\frac{3}{2}\tanh\left(\frac{2\zeta h}{a_c}\right) - 3\tanh\left(\frac{\zeta h}{a_c}\right) + \frac{\zeta h}{a_c}\left(\text{sech}^2\left(\frac{\zeta h}{a_c}\right) - \text{sech}^2\left(\frac{2\zeta h}{a_c}\right) \right) \right] \quad \text{(B.64)}$$

$$+ \frac{a_c^2 E_c(\alpha_c - \alpha_r)\sigma_a \Delta T}{2\zeta E_o}\left[2\tanh\left(\frac{\zeta h}{a_c}\right) - \tanh\left(\frac{2\zeta h}{a_c}\right) + \frac{2\zeta h}{a_c}\left(\text{sech}^2\left(\frac{\zeta h}{a_c}\right) - \text{sech}^2\left(\frac{2\zeta h}{a_c}\right) \right) \right]$$

The strain energy contribution from shear stresses, U_q, is given by

$$U_q = \frac{1}{2}\oint_v \int q\, d\gamma\, dV \quad \text{(B.65)}$$

where

$$d\gamma = \frac{dq}{G^{eff}} \quad \text{(B.66)}$$

Substituting Eq. (B.66) into Eq. (B.65) and integrating over dq,

166

$$U_q = \frac{1}{2} \oint_v \frac{q^2}{G^{eff}} \mathrm{dV} \tag{B.67}$$

Eq. (B.67) is integrated over the volume of the shear transfer region, which has a total thickness of $2a_q$ since shear is transferred at both the top and bottom of the cracking layer. The change in U_q when a new crack forms is

$$\Delta U_q = \left[2U_q\big|_h - U_q\big|_{2h} \right] \tag{B.68}$$

$2U_q\big|_h$ is the strain energy due to shear stresses of the volume element with cracks separated by a distance h. $U_q\big|_{2h}$, the strain energy with cracks separated by $2h$, can be found by solving Eq. (B.11) for G^{eff}, and substituting the result into Eq. (B.67), giving

$$U_q\big|_{2h} = \frac{1}{2} \int_{-h}^{h} \frac{2a_q q^2}{K a_q} \mathrm{dx'} \tag{B.69}$$

Simplifying,

$$U_q\big|_{2h} = \frac{2}{K} \int_0^h q^2 \mathrm{dx'} \tag{B.70}$$

Due to symmetry, we can once again integrate from 0 to h and multiply the result by two, rather than integrating from $-h$ to h. Placing Eqs. (B.41) and (B.45) into Eq. (B.10) and squaring,

$$q^2 = \frac{K^2 a_q^2 E_q^2}{a_r^2 E_c^2 E_r^2} \left[\frac{\sinh^2\left(\dfrac{2\zeta x'}{a_c}\right)}{\cosh^2\left(\dfrac{2\zeta h}{a_c}\right)} \right] \sigma_{c\infty}^2 \tag{B.71}$$

Substituting Eq. (B.71) into Eq. (B.70) and integrating,

$$U_q\big|_{2\lambda} = \frac{2Ka_o^2E_o^2}{a_r^2E_c^2E_r^2}\left[\frac{a_c^2}{8\zeta^2}\frac{\dfrac{a_c}{4\zeta}\sinh\left(\dfrac{4\zeta x'}{a_c}\right)-x'}{\cosh^2\left(\dfrac{2\zeta h}{a_c}\right)}\right]_0^{h}\sigma_{c_\infty}^2 \qquad (B.75)$$

Evaluating Eq. (B.75) from 0 to h,

$$U_q\big|_{2\lambda} = \frac{Ka_c^2a_o^2E_o^2}{4a_r^2E_c^2E_r^2\zeta^2}\left[\frac{\dfrac{a_c}{4\zeta}\sinh\left(\dfrac{4\zeta h}{a_c}\right)-h}{\cosh^2\left(\dfrac{2\zeta h}{a_c}\right)}\right]\sigma_{c_\infty}^2 \qquad (B.76)$$

Using the trigonometric relation $\sinh 2x = 2\sinh x\cosh x$, Eq. (B.76) can be reduced to:

$$U_q\big|_{2\lambda} = \frac{Ka_c^3a_o^2E_o^2}{16a_r^2E_c^2E_r^2\zeta^3}\left[2\tanh\left(\frac{2\zeta h}{a_c}\right)-\frac{4\zeta h}{a_c}\mathrm{sech}^2\left(\frac{2\zeta h}{a_c}\right)\right]\sigma_{c_\infty}^2 \qquad (B.77)$$

The strain energy due to normal stresses in the volume element when a new crack forms and with the cracks now separated by a distance h is

$$U_q\big|_{\lambda} = \frac{2}{K}\int_0^{h/2}\left(q^*\right)^2 dx' \qquad (B.78)$$

Due to symmetry, we integrate from 0 to $h/2$ and multiply the result by two. Also, in Eq. (4.33) q^* is the shear stress derived with the boundary conditions $\sigma_c^* = 0$ at $x' = \pm h/2$. Then, by analogy with $U_\sigma\big|_{2\lambda}$,

$$U_q\big|_{\lambda} = \frac{2Ka_o^2E_o^2}{a_r^2E_c^2E_r^2}\left[\frac{a_c^2}{8\zeta^2}\frac{\dfrac{a_c}{4\zeta}\sinh\left(\dfrac{4\zeta x'}{a_c}\right)-x'}{\cosh^2\left(\dfrac{\zeta h}{a_c}\right)}\right]_0^{\frac{h}{2}}\sigma_{c_\infty}^2 \qquad (B.79)$$

Evaluating Eq. (B.79) from 0 to $h/2$,

$$U_q\big|_h = \frac{Ka_c^2a_o^2E_o^2}{4a_r^2E_c^2E_r^2\zeta^2}\left[\frac{\frac{a_c}{4\zeta}\sinh\left(\frac{2\zeta h}{a_c}\right)-\frac{h}{2}}{\cosh^2\left(\frac{\zeta h}{a_c}\right)}\right]\sigma_{c_\infty}^2 \tag{B.80}$$

Using the trigonometric relation $\sinh 2x = 2\sinh x\cosh x$, Eq. (B.80) can be reduced to:

$$U_q\big|_h = \frac{Ka_c^3a_o^2E_o^2}{16a_r^2E_c^2E_r^2\zeta^3}\left[2\tanh\left(\frac{\zeta h}{a_c}\right)-\frac{2\zeta h}{a_c}\operatorname{sech}^2\left(\frac{\zeta h}{a_c}\right)\right]\sigma_{c_\infty}^2 \tag{B.81}$$

Substituting Eqs. (B.77) and (B.81) into Eq. (B.68),

$$\Delta U_q =$$
$$\frac{Ka_c^3a_o^2E_o^2}{16a_r^2E_c^2E_r^2\zeta^3}\left[4\tanh\left(\frac{\zeta h}{a_c}\right)-2\tanh\left(\frac{2\zeta h}{a_c}\right)+\frac{4\zeta h}{a_c}\left(\operatorname{sech}^2\left(\frac{2\zeta h}{a_c}\right)-\operatorname{sech}^2\left(\frac{\zeta h}{a_c}\right)\right)\right]\sigma_{c_\infty}^2$$

$$\tag{B.82}$$

Solving Eq. (B.22) for K and placing into Eq. (B.82) and substituting Eqs. (B.27), (B.24), and (B.25),

$$\Delta U_q = \frac{a_c^2a_rE_cE_r}{4\zeta a_oE_o}\left[\frac{a_0\sigma_a}{a_rE_r}-(\alpha_c-\alpha_r)\Delta T\right]^2$$
$$\left[2\tanh\left(\frac{2\zeta h}{a_c}\right)-\tanh\left(\frac{\zeta h}{a_c}\right)+\frac{2\zeta h}{a_c}\left(\operatorname{sech}^2\left(\frac{2\zeta h}{a_c}\right)-\operatorname{sech}^2\left(\frac{\zeta h}{a_c}\right)\right)\right] \tag{B.83}$$

The total change in strain energy when a crack appears, ΔU, is simply

$$\Delta U = \Delta U_\sigma + \Delta U_q \tag{B.84}$$

Substituting Eqs. (B.64) and (B.83) into Eq. (B.84),

$$\Delta U = \frac{a_c^2a_o^2E_c\sigma_a^2-a_c^2a_r^2E_c^2E_r(\alpha_c-\alpha_r)^2\Delta T^2}{2a_ra_oE_rE_o\zeta}\left[2\tanh\left(\frac{\zeta h}{a_c}\right)-\tanh\left(\frac{2\zeta h}{a_c}\right)\right] \tag{B.85}$$

The change in external work when a crack forms, ΔW, is given by

$$\Delta W = \left[2W|_h - W|_{2h} \right] \tag{B.86}$$

where $W|_{2h}$ and $2W|_h$ are the work done by the applied loading before and after the new crack forms, respectively. The former is found from

$$W|_{2h} = 2a_o \sigma_a u_r(h) \tag{B.87}$$

Evaluating Eq. (B.44) at $x'=h$,

$$u_r(h) = \frac{a_o \sigma_a h}{a_r E_r} - \frac{a_c E_c}{a_o E_o} \left[\frac{a_o \sigma_a}{a_r E_r} - (\alpha_c - \alpha_r)\Delta T \right] \left[h - \frac{a_c}{2\zeta} \tanh\left(\frac{2\zeta h}{a_c} \right) \right] + \alpha_r \Delta T \tag{B.88}$$

Substituting Eq. (B.88) into Eq. (B.87),

$$\begin{aligned} W|_{2h} &= \frac{2a_o^2 \sigma_a^2 h}{a_r E_r} \\ &- \left[\frac{a_c^2 a_o^2 E_c \sigma_a^2 - a_c^2 a_r a_o E_c E_r (\alpha_c - \alpha_r)\Delta T \sigma_a}{\zeta a_r a_o E_r E_o} \right] \left[\frac{2\zeta h}{a_c} - \tanh\left(\frac{2\zeta h}{a_c} \right) \right] + 2a_o \alpha_r \Delta T \sigma_a h \end{aligned}$$
$$\tag{B.89}$$

The work done by the applied loading after the new crack forms is given by

$$W|_h = 2a_o \sigma_a u_r^{\cdot}\left(\frac{h}{2} \right) \tag{B.90}$$

where $u_r^{\cdot}\left(\frac{h}{2} \right)$ is found from Eq. (4.22), derived using the boundary conditions $\sigma_c^{\cdot} = 0$ at $x' = \pm \frac{h}{2}$. By analogy with $W|_{2h}$,

$$\begin{aligned} W|_h &= \frac{a_o^2 \sigma_a^2 h}{a_r E_r} \\ &- \left[\frac{a_c^2 a_o^2 E_c \sigma_a^2 - a_c^2 a_r a_o E_r E_c (\alpha_c - \alpha_r)\Delta T \sigma_a}{\zeta a_r a_o E_r E_o} \right] \left[\frac{\zeta h}{a_c} - \tanh\left(\frac{\zeta h}{a_c} \right) \right] + a_o \alpha_r \Delta T \sigma_a h \end{aligned} \tag{B.91}$$

Substituting Eqs. (B.89) and (B.91) into Eq. (B.86),

$$\Delta W = \frac{2a_c^2 a_o^2 E_c \sigma_a^2 - 2a_c^2 a_r E_c E_r a_o (\alpha_c - \alpha_r)\sigma_a \Delta T}{2\zeta a_r a_o E_r E_o} \left[2\tanh\left(\frac{\zeta h}{a_c} \right) - \tanh\left(\frac{2\zeta h}{a_c} \right) \right]$$
$$\tag{B.92}$$

170

The strain energy release rate is found by placing Eqs. (B.85) and (B.92) into Eq. (B.46), yielding,

$$G = \frac{a_c E_c}{2 a_r a_o E_r E_o \zeta} \left[a_o \sigma_a - a_r E_r (\alpha_c - \alpha_r) \Delta T \right]^2 \left[2 \tanh\left(\frac{\zeta h}{a_c}\right) - \tanh\left(\frac{2\zeta h}{a_c}\right) \right] \quad \text{(B.93)}$$

Placing Eqs. (B.24), (B.25), and (B.27) into Eq. (B.93), the strain energy release rate may also be expressed as

$$G = \frac{a_c a_o E_o}{2\zeta a_r E_r E_c} \left[2 \tanh\left(\frac{\zeta h}{a_c}\right) - \tanh\left(\frac{2\zeta h}{a_c}\right) \right] \sigma_{c_\infty}^2 \quad \text{(B.94)}$$

Substituting Eq. (B.93) into Eq. (B.47), the cracking criterion becomes

$$\frac{a_c E_c}{2\zeta a_r a_o E_r E_o} \left[a_o \sigma_a - a_r E_r (\alpha_c - \alpha_r) \Delta T \right]^2 \left[2 \tanh\left(\frac{\zeta h}{a_c}\right) - \tanh\left(\frac{2\zeta h}{a_c}\right) \right] \geq G_{Ic} \quad \text{(B.95)}$$

APPENDIX C

COMPUTER CODE MANUAL AND DOCUMENTATION

****

USING CRACKOMATIC II

CODE FOR THE PREDICTION OF
MATRIX CRACKING

c 1995 Jason R. Maddocks and Hugh L. McManus
Massachusetts Institute of Technology
Rm 33-311, 77 Massachusetts Ave.
Cambridge MA 02139 (617) 253-0672

****
Version 2.1 1/95
WRITTEN IN MPW FORTRAN
c 1988,1989 Language Systems Corp.

****

This program is a research tool in the development stage
and is supplied "as is" for the purpose of
scientific collaboration.

****

L INTRODUCTION

CRACKOMATIC II Version 2.1 calculates matrix crack density and reduced laminate properties in every ply of any arbitrary laminate as functions of temperature, thermal cycles, or any thermomechanical load history.

II. INPUT FILES

CRACKOMATIC II requires four kinds of prepared input files: 1) a laminate file containing material and layup information, 2) a fatigue toughness file for thermal cyclic loading, 3) a load profile for thermomechanical loading, and 4) temperature/cycle dependent material property files (optional). These should be ASCII text files in the same folder or directory as the code.

Separate all entries by spaces and terminate every line, including the last one, with a carriage return.

IIa. LAMINATE FILE FORMAT

        NPLY
        NMATi ANGLEi THICKi FLAGi
        repeat above line NPLY times

        EXi EYi NUXYi GXYi
        ALPHA1i ALPHA2i BETA1i BETA2i
        repeat above 2 lines for each material

NPLY is the number of ply groups in the laminate
for each ply:
NMATi is the material number of that ply group (number materials consecutively from 1)
ANGLEi is the ply angle in degrees
THICKi is the ply thickness
FLAGi is a ply printing option. It should be set to 1 to print out the output data/results for ply i. Set to 0 if the printing of results for this ply is not needed. For each material:
EXi is the longitudinal ply modulus
EYi is the transverse ply modulus
NUXYi is the major Poisson's ratio
GXYi is the shear modulus
ALPHA1i is the longitudinal ply CTE
ALPHA2i is the transverse ply CTE
BETA1i and BETA2i are currently dormant ply CMEs- use 0.0

EXAMPLE: (A P75/934 [0/45/90/-45]s laminate, English units)

        7
        1 .005 0 0
        1 .005 45 1
        1 .005 90 1
        1 .010 -45 1
        1 .005 90 0
        1 .005 45 0
        1 .005 0 0
        34.3E6 0.9E6 .29 0.7E6
        -0.6E-6 16.E-6 0 0

IIb. FATIGUE TOUGHNESS FILE FORMAT

        NPOINTS
        Ni GCi
        repeat above line NPOINTS times

NPOINTS is the number of data points that defines the Gc vs N curve for each point:
Ni is the number of cycles
GCi is the measured transverse fracture toughness corresponding to that number of cycles

EXAMPLE: (P75/ERL1962, extrapolated from very limited data)

```
6
1          .59566
10         .55627
100        .51947
1000       .48512
10000      .45303
100000     .42307
```

IIc. THERMOMECHANICAL LOAD PROFILE

The thermomechanical load profile may accommodate any number of user-defined load increments, with thermal and mechanical loads applied either simultaneously or separately. Each increment is treated as a ramp, and loads are assumed to be quasi-static. Cycling effects are neglected.

The code always starts at the stress free temperature and ramps down to the first load in the load profile, which accounts for cooldown at the end of the cure cycle. Thus the first entry in the user's load profile should be the ambient conditions, i.e. room temperature and zero mechanical stress. The initial cure cycle ramp is not included in the output.

File format for thermomechanical loading:

```
NPROF
Ti SIGMAi
repeat above line NPROF times
```

NPROF is the number of increments in the load profile.
Ti and SIGMAi are the temperature and stress, respectively, at the ith increment. Ti is an actual temperature, not a ΔT.

EXAMPLE: (English units)

```
4
70 0
70 8.0E4
-100 8.0E4
-300 1.2E5
```

The laminate starts at ambient conditions, 70°F and zero applied mechanical stress. It is then loaded to 80 ksi with the temperature held constant. Next, with the mechanical stress held constant at 80 ksi, the temperature is reduced to -100°F. Finally, the temperature and mechanical stress are ramped simultaneously from the previous increment to -300°F and 120 ksi, respectively.

IId. TEMPERATURE/CYCLE DEPENDENT MATERIAL PROPERTY FILES

The temperature dependent material file is similar to the fatigue toughness file format. All material constants are listed.

File format:
        NPOINTS
        Ti EXi EYi NUXYi GXYi ALPHA1i ALPHA2i GCi
        repeat above line NPOINTS times

Ti is the temperature
Other variables are as previously described

EXAMPLE (P75/934)

```
        3
        -250   33.76E6   .9E6   .31   1.1E6   -0.43E-6    21.923E-6
.22791
        75    41.97E6   .83E6  .35   .61E6   -0.584E-6   19.18E-6
.22791
        250   45.36E6   .81E6  .30   .46E6   -0.365E-6   26.455E-6
.22791
```

File format for the material properties as function of cyclic loading is similar:
        NPOINTS
        Ni EXi EYi NUXYi GXYi ALPHA1i ALPHA2i GCi
        repeat above line NPOINTS times

III. INTERACTIVE SESSION

Once you have defined some layups and material files, run CRACKOMATIC. The following capitalized text refers to the questions/options during the interactive session.

The program will first ask for the laminate input file, give it one. Then it asks:

COMPUTE MINIMUM (1), MAXIMUM (2), OR AVERAGE (3) CRACK DENSITY?
Minimum seems to work best, so always choose it unless you specifically want to check theoretical maximum or average densities.

The code then outputs a review of the laminate, and a complete set of calculated laminate properties.

ANALYSIS TYPE-
1 = CRACK DENSITY AND PROPERTIES AS FUNCTION OF DELTA-T
2 = CRACK DENSITY AND PROPERTIES AS FUNCTION OF N
3 = CRACK DENSITY FROM THERMOMECHANICAL LOAD PROFILE
4 = READ NEW LAMINATE
5 = QUIT
Choices 1, 2, and 3 have their own sections below.
Choice 4 lets you pick a new laminate and/or change your choice of crack density. Choice 5 stops the code, leaving the session in an editable text window, where the results can be cut and pasted into other documents.

IIIa. ANALYSIS TYPE 1

This analysis calculates the progressive change in crack density and laminate properties as functions of decreasing temperature. The code asks:

GIVE G (TRANSVERSE PLY FRACTURE TOUGHNESS),
    SHEAR LAG FACTOR
    AND LAMINATE STRESS FREE TEMPERATURE
G is the critical strain energy release rate.
SHEAR LAG FACTOR is a geometric parameter which can reasonably range from around 0.5 to around 2.0.
LAMINATE STRESS FREE TEMPERATURE is usually the laminate cure temperature. The code then asks

GIVE TEMPERATURE RANGE AND INCREMENT:
INITIAL TEMP, FINAL TEMP, AND TEMP INCREMENT
User option variables to control the printed output

WANT TO SOFTEN LAMINATE AS IT PROGRESSES?
User option to include material softening effect (answer yes or no)

WANT TO INCORPORATE TEMPERATURE DEPENDENCE OF MATERIAL CONSTANTS (REQUIRES INPUT FILE)?
User option to include temperature dependent material properties, required input file with appropriate data (see format in Section IId.)

The output is a tab-separated table of temperatures, crack densities and laminate longitudinal stiffness and CTE. These can be used to generate plots of progressive cracking and changing laminate properties as the temperature is progressively decreased. At the final temperature, the program computes all the degraded laminate properties.

IIb. ANALYSIS TYPE 2

This analysis calculates the change in crack density and laminate properties as functions of numbers of constant thermal cycles. The code asks:

INPUT G(N) FILE NAME, OR HELP IF YOU NEED IT
Give it the name of a FATIGUE TOUGHNESS FILE (see format in Section IIb.).

GIVE SHEAR LAG FACTOR AND GREATEST DELTA-T
Give the shear lag factor described above, and the DELTA-T at the lowest temperature in the cycle. (The highest temperature or cycle R-value are assumed to be the same as those used to generate the data in the fatigue toughness file, so you don't input either of these).

INCREASE N LINEARLY (ENTER Y) OR EXPONENTIALLY (N)?
This choice controls the output. A "Y" will give output suitable for making a linear plot, while an "N" will generate output suitable for making a semi-log plot. If you choose Y, you are asked

GIVE MAXIMUM N AND INCREMENT
which is self-explanatory; if you choose N, you are asked
GIVE MAXIMUM N AND POINTS PER DECADE
which is almost so; points per decade is the number of plot
points generated for each power of ten on the plot.

WANT TO SOFTEN LAMINATE?
User option to include material softening effect

WANT TO INCORPORATE MATERIAL CONSTANTS AS FUNCTION OF THERMAL CYCLES (REQUIRES INPUT FILE)?
User option to include material properties as a function of thermal cycles, required input file with appropriate data.

The output is a tab-separated table of number of cycles, crack densities, and laminate longitudinal stiffness and CTE. These can be used to generate plots of cracking and changing laminate properties as the laminate is thermally cycled.

IIc. ANALYSIS TYPE 3

This analysis calculates the progressive change in crack density and laminate properties due to a user-defined thermomechanical load history. The code first asks:

PLEASE INPUT LOAD HISTORY FILE
Enter the name of the THERMOMECHANICAL LOAD PROFILE file (see format in Section IIc.)

GIVE G (TRANSVERSE PLY FRACTURE TOUGHNESS),

177

SHEAR LAG FACTOR
            AND LAMINATE STRESS FREE TEMPERATURE
G is the critical strain energy release rate.
SHEAR LAG FACTOR is a geometric parameter which can reasonably range
from around 0.5 to around 2.0.
LAMINATE STRESS FREE TEMPERATURE is usually the laminate cure
temperature. The code then asks

WANT TO SOFTEN LAMINATE AS IT PROGRESSES?
User option to include material softening effect

WANT TO INCORPORATE TEMPERATURE DEPENDENCE OF MATERIAL
CONSTANTS (REQUIRES INPUT FILE)?
User option to include temperature dependent material properties, required
input file with appropriate data (see format in Section IId.)

The output is a tab-separated table of temperatures, applied mechanical
stresses, crack densities and laminate longitudinal stiffness and CTE. These
can be used to generate plots of progressive cracking and changing laminate
properties with progressive changes in temperature, stress, or both. At the
final load, the program computes all the degraded laminate properties.

IV. A FEW USEFUL TRICKS

In the Macintosh version of the code, the output remains in an editable,
saveable text window following execution. The edit and file commands are
functional. Usually, all work in a session can be accessed by scrolling; very
long sessions save themselves in a file and must be closed and reopened using
an editor.

The outputs of Analysis Types 1, 2, and 3 are in tab-separated tables that can
be cut and pasted directly into spreadsheets or plotting programs. The code
expects all inputs in a consistent set of units. Make sure, for example, that if
you are using metric units you enter ply thicknesses in METERS, not
millimeters as they are usually reported.

A "hack" in the code allows you to give all properties in English units except
G_{Ic} (which is usually reported in metric) by entering negative G_{Ic} values; the
code converts the absolute value of G_{Ic} to English units.

V. SAMPLE SESSION

Three samples sessions are listed below. The first is an example of Analysis
Type 1. This example includes material softening effects and temperature
dependent material properties. The second session is an example of Analysis
Type 2 using material softening effects. The third shows an Analysis Type 3

including material softening effects and temperature dependent material properties. User input is in *bold italics*..

Va. SAMPLE SESSION A: ANALYSIS TYPE 1 OF P75/934 [0/45/90/-45]ₛ

INPUT LAYUP FILE OR HELP IF YOU NEED IT
p75934zfnf

| | | LAMINATE | |
PLY	MATERIAL	THICKNESS	ANGLE
1	1	0.0050	0.00
2	1	0.0050	45.00
3	1	0.0050	90.00
4	1	0.0100	-45.00
5	1	0.0050	90.00
6	1	0.0050	45.00
7	1	0.0050	0.00

MATERIAL PROPERTIES FOR MATERIAL 1-
E11   3.4300E+07   E22   9.0000E+05
NU12   2.9000E-01   G12   7.0000E+05
ALPHA1 -6.0000E-07   ALPHA2   1.6000E-05
BETA1   0.0000E+00   BETA2   0.0000E+00

ENGINEERING CONSTANTS FOR UNCRACKED LAMINATE-
E11 = 1.2317E+07 E22 = 1.2317E+07 G = 4.6943E+06
V12 = 3.1191E-01 V21 = 3.1191E-01
ALPHA1 = -6.0484E-08 ALPHA2 = -6.0484E-08 ALPHA12 = -4.8557E-19
BETA1 = 0.0000E+00 BETA2 = 0.0000E+00 BETA12 = 0.0000E+00

COMPUTE: (1) MINIMUM, (2) MAXIMUM, (3) AVERAGE CRACK SPACING
1

ANALYSIS TYPE-
1 = CRACK DENSITY AS FUNCTION OF DELTA-T
2 = CRACK DENSITY AS FUNCTION OF CYCLES (N)
3 = CRACK DENSITY FROM THERMOMECHANICAL LOAD PROFILE
4 = READ NEW LAMINATE
5 = QUIT
1

  GIVE G (TRANSVERSE PLY FRACTURE TOUGHNESS)
     SHEAR LAG FACTOR,
     LAMINATE STRESS FREE TEMPERATURE
-40 .65 350

  GIVE TEMPERATURE RANGE AND INCREMENT:
  INITIAL TEMP, FINAL TEMP, AND TEMP INCREMENT
75 -250 25

  WANT TO SOFTEN LAMINATE AS IT PROGRESSES?
y

WANT TO INCORPORATE TEMPERATURE DEPENDENCE OF
MATERIAL CONSTANTS (REQUIRES INPUT FILE) ?
y

PLEASE INPUT TEMPERATURE DEPENDENT MATERIAL FILE
p75934_tdep

TRANSVERSE PLY FRACTURE TOUGHNESS = 4.0000E+01 (METRIC)
TRANSVERSE PLY FRACTURE TOUGHNESS = 2.2791E-01
SHEAR LAG FACTOR =   0.65
STRESS FREE TEMPERATURE =   350.00

Temperature	* PLY 2 * Crack Density	* PLY 3 * Crack Density	* PLY 4 * Crack Density	LAMINATE Stiffness	CTE
75	0.0000E+00	0.0000E+00	0.0000E+00	1.4776E+07	-7.3510E-08
50	0.0000E+00	0.0000E+00	8.0141E+00	1.4571E+07	-5.7974E-08
25	0.0000E+00	0.0000E+00	1.5183E+01	1.4367E+07	-4.1396E-08
0	0.0000E+00	0.0000E+00	1.8989E+01	1.4173E+07	-1.9946E-08
-25	0.0000E+00	0.0000E+00	2.2130E+01	1.3981E+07	2.6973E-09
-50	0.0000E+00	0.0000E+00	2.4945E+01	1.3788E+07	2.6106E-08
-75	2.6459E+01	3.6858E+01	2.7567E+01	1.3517E+07	-1.3391E-08
-100	3.3482E+01	4.6949E+01	3.0048E+01	1.3300E+07	-8.4506E-09
-125	3.9021E+01	5.4842E+01	3.2430E+01	1.3086E+07	-1.4497E-10
-150	4.3892E+01	6.1767E+01	3.4737E+01	1.2872E+07	9.5830E-09
-175	4.8371E+01	6.8126E+01	3.6984E+01	1.2660E+07	2.0111E-08
-200	5.2588E+01	7.4108E+01	3.9184E+01	1.2446E+07	3.1153E-08
-225	5.6616E+01	7.9821E+01	4.1345E+01	1.2233E+07	4.2564E-08
-250	6.0469E+01	8.5284E+01	4.3457E+01	1.2027E+07	5.3318E-08

ALL LAMINATE PROPERTIES AT FINAL TEMPERATURE
E11 = 1.2027E+07 E22 = 1.2026E+07 G = 4.6281E+06
V12 = 3.0888E-01 V21 = 3.0887E-01
ALPHA1 = 5.3318E-08 ALPHA2 = 5.2551E-08 ALPHA12 = -4.8800E-08
BETA1 = 0.0000E+00 BETA2 = 0.0000E+00 BETA12 = 0.0000E+00

ANALYSIS TYPE-
1 = CRACK DENSITY AS FUNCTION OF DELTA-T
2 = CRACK DENSITY AS FUNCTION OF CYCLES (N)
3 = CRACK DENSITY FROM THERMOMECHANICAL LOAD PROFILE
4 = READ NEW LAMINATE
5 = QUIT
5

Vb SAMPLE SESSION B: ANALYSIS TYPE 2 OF P75/ERL1962 [0/90/0/90]s

INPUT LAYUP FILE OR HELP IF YOU NEED IT
p75znzn

PLY	MATERIAL	LAMINATE THICKNESS	ANGLE
1	1	0.0050	0.00
2	1	0.0050	90.00
3	1	0.0050	0.00
4	1	0.0100	90.00
5	1	0.0050	0.00
6	1	0.0050	90.00
7	1	0.0050	0.00

MATERIAL PROPERTIES FOR MATERIAL 1-
E11   3.4300E+07   E22   9.0000E+05
NU12   2.9000E-01   G12   7.0000E+05
ALPHA1 -5.3000E-07   ALPHA2   2.2000E-05
BETA1   0.0000E+00   BETA2   0.0000E+00

ENGINEERING CONSTANTS FOR UNCRACKED LAMINATE-
E11 = 1.7635E+07   E22 = 1.7635E+07   G =   7.0000E+05
V12 = 1.4830E-02   V21 = 1.4830E-02
ALPHA1 = 2.0225E-07   ALPHA2 = 2.0225E-07   ALPHA12 = -6.8180E-18
BETA1 = 0.0000E+00   BETA2 = 0.0000E+00   BETA12 = 0.0000E+00

COMPUTE: (1) MINIMUM, (2) MAXIMUM, (3) AVERAGE CRACK SPACING
1

ANALYSIS TYPE-
 1 = CRACK DENSITY AS FUNCTION OF DELTA-T
 2 = CRACK DENSITY AS FUNCTION OF CYCLES (N)
 3 = CRACK DENSITY FROM THERMOMECHANICAL LOAD PROFILE
 4 = READ NEW LAMINATE
 5 = QUIT
2

 INPUT G(N) FILE NAME OR HELP IF YOU NEED IT
p75gs

 GIVE SHEAR LAG FACTOR AND GREATEST DELTA-T
.65 -600

 INCREASE N LINEARLY (ENTER Y) OR EXPONENTIALLY (N)?
y

 GIVE MAXIMUM N AND INCREMENT
500 25

 WANT TO SOFTEN LAMINATE?
y

 WANT TO INCORPORATE MATERIAL CONSTANTS
 AS FUNCTION OF CYCLES?

181

n

FRACTURE TOUGHNESS AS A FUNCTION OF CYCLE

N	FRACTURE TOUGHNESS
1.0000E+00	5.9566E-01
1.0000E+01	5.5627E-01
1.0000E+02	5.1947E-01
1.0000E+03	4.8512E-01
1.0000E+04	4.5303E-01
1.0000E+05	4.2307E-01

SHEAR LAG FACTOR =   0.65
MAXIMUM DELTA-T = -600.00

Cycle	* PLY 1 * Crack Density	* PLY 2 * Crack Density	* PLY 4 * Crack Density	LAMINATE Stiffness	CTE
0	1.8201E+01	1.8037E+01	3.5615E+01	1.7558E+07	9.5881E-08
25	3.4207E+01	3.4483E+01	3.7763E+01	1.7540E+07	6.3889E-08
50	3.5999E+01	3.6245E+01	3.8244E+01	1.7538E+07	5.9886E-08
75	3.7677E+01	3.7901E+01	3.8733E+01	1.7536E+07	5.6050E-08
100	3.9273E+01	3.9480E+01	3.9231E+01	1.7533E+07	5.2329E-08
125	3.9423E+01	3.9629E+01	3.9280E+01	1.7533E+07	5.1975E-08
150	3.9568E+01	3.9773E+01	3.9326E+01	1.7533E+07	5.1633E-08
175	3.9712E+01	3.9916E+01	3.9374E+01	1.7533E+07	5.1291E-08
200	3.9856E+01	4.0059E+01	3.9421E+01	1.7533E+07	5.0950E-08
225	4.0000E+01	4.0201E+01	3.9468E+01	1.7532E+07	5.0609E-08
250	4.0143E+01	4.0343E+01	3.9516E+01	1.7532E+07	5.0269E-08
275	4.0286E+01	4.0485E+01	3.9563E+01	1.7532E+07	4.9930E-08
300	4.0429E+01	4.0626E+01	3.9610E+01	1.7532E+07	4.9591E-08
325	4.0572E+01	4.0767E+01	3.9658E+01	1.7532E+07	4.9252E-08
350	4.0713E+01	4.0907E+01	3.9706E+01	1.7531E+07	4.8915E-08
375	4.0854E+01	4.1047E+01	3.9754E+01	1.7531E+07	4.8575E-08
400	4.0995E+01	4.1187E+01	3.9802E+01	1.7531E+07	4.8239E-08
425	4.1135E+01	4.1327E+01	3.9850E+01	1.7531E+07	4.7902E-08
450	4.1275E+01	4.1465E+01	3.9898E+01	1.7531E+07	4.7566E-08
475	4.1415E+01	4.1604E+01	3.9946E+01	1.7530E+07	4.7230E-08
500	4.1555E+01	4.1742E+01	3.9995E+01	1.7530E+07	4.6894E-08

ALL LAMINATE PROPERTIES AT FINAL TEMPERATURE

E11 = 1.7530E+07 E22 = 1.7564E+07 G = 5.6136E+05
V12 = 1.1942E-02 V21 = 1.1965E-02
ALPHA1 = 4.6894E-08 ALPHA2 = 7.6861E-08 ALPHA12 = -7.6337E-18
BETA1 = 0.0000E+00 BETA2 = 0.0000E+00 BETA12 = 0.0000E+00

ANALYSIS TYPE-
1 = CRACK DENSITY AS FUNCTION OF DELTA-T
2 = CRACK DENSITY AS FUNCTION OF CYCLES (N)
3 = CRACK DENSITY FROM THERMOMECHANICAL LOAD PROFILE
4 = READ NEW LAMINATE
5 = QUIT
5

INPUT LAYUP FILE OR HELP IF YOU NEED IT
p75934zfnf

PLY	MATERIAL	LAMINATE THICKNESS	ANGLE
1	1	0.0050	0.00
2	1	0.0050	45.00
3	1	0.0050	90.00
4	1	0.0100	-45.00
5	1	0.0050	90.00
6	1	0.0050	45.00
7	1	0.0050	0.00

MATERIAL PROPERTIES FOR MATERIAL 1-
$E11$ 3.4300E+07 $E22$ 9.0000E+05
$NU12$ 2.9000E-01 $G12$ 7.0000E+05
$ALPHA1$ -6.0000E-07 $ALPHA2$ 1.6000E-05
$BETA1$ 0.0000E+00 $BETA2$ 0.0000E+00

ENGINEERING CONSTANTS FOR UNCRACKED LAMINATE-
$E11$ = 1.2317E+07 $E22$ = 1.2317E+07 G = 4.6943E+06
$V12$ = 3.1191E-01 $V21$ = 3.1191E-01
$ALPHA1$ = -6.0484E-08 $ALPHA2$ = -6.0484E-08 $ALPHA12$ = -4.8557E-19
$BETA1$ = 0.0000E+00 $BETA2$ = 0.0000E+00 $BETA12$ = 0.0000E+00

COMPUTE: (1) MINIMUM, (2) MAXIMUM, (3) AVERAGE CRACK SPACING
1

ANALYSIS TYPE-
1 = CRACK DENSITY AS FUNCTION OF DELTA-T
2 = CRACK DENSITY AS FUNCTION OF CYCLES (N)
3 = CRACK DENSITY FROM THERMOMECHANICAL LOAD PROFILE
4 = READ NEW LAMINATE
5 = QUIT
3

PLEASE INPUT LOAD HISTORY FILE
p75934_profile

GIVE G (TRANSVERSE PLY FRACTURE TOUGHNESS)
    SHEAR LAG FACTOR,
    LAMINATE STRESS FREE TEMPERATURE
-40 .65 350

WANT TO SOFTEN LAMINATE AS IT PROGRESSES?
y

WANT TO INCORPORATE TEMPERATURE DEPENDENCE OF

MATERIAL CONSTANTS (REQUIRES INPUT FILE) ?
y

PLEASE INPUT TEMPERATURE DEPENDENT MATERIAL FILE
p75934_tdep

TRANSVERSE PLY FRACTURE TOUGHNESS = 4.0000E+01 (METRIC)
TRANSVERSE PLY FRACTURE TOUGHNESS = 2.2791E-01
SHEAR LAG FACTOR =   0.65
STRESS FREE TEMPERATURE =   350.00

Temp	Applied Stress	* PLY 2 * Crack Density	* PLY 3 * Crack Density	* PLY 4 * Crack Density	LAMINATE Stiffness	CTE
75	0.000E+00	0.000E+00	0.000E+00	0.000E+00	1.4776E+07	-7.3510E-08
50	0.000E+00	0.000E+00	0.000E+00	8.014E+00	1.4571E+07	-5.7974E-08
25	0.000E+00	0.000E+00	0.000E+00	1.518E+01	1.4367E+07	-4.1396E-08
0	0.000E+00	0.000E+00	0.000E+00	1.899E+01	1.4173E+07	-1.9946E-08
-25	0.000E+00	0.000E+00	0.000E+00	2.213E+01	1.3981E+07	2.6973E-09
-50	0.000E+00	0.000E+00	0.000E+00	2.495E+01	1.3788E+07	2.6106E-08
-75	0.000E+00	2.646E+01	3.686E+01	2.757E+01	1.3517E+07	-1.3391E-08
-100	0.000E+00	3.348E+01	4.695E+01	3.005E+01	1.3300E+07	-8.4506E-09
-125	1.143E+04	4.319E+01	6.311E+01	3.438E+01	1.3061E+07	-1.6840E-08
-150	2.286E+04	5.129E+01	7.633E+01	3.847E+01	1.2828E+07	-2.1044E-08
-175	3.429E+04	5.862E+01	8.825E+01	4.240E+01	1.2596E+07	-2.3427E-08
-200	4.571E+04	6.549E+01	9.940E+01	4.622E+01	1.2365E+07	-2.4731E-08
-225	5.714E+04	7.207E+01	1.101E+02	4.995E+01	1.2134E+07	-2.5275E-08
-250	6.857E+04	7.840E+01	1.204E+02	5.360E+01	1.1912E+07	-2.6036E-08
-275	8.000E+04	8.357E+01	1.288E+02	5.661E+01	1.1883E+07	-4.5323E-08

ALL LAMINATE PROPERTIES AT FINAL TEMPERATURE
E11 = 1.1883E+07 E22 = 1.1910E+07 G = 4.5773E+06
V12 = 3.1317E-01 V21 = 3.1389E-01
ALPHA1 = -4.5323E-08 ALPHA2 = 4.9401E-09 ALPHA12 = -4.7435E-08
BETA1 = 0.0000E+00 BETA2 = 0.0000E+00 BETA12 =   0.0000E+00

ANALYSIS TYPE-
1 = CRACK DENSITY AS FUNCTION OF DELTA-T
2 = CRACK DENSITY AS FUNCTION OF CYCLES (N)
3 = CRACK DENSITY FROM THERMOMECHANICAL LOAD PROFILE
4 = READ NEW LAMINATE
5 = QUIT
5

184

APPENDIX D

CRACK DENSITY DATA AND ANALYTICAL PREDICTIONS

This appendix presents all results of the progressive thermal and mechanical loading tests of the $[0_4/45_4/90_4/-45_4]_s$, $[0_2/45_2/90_2/-45_2]_s$, and $[0_2/60_2/-60_2]_s$ laminates. Thermal results comprise crack data from both interior and edge inspections. Average observed crack density is plotted as a function of applied load or decreasing temperature. Error bars represent one standard deviation. Predicted crack density curves are plotted on the same graphs as the experimental data.

$[0_4/45_4/90_4/-45_4]_s$
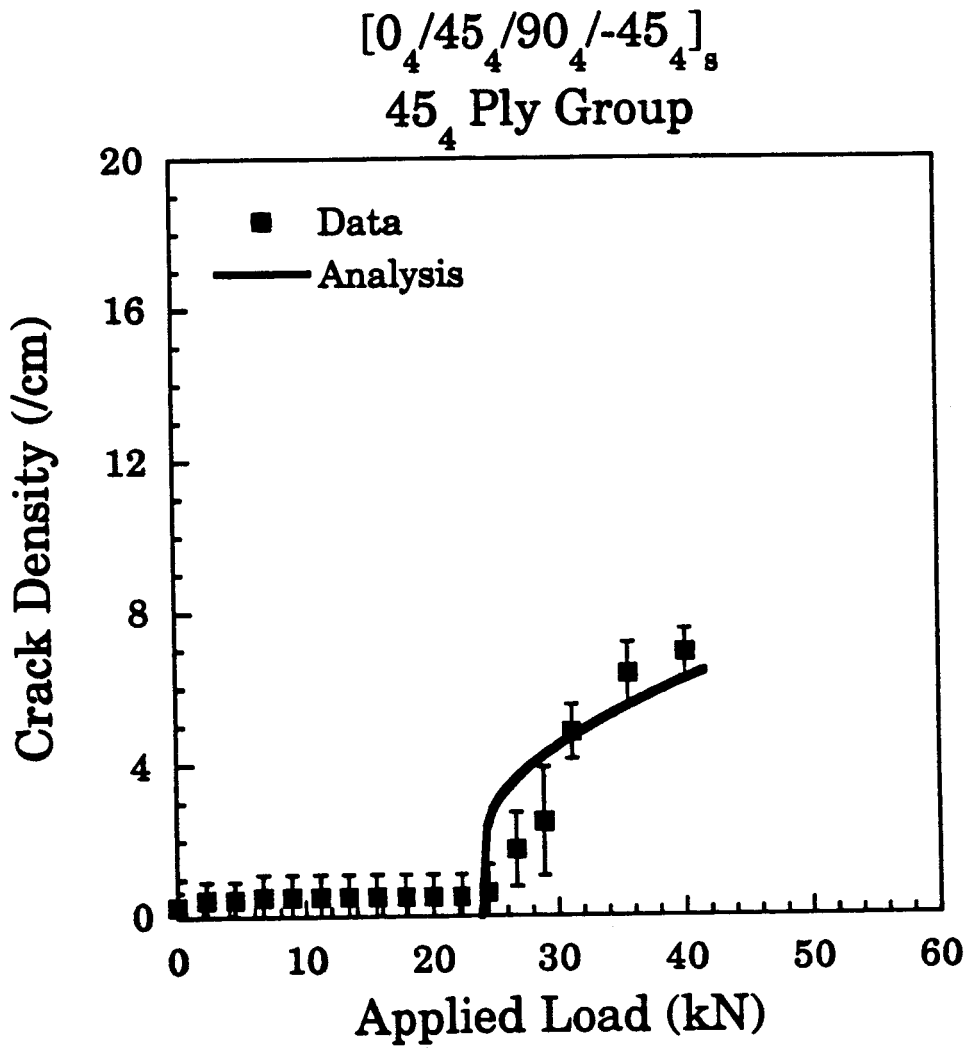
45_4 Ply Group

Figure D.1 Experimental results and analytical predictions of crack density vs. progressive applied load. 45_4 ply group of $[0_4/45_4/90_4/-45_4]_s$ laminate.

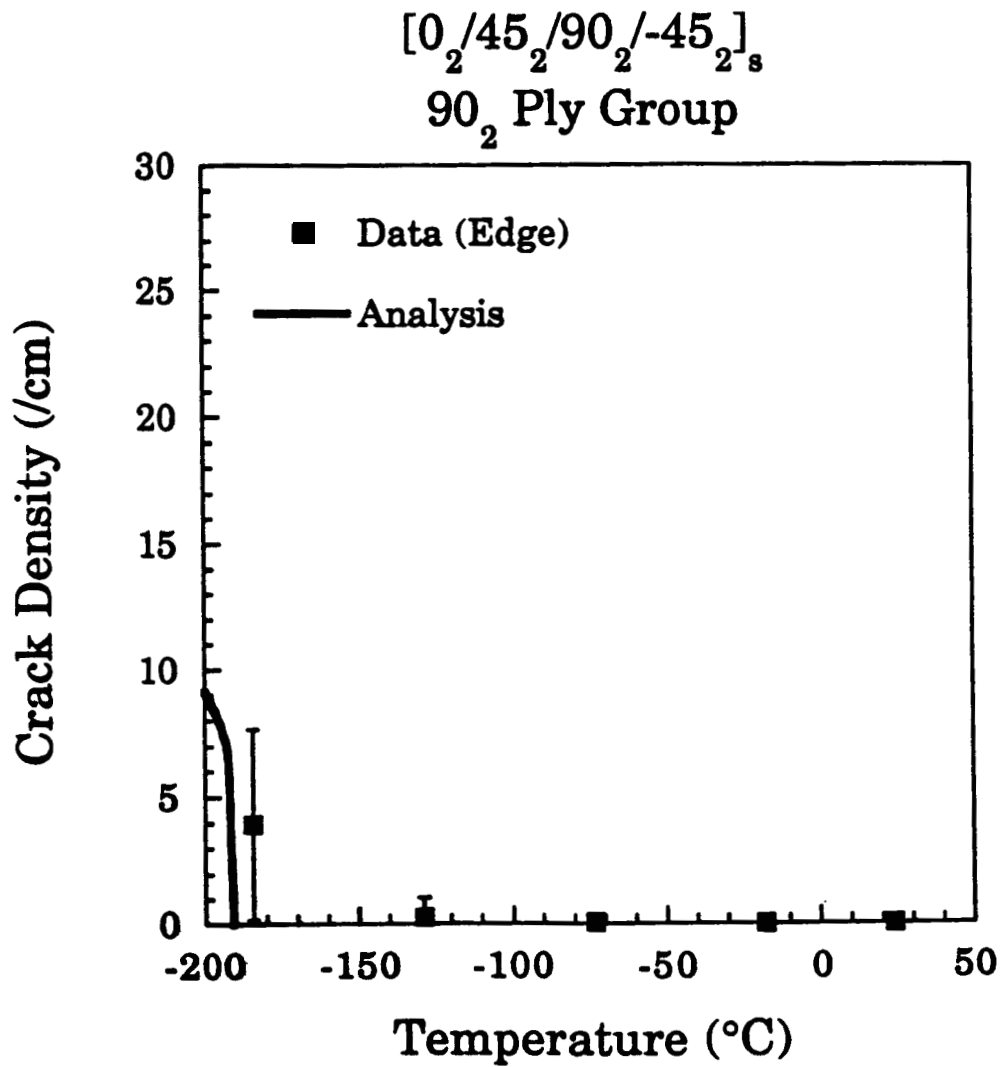$$[0_4/45_4/90_4/-45_4]_s$$
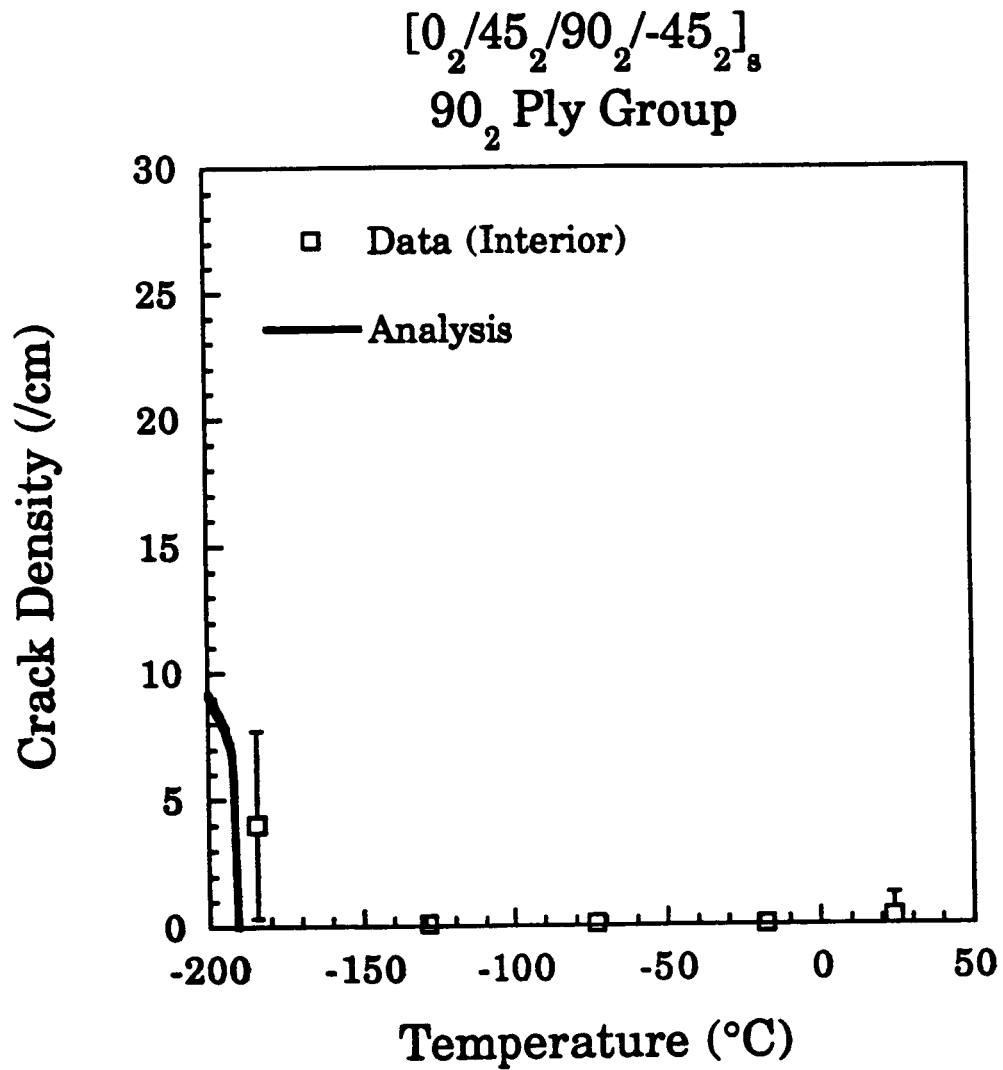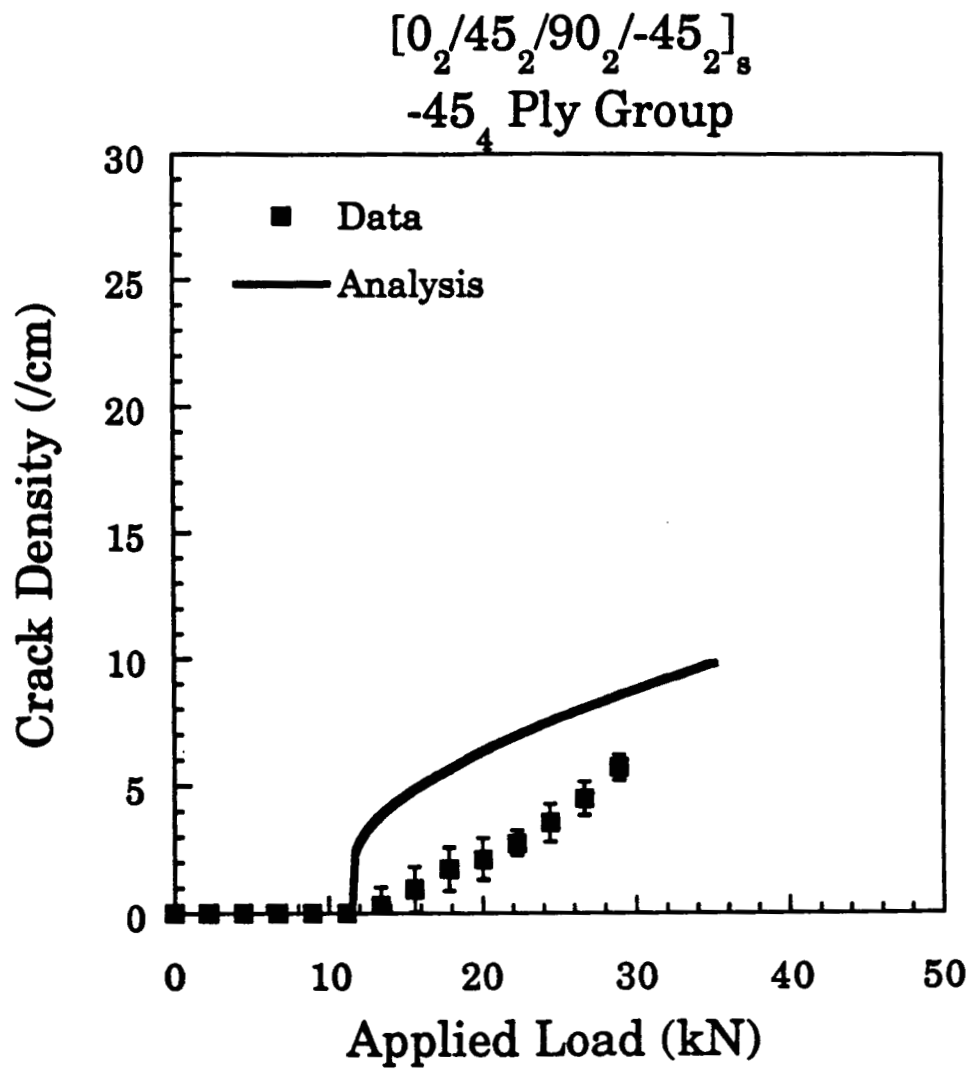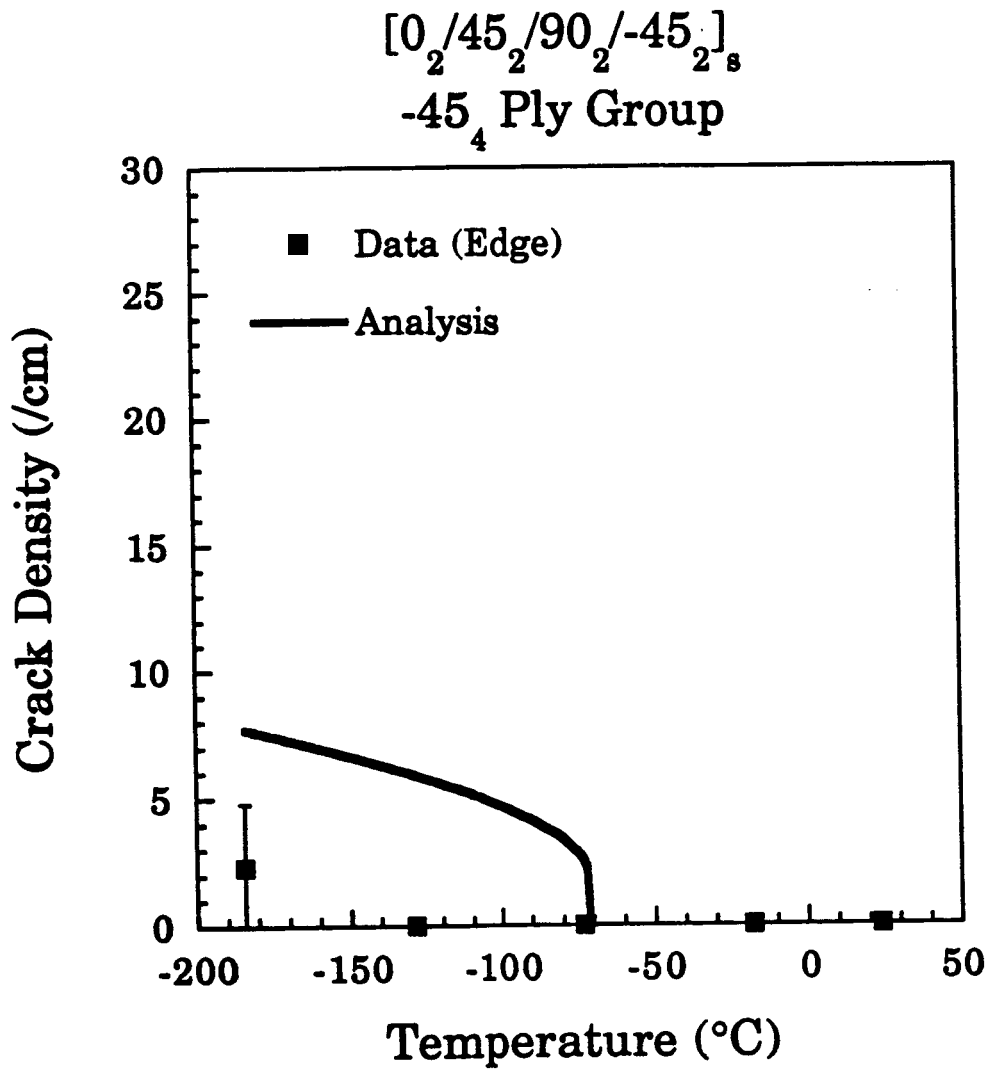$$45_4 \text{ Ply Group}$$
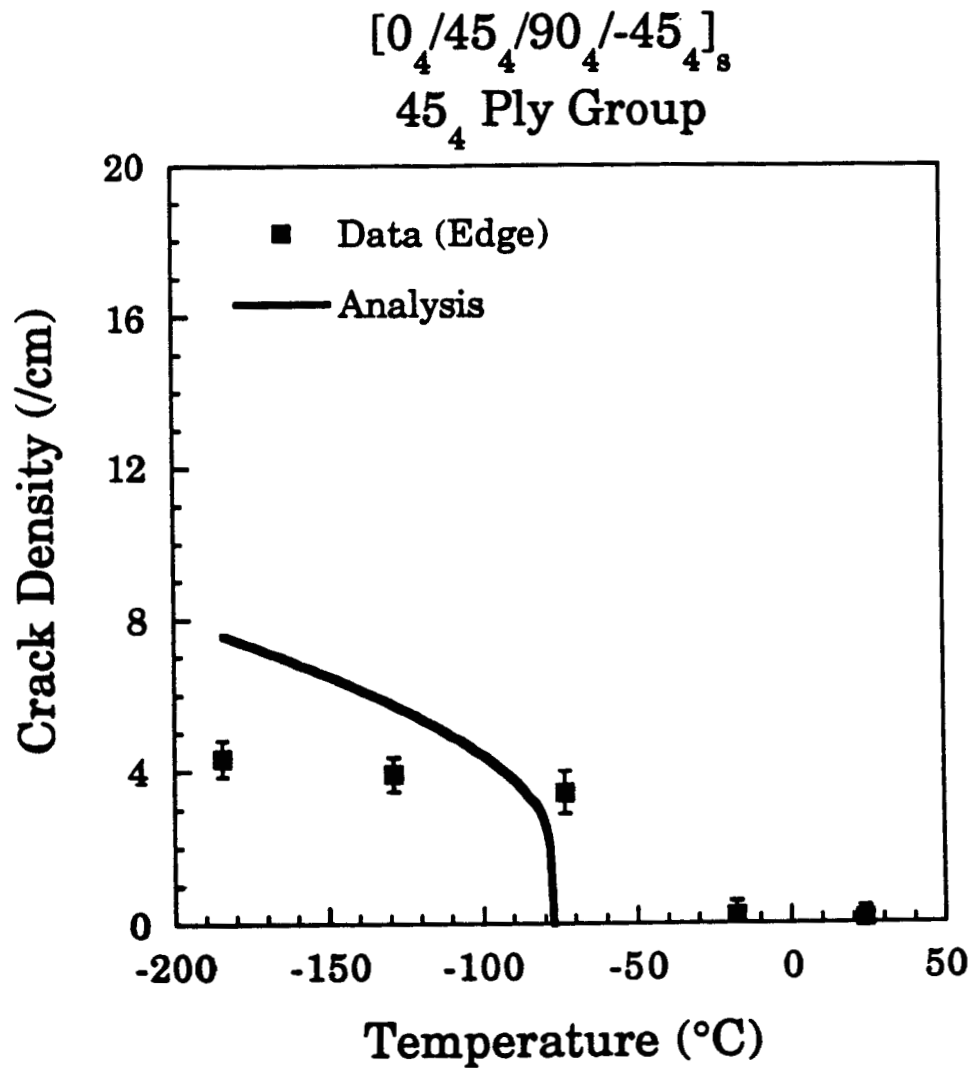
Figure D.2 Experimental results and analytical predictions of crack density vs. progressively decreasing temperature. 45_4 ply group of $[0_4/45_4/90_4/-45_4]_s$ edge specimens.

$$[0_4/45_4/90_4/-45_4]_s$$
$$45_4 \text{ Ply Group}$$
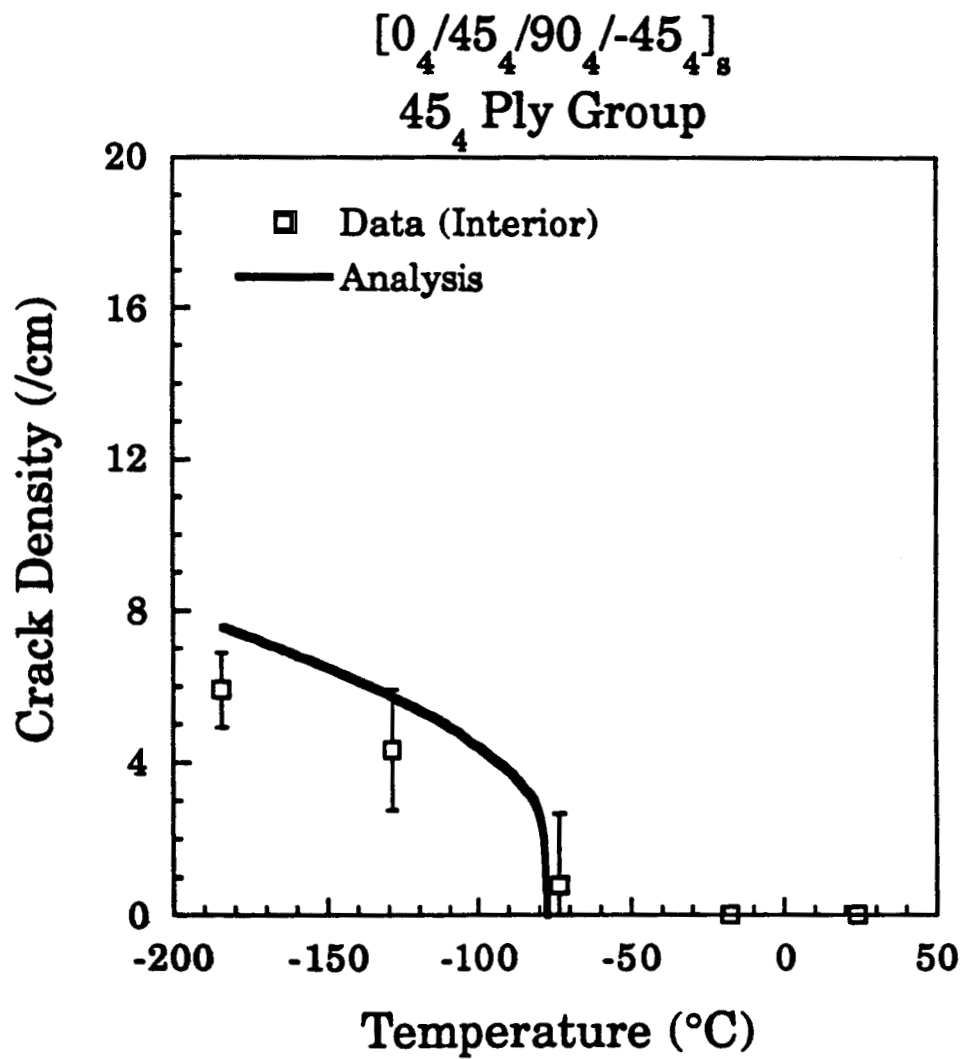
Figure D.3   Experimental results and analytical predictions of crack density vs. progressively decreasing temperature. 45_4 ply group of $[0_4/45_4/90_4/-45_4]_s$ interior specimens.

$$[0_4/45_4/90_4/-45_4]_s$$
$$90_4 \text{ Ply Group}$$
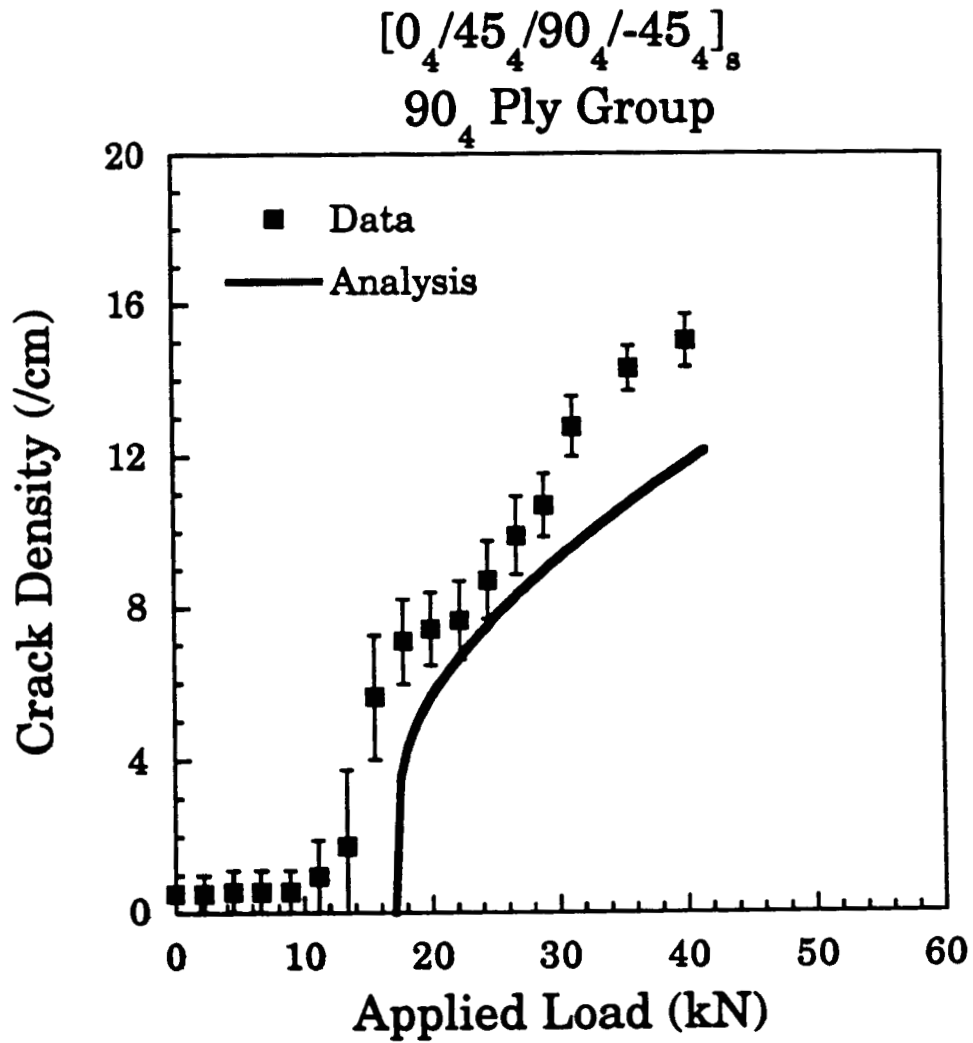
Figure D.4 Experimental results and analytical predictions of crack density vs. progressive applied load. 90₄ ply group of [0₄/45₄/90₄/-45₄]ₛ laminate.
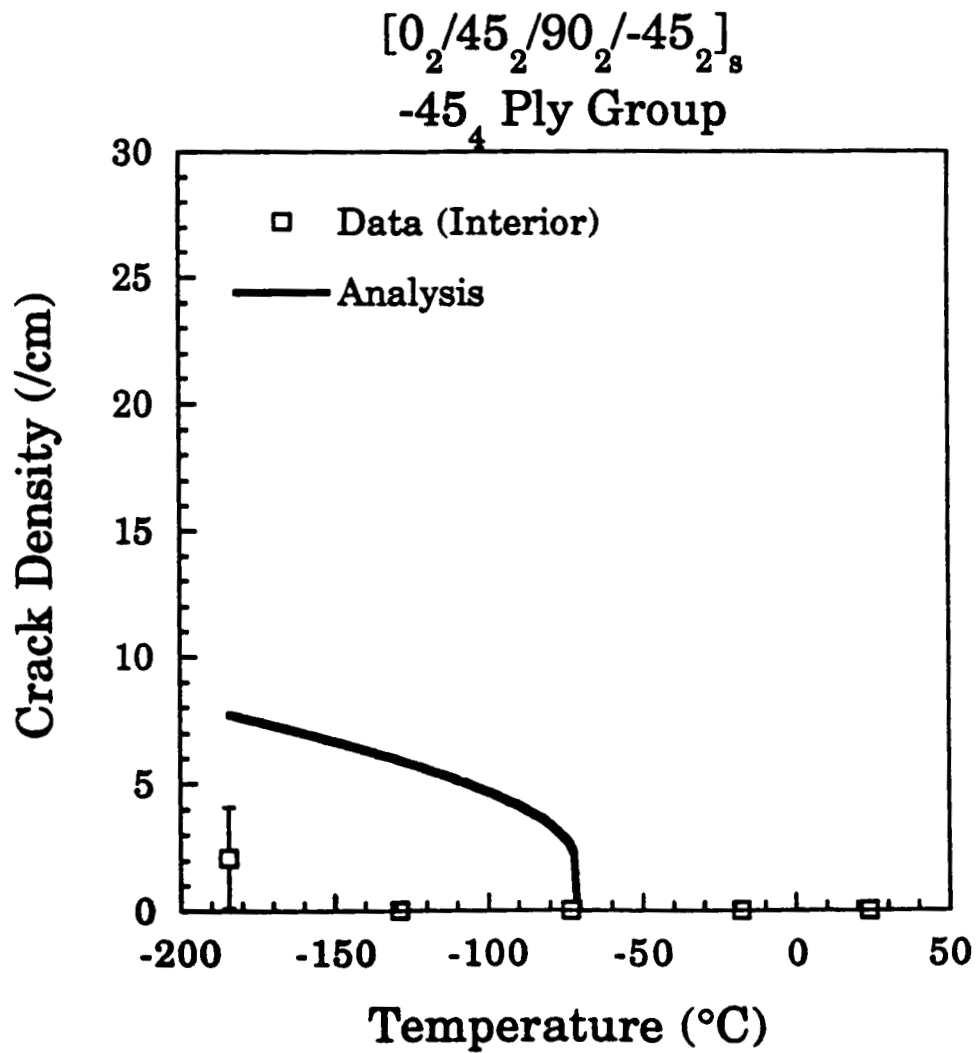
$[0_4/45_4/90_4/-45_4]_s$
90$_4$ Ply Group
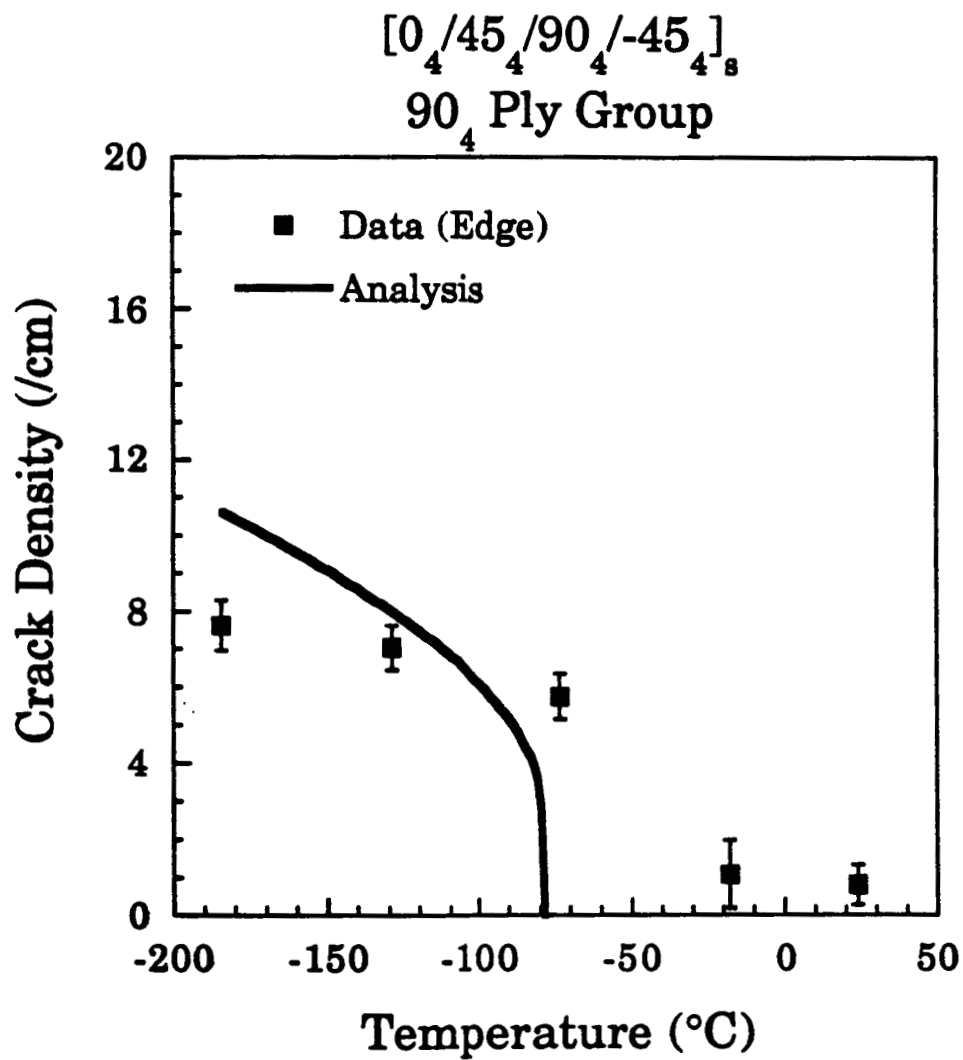
Figure D.5   Experimental results and analytical predictions of crack density vs. progressively decreasing temperature. 90$_4$ ply group of $[0_4/45_4/90_4/-45_4]_s$ edge specimens.

$$[0_4/45_4/90_4/-45_4]_s$$
$$90_4 \text{ Ply Group}$$
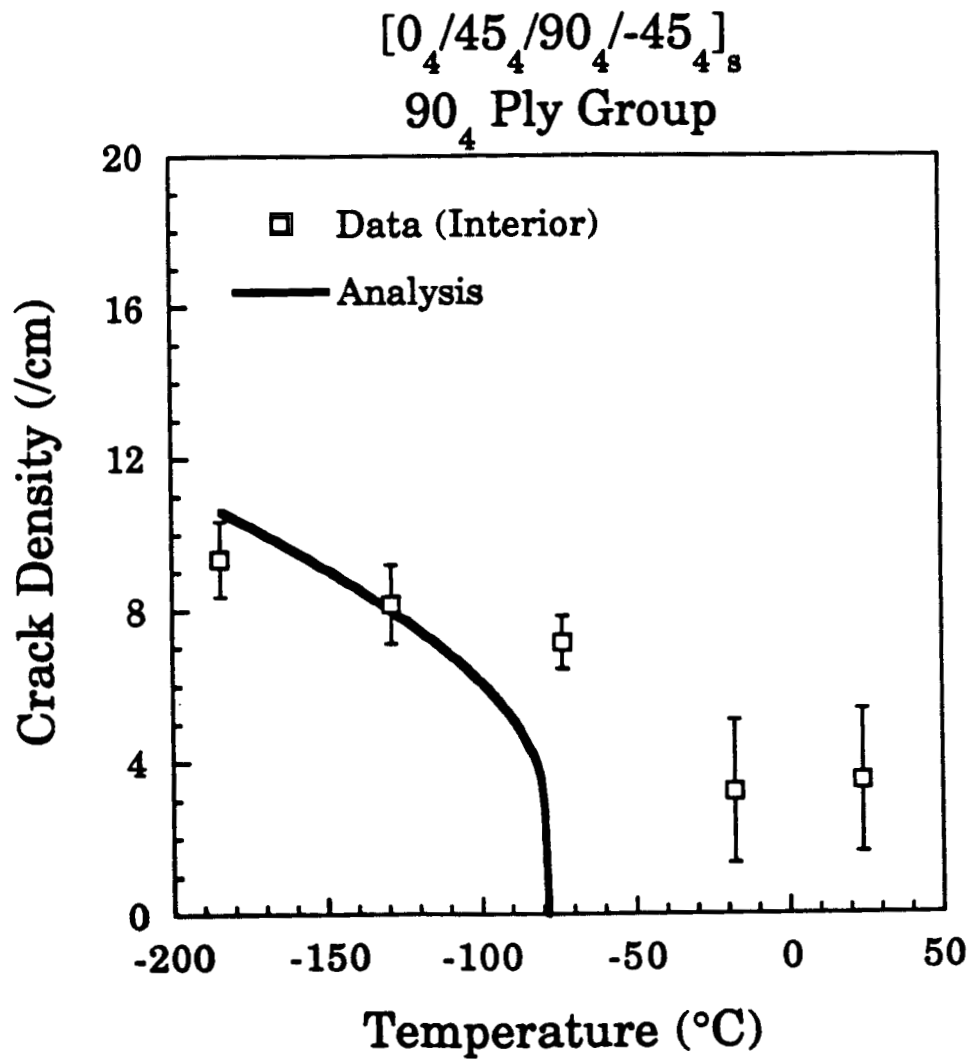
Figure D.6 Experimental results and analytical predictions of crack density vs. progressively decreasing temperature. 90_4 ply group of $[0_4/45_4/90_4/-45_4]_s$ interior specimens.
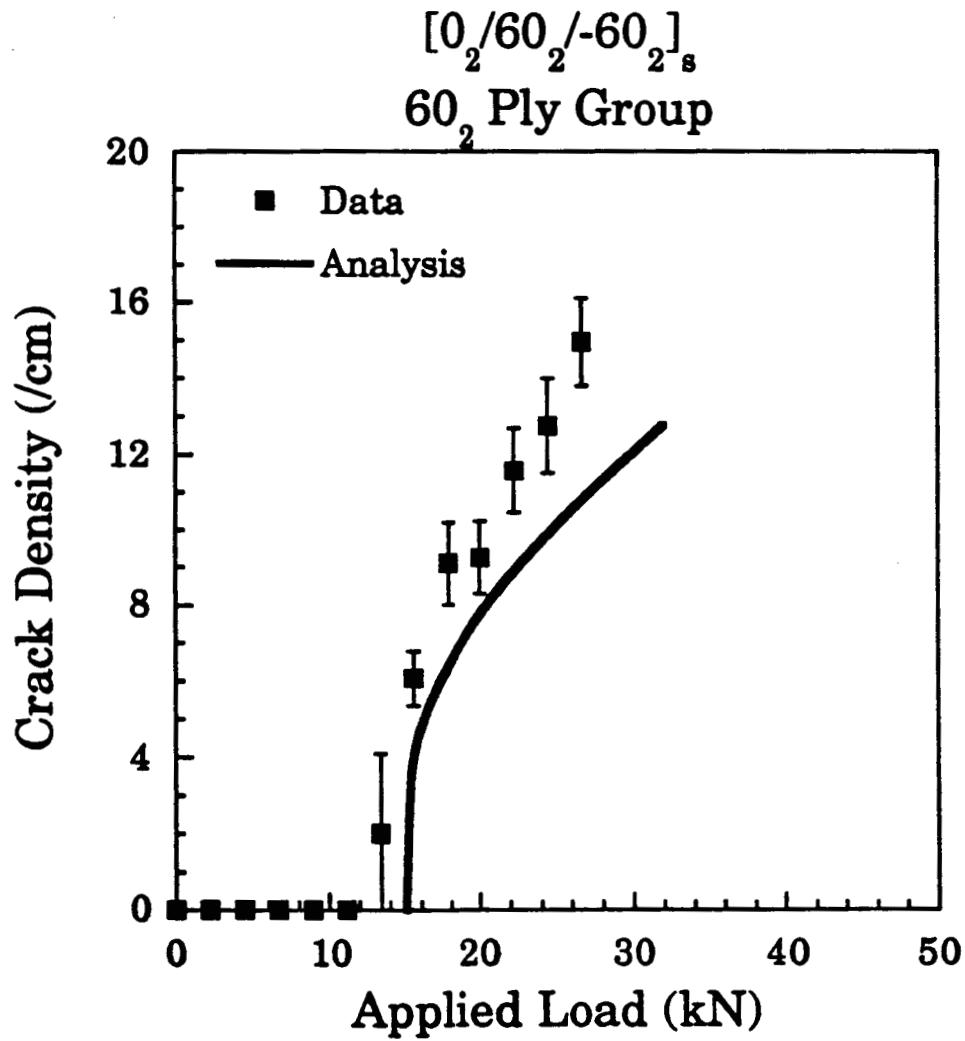
$[0_4/45_4/90_4/-45_4]_s$

-45_8 Ply Group

Figure D.7 Experimental results and analytical predictions of crack density vs. progressive applied load. -45_8 ply group of $[0_4/45_4/90_4/-45_4]_s$ laminate.
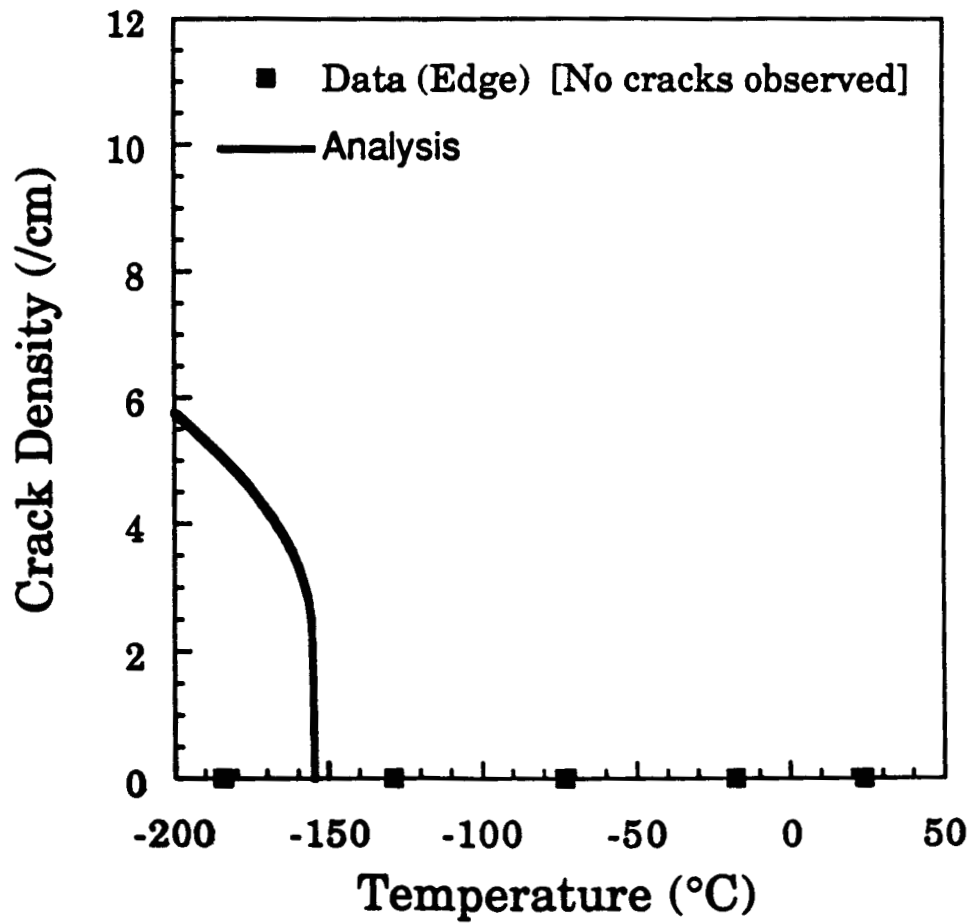
$$[0_4/45_4/90_4/-45_4]_s$$
$$-45_8 \text{ Ply Group}$$
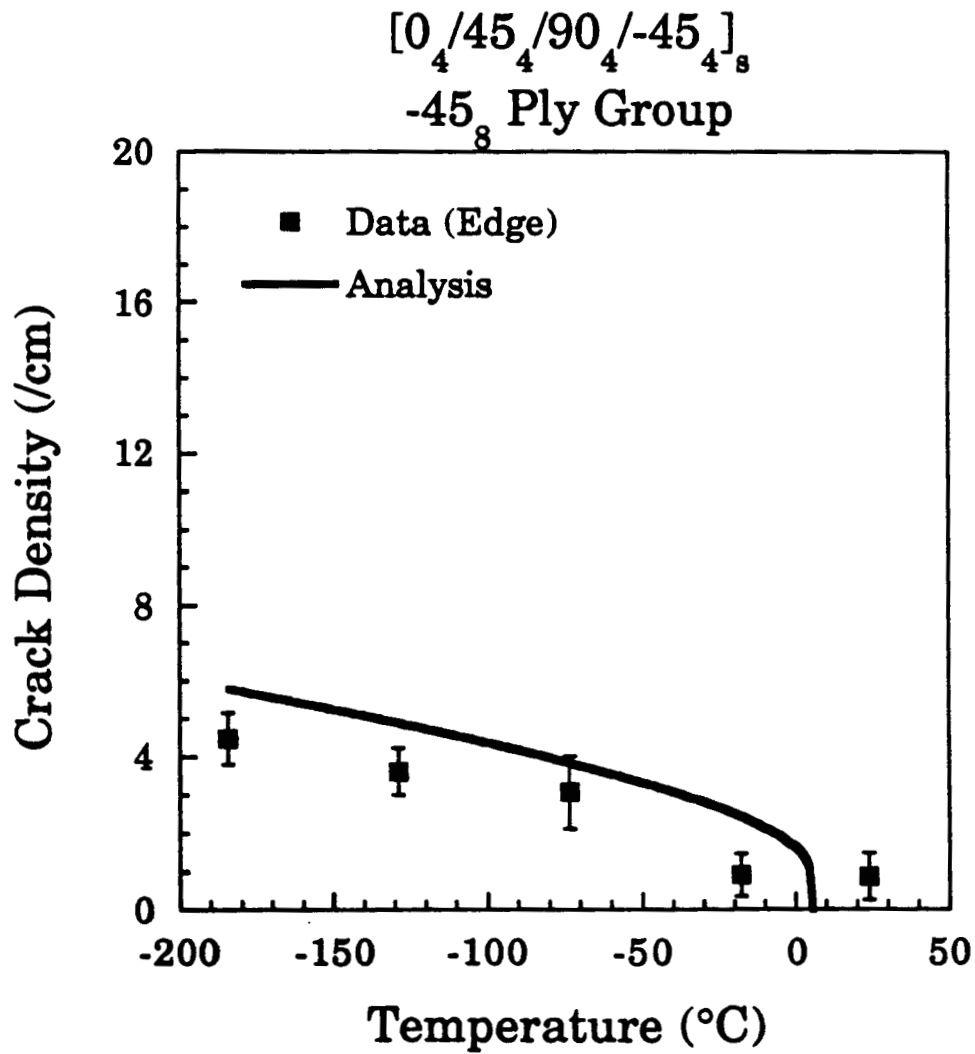
Figure D.8 Experimental results and analytical predictions of crack density vs. progressively decreasing temperature. -45$_8$ ply group of [0$_4$/45$_4$/90$_4$/-45$_4$]$_s$ edge specimens.
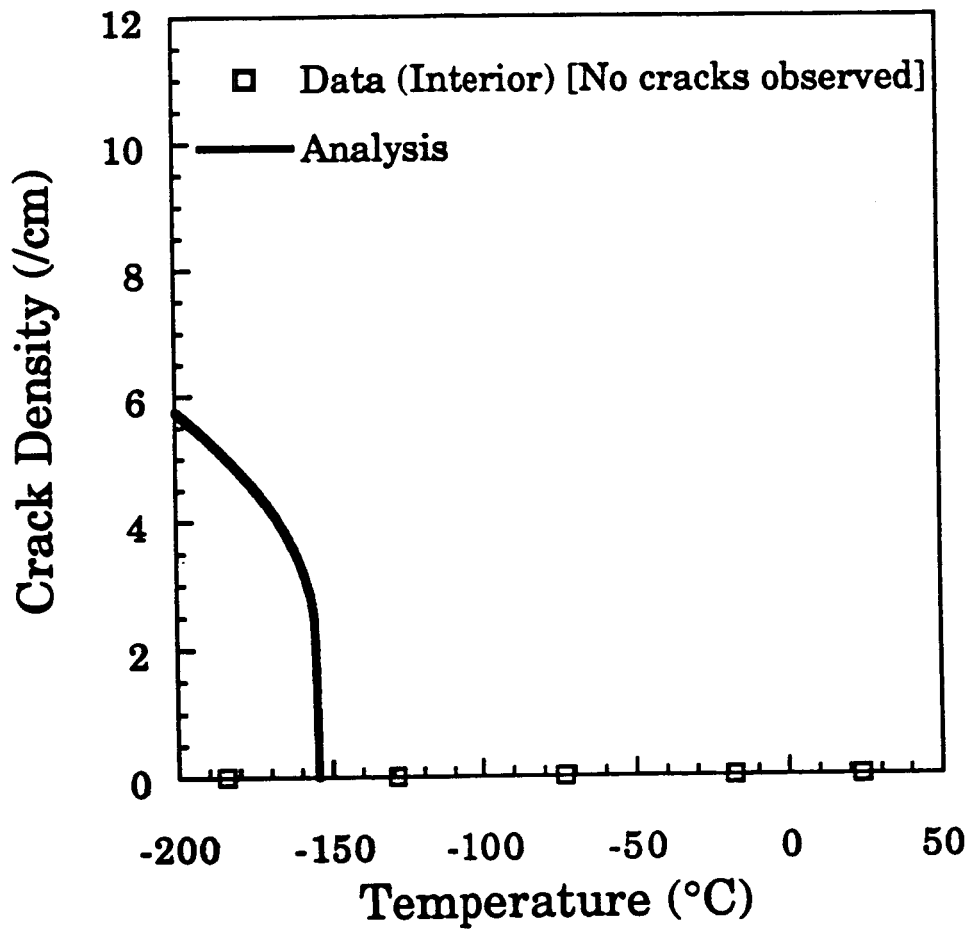
$[0_4/45_4/90_4/-45_4]_s$
-45_8 Ply Group
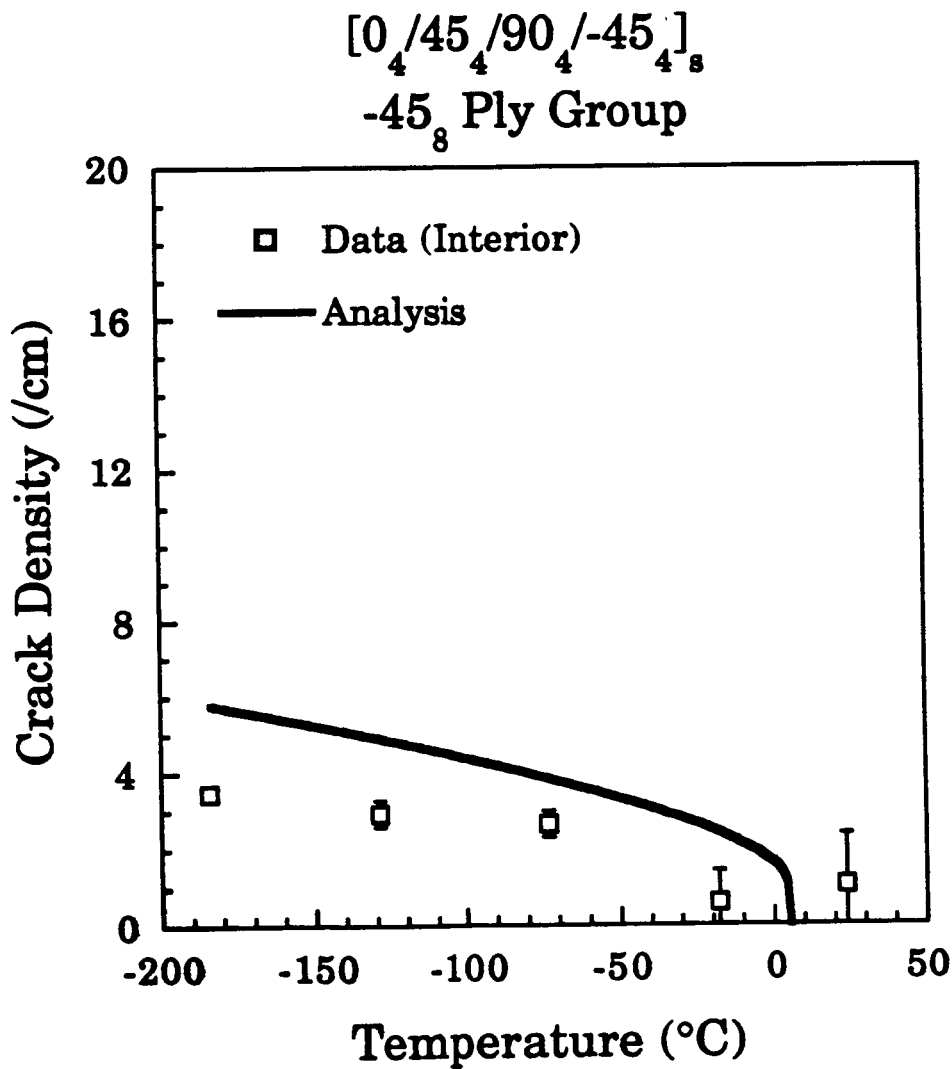
Figure D.9 Experimental results and analytical predictions of crack density vs. progressively decreasing temperature. -45_8 ply group of $[0_4/45_4/90_4/-45_4]_s$ interior specimens.
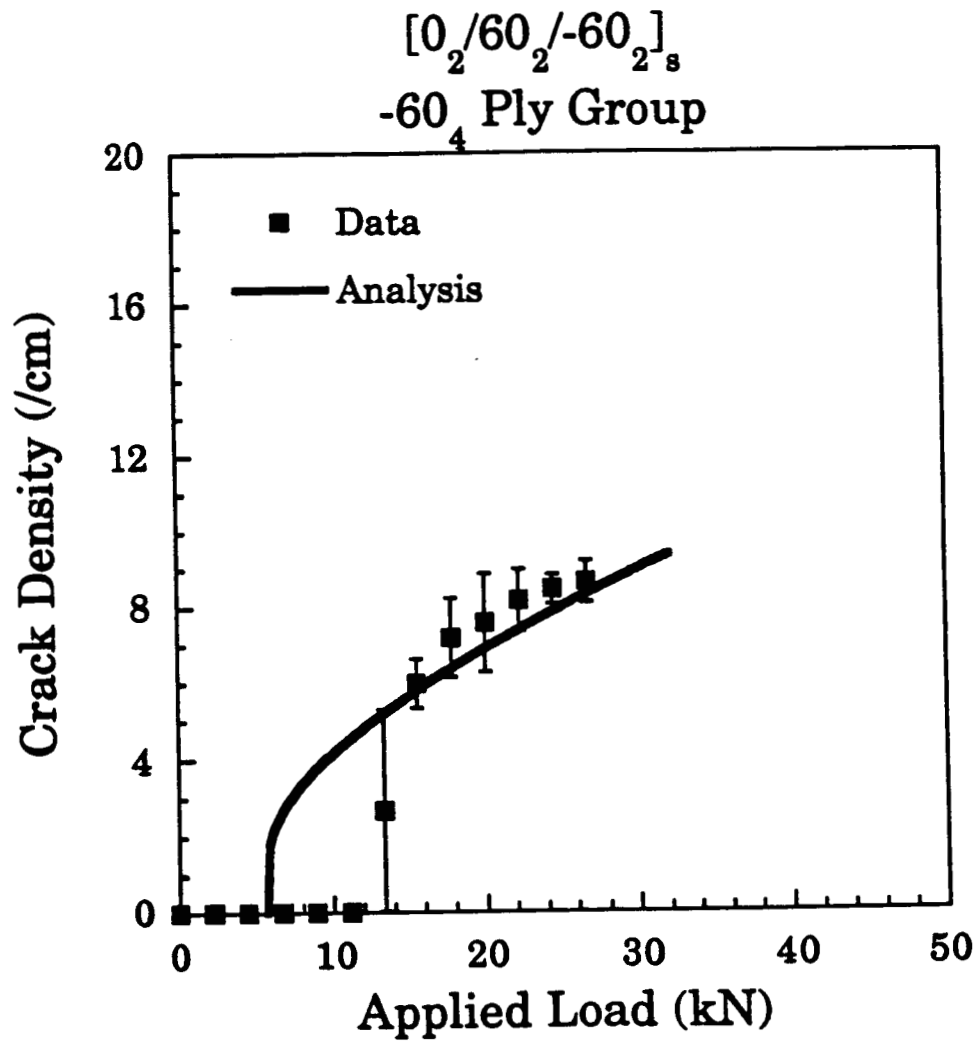
C-3.

$[0_2/45_2/90_2/-45_2]_s$

45_2 Ply Group

Figure D.10 Experimental results and analytical predictions of crack density vs. progressive applied load. 45_2 ply group of $[0_2/45_2/90_2/-45_2]_s$ laminate.

$$[0_2/45_2/90_2/-45_2]_s$$
$$45_2 \text{ Ply Group}$$
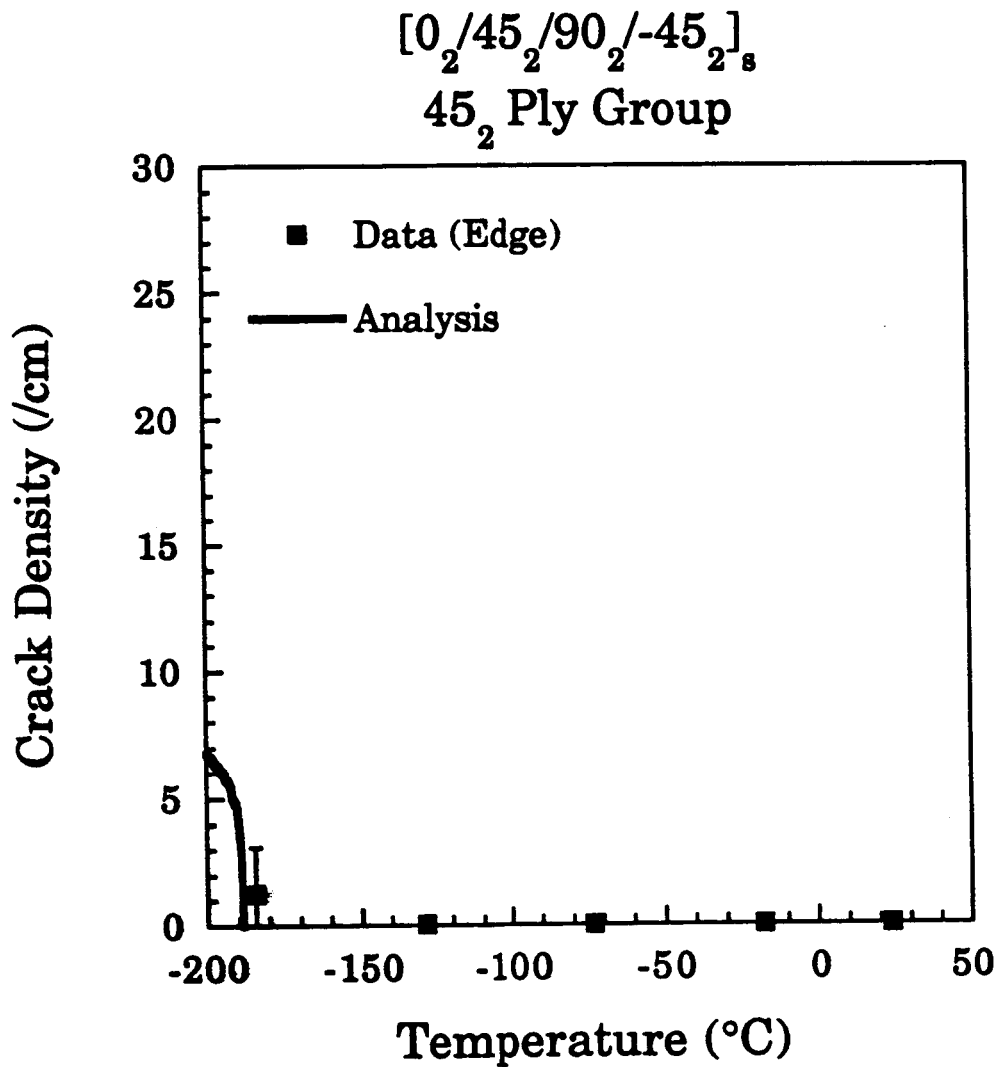
Figure D.11 Experimental results and analytical predictions of crack density vs. progressively decreasing temperature. 45_2 ply group of $[0_2/45_2/90_2/-45_2]_s$ edge specimens.

$$[0_2/45_2/90_2/-45_2]_s$$
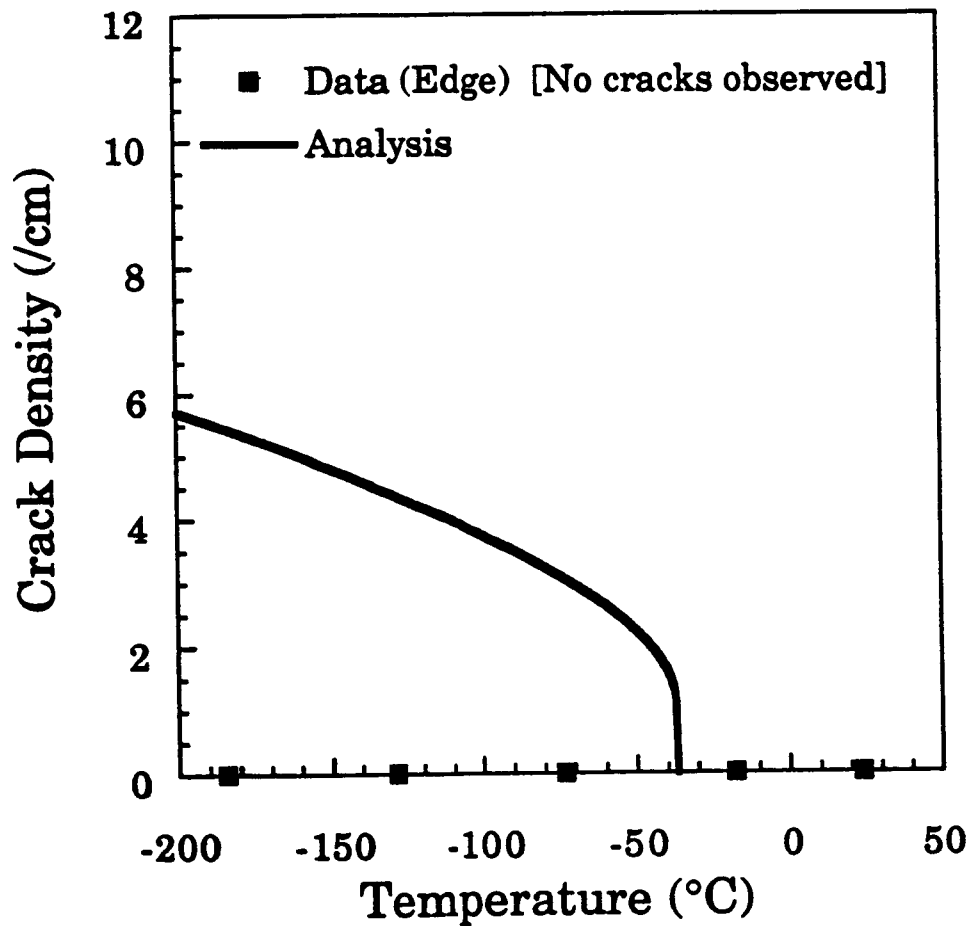$$45_2 \text{ Ply Group}$$
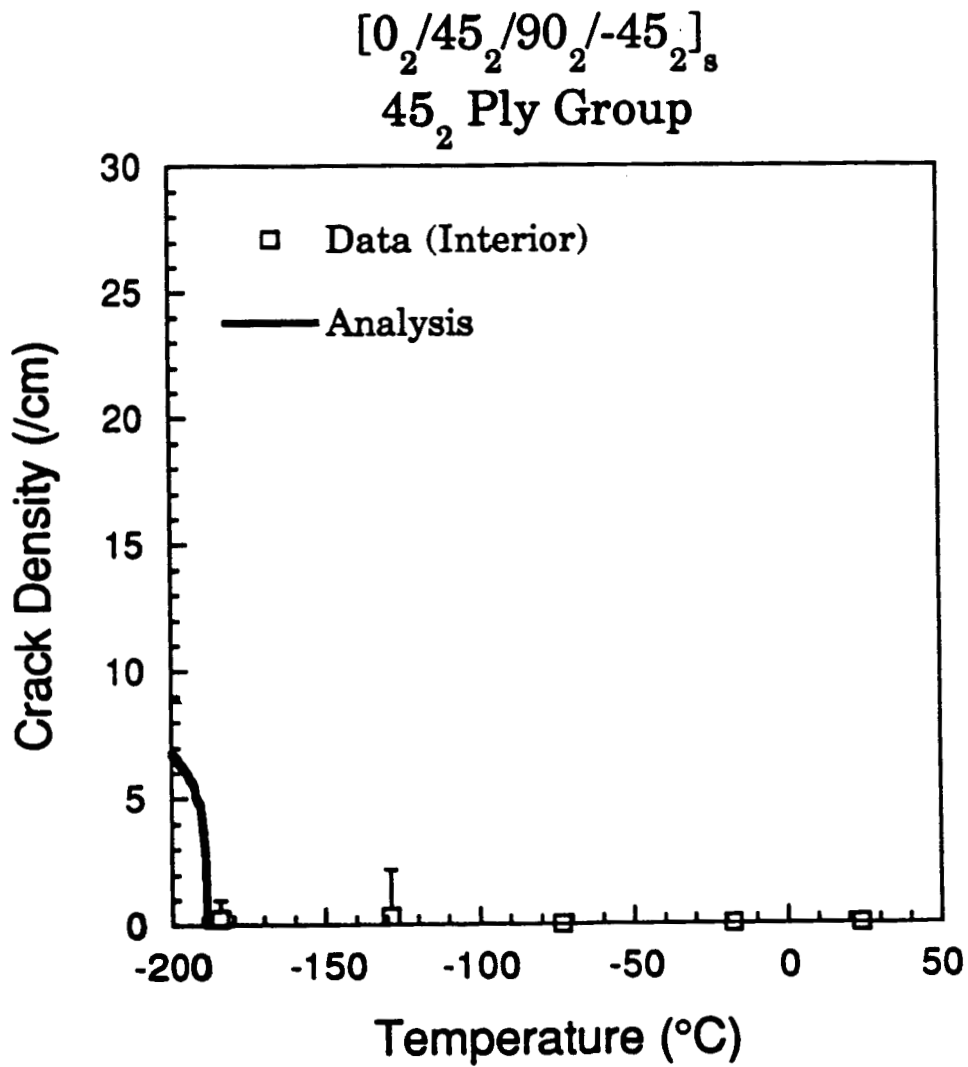
Figure D.12 Experimental results and analytical predictions of crack density vs. progressively decreasing temperature. 45_2 ply group of $[0_2/45_2/90_2/-45_2]_s$ interior specimens.

$$[0_2/45_2/90_2/-45_2]_s$$
$$90_2 \text{ Ply Group}$$
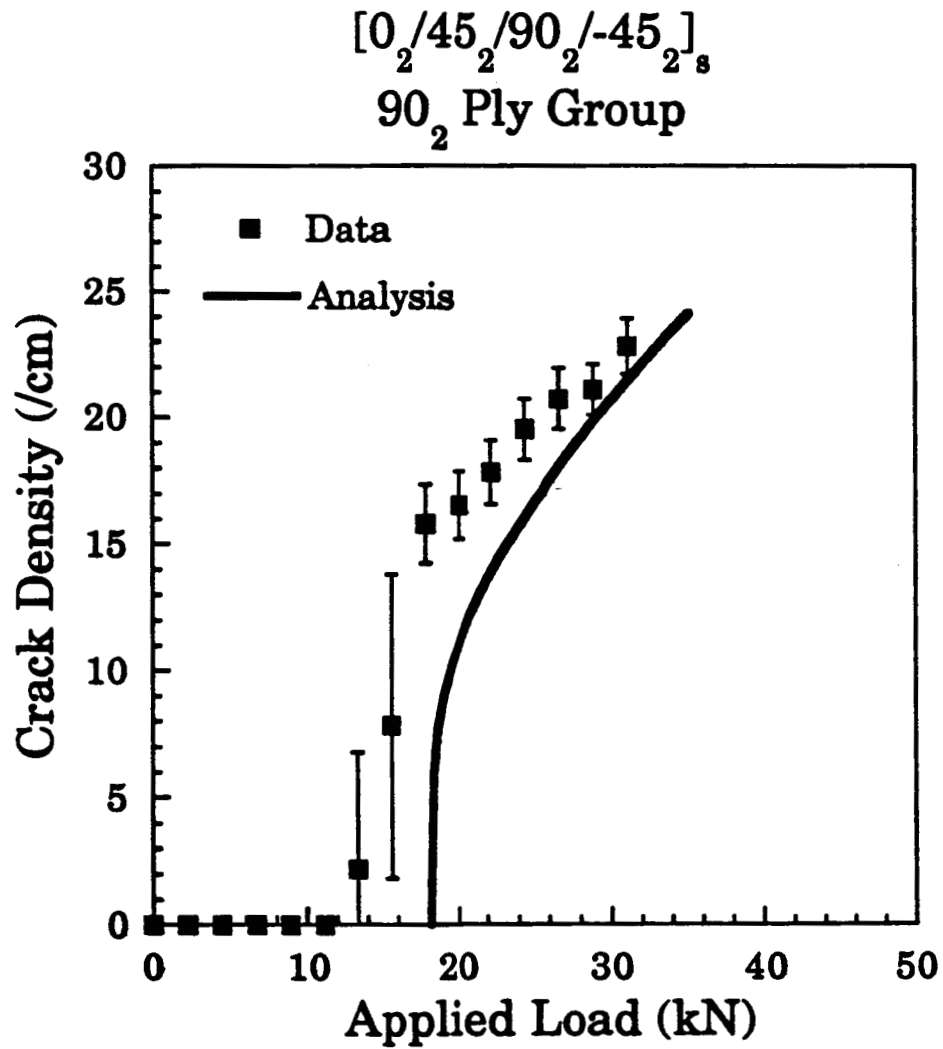
Figure D.13 Experimental results and analytical predictions of crack density vs. progressive applied load. 90_2 ply group of $[0_2/45_2/90_2/-45_2]_s$ laminate.

$$[0_2/45_2/90_2/-45_2]_s$$
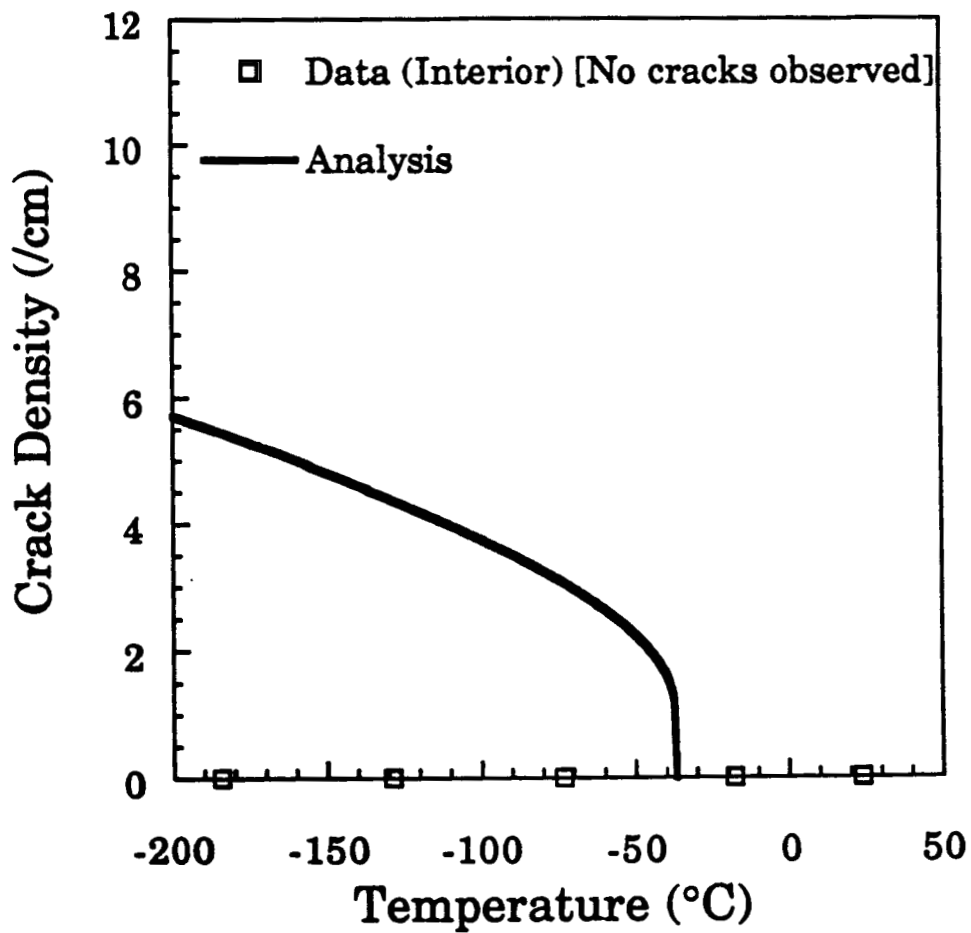$$90_2 \text{ Ply Group}$$

Figure D.14 Experimental results and analytical predictions of crack density vs. progressively decreasing temperature. 90_2 ply group of $[0_2/45_2/90_2/-45_2]_s$ edge specimens.

$$[0_2/45_2/90_2/-45_2]_s$$
$$90_2 \text{ Ply Group}$$

Figure D.15 Experimental results and analytical predictions of crack density vs. progressively decreasing temperature. 90_2 ply group of $[0_2/45_2/90_2/-45_2]_s$ interior specimens.

$$[0_2/45_2/90_2/-45_2]_s$$

-45$_4$ Ply Group

Figure D.16 Experimental results and analytical predictions of crack density vs. progressive applied load. -45$_4$ ply group of $[0_2/45_2/90_2/-45_2]_s$ laminate.

$[0_2/45_2/90_2/-45_2]_s$

-45_4 Ply Group

Figure D.17 Experimental results and analytical predictions of crack density vs. progressively decreasing temperature. -45_4 ply group of $[0_2/45_2/90_2/-45_2]_s$ edge specimens.

$[0_2/45_2/90_2/-45_2]_s$

-45_4 Ply Group

Figure D.18 Experimental results and analytical predictions of crack
density vs. progressively decreasing temperature. -45_4 ply
group of $[0_2/45_2/90_2/-45_2]_s$ interior specimens.

$[0_2/60_2/-60_2]_s$

60_2 Ply Group

Figure D.19 Experimental results and analytical predictions of crack density vs. progressive applied load. 60_2 ply group of $[0_2/60_2/-60_2]_s$ laminate.

$[0_2/60_2/-60_2]_s$

60_2 Ply Group

Figure D.20 Experimental results and analytical predictions of crack density vs. progressively decreasing temperature. 60_2 ply group of $[0_2/60_2/-60_2]_s$ edge specimens.

$$[0_2/60_2/-60_2]_s$$
$$60_2 \text{ Ply Group}$$

Figure D.21 Experimental results and analytical predictions of crack density vs. progressively decreasing temperature. 60_2 ply group of $[0_2/60_2/-60_2]_s$ interior specimens.

Figure D.22 Experimental results and analytical predictions of crack density vs. progressive applied load. -60₄ ply group of [0₂/60₂/-60₂]ₛ laminate.

$$[0_2/60_2/-60_2]_s$$
$$-60_4 \text{ Ply Group}$$

Figure D.23 Experimental results and analytical predictions of crack density vs. progressively decreasing temperature. -60_4 ply group of $[0_2/60_2/-60_2]_s$ edge specimens.

$$[0_2/60_2/-60_2]_s$$

$$-60_4 \text{ Ply Group}$$

Figure D.24 Experimental results and analytical predictions of crack density vs. progressively decreasing temperature. -60_4 ply group of $[0_2/60_2/-60_2]_s$ interior specimens.

APPENDIX E

FIRST-PLY-FAILURE STRESS-STRAIN DATA

This appendix presents stress-strain data for the $[0_4/45_4/90_4/-45_4]_s$, $[0_2/45_2/90_2/-45_2]_s$, and $[0_2/60_2/-60_2]_s$ tensile coupons. Stress-strain curves for the loadings after which first ply failure was observed are plotted. The specimen name is included with each plot. The first character indicates the layup: "E", "F", and "G" represent $[0_2/60_2/-60_2]_s$, $[0_2/45_2/90_2/-45_2]_s$, and $[0_4/45_4/90_4/-45_4]_s$, respectively. The second character represents the panel from which the specimen was cut, and the third indicates the specimen's position on the cutting plan in Figure 5.1. The final character is either "N", "W", or "M": narrow thermal specimen, wide thermal specimen, or tensile coupon, respectively.

Specimen GA-1M
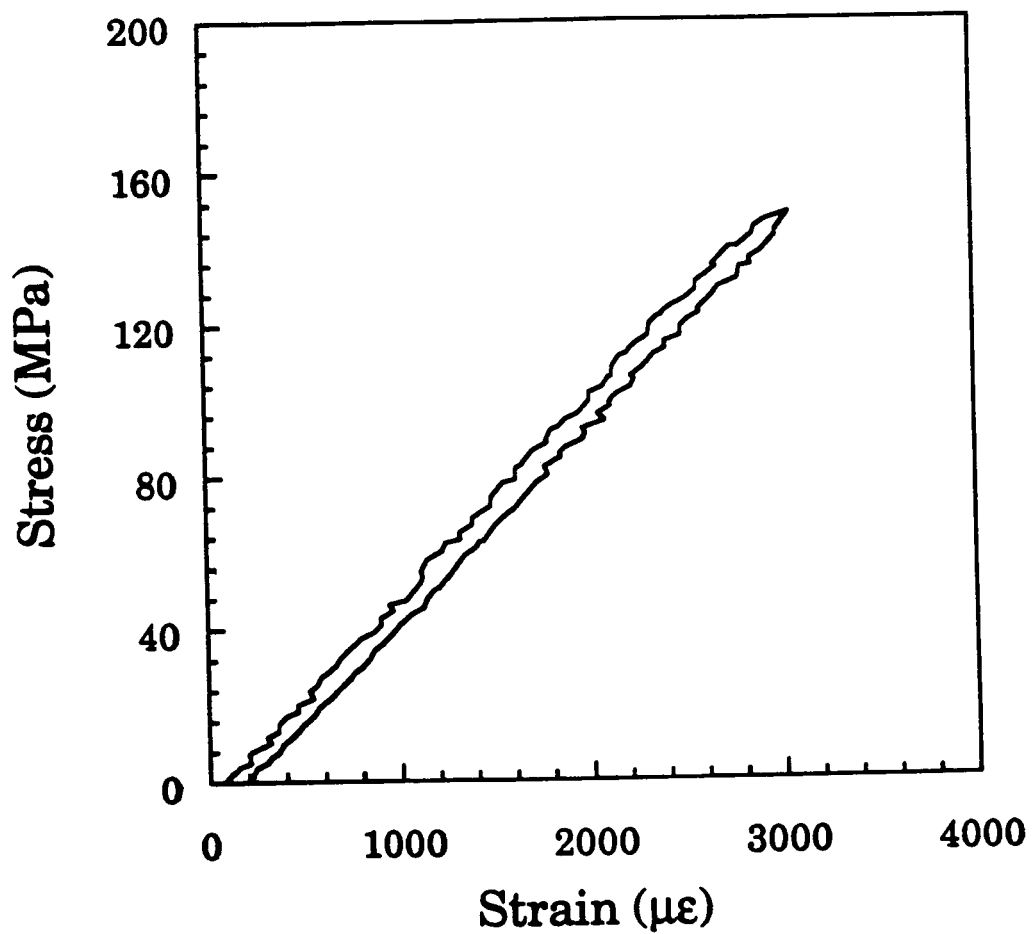
Figure E.1 Stress-strain plot for GA-1M [0₄/45₄/90₄/-45₄]ₛ tensile coupon progressively loaded to 15.6 kN.

Specimen GA-2M
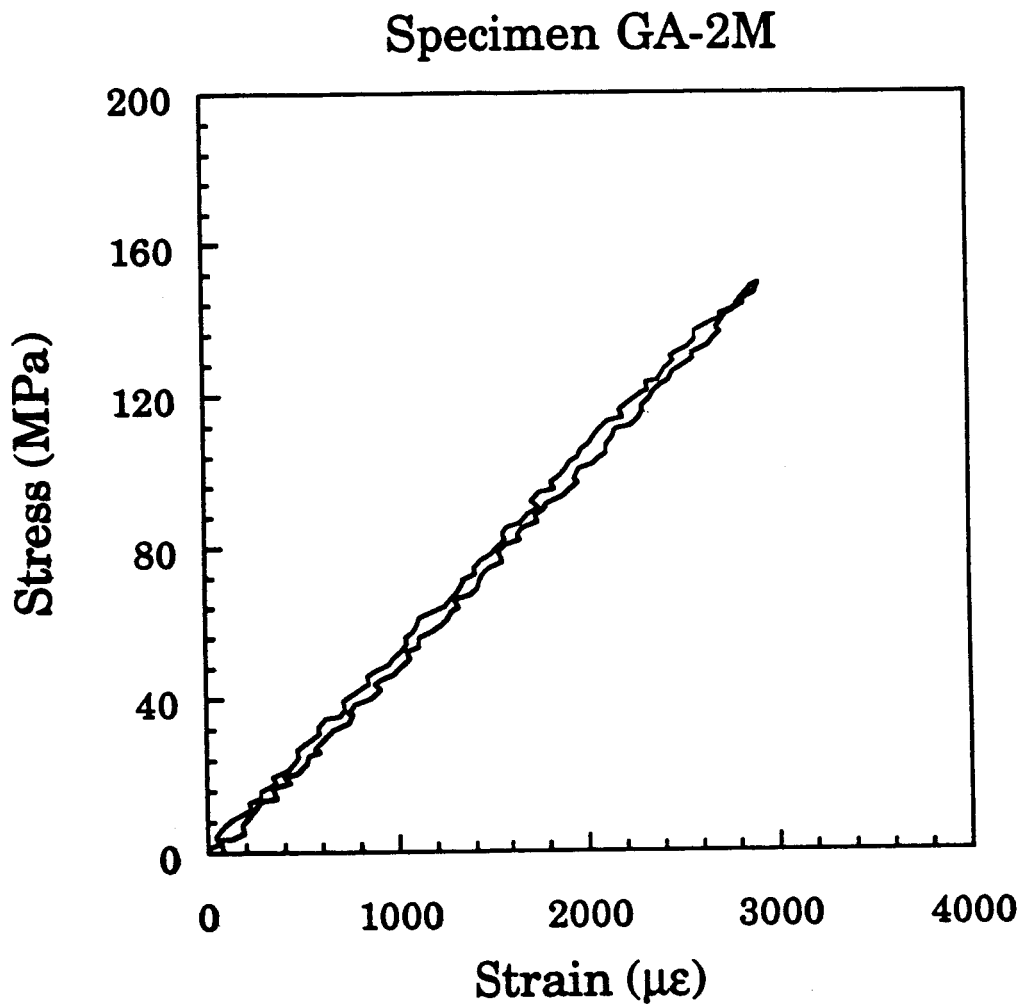
Figure E.2   Stress-strain plot for GA-2M [0₄/45₄/90₄/-45₄]ₛ tensile coupon
progressively loaded to 15.6 kN.

Specimen GA-3M
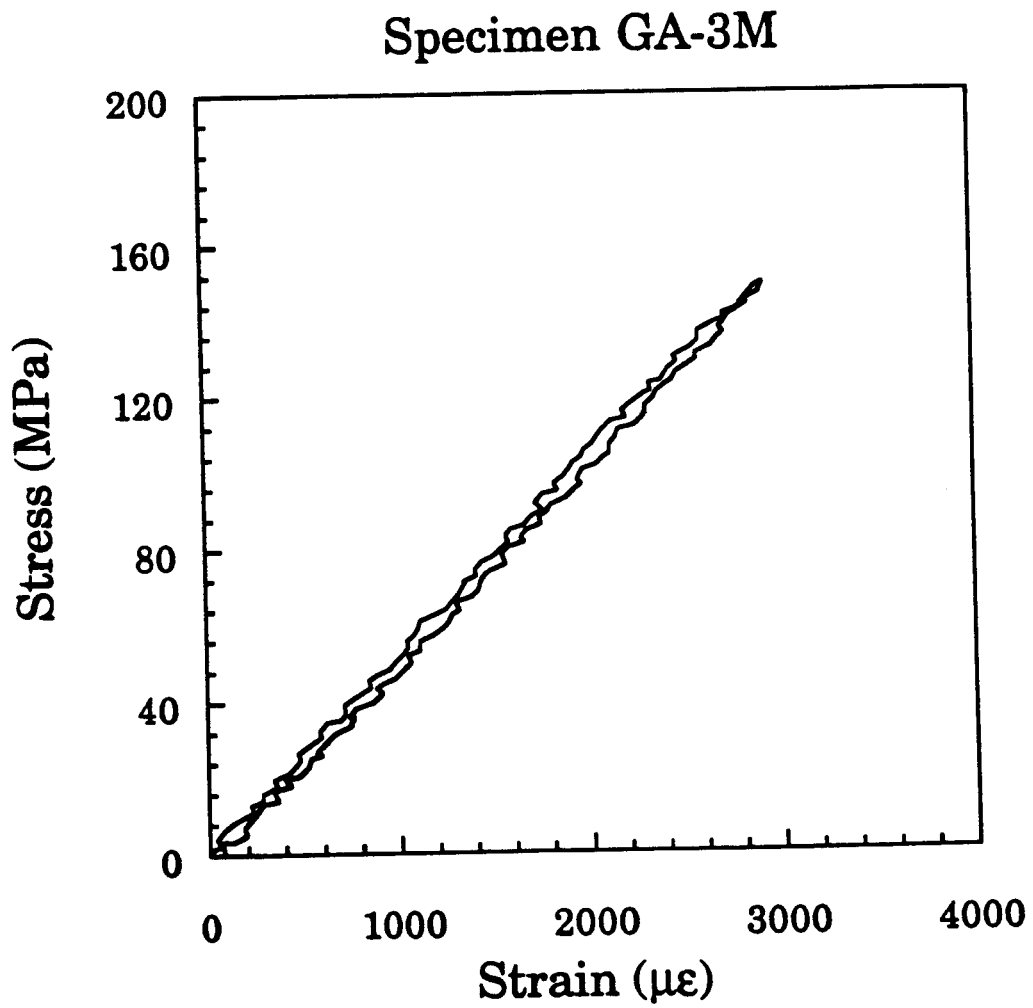
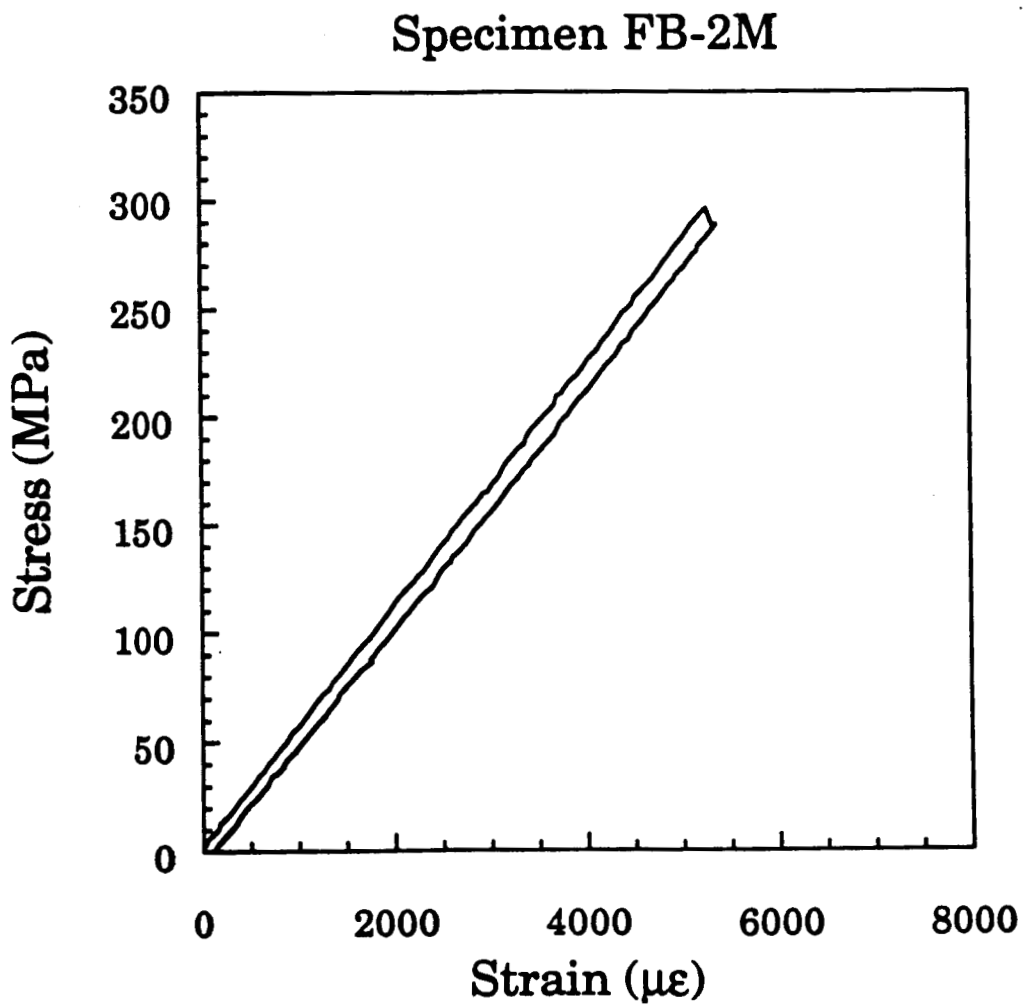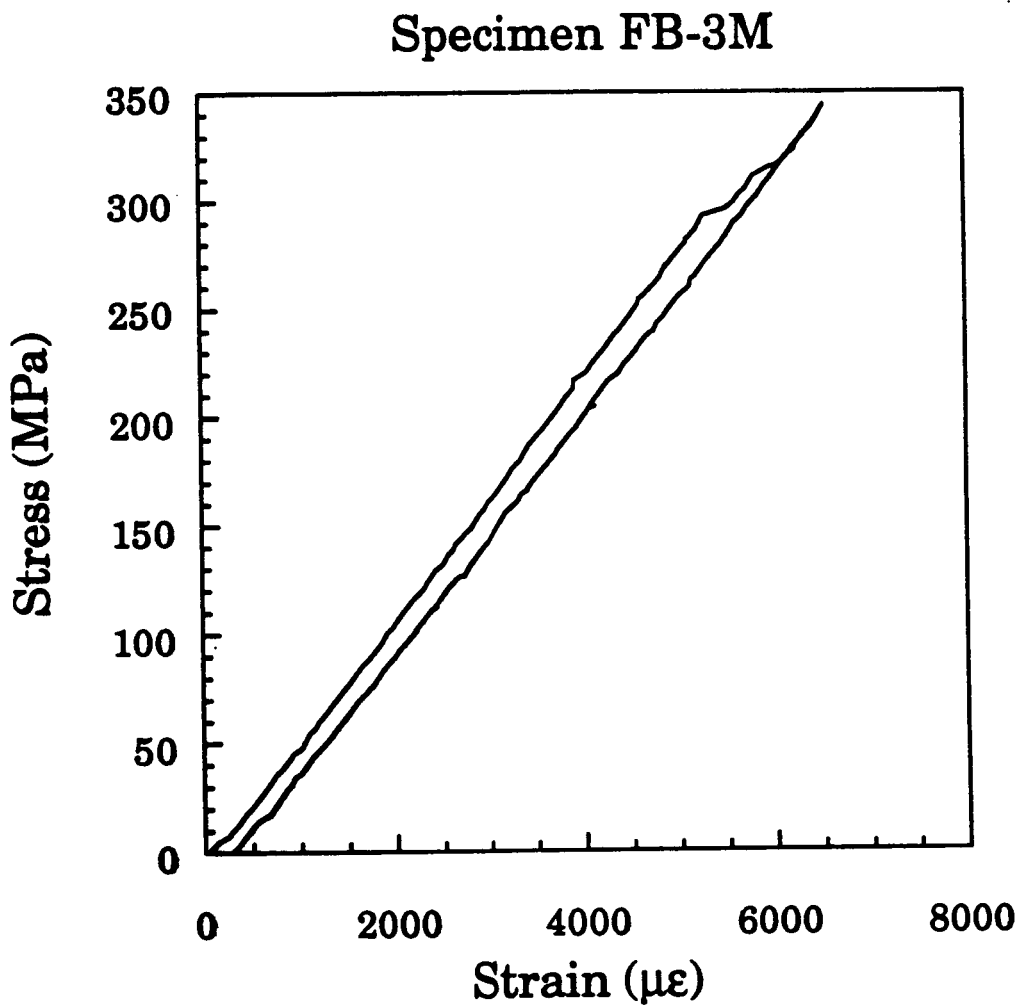Figure E.3   Stress-strain plot for GA-3M [0₄/45₄/90₄/-45₄]ₛ tensile coupon progressively loaded to 15.6 kN.

Specimen GB-2M
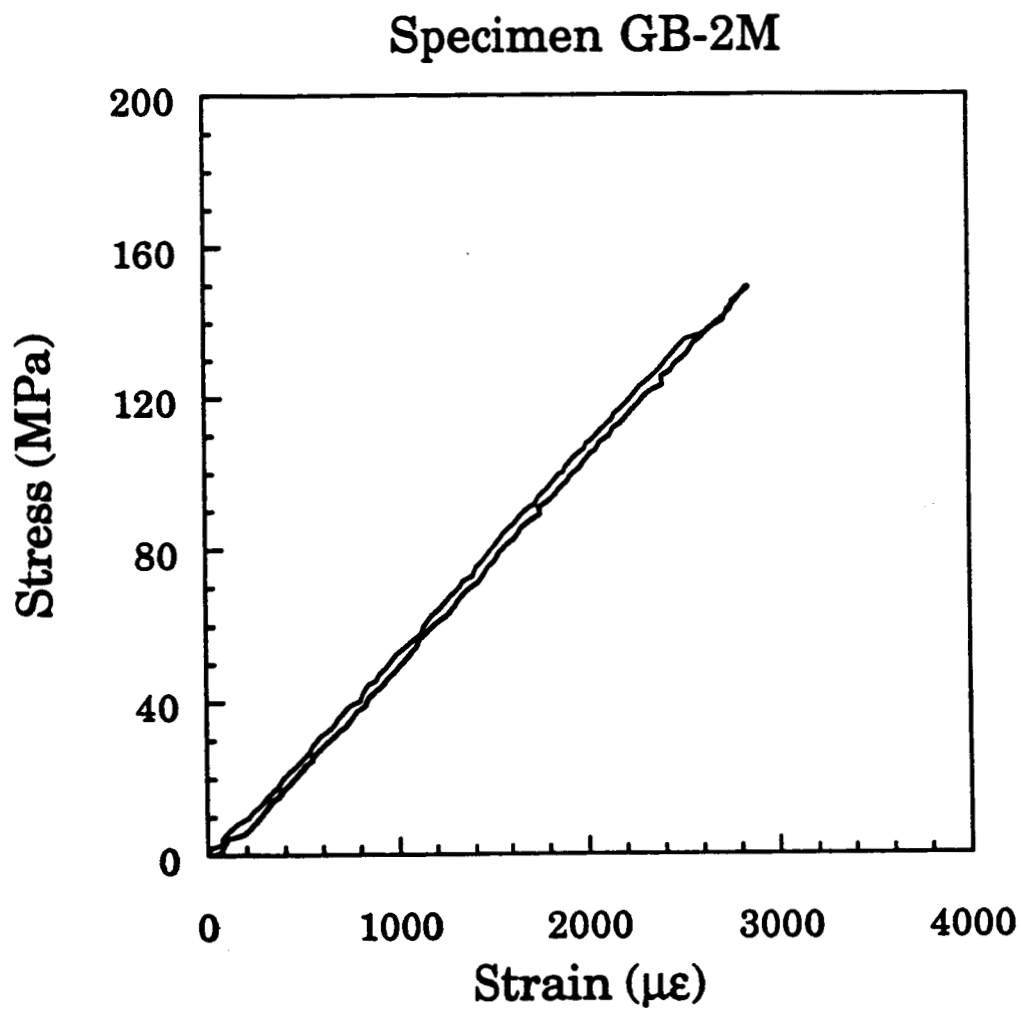
Figure E.4   Stress-strain plot for GB-2M [0₄/45₄/90₄/-45₄]ₛ tensile coupon progressively loaded to 15.6 kN.
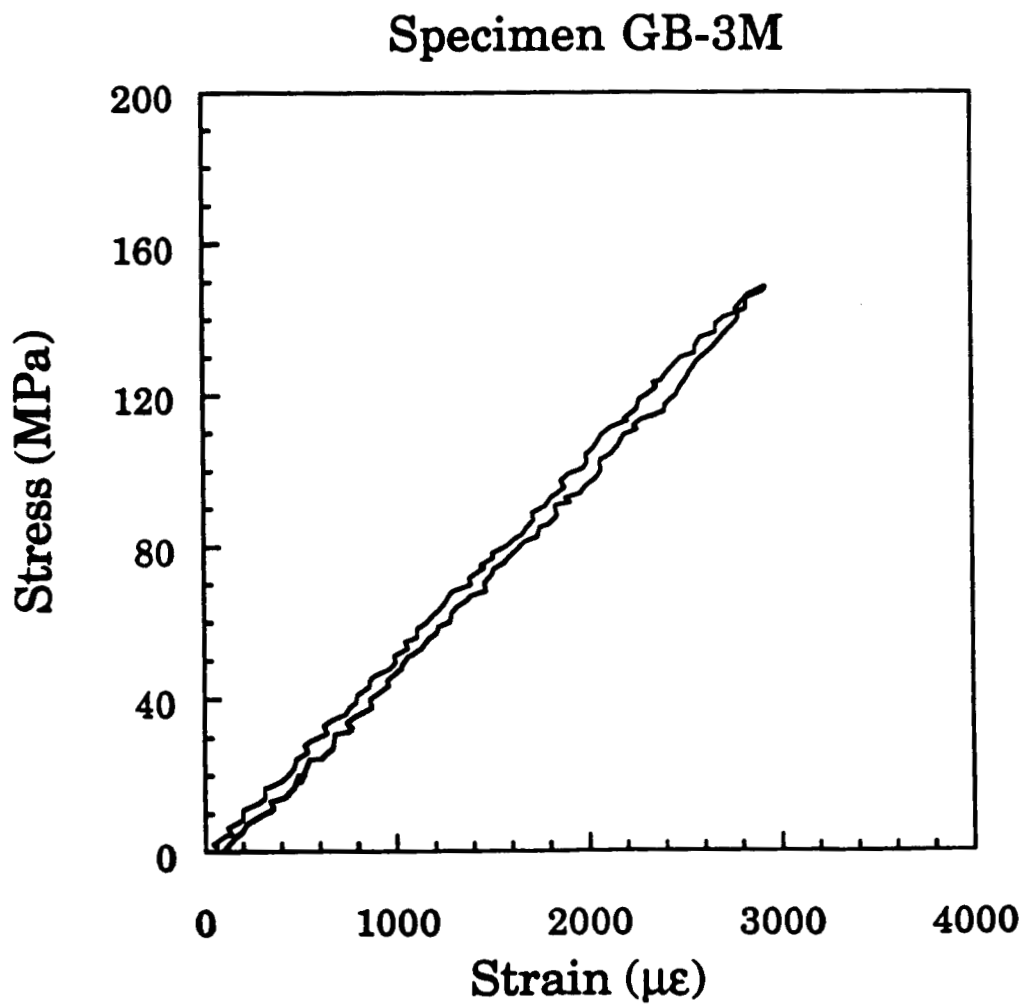
Specimen GB-3M

Figure E.5   Stress-strain plot for GB-3M [0./45./90./-45.]ₛ tensile coupon progressively loaded to 15.6 kN.
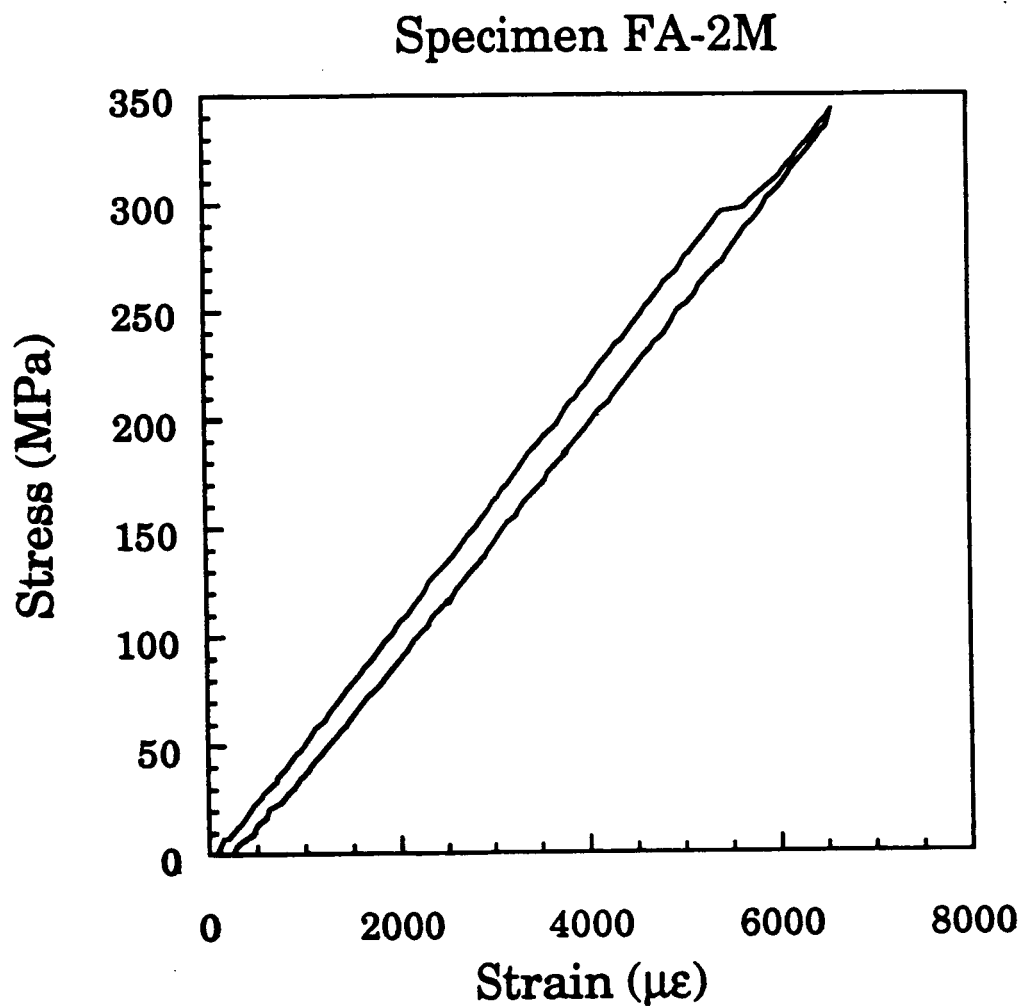
Specimen FA-2M

Figure E.6   Stress-strain plot for FA-2M $[0_2/45_2/90_2/-45_2]_s$ tensile coupon
progressively loaded to 17.8 kN.

Figure E.7   Stress-strain plot for FA-3M [0$_2$/45$_2$/90$_2$/-45$_2$]$_s$ tensile coupon progressively loaded to 17.8 kN.
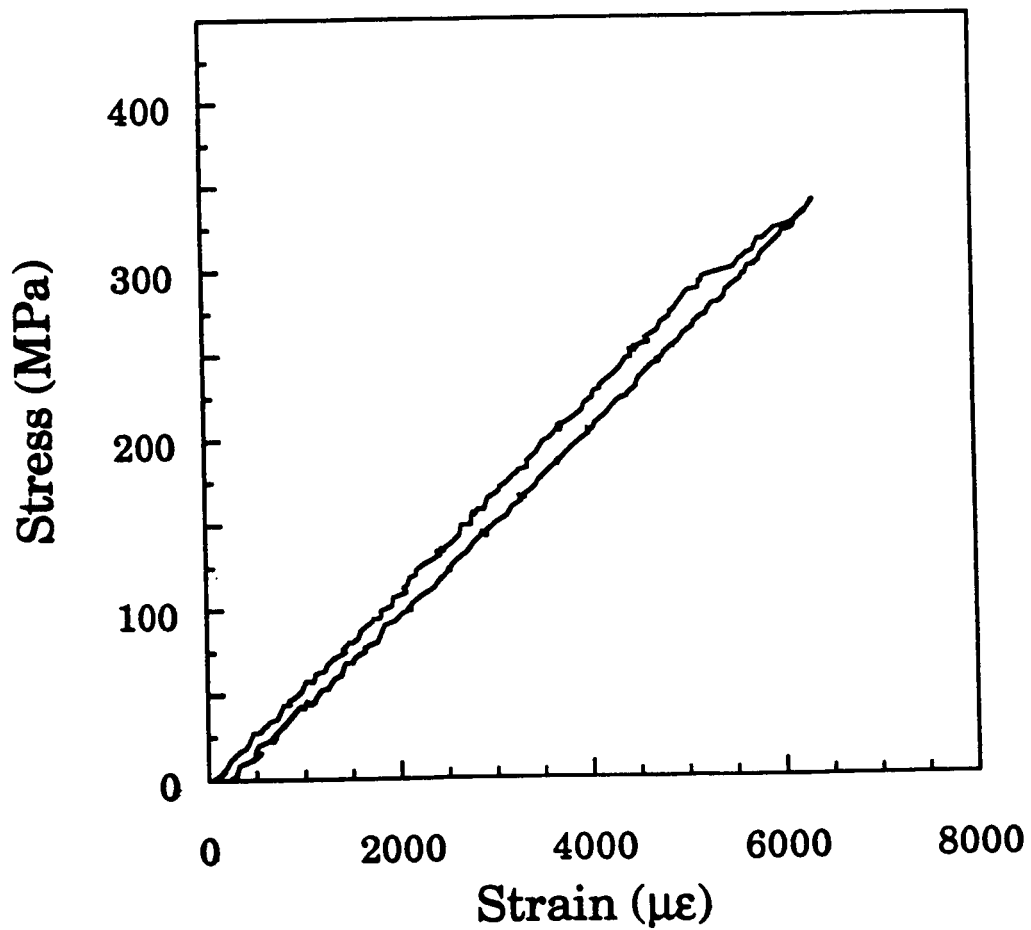
Specimen FB-1M
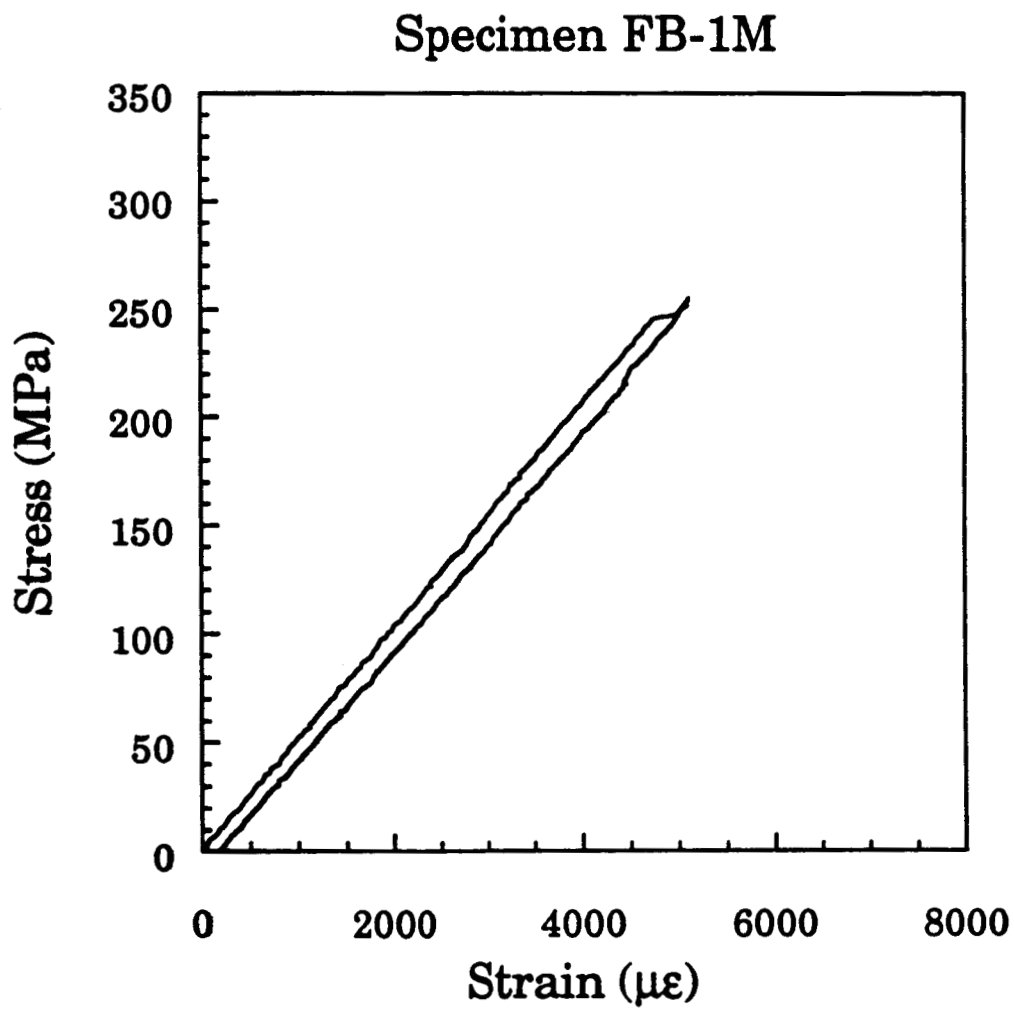
Figure E.8   Stress-strain plot for FB-1M [0₂/45₂/90₂/-45₂]ₛ tensile coupon
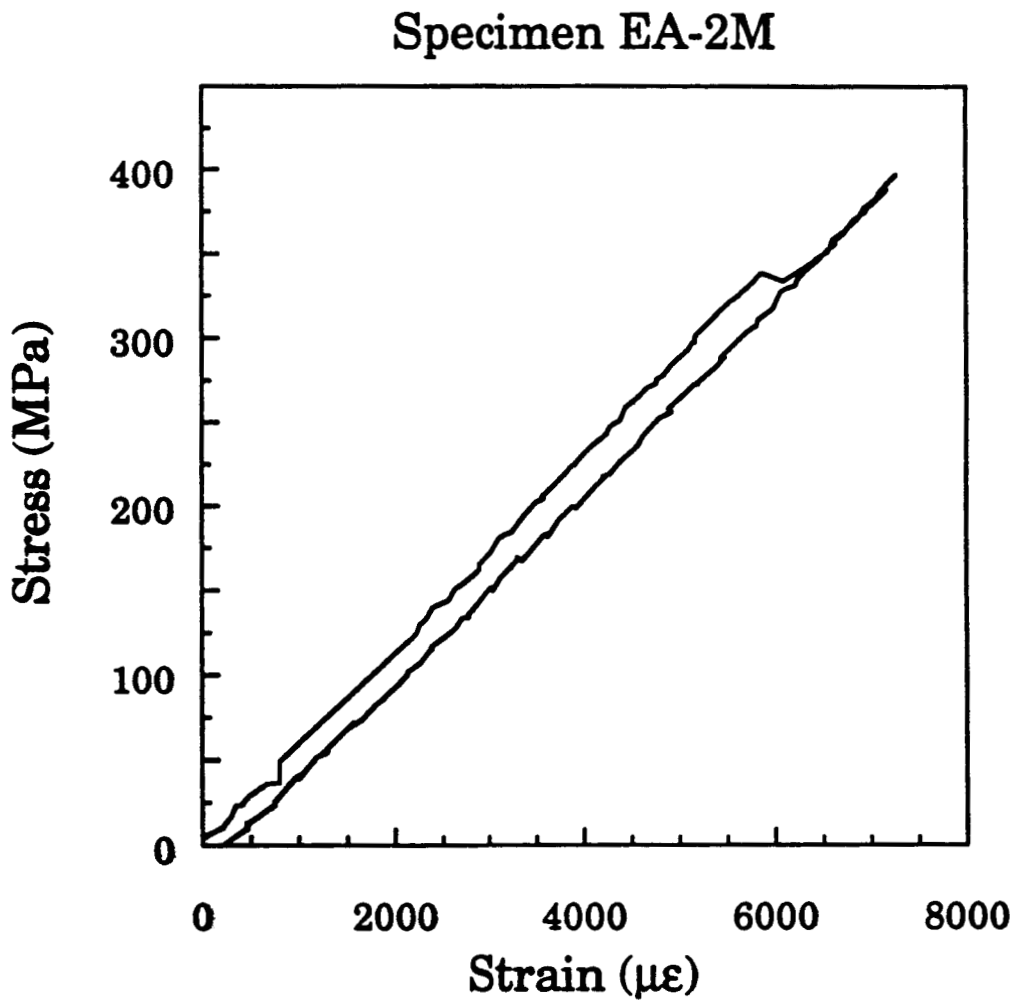progressively loaded to 13.3 kN.

Specimen FB-2M

Figure E.9   Stress-strain plot for FB-2M $[0_2/45_2/90_2/-45_2]_s$ tensile coupon progressively loaded to 15.6 kN.

Specimen FB-3M

Figure E.10 Stress-strain plot for FB-3M [0$_2$/45$_2$/90$_2$/-45$_2$]$_s$ tensile coupon progressively loaded to 17.8 kN.

Figure E.11 Stress-strain plot for EA-1M [0₂/60₂/-60₂]ₛ tensile coupon progressively loaded to 13.3 kN.
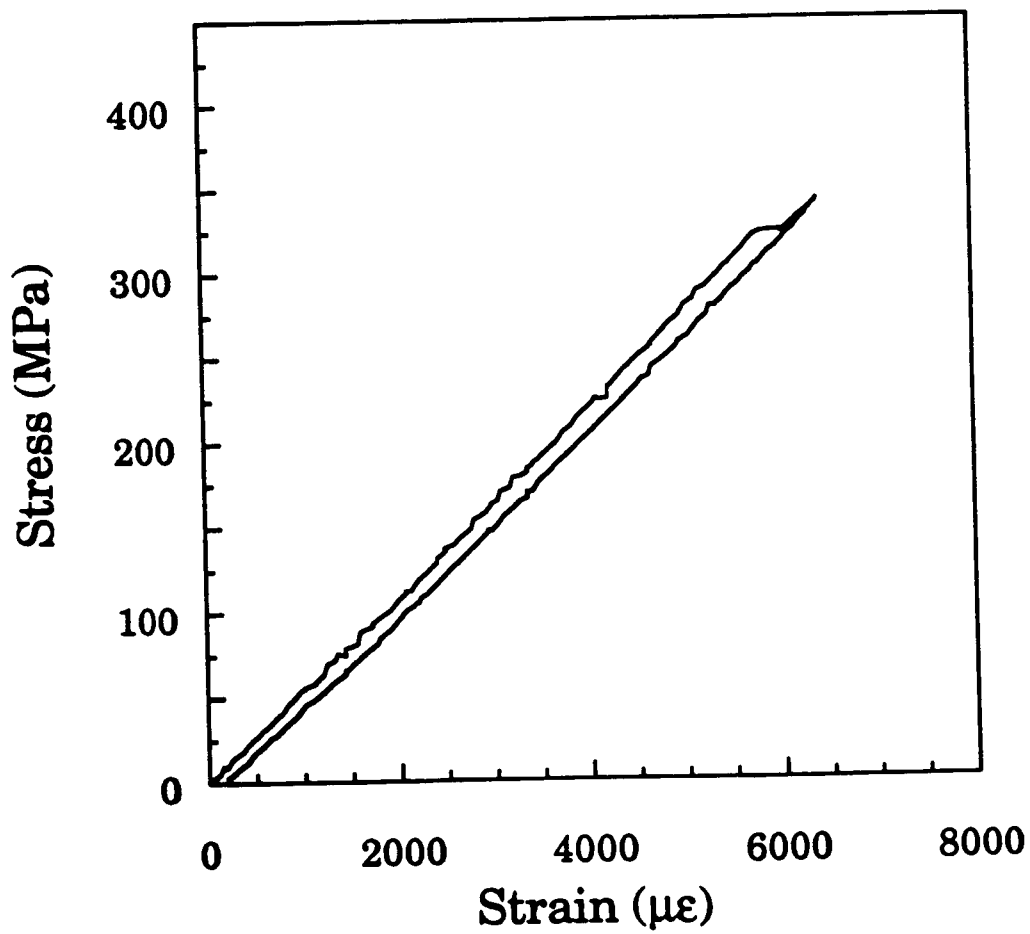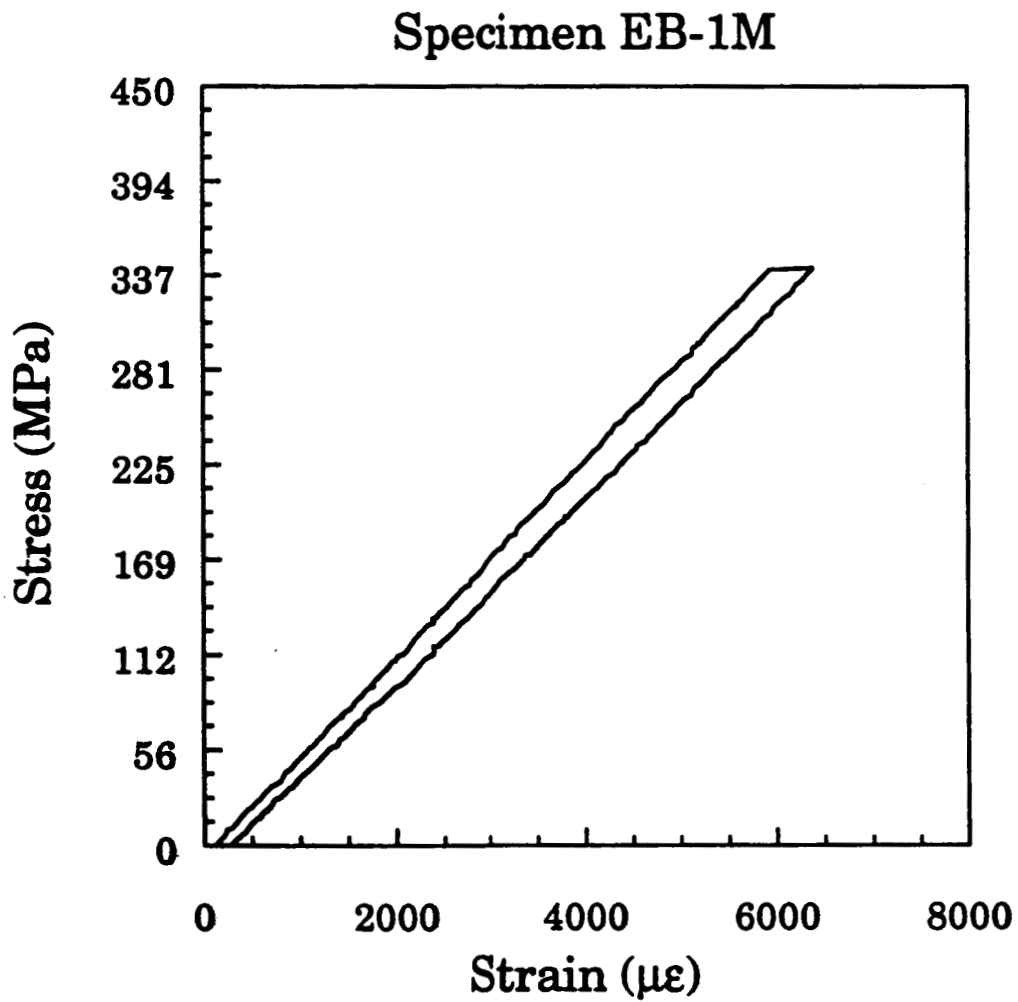
Specimen EA-2M

Figure E.12 Stress-strain plot for EA-2M [0$_2$/60$_2$/-60$_2$]$_s$ tensile coupon progressively loaded to 15.6 kN.

Specimen EA-3M

Figure E.13 Stress-strain plot for EA-3M $[0_2/60_2/-60_2]_s$ tensile coupon progressively loaded to 13.3 kN.
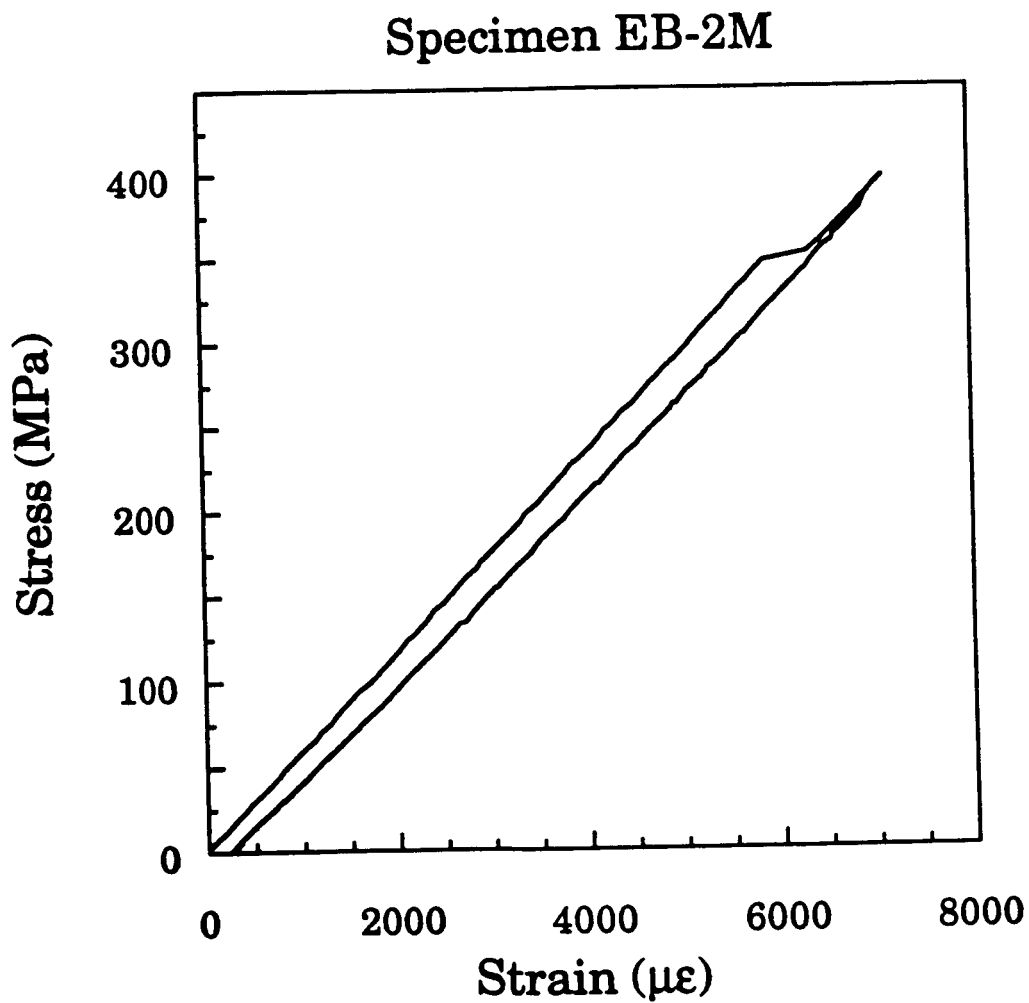
Specimen EB-1M

Figure E.14 Stress-strain plot for EB-1M $[0_2/60_2/-60_2]_s$ tensile coupon progressively loaded to 13.3 kN.

Figure E.15 Stress-strain plot for EB-2M $[0_2/60_2/-60_2]_s$ tensile coupon progressively loaded to 15.6 kN.